

**Inverse Modelling of Material Parameters for
Rubber-like material: Create a New Methodology of
Predicting the Material Parameters using
Indentation Bending Test**

Jensen Aw Chee Seng

**A thesis submitted in partial fulfilment of the
requirements of the Liverpool John Moores
University for the degree of
Doctor of Philosophy**

August 2015

ACKNOWLEDGEMENTS

I would like to express my sincere gratitude and special thanks to my supervisors, Prof. James Ren, Dr. Dave Allanson, Prof. R. Li, who has provided guidance, advice and encouragement during this research study. I am also grateful for my current employer Nottingham University and Mr. Edward for their support in completing the thesis while work as a KTP associate.

Many other academic, secretarial and technical members of staff have facilitated the realisation of this thesis and I express them all my gratitude. I would like to thank Mr. Clive Eyre and Mr. Anthony Dunmore for their invaluable technical support with material testing and sample manufacturing process.

I would like to take this opportunity to thank my group mates, Dr. Hongyi Zhao, Mr. Andrew Norbury and Dr. Nyoman Budiarsa for their friendship and sharing their experience. I am also grateful of the help from my friends, who gave me help in many ways and shared a great time in my studies and life at Liverpool John Moores University.

Finally, I would like to thank my family and my wife for sustained encouragement that gave me motivation during my studies continuous and unselfish love and support all the time.

Jensen Aw Chee Seng

Abstract

Rubber-like materials and thin membrane materials have been widely used in industries, such as engineering fields and biomedical fields. The mechanics of membranes and material parameters identification is an important research area. In this work, different inverse FE modelling approaches to extract material parameters (Ogden model) has been assessed supported by several newly developed programs in producing or analysing the data. The effects of new material properties (e.g. negative Poisson's ratio) are also studied.

In this work, the use of inverse FE modelling and indentation bending test for material property identification has been systematically studied. A parametric FE model has been developed and validated simulating the indentation bending tests of thin latex rubber samples made in the laboratory. Rubber samples were tested in standard uniaxial tensile, planar tests, the hyperelastic material parameters are determined and used as the target for an inverse materials parameter identification program. An ABAQUS add-on program has been developed to automatically update the material parameters and extract the force-displacement data. Simulation spaces over a wide range of material parameters have been developed, which successfully provided the numerical data for the inverse approach for material property prediction. Different curve analysis approaches in representing the force-displacement curve have been proposed including (1) using ratio of P/h^3 for the low load region, (2) using the effective slope at higher load and (3) using the second order polynomial curve fitting parameters. The result shows that use of these curve fitting parameters could effectively simplify the inverse FE modelling process and allow the use of surface plot equations to establish a mathematical relationship between curve coefficients and material parameters. These relationships could effectively open up the possibility of improving the uniqueness of inversely predicted material property sets by combining either data from different testing conditions or different curve data from the same test.

As an important part of the work, several new programs have been developed to process and analyse the data. A MatLab program has been developed to determine

the surface equation between the key curve coefficients and the material parameters based on FE data with an Ogden model. Work based on the data from a single indenter test shows that there are multiple material property sets that could produce identical force-displacement data. This confirms that the results are not unique. Several approaches have been evaluated by combining the surface equation for different curve parameters or testing conditions (i.e. sample sizes) to improve the robustness of the inverse prediction. A program has been developed and implemented by the inverse FE modelling which allows systematic studies with different approaches including dual chamber size, thickness or combining a two curve parameter approach. The results demonstrate combining different curve fitting approaches with a smaller chamber size is more effective than using the dual chamber size approach. Relaxation indentation bending test have been performed and different inverse FE program has been comparatively applied to estimate the viscoelastic parameters from the test data. One program is based on full objective function approach; the other is a two staged interactive searching approach. This program has been evaluated in both training data using numerical data as the target and relaxation test data of the natural latex rubber sample.

The deformation of circular elastic membranes with a clamped edge under point loading or finite contact conditions is systematically studied incorporating auxeticity behaviour (Negative Poisson's ratio). The effect of Poisson's ratio on the deformation of the material is established. The feasibility and limitation of an analytical solution is assessed. The work shows that the P/h^3 relationship is applicable to describe the force displacement data over the membrane domain for both point loading and finite contact conditions. It is shown that negative Poisson's ratio has shown clear influence on the membrane deformation domain; the resistance force of a membrane with a negative Poisson's ratio is relatively lower, which could be beneficial for application such as sensors, as the material will be more sensitive to load change. This work has highlighted some important characteristics of membranes with negative Poisson's ratio, further work is required to quantify these effects with consideration of relative dimensions between sample thickness and chamber size.

Contents

Acknowledgement

Abstract

Contents

Symbols (In order of appearance)

List of Figures

Chapter 1 Introduction	1
1.0 Introduction	2
1.1 Indentation bending tests of thin membranes and materials parameters identification	2
1.2 Aims and objectives	6
1.3 Outline of the thesis	7
Chapter 2 Literature review	9
3.2 Background and literature review	10
2.1 Introduction	10
2.2 Rubber-like materials and thin membranes	11
2.3 The properties of rubber like material and plastics material	15
2.4 Strain energy functions for rubber, foams and biological materials	18
2.5 Viscoelastic properties for rubber and plastic material	25
2.6 Mechanical tests of materials and applications	33
2.6.1 Material testing with standard tests	33
2.7 Indentation and indentation bending test	36
2.8 FE modelling and inverse properties prediction	45
2.9 Different inverse modelling approaches and their applications in material	

Properties prediction.....	49
2.9.1 Inverse parameter identification based interactive property searching approach.....	50
2.9.2 Artificial Neural Network (ANN).....	53
2.9.3 An optimisation method with post data processing –the Kalman filter method.....	55
2.9.4 An objective functions method for optimization.....	57
2.10 Main challenges testing thin membranes and properties identification..	58

Chapter 3 Inverse finite element (FE) modelling method to determine the hyperelastic material parameters based on indentation bending tests.....60

3.1 Introduction.....	61
3.2 Experimental works and results.....	64
3.2.1 Rubber sheet sample preparation.....	64
3.2.2 Uniaxial and planar tests of the rubber material and results.....	65
3.2.3 Indentation bending tests and results.....	69
3.3 FE modelling of indentation bending test and validation.....	74
3.3.1 Hyperelastic FE model of indentation bending test.....	74
3.3.2 Mesh sensitivity tests and results.....	78
3.3.3 Validation of the FE with testing data and selection of suitable strain energy function for direct and inverse analysis.....	80
3.4 Inverse FE modelling for material parameters prediction.....	83
3.5 Structure of the data analysis and inverse material parameters identification Program.....	89
3.6 P/h^3 Curvature approach and results.....	93
3.7 Slope method and results.....	99
3.8 Polynomial curve fitting approach and results.....	106
3.9 Inverse materials properties identification based on combination of different curve parameters.....	116
3.10 Use of the inverse approach in analysing experimental data and comparison with the full curve objective function approach.....	124
3.11 Discussion.....	129
3.12 Conclusion.....	132

Chapter 4 Characterisation of the viscoelastic material parameters of materials from indentation bending tests.....	134
4.1 Introduction.....	135
4.2 Experimental work and results.....	137
4.2.1 Materials.....	137
4.2.2 Relaxation tensile test.....	137
4.2.3 Indentation bending test and relaxation tests.....	139
4.3 FE model and inverse identification of creep parameters.....	140
4.4 Inverse program and results.....	145
4.5 Development of a stage interactive searching program in Python and results.....	151
4.6 Summary.....	157
 Chapter 5 Effect of Poisson's ratio on the deformation of thin membrane structures under indentation	 158
5.1 Introduction.....	159
5.2 Experimental and FE models.....	161
5.3 Result and discussion.....	164
5.3.1 Comparison between experimental data and FE modelling...164	
5.3.2 Deformation of a thin membrane under point loading conditions.....	165
5.3.3 Effect of Poisson's ratio on the deformation of membranes under finite contact conditions.....	168
5.4 Summary.....	177
 Chapter 6 Conclusions and Future works.....	 178
6.1 Summary and conclusions.....	179
6.2 Recommendations for future works.....	181
 References.....	 182
 Publication list.....	 202

Symbols (In Order of Appearance)

2.3 The properties of rubber material and plastic material

- σ_x The tensile stress
- ε_x The tensile strain
- E The Young's modulus
- ν The Poisson's ratio
- G The shear modulus
- ε^E The elastic strain
- ε^P The plastic strain

2.4 Strain energy functions for rubber, foams and biological materials

- W, \tilde{W} Strain energy function
- U Strain energy density
- F The deformation gradient tensor
- C The right Cauchy-Green deformation tensor, $C = F^T F$
- I_1 The first invariant of C , $I_1 = \text{tr} C$
- I_2 The second invariant of C , $I_2 = (\text{tr} C)^2 - \text{tr} C^2$
- I_3 The third invariant of C , $I_3 = \det C$
- J The Jacobian matrix of the deformation, $J = \det F$
- D_1 The material constant
- C_1, C_2 The material constant
- $\lambda_i (i = 1, 2, 3)$ The principal stretches
- μ The shear modulus
- κ The bulk modulus
- μ_0 The initial shear modulus
- κ_0 The initial bulk modulus
- B The left Cauchy-Green deformation tensor, $B = FF^T$
- b_1, b_2, b_3 The principle values of B
- J^{el} The elastic volume ratio

2.5 Viscoelastic properties for rubber and plastic material

- σ The tensile stress
- η The coefficient of viscosity
- $\dot{\varepsilon}$ The strain rate
- τ The time
- k The spring constant
- ε_{total} The total strain
- ε_D The strain of dashpot
- ε_s The strain of spring
- σ_D The stress of dashpot
- σ_s The stress of spring
- $G(t)$ The shear modulus in the function of time
- $\kappa(t)$ The bulk modulus in the function of time
- G_0 The initial shear modulus
- κ_0 The initial bulk modulus
- E_0 The initial Young's modulus
- $E(t)$ The Young's modulus in the function of time
- E_κ The Young's modulus of element number of κ
- s_1, s_2 The Maxwell spring one and spring two
- D The Maxwell dashpot
- m The Maxwell model
- ε_m The strain of Maxwell model
- σ_m The stress of Maxwell model
- ε_{tot} The total strain
- σ_{tot} The total stress

2.8 FE modelling and inverse properties prediction

- $[k]$ The stiffness matrix
- $\{U\}$ The vector of (unknown) nodal displacement or temperature

- $\{F\}$ The vector of applied nodal forces

2.9 Different inverse modelling approaches and their applications in material properties prediction

- W_R The works done
- W_t The total energy
- C_1 / C_2 The ratio of two different indenter angles

3.3.3 Validation of the FE with testing data and strain energy selection

- C_{01}, C_{10} The material constant
- β^i The temperature-dependent material parameters, which is related to the Poisson's ratio

3.4 Inverse FE modelling for material parameters prediction

- C The curvature value
- P The indentation bending force
- h The indentation bending depth
- a The diameter of chamber
- t The sample thickness
- E The Young's modulus
- $f(\nu)$ The Poisson's ratio of material constant
- μ The Ogden material parameter (mu)
- α The Ogden material parameter (Alpha)

3.7 Slope method and results

- \bar{x}, \bar{y} The sample mean of the known x's and known y's

3.8 Polynomial curve fitting approach and results

- $a_k (k = 0,1,2)$ The polynomial parameters

4.3 FE model and inverse parameter identification

- $G_R(t)$ The time dependent shear relaxation modulus

- $E(t)$ The time dependent Young's modulus
- g_{∞} The long term normalised shear modulus
- G_{∞} The long term shear modulus
- G_i The shear modulus at the observation i
- t The time in second
- τ_i The material constant (τ_i)

List of Figures

Chapter 2

Figure 2.1 Rubber and rubber-like materials and typical applications.....	13
Figure 2.2 Schematics showing the linear elastic (a) and nonlinear material behaviours (b-c).....	16
Figure 2.3 Schematics to show viscoelastic material behaviour in loading and unloading.....	17
Figure 2.4 Different types of viscoelastic material models.....	32
Figure 2.5 Deformation modes of various experimental tests for measuring material parameters.....	33
Figure 2.6 Different indentation/bending tests for characterising rubber-like materials and plastics.....	38
Figure 2.7 Large displacement indentation bending tests of a rubber sheet.....	40
Figure 2.8 Indentation test for elastic membranes with a complex shape.....	41
Figure 2.9 Characterisation of hyperelastic rubber-like materials by stretching in a bulge test.....	43
Figure 2.10 Indentation test of hydrogel with high cross-linked polymeric network.....	48
Figure 2.11 Inverse modelling approaches for characterising rubber materials based on indentation tests.....	51
Figure 2.12 Typical parametric studies based inverse FE modelling method for inverse material properties identification of rubber block based on a surface tension test.....	52
Figure 2.13 Structure of direct and inverse neural network modelling.....	53
Figure 2.14 A single ANN system used in predicting plastic properties based on conical indentation (a) and the surface equations representing the relationship between the P-h curve parameters and material properties (b).....	54
Figure 2.15 Post-modelling approach based on the Kalman Filter method.....	56

Chapter 3

Figure 3.1 Flow Chart showing the research work: the experimental tests, numerical modelling and inverse FE modelling.....	62
Figure 3.2 Samples of rubber sheets used in the indentation bending tests, Uniaxial tensile test and planar tests.....	65
Figure 3.3 Tensile test machine (a) and the setup of the Uniaxial tensile test (b) and planar tensile tests (c).....	66
Figure 3.4 Typical force and displacement data of the Uniaxial tensile test (a) and Planar tensile test (b).....	67
Figure 3.5 Stress-strain curves for uniaxial tensile test (a) and Planar tensile test (b) of the rubber sheet.....	68
Figure 3.6 Structure and setup of the indentation bending test system (a&b), the sample holder (c&d), smaller load cell and typical force-displacement curve (e&f).....	70
Figure 3.7 Typical experimental force-displacement data showing the repeatability of the test. (Chamber size, diameter=20mm, Sample thickness=0.8mm).....	71
Figure 3.8 Typical testing data with different loading rates. (Sample Thickness=0.8mm; Chamber size diameter=30mm).....	72
Figure 3.9 Force-displacement data of rubber sheet of different thicknesses.....	73
Figure 3.10 Flow chart showing the key procedure to build the ABAQUS model of the indentation bending test, which is used to produce the .RPY file.....	76
Figure 3.11 3D finite element model of the indentation bending tests (a) FE model; (b) Mesh of the model; (c) typical deformed shape (vertical displacement, U3); (d) a typical force displacement data.....	77
Figure 3.12 Mesh size sensitivity tests and results. (a-c): FE models with different mesh sizes for chamber diameter=30mm; (d) typical force and displacement data of FE models of different element size ($E=1.25\text{MPa}$, $\nu=0.495$).....	79
Figure 3.13 Comparison between experiment result and FE results with different material models based on the combination of tensile test and planar test data of the rubber sheet.....	81
Figure 3.14 Typical feature of the P-h curve that provides coefficients representing the force displacement data to be used in the inverse FE modelling program.....	86
Figure 3.15 Structure of the program to estimate the material parameters.....	91

Figure 3.16(a) Screen print of the add-on program.....	91
Figure 3.16(b) Large range of material parameters (μ :0.2-1, α : 1-4.5).....	92
Figure 3.17 Surface plot for Curvature vs. (μ , α) (Sheet thickness=0.3mm).....	94
Figure 3.18 The p - h curves used in the training data as the target; (b & c) predicted material parameters with two different chamber size based on the curvature approach. (Sheet thickness=0.3mm).....	98
Figure 3.19 Surface plot for slope vs. (μ , α) (t =0.3mm). (a) Chamber size =20, and (b) Chamber size =30mm.....	103
Figure 3.20 Typical materials sets predicted based on the surface plot equations of the slope and the use of data from two chamber sizes to predict the material parameters (Sheet thickness=0.3mm).....	104
Figure 3.21 Typical correlation coefficients when fitting the force-displacement data with 2 nd order polynomial trendlines.....	108
Figure 3.22 Surface plot for second order coefficient a vs. (μ , α) (t =0.8mm, chamber size =20 (a) and 30mm (b)).....	110
Figure 3.23 Typical material sets predicted based on the surface plot equations of the second order polynomial coefficient ' a ' and the use of data from two chamber sizes to predict the material parameters (Sheet thickness=0.3mm).....	111
Figure 3.24 Typical materials sets predicted based on the surface plot equations of the first order polynomial coefficient ' b ' and the use of data from two chamber sizes to predict the material parameters (Sheet thickness=0.3mm).....	112
Figure 3.25 Typical materials sets predicted based on the surface plot equations of the second order polynomial coefficient ' a ' and the use of data from two chamber sizes to predict the material parameters (Sheet thickness=0.8mm).	113
Figure 3.26 Typical materials sets predicted based on the surface plot equations of the first order polynomial coefficient ' b ' and the use of data from two chamber sizes to predict the material parameters (Sheet thickness=0.8mm).....	114
Figure 3.27 (a&b) Data to show the concept of combining the material sets based surface equation for the slope and interception method (a) and the material sets based surface equation for the second order and first order polynomial coefficients. (Chamber size=20mm, Sheet thickness=0.8mm).....	120
Figure 3.27 (c&d) Data to show the concept of combining the material sets based surface equation for the slope and interception method (a) and the material sets based	

surface equation for the second order and first order polynomial coefficients. (Chamber size=30mm, Sheet thickness=0.8mm).....	121
Figure 3.28 (a&b) Data to show the concept of combining the material sets based surface equation for the slope and interception method (a) and the material sets based surface equation for the second order and first order polynomial coefficients. (Sample diameter=20mm, Sheet thickness=0.3mm).....	122
Figure 3.28 (c&d) Data to show the concept of combining the material sets based surface equation for the slope and interception method (a) and the material sets based surface equation for the second order and first order polynomial coefficients. (Sample diameter=30mm).....	123
Figure 3.29 (a&b) Materials parameters prediction based on the experimental data with the combined curvature and slope approach for chamber size 20 (a) and chamber size 30 (b) (Sheet thickness=0.8mm, Target value: $\mu=0.35$, $\alpha=2.4$).....	125
Figure 3.29 (c&d) Materials parameters prediction based on the experimental data with the combined slope and intercept approach for chamber size 20 (a) and chamber size 30(b) (Sheet thickness=0.8mm, Target value: $\mu=0.35$, $\alpha=2.4$).....	126
Figure 3.29 (e&f) Materials parameters prediction based on the experimental data with the combined 2 nd and 1 st polynomial equation coefficients approach for chamber size 20 (a) and chamber size 30(b). (Sheet thickness=0.8mm, Target value: $\mu=0.35$, $\alpha=2.4$).....	127
Figure 3.30 A Bar chart comparing the predicted data from different approaches.....	128

Chapter 4

Figure 4.1 Flow chart showing the main work in developing an inverse modelling procedure to extract the relaxation coefficients from indentation bending tests.....	136
Figure 4.2 Latex liquid emulsion and specimen material.....	137
Figure 4.2 (c) Typical force-time data for relaxation tensile test of the latex rubber material.....	138
Figure 4.3 Force-time data with different loading rate.....	138

Figure 4.4 Typical force-time data of relaxation indentation bending test on samples of different thicknesses (R=4mm, Chamber size=30mm, and thickness=0.24, 0.34, 1.9mm).....	139
Figure 4.5 Typical normalised shear modulus-time for ABAQUS input parameters to fit the Prony series coefficients.....	141
Figure 4.6 Typical FE modelling result using the tensile relaxation as direct input to the FE model.....	143
Figure 4.7 Comparison between experiment result and FE results with different material model.....	144
Figure 4.8 Comparison between fitted standard test data versus the data based on predicted material parameters.....	144
Figure 4.9 Flow chart to show the inverse modelling approach to predict the visco-hyperelastic properties.....	145
Figure 4.10 Simulation space for Prony series properties.....	146
Figure 4.11 Numerical data used as a target in the training data to predict the visco-hyperelastic parameters.....	147
Figure 4.12 Surface plots of the Objective Functions for training data with known material properties.....	147
Figure 4.13 Typical objective function values for some property sets against target ($G=0.2$ and $\tau=250$).....	148
Figure 4.14 Surface plot of objective function against the experimental data.....	148
Figure 4.15 Typical objective function values of some material property sets against the experimental data. The results show that the inverse program method has produced a result close to the true material properties extracted from the standard tensile relaxation tests.....	149
Figure 4.16 Typical force-time curve based on predicted material parameters with low objective function values together with experimental curve.....	150
Figure 4.17 Flow chart to show the procedure of the python program to search for G and τ of the Prony series parameter.....	152
Figure 4.18 Sensitivity test of Prony series parameters.....	153
Figure 4.19(a) Comparison between the predicted G modulus based on the Objective function approach and the interactive searching approach and the target value (based on the standard tensile stress relaxation test).	155

Figure 4.19(b) Comparison between the predicted τ based on the Objective function approach and the interactive searching approach and the target value (based on the standard tensile stress relaxation test).....156

Figure 4.20 Comparison between experimental relaxation data and numerical force-time data using the predicted relaxation parameters in an indentation bending tests.....156

Chapter 5

Figure 5.1 Setup of a typical indentation bending tests (a) and FE model for finite contact (b) and point loading (c) of thin membranes. The rim of the circular membrane is fixed at all degree of freedom.....163

Figure 5.2 Comparison of experimental and numerical data with Elastic and hyperelastic model to validate the FE model.....165

Figure 5.3 Comparison between FE and analytical solution for point Loading Condition of circular membrane with negative and positive poisson's ratio.....166

Figure 5.4 Variation of curvature parameter (P/δ^3) with positive and negative Poisson's ratio for samples of different thicknesses under point loading.....167

Figure 5.5 Force displacement curves for Limit Contact Model. The solid and dash lines are data based on analytical solution for point loading (Eq. 5.1).....169

Figure 5.6 Curvature Parameter (P/δ^3) vs. depth for different indenter sizes (R1, 2, and 4mm, sample thickness=0.1mm).....170

Figure 5.7 Effect of auxeticity on the P/δ^3 for samples of different thickness.....171

Figure 5.8 Effect of auxeticity on the displacement (Vertical displacement, U_2) profile with different sample thickness.....172

Figure 5.9 Axial displacement (U_1) Profile with different sample thicknesses.....174

Figure 5.10 Effect of Poisson's Ratio on the contact stress showing the effect of auxeticity on the contact area.....175

CHAPTER ONE

INTRODUCTION

1.0 Introduction

1.1 Indentation bending tests of thin membranes and materials parameters identification

Many engineering and medical conditions involve deformation/deflection of thin shells/membranes with a clamped boundary, such as pressure sensors, valves and actuators. (Ju B.F. et al, 2005; Egan P. et al, 2007; Scott O.N. et al, 2004; Selvadurai A.P.S., 2006; Ahearne M. et al, 2010). Many biological structures are also thin walled and filled with different fluidic medium (air/water), for example cells, blood vessel, bladder and rectum, etc. (Humphrey, 2002). The mechanical properties of thin elastic membranes and structures are of wide interest to improve the performance of these materials/structures, as well as the functions of biological tissue, including the filling process of the human or animal bladders. The material deformation in these cases covers a wide spectrum of strain levels from small deformation to large displacement with samples of different thicknesses. A convenient way to test the material behaviour is by using indentation bending tests in which an indenter/sphere is pressed onto a thin sample fixed along its rim of either a regular (round, square) or arbitrary shape (Ju B.F. et al, 2005; Ahearne M. et al, 2010). The resulting force displacement curve (P - h curves) is dependent on the properties of the material, the structure and dimensions of the sample. A detailed understanding of the deformation mechanism of different materials/structures under such a loading condition is of great significance to materials testing and product development.

In a continuous indentation bending test, an indenter is pressed onto the sample surface and the resistance of the material is represented by the force displacement/deflection data. (Begleya M. R. et al, 2004; Scott O. N. et al, 2004; Ju B. F. et al, 2005; Ahearne M. et al, 2010; Cao Y. P. et al, 2009). A range of testing methods with different facilities have been developed and used to characterise different materials (Diridollou S. et al, 1997; Selvadurai A.P.S., 2006; Sasso M. et al, 2008; Aernouts J. et al, 2010; Hosseini M. et al, 2013; Koumi E.K. et al, 2014; Budday S. et al, 2015). Due to its intrinsic experimental simplicity in terms of facilities and sample requirements, and effort has been made to explore its use to

directly/reversely probe the properties of materials and investigate the mechanical behaviour of thin shell/membrane materials rather than using standard testing methods (such as tensile, planar), which require the use of large samples in order to produce stress-strain data with well-defined deformation fields. In some case, such as biological materials such as bladder, standard samples are not readily available or extremely costly due to limited availability, etc. Apart from using the method to determine material properties, it is also of significant importance to further study the mechanics of materials with abnormal properties.

In comparison with other testing methods, such as indentation test which sample is supported from the base, and the sample for indentation bending tests is fixed from the edge. The testing or material property prediction could be affected by many factors including the selection of material models and strain energy functions as well as the testing conditions. The effect of the sample size and the indenter size is also not well defined, which may vary with the materials and strain levels. This makes it much more difficult to establish a robust inverse program and data analysis procedure. For an inverse program, the accuracy, robustness and the uniqueness is very important. For situations where a unique results is not attainable, effort has to be made to define a procedure (such as a larger data set) in order to determine a set of material data which is sufficiently accurate. In such a case, a wide range of material parameters set will be required for the inverse modelling program to search the optimum material parameters set. This requires expensive modelling works to build a large simulation space. Analysis of the data and editing the material parameters manually is very time-consuming and ineffective. Inverse modelling programs with automatic/semi-automatic program have to be used to improve the accuracy and decrease the time of data mining. In ABAQUS, some users interactively modify or read data by linking the program with FORTRAN and C++ to run user-subroutine codes such as VUMAT and UMAT ([Lee W. B. and Chen Y. P., 2010](#); [Toda N. et al, 2010](#); [Mishnaevsky L. et al, 2014](#)). These developments offer an opportunity to develop a data processing program combining FE modelling, parametric studies, data process and analysis to reduce the complexity of the inverse program, This is very important for application oriented development of inverse modelling. Python is more user friendly and flexible program, which is increasingly being used within or linked to ABAQUS. When dealing with complex materials models, it is essential to develop

a modern Python programming language to be used as a tool for running multiple parametric models over a wide range of material parameters in a smart and quicker method to characterise the material properties, rather than relying on manually changing the parameters. This is applicable to both hyperelastic parameters and the time dependent viscoelastic properties. The work will cover developing models, automatic fitting curve parameters, automatically compare results and determine the parameters of different materials models.

Another area which requires further study is the mechanics of indentation bending tests for some new materials (such as negative Poisson's ratio materials). Smart materials are increasingly being used in area involves thin shells/membranes. A detailed understanding of the deformation mechanism of different materials/structures under such a loading condition is of great significance to materials developments. Most of the work has been focused on material stiffness (represented by the Young's modulus) with a fixed Poisson's ratio. With the rapid development in materials with different Poisson's ratios, including material with negative Poisson's ratios at different length scales ([Evans K.E. and Alderson A., 2000](#); [Pozniak A.A. and Wojciechowski K.W., 2014](#); [Sanami M. et al, 2014](#); [Sun G.Y. et al, 2014](#); [Alderson K. et al, 2014](#); [Ge Z. and Hu H., 2015](#); [Lim T.C., 2015](#); [Shufrin I. et al, 2015](#)), it is important to investigate the potential effects of Poisson's ratio and auxeticity on the force-displacement data, the material deformation modes and its interaction with the indenter. Due to the nature of loading and sample configuration, the effect of Poisson's ratio for a sample with clamped edge conditions is complicated, being affected by material properties as well as the experimental conditions (such as sample thickness and indenter size, etc.). Within the loading strain domain, the deformation mode may change with depth. In the bending/plate domain, the load is known to be not affected by the auxeticity of the materials ([Timoshenko S. et al, 1951](#)). But in the membrane or transition between plate and membrane behaviour, positive or negative Poisson's ratio theoretically would potentially have different effects under localised loading conditions ([Timoshenko S. and Woinowski-Krieger S., 1987](#); [Komaragiri U. et al, 2005](#)). It is essential to investigate the effect of Poisson's ratio on the material behaviour in both point loading and finite contact conditions (such in the case of a spherical indenter). Under these conditions which are different from the loading conditions of standard tests

(e.g. tensile tests), the effect of material properties on the material behaviour is directly influenced by the dimensions of the experimental samples as well as the loading conditions. A detailed understanding of these factors will help to establish the effects of the Poisson's ratio with a focus on the influence of auxeticity, which will help to further develop material testing methods and extend the use of auxetic materials in many relevant industrial fields.

1.2 Aims and objectives

The work aimed to develop python based program/framework for a combined experimental and numerical method to inversely predict the material properties of thin membranes for both hyperelastic material and viscoelastic material.

The main objectives are:

- To develop and validate an FE model simulating indentation bending tests of thin rubber sheets
- To develop a python based FE program with fully parametrised material properties and dimensional parameters.
- To evaluate the feasibility of representing the force-displacement data using different curve parameters in order to simplify the curve fitting and searching process.
- To develop an inverse FE program for hyperelastic parameters prediction and validate the results with training set and testing data of thin rubber sheet.
- To develop programs to inversely calculate the viscoelastic properties for different viscoelastic material.
- To investigate the effect of Poisson's ratio on the deformation of thin membrane under finite contact condition.

1.3 Outline of the thesis

In chapter two, background information and current research on testing thin rubber sheets such as indentation bending tests and inverse modelling and their applications in characterisation of material properties have been reviewed. The basic theories of linear and nonlinear mechanics and strain energy functions are reviewed with the key controlling materials discussed. The viscoelastic behaviour of rubber and polymer are reviewed, different creep material behaviour model are discussed in details.

The main results on the indentation bending and material properties characterisation is presented in Chapter 3. An inverse FE modelling program based on the indentation bending tests has been developed and applied to characterise the nonlinear elastic material properties of thin sheet. Three different approaches have been evaluated to present the force-displacement curve using different curve parameters, which effectively simplify the data set. The methodology has been studied in terms of accuracy, convergence and robustness of the predicted results, which are important for materials characterisation. The method is evaluated using training data with known material properties first then, used to predict the material properties of natural latex rubber made in the laboratory. Several approaches have been evaluated to improve the robustness by combining data at different indentation depths or sample sizes.

The work on the FE modelling of the relaxation indentation bending test is presented in Chapter 4. In this work, the inverse FE program is developed to simulate the relaxation tests of latex rubber sheet. A set of relaxation tests based on the indentation bending test has been conducted. Latex rubber with different thicknesses were produced and tested. The viscoelastic properties of the latex rubber are inversely estimated by combined experimental data and FE modelling program. The accuracy of the predicted viscoelastic parameters is assessed by comparing the testing results with standard relaxation tensile tests.

In Chapter 5, the effects of Poisson's ratio on the material behaviour are investigated including the force-displacement data, material movement and the contact conditions.

Overall conclusions are given in Chapter 6. Future works are highlighted based the work reported.

CHAPTER TWO

LITERATURE REVIEW

2.0 Background and literature review

2.1 Introduction

In this chapter, the main properties of rubber materials and their applications in different industrial fields has been reviewed. Different types of mechanical tests, in particular those suitable for thin samples are given in details. Main hyperelastic strain energy functions widely used for rubber like materials are presented and the advantages and disadvantages of each model is discussed. Different testing methods for thin membranes are reviewed including different testing setups. The theoretical framework and current research on inverse FE modelling method and optimisation programs have been critically reviewed and potential improvements are discussed. The difficulties and challenges for inverse FE modelling approach based the indentation bending tests to predict the hyper-elastic, elastic-plastic, and viscoelastic properties are reviewed and discussed.

2.2 Rubber-like materials and thin membranes

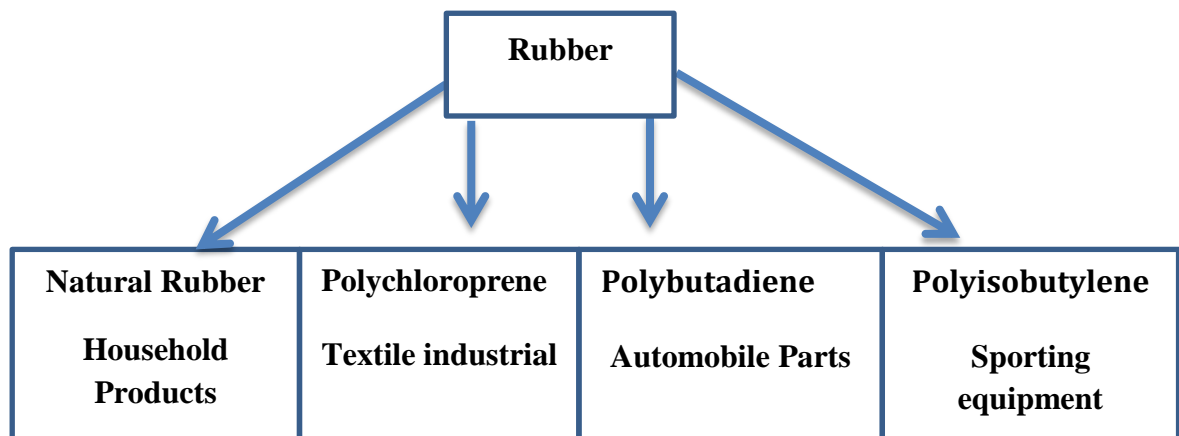
Rubber and rubber-like materials are used in a wide range of industries such as automotive industries (vehicle tires, oil seal ring, and vibration absorber), engineering field (conveyor belt, bearing, adhesives, etc.) and marine industries (fume scrubbers, cooling pipe work and fender) (*Mazurkiewicz D., 2009; Samad M.S.A. et al, 2011; Zanchet A. et al, 2012*). Rubbers are also widely used in medical fields such as diagnosis and treatment equipments, tubes, gloves as well as biological organs or morphogenesis (*Thein-Han et al, 2009*). Figure 2.1(a) list different types of rubbers and their applications (*Peyraut F. et al, 2009; Bechir et al, 2010; Huang H. et al, 2013*). Natural rubber normally can be found in household applications such as gloves, rubber-bands, flooring mats, hot water bags, etc. Natural rubber is a high molecular weight polymeric substance. Isoprene is a diene and 1, 4 addition leaves a double bond in each of the isoprene unit in the polymer (*Charles J. & Gunasekaran S., 2015*). Raw natural rubber has low tensile strength and abrasion resistant, however vulcanised natural rubber can improve its properties and modify the properties of the natural rubber. Typical example is radiation or hot vulcanisation process, in which heat, sulphur, zinc oxide and accelerator are combined to modify the rubber structure and properties (*Chaudhari C.V. et al, 2005, Jaunich M. & Stark W., 2009*).

The type of rubber widely used in the textile industries is polychloroprene or known as poly 2 chlorobutadiene for making household product (e.g. carpet, rugs, and bedding) as it has good chemical resistance and flexibility over a wide temperature range. This polymer is prepared by free radical emulsion polymerisation. The chloroprene in the form of liquid emulsion is converted into homopolymers or copolymers with the aid of radical initiators. The polymerisation is stopped by agent and polymer is frozen by refrigeration and drawn as a thin rubber sheet (*Gac P.Y.L. et al, 2014*). In term of mechanical properties, the chloroprene rubbers are homopolymers of chloroprene and the polymer chains have an almost entirely *trans*-1-4-configuration. Because of this high degree of stereoregularity they are able to crystallise during stretching and elongation at break is between 250 to 500% (*Ismail H. & Leong H.C., 2001, Ha-Anh T. & Vu-Khanh T., 2005*).

Another type of rubber is polybutadiene, this type of rubber is a synthetic rubber with a high resistance to wear. Polybutadiene forms by linking many 1,3-butadiene monomers to make a longer polymer chain molecule. The catalysts used to form a polybutadiene are neodymium, cobalt, nickel, titanium and lithium. Different catalyst can influence the material properties, for example, using cobalt resulting in a low viscosity material that is easy to use but low in mechanical strength and with neodymium can form an end-to-end (higher *cis*) linear structure and increase the mechanical strength ([Oehme A. et al, 1993](#), [Kwag G. H. et al, 2005](#), [Li H. et al, 2011](#), [Srivastava V. K. et al, 2011](#)). One of its typical applications is in manufacture of tyres.

Polyisobutylene consists of 98.5% of isobutylene and 1.5% of isoprene. Polymerisation of isoprene results in the incorporation of an alkene into the polymer chain. The sulphur added vulcanised and formed a network structure in the form of crosslinked rubber. The material has high chemical stability, biocompatibility and low permeability to gases and solvent, these made them suitable being used in the manufacture of adhesives, sporting equipment, protection masks and in chewing gum. ([Pinchuk L. et al, 2008](#), [Roh J. H. et al, 2015](#), [Trant J. F. et al, 2015](#))

Some specific examples of rubber products are shown in Figure 2.1(b-e) including tyre, seal, sensor and bearing. Oil seal and water seal (Figure 2.1(b)) is used in industrial field to prevent leaking from the joint pipe ([Chandrasekaran, 2010](#)). Damping facilities such as vibration suspension and shock absorber of automobile normally use viscoelastic rubber seal, as shown in Figure 2.1(c), for achieving the damping effect. Due to their wide range of applications, it is important to develop proper experimental techniques to characterise the material properties of rubbers and rubber-like materials.



(a) Different types of rubber and typical areas of applications.

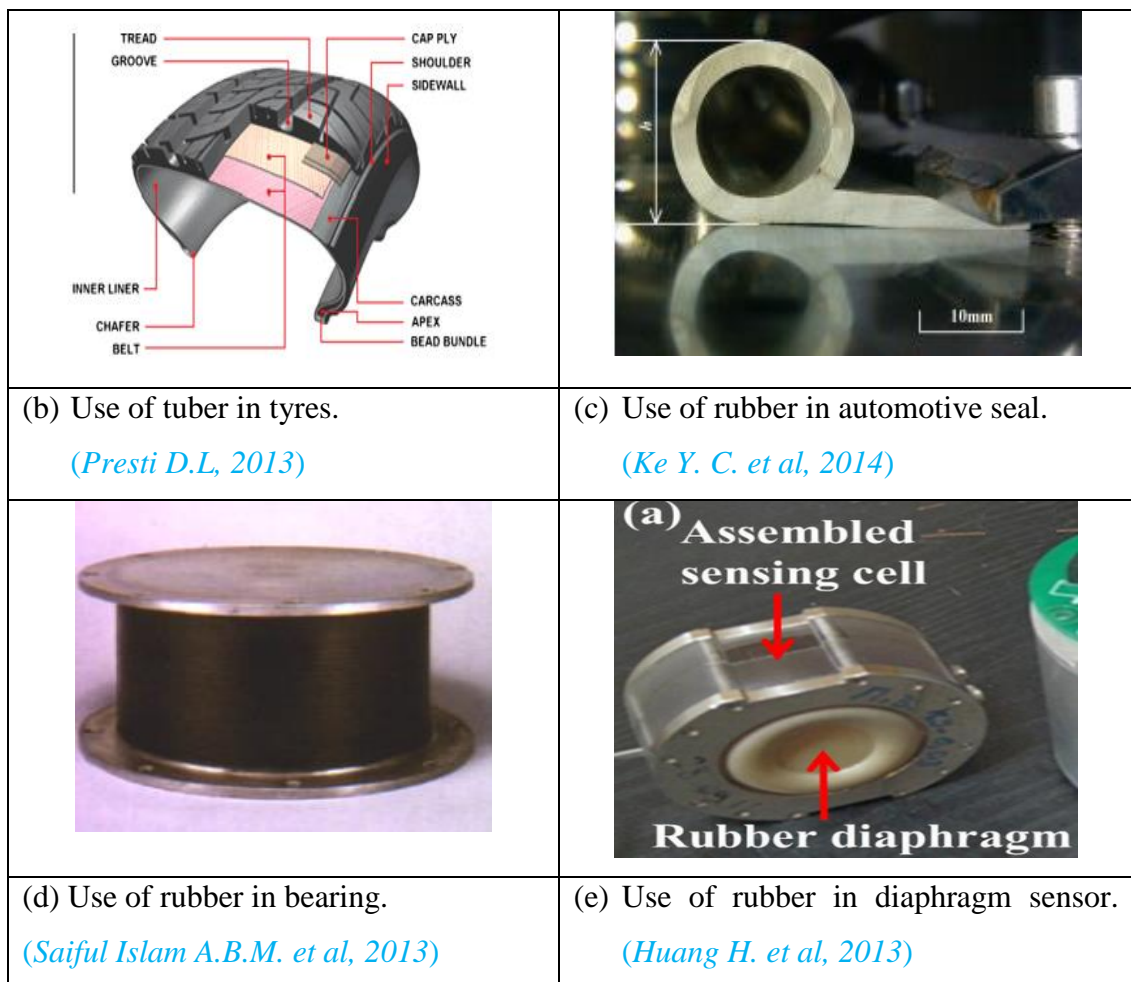


Figure 2.1 Rubber and rubber-like materials and typical applications.

Rubber components are normally used in different form/geometries or under various strain range in different applications. For example, for tyre and bearing, the rubber materials are in a form of bulk material. While the material for seals/gaskets is in the form of thin sheet, the thinner the seal is the better the performance. Diaphragms are used to detect the change of pressure, so thin membranes are used to meet the requirement on functionality. Thin rubber like membranes are also widely used in applications such as surgical gloves, pressure valves, actuators and etc. (*Nguyen et al, 2004; Daisley et al, 2006; Kabwe A.M. et al, 2010; Taniguchi H., 2013*). Thin rubber like material are increasingly being used for artificial tissues such as blood vessels, fibrous interface membrane, bladder, rectum and etc. (*Haslach and Humphrey, 2004; Chan and Crosby, 2006; Kraaij G. et al, 2014; Lee A.Y. et al, 2014*). These types of sample are more difficult to test and characterise than rubbers in a bulk form. The choice of testing always depends on the materials concerned, the boundary condition in service, the strain level and the main functional requirements. In addition, for different condition, the same material may need to be represented by different types of material models when simulating the material deformation.

2.3 The properties of rubber like material and plastics material

Figure 2.2(a-c) shows schematically the three main types of stress strain relationships in materials. Figure 2.2(a) illustrate a simple case of linear elastic behaviour, in which stress is proportional to strain and the strain is recoverable if the stress is removed, i.e. the specimen returns to its original dimensions.

A linear elastic relationship between compressive or tensile stress and strain can be described by:

$$\sigma_x = E\varepsilon_x \quad (2.1)$$

Where the constant E is the Young's modulus.

The absolute value of the ratio between the lateral strains to the longitudinal strain is the Poisson's ratio:

$$\nu = -\frac{\varepsilon_y}{\varepsilon_x} \quad (2.2)$$

The Poisson's ratio for rubber is close to 0.5 as the material is incompressible. For an isotropic material, the shear modulus G can be calculated using:

$$G = 2E(1 + \nu) \quad (2.3)$$

As a comparison, Figure 2.2(b) shows a typical elastic-plastic behavior, this material behavior is commonly found in plastics and metals. For elastic-plastic behaviour, the strain can be divided into two parts: elastic part and plastic part. Elastic part is linear and revisable, normally these two stages is separated by yielding point which is the point that material starts to undergo plastic deformation which is an irreversible process. The total strain is the sum of the elastic and plastic strain:

$$\varepsilon = \varepsilon^E + \varepsilon^P \quad (2.4)$$

When unloading in the plastic region, the behaviour is again elastic. After complete unloading, the remaining strain is the plastic strain ε^P .

As shown in Figure 2.2(c), a non-linear relationship or so called hyperelastic material is usually found in rubber-like material. Rubber-like materials are elastic in the

classical sense. During unloading, the stress-strain curve is revisable and no permanent deformation. Rubber-like materials are initially isotropic elastic body, and usually defined in terms of invariants of stretch ratios. There are some phenomena of hyperelastic material model such as material is isotropic and non-linear, exhibit instantaneous elastic response up to large strains (*Malvern L. E., 1969, Johannknecht R. & Jerrams S. J., 1999, Shabana A. A., 2012*). The non-linear relationships between stress and strain are usually convex upwards. When materials are under cyclic loading, it will exhibit a typical viscoelastic material behaviour as shown in Figure 2.3. This type of deformation is the mechanical characteristic of viscous flow and elastic deformation (*Love A. E. H., 1944, Timoshenko S. & Goodier J. N., 1951, Slaughter W. S., 2002, Mills et al, 2003*).

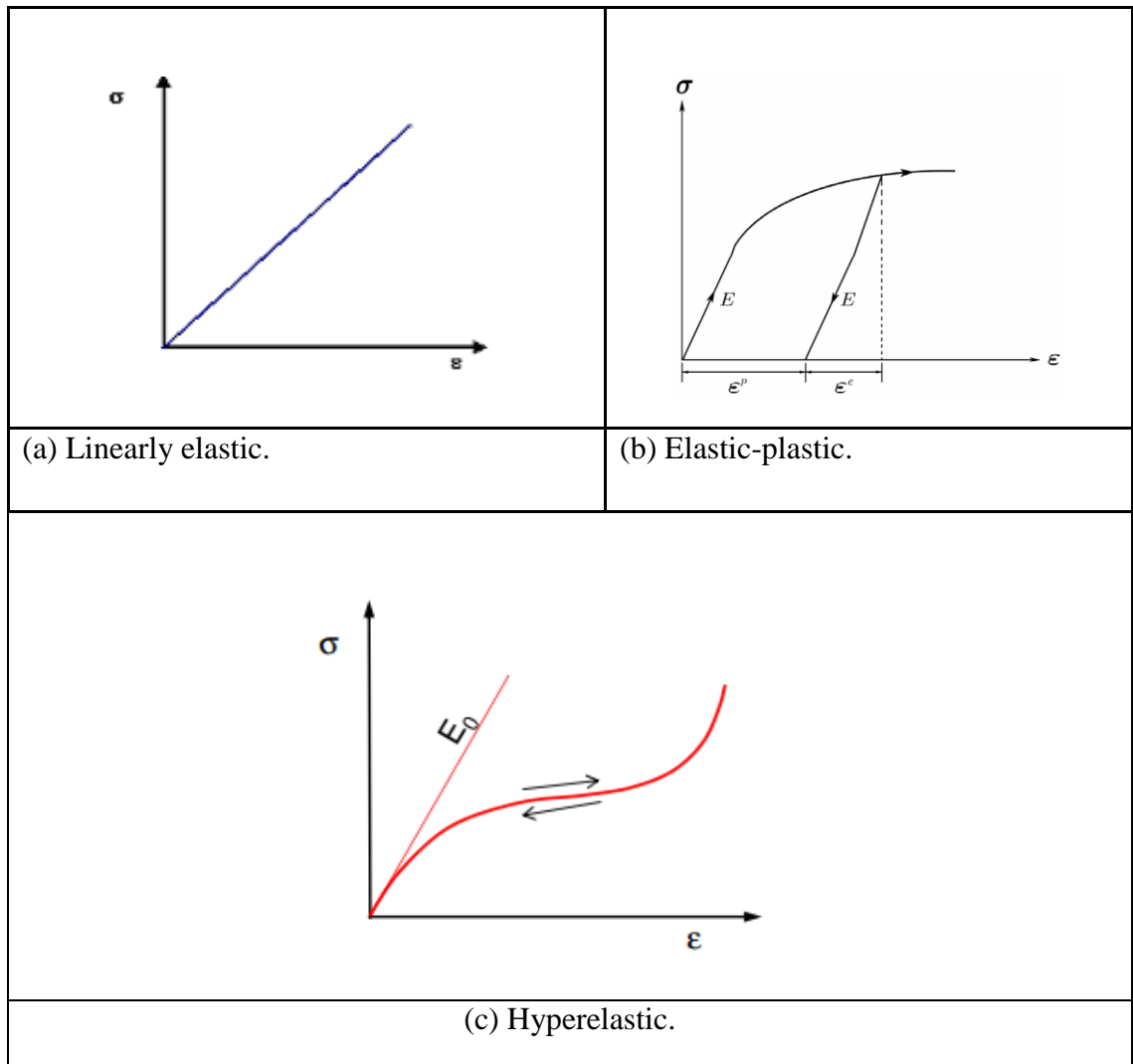


Figure 2.2 Schematics showing the linear elastic (a) and nonlinear material behaviours (b-c).

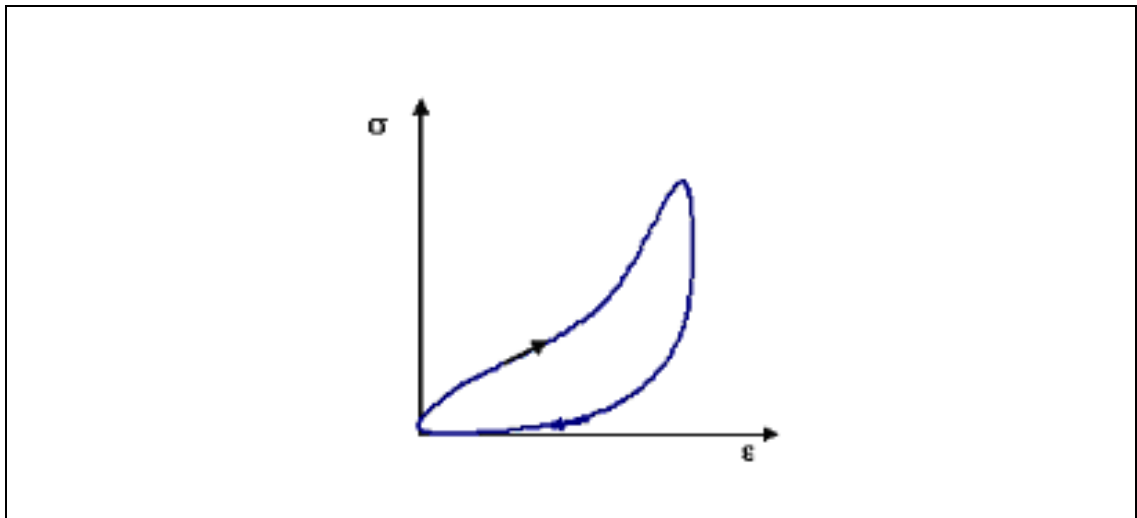


Figure 2.3 Schematics to show viscoelastic material behaviour in loading and unloading.

2.4 Strain energy functions for rubber, foams and biological materials

For a linear elastic material, its behaviour can be simply represented by the Young's modulus and Poisson's ratio. For an elastic-plastic material, the material's behaviour could normally be represented by the yield stress and working hardening coefficients. For hyperelastic materials, their behaviour is more complicated, which can only be described by complex strain energy functions, this make the testing and modelling of this group of materials much more difficult.

Strain energy refers to the potential energy stored in an object by virtue of deformation ([Ogden et al, 2004](#)). For a perfectly elastic material the strain energy is equal to the work that must be done to produce both normal and shear strains. The strain energy is recovered when the stress causing the strain is removed. Total recovery is achieved for perfectly elastic material and the recovery is partial for plastic material due to energy dissipation. **The strain energy function, W** , is a function which relates the strain of a material to the energy developed by this deformation. **Strain energy density (U):** Strain Energy Density (SED) is strain energy measured per unit volume of the body. SED is a better indication of the material since it is normalized to the size of the body. The strain energy function can be regarded as a generalisation of Hooke's law that enables the description of complex elastic components in a systematic way ([Afshar and Berto, 2011](#); [Boulenouar A. et al, 2013](#)).

Many materials can undergo a very large deformation (known as hyperelastic behaviour) including foams, rubber and many biological tissues ([Aernouts et al, 2012](#); [Ahearne et al, 2010](#)). For an elastic material, the stress at any point can be defined solely as a function of the deformation gradient \mathbf{F} at that point. A change in stress arises only in response to a change in configuration irrespective of the manner in which the change in configuration arises in space and time. For a hyperelastic material, in addition to the above definition, an additional scalar function also exists from which the stress can be derived at each point. The scalar function is the stored energy or strain energy function, W , which can also be defined in terms of the deformation gradient. ([Weiss and Gardiner, 2001](#)).

$$W = \tilde{W}(F) \quad (2.5)$$

The strain energy, W , must obey the principle of material frame indifference. With this principle, rigid body motions will not change the value of the strain energy function. Consequently, W may be expressed in the form of:

$$W = \tilde{W}(C) \quad (2.6)$$

Where C is the right Cauchy-Green strain tensor. Then, the second Piola-Kirchhoff stress is derived directly from the strain energy as:

$$S = 2 \frac{\partial W}{\partial C} \quad (2.7)$$

Hyperelasticity provides a convenient framework for the formulation of constitutive equations for materials such as rubber, foams or biological soft tissues as it allows for large deformations and anisotropy ([Weiss and Gardiner, 2001](#)).

A hyperelastic material might be represented by a strain energy function. For Hookean (linear) elastic materials, this takes the following form:

$$W = W(I_1, I_2, I_3) \quad (2.8)$$

For an isotropic material W can depend on C through only the three principle invariants of C :

$$\text{Where} \quad I_1 = \text{tr}C; \quad I_2 = \frac{1}{2}[(\text{tr}C)^2 - \text{tr}C^2]; \quad I_3 = \det C$$

and “tr” denotes the trace of the tensor. The isotropic hyperelastic material reduces to linearised elasticity when appropriate assumptions regarding the magnitude of strains and rotations are made ([Ericksen and Rivlin, 1948](#); [Weiss and Gardiner, 2001](#); [Monteiro E. et al, 2011](#); [Dias V. et al, 2014](#)).

Finite Element analysis for nonlinear elasticity, the solution process often proceeds by searching for a configuration that is close to a known equilibrium state that provides a balance between incrementally applied loads and the current stress field in the material. In this case, the elasticity tensor plays an important role in the iterative

solution process (*Brunig, 1998; Weiss and Gardiner, 2001; Arciniega and Reddy, 2007*). Nonlinear problems are solved iteratively using the Newton-Raphson method (*ABAQUS Theory Manual 6.11*). The Newton-Raphson method is a powerful technique for solving equations numerically. It is based on the simple idea of linear approximation. The Newton-Raphson method is widely used in root-finding procedures with combination of simplicity and power. The Newton-Raphson method has the form for the solution of the nonlinear equation where given $f(x) = 0$, and the first estimation of $x_1 = x_0 - \frac{f(x_0)}{f'(x_0)}$ and x_2 is obtained from x_1 . By continue this way, if x_n is the current estimate, then the next estimate is given by:

$$x_{p+1} = x_p - \frac{f(x_p)}{f'(x_p)} \quad (P=0, 1, 2, \dots)$$

A nonlinear problem will require many times the computer resource compare with linear problem (*Israel A. B., 1966, Traub J. F. & Wuzniakowski H., 1979, Galantai A., 2000*).

Many strain energy function models have been developed to characterise different material systems which undergo large deformation, typically Mooney-Rivlin model, neo-Hookean form, Ogden model and Yeoh (*Ogden, 1972; Petre M. T. et al, 2007; Renaud C. et al, 2009*). They are generally used to describe incompressible materials (such as rubber and liquid filled structures). Some models have been extended to compressible materials such as hyperfoam models (*Verdejo R. and Mills N.J., 2004; Fontanella C.G. et al, 2013*). These material models have been employed in a range of computational software including ABAQUS, which are briefly described:

Neo-Hookean model

A Neo-Hookean model is similar to the Hooke's law, which can be used for predicting the nonlinear stress-strain behavior of material under large range of deformation. The model was developed by Ronald Rivlin in 1948 (*Ericksen J. L. & Rivlin R. S., 1948; Martins et al, 2007*). This model is based on the statistical thermodynamic of cross-linked polymer chains and is usable for rubber-like and

plastic materials. The initial stage of cross-linked polymer acts in a Neo-Hookean manner which moves relative to each other when stress applied.

The form of the Neo-Hookean strain energy potential follows the format given below:

$$W = C_1(I_1 - 3) \quad (2.9)$$

where C_1 is a material constant, and I_1 is the first invariant of the left Cauchy-Green deformation tensor as defined in equation 2.10.

For a compressible Neo-Hookean material the strain energy density function is given by

$$W = C_1(I_1 - 3) + D_1(J - 1)^2; J = \det(F) = \lambda_1\lambda_2\lambda_3 \quad (2.10)$$

Where D_1 is a material constant, $\bar{I}_1 = J^{-2/3}I_1$ is the first invariant of the deviatoric part of the left Cauchy-Green deformation tensor, and F is the deformation gradient. There are several alternative formulations for compressible Neo-Hookean materials, for example.

$$W = C_1(\bar{I}_1 - 3 - 2\ln J) + D_1(J - 1)^2 \quad (2.11)$$

To be consistent with linear elasticity,

$$C_1 = \frac{\mu}{2}; D_1 = \frac{\kappa}{2} \quad (2.12)$$

where μ is the shear modulus and κ is the bulk modulus.

From the analysis given above, the Neo-Hooke's law is an extension of Hooke's law for the large deformations material such as plastic and rubber-like substance. However, Neo-Hookean material model is only accurate and sufficient for material over a strain range up to 30-70%. ([Zhu Y.F., 2010](#)).

Mooney-Rivlin model

Several assumptions had been made when developing the original Mooney model as the strain energy function for rubber starting from: (1) The material is homogeneous and free from hysteresis; (2). The material is isotropic initially and throughout the deformation; (3) The deformations occur without change in volume; (4) The traction in simple shear in any isotropic plane is proportional to the shear ([Mooney, 1940](#)).

Mooney initially proposed the linear form of strain energy functions as:

$$W = C_1(I_1 - 3) + C_2(I_2 - 3) \quad (2.13)$$

where C_1 and C_2 are constants and I_1 and I_2 are the first and the second invariant of the unimodular component of the left Cauchy–Green deformation tensor:

$$\bar{I}_1 = J^{-2/3} I_1; I_1 = \lambda_1^2 + \lambda_2^2 + \lambda_3^2; J = \det(F) \quad (2.14)$$

$$\bar{I}_2 = J^{-4/3} I_2; I_2 = \lambda_1^2 \lambda_2^2 + \lambda_2^2 \lambda_3^2 + \lambda_3^2 \lambda_1^2 \quad (2.15)$$

For an incompressible material such as rubber, $J = 1$.

This general form based on a linear relationship between stress and strain in simple shear was referred to as the Mooney-Rivlin model, this equation gives a marginally better fit to some of the experimental data of rubber than pure elastic models with suitable choices of C_1 and C_2 (Mooney, 1940; Ali A. et al, 2010; Crocker L.E. et al, 2011). The Mooney-Rivlin material was originally developed for rubber, but is today often applied to describe general incompressible biological tissue. For modelling rubbery and biological materials at even higher strains, the more sophisticated **Ogden material model** has been used. (Breslavsky I.D. et al, 2014; Kraaij G. et al, 2014).

Ogden form models

This model was developed by Ray W. Ogden in 1972 (Ogden, 1972). It is used to describe the non-linear stress-strain behaviors of complex materials such as rubbers, polymers and biological tissue. Similar to the other hyperelastic material models, the Ogden model was based on an assumption that the material behavior can be described by strain energy density function, which is isotropic, incompressible and strain rate independent.

For small strains the shear modulus and bulk modulus for the Ogden form are given by

$$\mu_0 = \sum_{i=1}^N \mu_i, K_0 = K_1 \quad (2.16)$$

According to the Ogden model (Ogden, 1972a), U is a function of the principal values b_1, b_2, b_3 of \mathbf{B} .

$$U = \sum_n (\mu_n / \alpha_n) (b_1^{\alpha_n} + b_2^{\alpha_n} + b_3^{\alpha_n} - 3) \quad (2.17)$$

Where μ_n is constant, and α_n is not necessarily integer and may be positive or negative. \mathbf{B} is left Cauchy-Green strain tensor,

$$\mathbf{B} = \mathbf{F}\mathbf{F}^T \quad (2.18)$$

and b_1, b_2, b_3 are principle values of \mathbf{B} .

Equation 2.19 shows the general form of the Ogden strain energy potential

$$U = \sum_{i=1}^N \frac{2\mu_i}{\alpha_i^2} (\bar{\lambda}_1^{\alpha_i} + \bar{\lambda}_2^{\alpha_i} + \bar{\lambda}_3^{\alpha_i} - 3) + \sum_{i=1}^N \frac{1}{D_i} (J^{el} - 1)^{2i} \quad (2.19)$$

where $\bar{\lambda}_i$ are the deviatoric principal stretches; λ_i are the principal stretches; μ_i and α_i is a material parameter; and D_i are temperature-dependent material parameters ([ABAQUS Theory Manual 6.11](#)). Ogden model is widely used for rubber components such as seal and O-ring where the model is sufficient to represent test data up to 700% of the tensile test result. In addition, the Ogden model is much more flexible in describing the experiment data than Mooney-Rivlin model. ([Yeoh O.H., 1993](#); [Kim B.K. et al, 2012](#))

Yeoh Model

The **Yeoh** hyperelastic material model is also called the third-order reduced polynomial form, which is suitable for describing isotropic almost incompressible rubber-like materials ([Renaud C. et al, 2011](#)). This model is based on Ronald Rivlin's observation that the elastic properties of rubber may be described using a strain energy density function which is a power series in the strain invariants $I_1 I_2 I_3$. The Yeoh model for incompressible rubber is a function only of I_1 and the strain energy potential is given by

$$W(I_1) = \sum_{i=1}^3 C_{10} (I_1 - 3)^i$$

For compressible rubbers, $I_3 = J^2$, so the dependence is included and used for compressible materials. The strain energy density function for this model is written as

$$W = \sum_{i=1}^n C_{i0} (\bar{I}_1 - 3)^i + \sum_{k=1}^n C_{k1} (J - 1)^{2k} \quad (2.20)$$

Where $I_3 = J^{-2/3} I_1$, and C_{i0}, C_k are material constants. The quantity C_{10} is half of the initial shear modulus, while C_{11} is half of the initial bulk modulus. The compressible Yeoh model could be reduced to the Neo-Hookean model for compressible materials when $n=1$. ([Renaud C. et al, 2009](#)).

All these strain energy functions have found applications for different situation where the model is most suitable. Due to the fact these models are developed based on mathematical formation, sometimes it is difficult to derive values for the key parameters. As briefly illustrated in the equations, in several cases, a combination of parameters is linked to the initial shear modulus. This directly influences the accuracy, robustness and uniqueness of materials parameter estimation and choice of material models in different situations.

2.5 Viscoelastic properties for rubber and plastic materials

Viscoelasticity is a time dependent mechanical behaviour where the material response is dependent on the current state of deformation and deformation history ([Zhang H.H. and Li L.X., 2009](#)). Typical viscoelastic materials include rubbers, fibers, human muscle tissues and plastics ([Tobolsky A.V. and Andrews R.D., 1944](#)). The viscoelastic behaviour can be observed/measured by following tests: Creep test under constant load and stress relaxation test under constant deformation. When a constant strain is applied to a rubber sample, the stress necessary to keep the strain would be decreased over time. This means that the material resistance against the deformation is decreasing gradually. This behaviour is named “stress relaxation”. On the other hand, when an elastomeric specimen is subjected to a constant stress, the strain gradually increase leading to a phenomenon known as “creep”. Chemical processes within the material could lead to relaxation as well as creep in higher temperature. An increase in temperature results in thermal expansion among polymer molecule, then expansion result in an increase in the average distance between sequential segments in a strand and between network chains. The increase of the distance may cause the intermolecular and intramolecular force decrease and reduction of elastic moduli. This mean the rubber material will creep more at higher temperatures, so temperature is known to strongly influence the creep properties of rubber material. Chemical processes occur which may result in either main chain scission or cross-link scission. There are several factors which could lead to chemical process such as thermal effects, chemical properties, oxygen and ozone attack and light aging effect. ([Drozdov A.D. et al, 1999](#), [South J. T., 2001](#); [Hamaguchi H. et al, 2009](#); [Woo C. S. and Park H. S., 2011](#); [Cui T et al, 2013](#); [Le Gac P. Y. et al, 2015](#)). However, at room temperature this effect can be neglected and the most dominant sort of relaxation comes from physical processes. ([Brown R.P. and Bennett, F.N.B., 1981](#); [Mottahedi M. et al, 2010](#)).

Viscoelastic is a combination of elastic and visco behaviour. The elastic behaviour can be simply represented by the Hook’s law with Young’s Modulus. The visco material behaviour in elastomer “The entropic uncoiling process” is fluid-like in nature, and can be modelled by a “Newtonian dashpot”, in which the stress produces not a strain but a strain rate:

$$\sigma = \eta \dot{\varepsilon} \quad (2.21)$$

The overdot in equation 2.21 denotes time differentiation and η is a viscosity. In many of the relations to follow, it will be convenient to employ the ratio of viscosity to stiffness:

$$\tau = \frac{\eta}{k} \quad (2.22)$$

The unit of τ is time, k is the spring constant; and it will be seen that this ratio is a useful measure of the response time of the material's viscoelastic response. For viscoelastic materials, the two important material parameters are stiffness ' E ' and the material coefficient of viscosity ' η '. (*Roylance D., 2001*).

As shown in Figure 2.4, many theoretical models have been developed for describing viscoelastic material behaviour under different situation and configurations including the Maxwell model, Kelvin-voight model, Prony series model, Standard linear solid model, etc. These models represent materials under different loading conditions in different configurations balancing the elastic and viscoelastic behaviour, normally represented by spring and dashpot, respectively. Springs perform like an elastic material and a dashpot performs like a pure viscous material. Elastic materials strain when stretched and return to their original state once the stress is removed. While dashpots exhibit time dependent recovery behaviour. Viscoelastic materials have elements of both properties and, as such, exhibit time-dependent strain. The basic theory and mathematical formula of some commonly used viscoelastic model are to be briefly presented in this section.

Kelvin–Voigt model

The Kelvin–Voigt model consists of a Newtonian damper and Hookean elastic spring connected in parallel. It is used to describe the creep behaviour of polymers. As shown in Figure 2.4(a), the two components of the model are arranged in parallel, the strains in each component are identical:

$$\varepsilon_{Total} = \varepsilon_D = \varepsilon_S \quad (2.23)$$

Where ε_D is the strain of the dashpot; ε_S is the strain of the spring. Similarly, the total stress will be the sum of the stress in each component:

$$\sigma_{Total} = \sigma_D + \sigma_S \quad (2.24)$$

Where σ_D is the stress of the dashpot; σ_S is the stress of the spring based on these equations in a Kelvin–Voigt material, stress σ , strain ε and their rates of change with time t are governed by equations of the form:

$$\sigma(t) = E\varepsilon(t) + \eta \frac{d\varepsilon(t)}{dt} \quad (2.25)$$

Where η is the viscosity of the material. Based on this model, the material deforms at a decreasing rate upon application of a constant stress, asymptotically approaching to a steady-state strain. When the stress is released, the material gradually relaxes to its original undeformed state. At constant stress (creep), the model is quite realistic as it predicts strain to approach to σ/E as time continues to infinity. Many works has used the Kelvin–Voigt model ([Taylor L.S. et al, 2002](#); [Rajagopal K.R, 2009](#); [Licht C., 2013](#)).

Maxwell Model

The Maxwell model is commonly used in many works. As shown in Figure 2.4 (b), it consists of one Hookean spring and one Newtonian dashpot being connected in series. This model was designed to describe the stress relaxation behaviour of materials. When the load is released and the spring gradually recovers to its original shape by pulling the dashpot with it and stress on the spring release over time. The spring can be represented by the stiffness (E) and dashpot can be described by viscosity coefficient (η).

In a Maxwell material, stress σ , strain ε and their rates of change with respect to time t are governed by equations in the form of:

$$\frac{d\varepsilon_{Total}}{dt} = \frac{d\varepsilon_D}{dt} + \frac{d\varepsilon_S}{dt} = \frac{\sigma}{\eta} + \frac{1}{k} \frac{d\sigma}{dt} \quad (2.26)$$

Multiplying by k and using $\tau = \eta/k$:

$$k \dot{\epsilon} = \dot{\sigma} + \frac{1}{\tau} \sigma \quad (2.27)$$

This is a “constitutive” equation for theoretical Maxwell material. Since the equation contains time derivatives, simple constant of proportionality between stress and strain is no longer applicable. In this case, the concept of “modulus” – the ratio of stress to strain – needs to be broadened to account for this more complicated behaviour. The equation can be applied either to the shear stress or to the uniform tension in a material. In the former case, the viscosity corresponds to that for a Newtonian fluid. In the latter case, it has a slightly different meaning relating stress and rate of strain. The model is usually applied to the case of small deformations (*Boubaker M.B. et al, 2013; Jiang T.Z. et al, 2014*). For the large deformations some geometrical non-linearity has to be included.

Generalized Maxwell Model (Prony series)

Maxwell model has a problem when being applied to relaxation test due to the fact that it resulted in a zero stress at the infinity time. The general Maxwell model was developed to solve this problem and was found to be able to model complicated viscoelastic materials. The main idea behind the general Maxwell model is that the relaxation does not occur at a single time, but at a distribution of times as illustrated in Figure 2.4(c). Viscoelastic behaviour can be divided into two types of deformation (small or large). In large deformation of viscoelastic, the hyperelastic properties need to be taken into account. For small strain model, the initial values of shear and bulk modulus would be enough as the starting values of the material properties over the time. The shear and bulk modulus are representative of deviatoric and volumetric parts of the stress respectively to the equation below (*Yang L.M. et al, 2000*).

$$\sigma = \sigma_{deviatoric} + \sigma_{volumetric} \quad (2.28)$$

$$\sigma = \int_0^t 2G(t-\tau) \frac{de}{d\tau} d\tau + I \int_0^t \kappa(t-\tau) \frac{d\Delta}{d\tau} d\tau \quad (2.29)$$

Where σ is Cauchy stress, e and Δ are deviatoric and volumetric part of the strain. $G(t)$ and $\kappa(t)$ are shear and Bulk modulus functions, t and τ are current and past

time and I is identity matrix. Prony series was then proposed by the following formulas (2.30) and (2.31) relating shear and bulk modulus over the time.

$$G = G_0[\alpha_\infty^G + \sum_{i=1}^{nG} \alpha_i^G \exp\left(-\frac{t}{\tau_i^G}\right)] \quad (2.30)$$

$$\kappa = \kappa_0[\alpha_\infty^K + \sum_{i=1}^{nK} \alpha_i^K \exp\left(-\frac{t}{\tau_i^K}\right)] \quad (2.31)$$

Where superscript is used to show the belonging to shear or bulk modulus, and subscript indices the number of series component.

$\alpha_i = \frac{G_i}{G_0}$ and τ_i is relaxation time constant for each Prony series component.

α_∞ could be simply calculated by time equal to zero. Then we have

$$G_0 = G_0[\alpha_\infty^G + \sum_{i=1}^{nG} \alpha_i^G] \quad (2.32)$$

Where the term $\alpha_\infty + \sum_{i=1}^n \alpha_i$ should then be equal to 1. It means that $\alpha_\infty = 1 - \sum_{i=1}^n \alpha_i$. Hence, the only constant of the formula are α_i and τ_i which should be determined by a relaxation test. Where the initial values of G and K would be calculated when time equal to zero. For incompressible material like elastomer, the Poisson's ratio can be assumed as 0.5 or infinite bulk modulus. The generalized Maxwell model can be express in term of E instead of G which $G=E/(2(1+\nu))$.

$$E(t) = E_0 + \sum_{k=1}^n E_k e^{-t/\tau_k} \quad (2.33)$$

Where τ_k is the relaxation time of an element k, $\tau_k = \eta_k / E_k$, and E_0 is the quasi-equilibrium value of the modulus of elasticity, n is the total number of Maxwell elements, E_k is the Young's modulus for element number k and η_k is the coefficient of viscosity of the Maxwell element.

In most cases, equations (2.31) and (2.32) can be used instead of some additional different boundary condition for example in different temperatures ([Mottahedi et al, 2010](#)). According to [Sato et al \(2004\)](#), generalised Maxwell model was successfully used in representing the viscoelastic behaviour of different materials, such as nitrile

butadiene rubber and damper used in seismic isolation. (*Park S.W. and Schapery R.A., 1999; Renaud F. et al, 2011; Lu L.Y. et al, 2012; Hassan M.A. et al, 2012*).

Standard Linear Solid Model

Figure 2.4(d) shows the standard linear solid model with a linear combination of spring and dashpots. In this model, the Elastic response of the material is represented by spring and viscosity is represented by dashpots. This model, to certain extent combined Kelvin-Voigt model and Maxwell Model in order to overcome the limitation of these models. For example, the Maxwell model does not describe creep or recovery, and the kelvin-Voigt model does not describe stress relaxation. In contrast to the Maxwell and Kelvin–Voigt models, the SLS is slightly more complex, involving elements both in series and in parallel. This model consists of two systems in parallel. The first, referred to as the Maxwell arm, contains a spring ($E = E_2$) and dashpot (viscosity η) in series. The other system contains only a spring ($E = E_1$). In order to establish this system, the following physical relations must be realised:

For the parallel components: $\sigma_{tot} = \sigma_1 + \sigma_2$, and $\epsilon_{tot} = \epsilon_1 = \epsilon_2$

For the series components: $\sigma_{tot} = \sigma_1 = \sigma_2$, and $\epsilon_{tot} = \epsilon_1 + \epsilon_2$

These relationships help with relating the various stresses and strains in the overall system and the Maxwell arm:

$$\sigma_{tot} = \sigma_m + \sigma_s$$

$$\epsilon_{tot} = \epsilon_m = \epsilon_{s1}$$

$$\sigma_m = \sigma_D = \sigma_{s2}$$

$$\epsilon_m = \epsilon_D + \epsilon_{s2}$$

Where the subscripts m , D , s_1 and s_2 refer to Maxwell, dashpot, spring one, and spring two, respectively.

Using these relationships, the time derivatives of these functions, and the stress-strain relationships above for the spring and dashpot elements, the system can be modelled as follows:

$$\frac{d\varepsilon(t)}{dt} = \frac{\frac{E_2}{\eta} \left(\frac{\eta}{E_2} \frac{d\sigma(t)}{dt} + \sigma(t) - E_1 \varepsilon(t) \right)}{E_1 + E_2} \quad (2.34)$$

The equation can also be expressed as:

$$\frac{d\varepsilon(t)}{dt} = (E_1 + E_2)^{-1} \cdot \frac{d\sigma(t)}{dt} + \frac{E_2}{\eta} \sigma(t) - \frac{E_1 E_2}{\eta} \varepsilon(t) \quad (2.35)$$

The relaxation time τ is different for each material and is equal to $\frac{\eta}{E_2}$.

The Standard Linear Solid Model has been used in modelling more complex materials, such as building material, composite material, auxetic material and biological material (tissue, tendon, ligaments, and articular cartilage) ([Lakes R. et al, 2009](#); [Almagableh A. et al, 2009](#); [Argatov I.I., 2012](#); [Wang X. et al, 2013](#); [De Haan Y.M. and Sluimer G.M., 2014](#)).

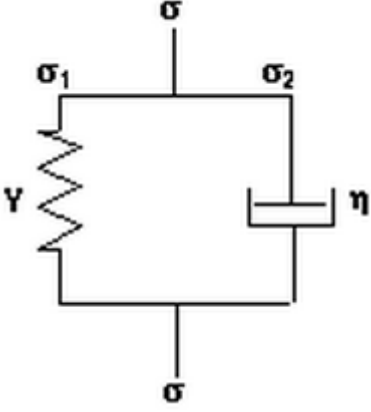
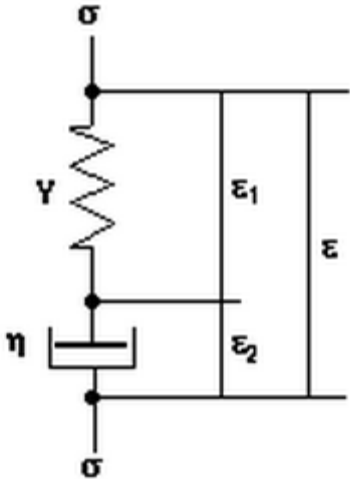
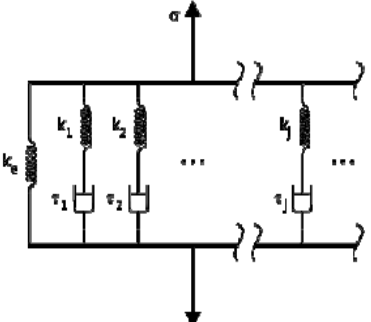
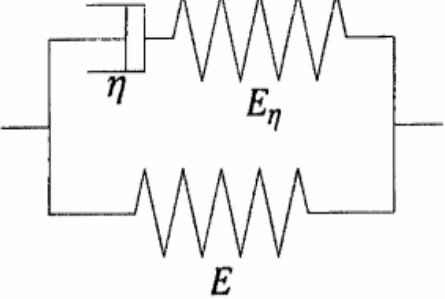
	
<p>(a) Kelvin–Voigt material. (Chandra P.K. and Sobral P. J. do A., 2000)</p>	<p>(b) Maxwell material. (Chandra P.K. and Sobral P. J. do A., 2000)</p>
	
<p>(c) Generalized Maxwell Model. (Prony series) (Mottahedi M. et al, 2010)</p>	<p>(d) Standard Linear Solid Model. (De Haan Y.M. and Sluimer G.M., 2001)</p>

Figure 2.4 Different types of viscoelastic material models.

2.6 Mechanical tests of materials and applications

2.6.1 Material testing with standard tests

As presented in section 2.4, most of these linear and nonlinear materials behaviours can be described with one or more material parameter. It is a challenging task to accurately derive the key parameters of these functions. Conventionally, the determination of material parameters is based on the use of test samples with a standardised geometry and strain state as shown in Figure 2.5. Such that particular conditions on the stress and strain field are satisfied in the sample/or part of the sample. Then the unknown model parameters are obtained via curve fitting from experimental data. Current standard approaches normally require large numbers of tests and samples with well-defined geometries (*Mills and Zhu, 1999; Mills et al, 2003; Moreu and Mills, 2004; Petre et al, 2007*).

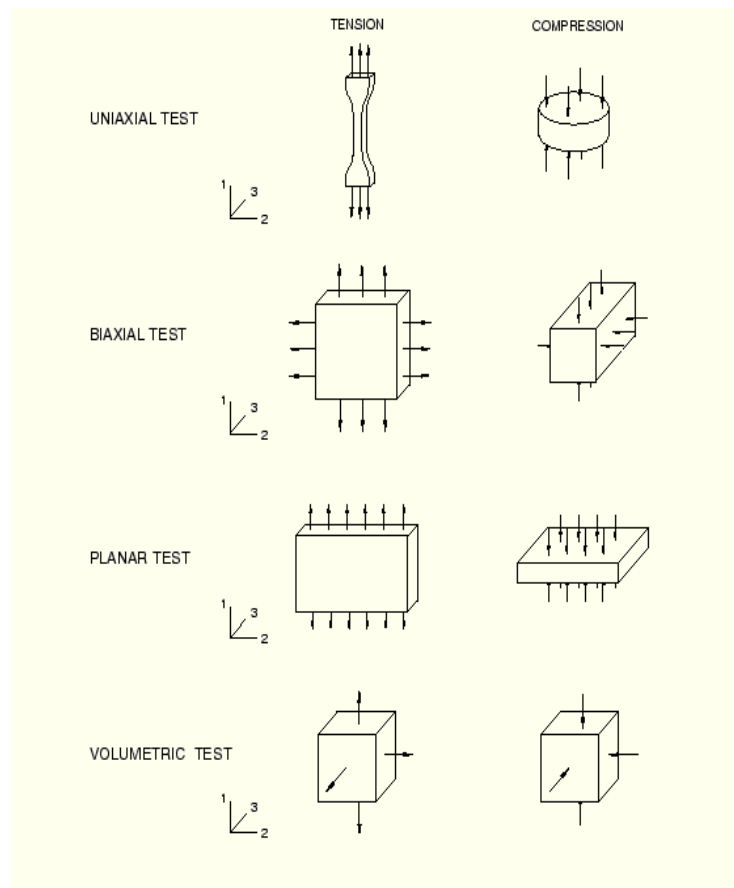


Figure 2.5 Deformation modes of various experimental tests for measuring material parameters (*ABAQUS User Manual 6.11*).

Most of the tests has been done with standard tests, but in some cases, the method is inconvenient or even impossible where standard specimens are not readily available, or for *in situ* monitoring of the mechanical strength of the materials. Recently, some effort has been made to use non-standard test under more complex conditions to determine the material parameters. The use of a range of tests have been explored including tension, compression, suction, and bending test or indentation. ([Diridollou S. et al, 1997](#); [Bader D. L. and Knight M. M., 2008](#); [Ridha H. and Thurner P. J., 2013](#); [Budday S. et al, 2015](#)). The indentation test has been used to charcaterise material properties of the gray and white matter brain tissue. Different diameter of the circular flat punch has been used to indent the brain tissue with 400 μ m and measuring the force. By using the analytical solution method, constant samples elastic moduli were calculated. The testing method presented an easy-to-use, robust, reliable and repeatable to characterise the mechanical properties of brain tissue ([Budday S. et al, 2015](#)). Another testing method with an air suction device to measure the material properties of human skin were developed by [Diridollou S. et al, \(1997\)](#). The cylindrical chamber is attached to the skin using double-sided adhesive tape and vacuum is applied to deform the skin by air suction. By using the ultrasonic detection, skin deformation and position was recorded. The results are plotted in suction pressure over displacement. This study is to monitor the actual skin and subcutaneous fat thickness changes while under suction, the technique should prove the difference between healthy and diseased skin to mechanical deformation. In other words, to develop a mathematical model of the physical properties of skin to define material parameters for differentiating skins.

Generally, these tests involve applying a predefined stress /deformation on the sample surface and monitor the displacement/load. Then the material properties/parameters were determined through mathematical or inverse FE modeling by finding the material parameters that give numerical results matching experimental data. One testing mode which is particularly relevant to thin membranes/sheet is the indentation bending tests ([Ju B. F. et al, 2005](#); [Ahearne M. et al, 2009](#)), which combines localized indentation and bending of the sample that is ideal for samples in the form of thin sheet. In addition, creep and relaxation are normally associated with the functions and performance of thin membranes, it is also

interest to investigate how to use these nonstandard tests and inverse modelling to determine the time dependent material behaviors in creep and relaxation.

2.7 Indentation and indentation bending test

In an indentation test, indenters of different shapes are pressed onto the sample surface while the force and displacement is recorded, either continuously or with fixed load/displacement, to represent the resistance of the material to deformation. There are many types of shaped indenter, such as cylindrical, spherical, pyramid tip indenter, are developed and all of these have found applications in testing different types of materials (*Swain M.V., 1998; Lim Y.Y. and Chaudhri M.M., 2006; Chicot D. et al, 2013; Hosseini M. et al, 2013; Koumi E.K. et al, 2014*). For example, the pyramid tip indenter (such as the Vickers Indenter) is mostly used for hard material such as metals, ceramics and plastics, while blunt indenter (spherical or flat) is commonly used for softer materials. Recently, the application of indentation tests has also been increasingly used to determine mechanical properties of materials with time-dependent deformation behaviour including polymers and rubber-like materials (*Carter F.J. et al., 2001; Delalleau A. et al, 2006; Giannakopoulos A.E. et al, 2007; Carson W.C. et al, 2011*). There have been several works using flat and spherical indenters to test biological materials such as skin, heel pad, etc. (*Han L.H. et al, 2002; Erdemir A. et al, 2006; Li B, 2009; Pamplona D.C. et al, 2014; Zhang M.G. et al, 2014*). In addition, flat punches type indenters can also be used to determine the viscoelastic properties of soft layer bonded to hard substrates shown in Figure 2.6(a) (*Cao Y. P. et al, 2008*). Bending tests are another form of experiment to test the resistance of material to localised loading. Bending is a common deformation in many thin sheet structures such as (mobile phone, pressure sensors, bio-tissues, packaging, laptop casing, household, automotive, and etc.). Figure 2.6(b) shows schematically the setup of a bending tests, which has been used in the work of testing the deformation in a mobile phone cover (*Fredrik N. 2006*).

Indentation bending test is a combination of indentation and bending tests, as illustrated in Figure 2.6(c). It is able to characterise the mechanical properties of the material in the form of a thin sheet such as Young modulus, yielding stress and viscoelastic (*Huber N. et al, 1999; Begleya M. R. et al, 2004; Scott O. N. et al, 2004; Cao Y. P. et al, 2009*). In the test, an indenter is pressed onto the surface of the material which is firmly clamped around the rim/edge. The force and displacement curve data is used to measure the properties of the material. This test can be of different scale from nano, micro to macro tests and the shape of the sheet being

indented can be a circular, square or irregular shape ([Chen and Soh, 2008](#); [Heinrich C. et al, 2009](#)). Figure 2.6(d) shows the experimental setup of a test used to predict the young modulus of the thin polymer membrane using an atomic force microscope by [Ju B. F. et al, \(2005\)](#). This research mainly focuses on very thin polymer membrane with a thickness of 120 μm . Figure 2.6(e) shows a setup of a tester used to study the indentation deformation of freestanding circular elastomer films with spherical indenters. In the work, a spherical indenter is used to test very soft thin film made of poly (dimethyl siloxane) and biological material (membrane) as the specimen. In this work, an analytical solution has been evaluated (classical Begley/Mackin finite contact solution and classical Schwerin solution) in predicting the testing result using linear elastic model. The limitation of Schwerin point-load solution is that it only works for a small indenter, in other way Begley/Mackin finite contact solution can potentially work for all size of indenter ([Scott et al, 2004](#)).

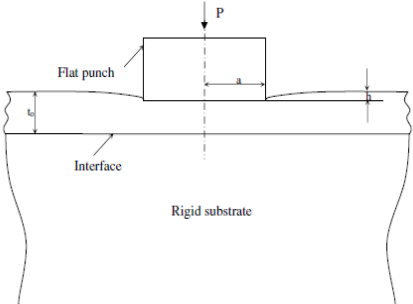
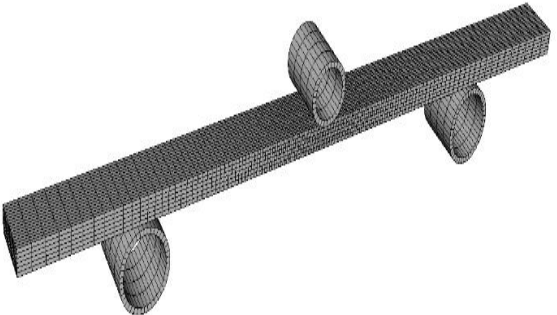
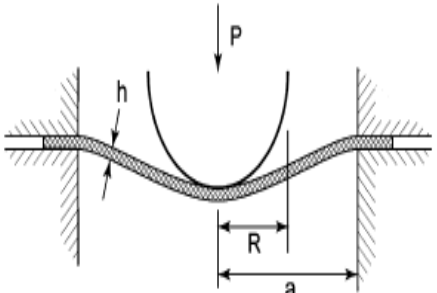
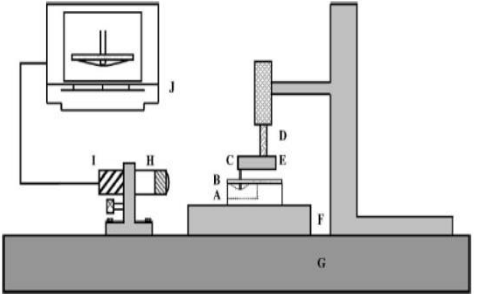
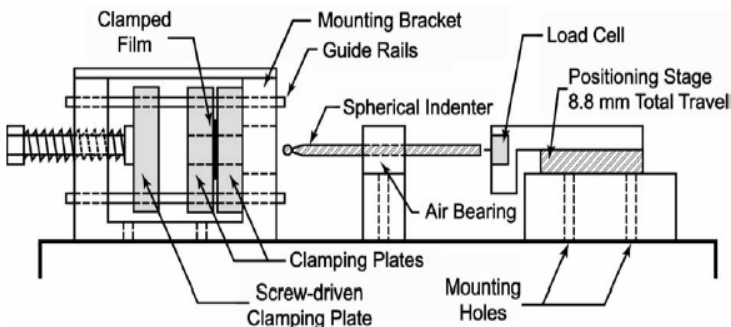
	
<p>(a) Flat punch test of sample within a thin layer on top of a rigid substance. (Cao Y. P. et al, 2009)</p>	<p>(b) Setup of a bending test for mobile phone material. (Plastic). (Nordgren F. et al, 2006)</p>
	
<p>(c) Schematic to show indentation bending tests of free standing film.(Scott O.N. et al, 2004)</p>	<p>(d) Schematic diagram of the vertical indentation bending test based on Atomic Force Microscope (AFM). (Ju B. F. et al, 2005)</p>
	
<p>(e) A horizontal indentation bending test. (Scott O. N. et al, 2004)</p>	

Figure 2.6 Different indentation/bending tests for characterising rubber-like materials and plastics.

In the study done by [Selvadurai \(2006\)](#) (Figure 2.7), the problem of the large transverse deflection of a natural rubber membrane that is fixed along a circular boundary was investigated. In the work, uniaxial experiments were performed first in order to characterise the constitutive behaviour of the rubber material and the data is analysed with several constitutive models available. These constitutive models were used to develop a computational model for the quasi-static load–displacement response of a rigid spherical indenter that deflects the rubber membrane in a controlled fashion and to determine the deflected shape of the membrane at specified load levels. Both axisymmetric and asymmetric deflections of the rubber membrane were investigated. The study provided comparison between the experimental results for the membrane deflections with results derived from FE simulations. The work showed that many of the existing models can, in general, describe the material at both moderate and large strain levels and the Mooney–Rivlin type of strain energy functions were found to be the most suitable for deformation at lower strain level (Figure 2.7(d)). Similarly the Ogden model also showed a reasonable accuracy in predicting the force deflection data.

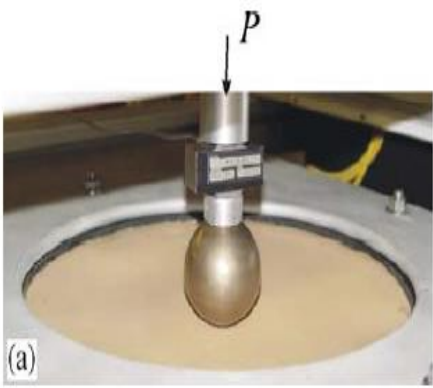
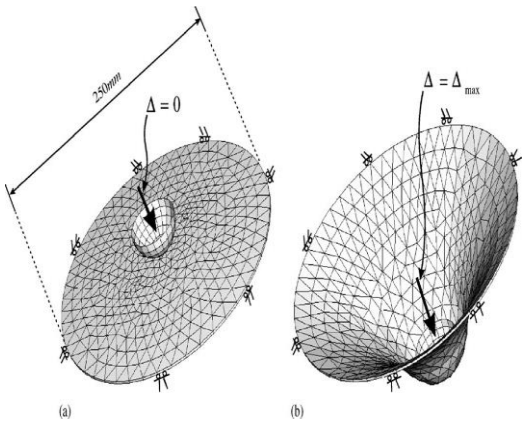
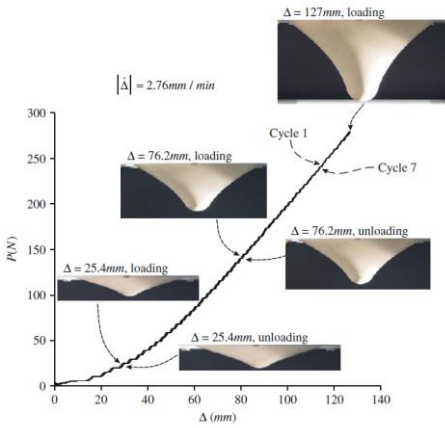
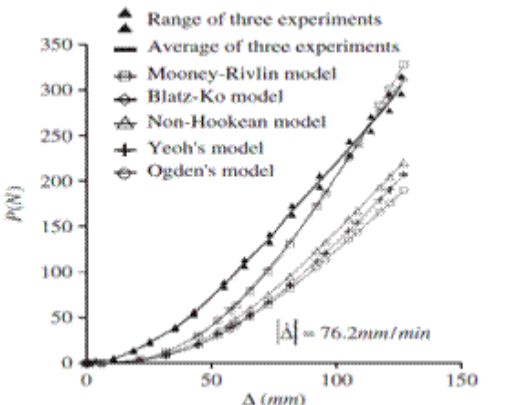
	
<p>a) Axisymmetric indentation.</p>	<p>b) FE model of indentation bending tests.</p>
	
<p>c) Deflection of rubber membrane during a large displacement indentation bending test.</p>	<p>d) Comparison between experimental and numerical data with different material models.</p>

Figure 2.7 Large displacement indentation bending tests of a rubber sheet. (Selvadurai, 2006)

In another study, Aernoutset (2010) used a similar setup to characterise membranes with a complex shape using point indentation measurements as shown in Figure 2.8. The sample made of latex rubber which was clamped with a circular boundary. The indenter used is a flat cylindrical with a diameter of 1.7mm. The main objective of

the work was to use the indentation technique to determine the elasticity parameters of a rubber-like material with a complex surface and shape. In the work, an inverse modelling method is developed to predict the material properties by using First-order Mooney-Rivlin and second-order Ogden material to define the material parameters. This research also extended to the modelling of a human tympanic membrane that has a complex shape. The test demonstrate a clear advantage in using indentation bending tests to study the behaviour of tympanic membrane and middle ear ossicular prosthesis, which is difficult to be tested using other methods.

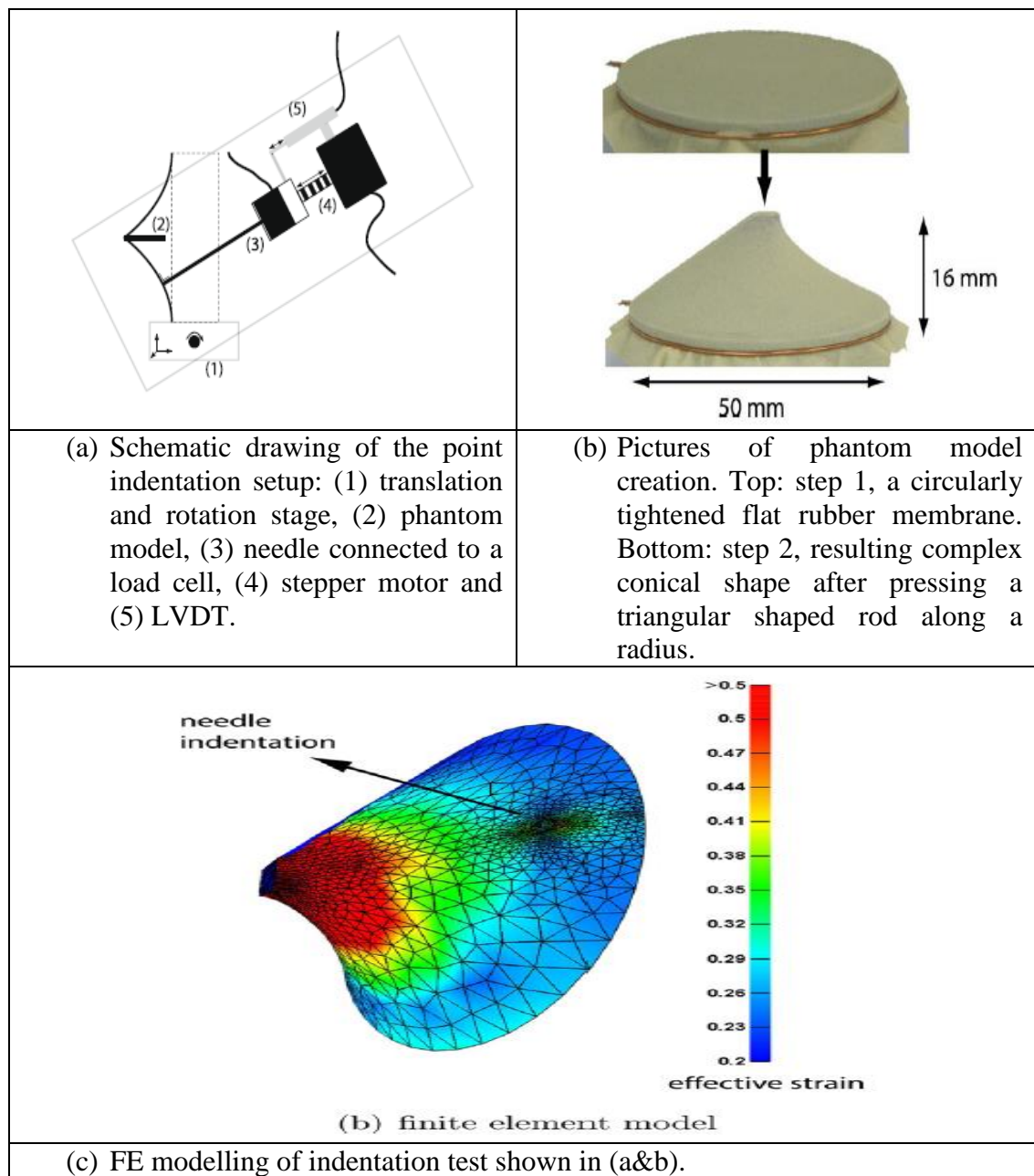


Figure 2.8 Indentation test for elastic membranes with a complex shape. (*Aernouts J. et al, 2010*).

Instead of indentation test, bulge test has also been used by researchers (e.g. [Sasso M. et al, 2008](#)) on thin membranes to predict the material properties. As shown in Figure 2.9(a), a bulge test is conducted by applying a fluid pressure which stretches the sample without any direct contact and the change of thickness and depth of the sample is recorded by two high resolution cameras and pressure is measured by fluid pressure gauge. Figure 2.9(c) shows the FE model and the boundary condition used to fix the circular edge. Typical pressure-depth is shown in Figure 2.9(d) where Ogden and second order of Mooney-Rivlin model are comparable to the experimental result. Both give a good description of the non-linear behaviour.

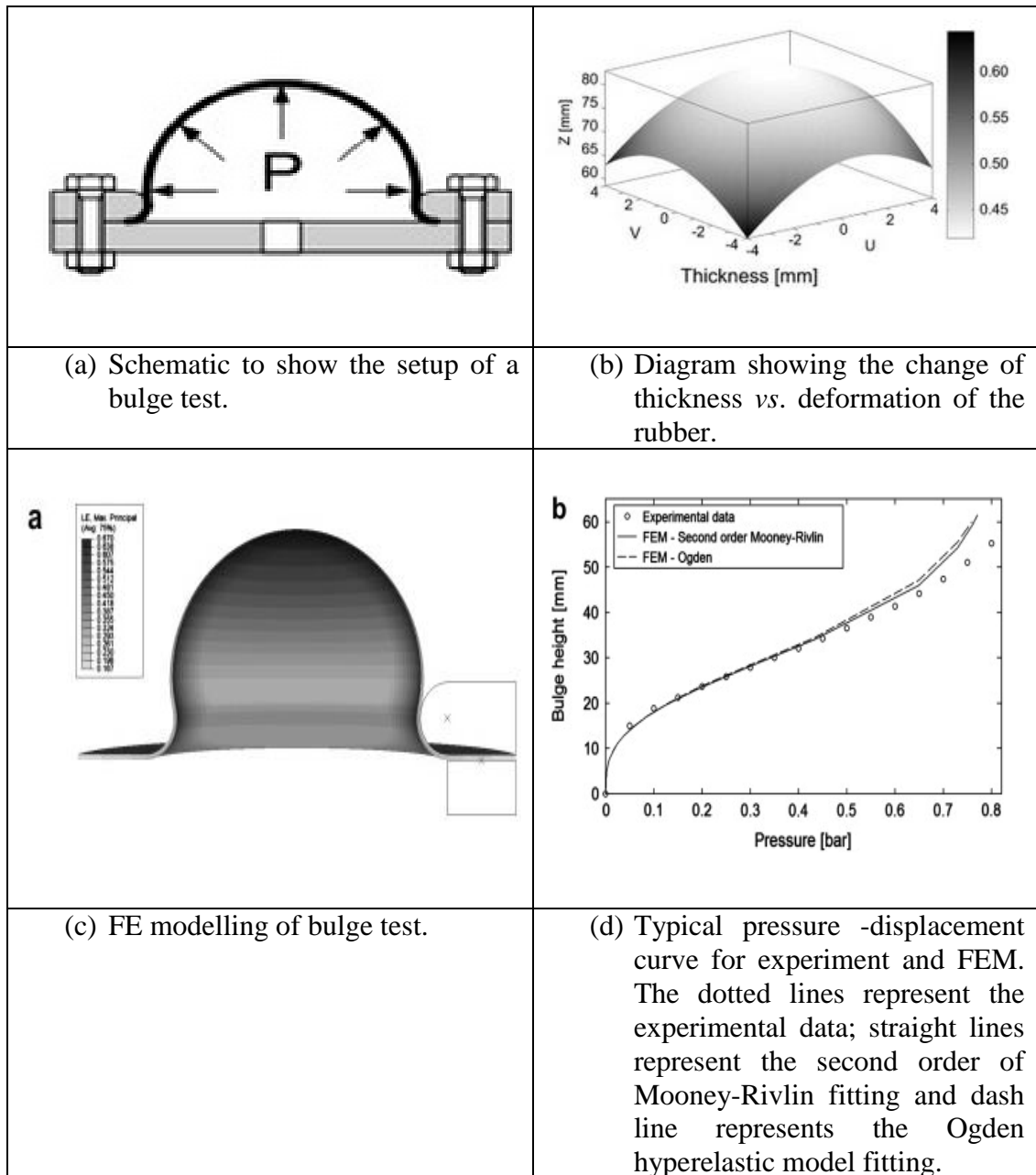


Figure 2.9 Characterisation of hyperelastic rubber-like materials by stretching in a bulge test. (*Sasso M. et al, 2008*).

An indentation bending test does not required any expensive instrumentation. The main measurable variables are force and displacement, which can easily be captured by load cell or displacement sensors. The test can be set up with a complex shape of the product and only require a small piece of the material sample to run the test. However, the indentation bending test is not a standard test which cannot directly measure the properties of the material. In addition, due to the fact that the deformation domain may change between plate theory to membranes depending on

the size of the sample, indenter shape, materials properties and strain level, it is difficult to use a robust analytical solution which is universally applicable to all materials. In order to characterise materials using indentation bending test, FE inverse modelling offers a better option to estimate the materials properties from the tests. Typical inverse modelling method and applications are briefly discussed in the next section.

2.8 FE modelling and inverse properties prediction

Finite element method is a numerical technique used to solve engineering and scientific problems. The methods are widely used to solve structural, fluid, multiphysics problems. (*Fagan, 1992; Dai X. H. et al, 2010; Khor C. Y. et al, 2011; Coombs D.J. et al, 2012*). There are many commercial packages available which are being widely used nowadays such as ABAQUS, ANSYS, COSMOL and etc. The finite element approach involves dividing the continuum into small elements for the stress or displacement fields (or other physical parameters) to be approximated with displacements (or other variables) that is continuous and is in equilibrium, thus satisfying the problem's boundary conditions. The approximation is determined by transforming the differential equation approach into an algebraic problem, wherein the finite elements or small subdomain have all the complex equations solved for a simple shape and transformed to a more complex equation over a larger domain. Structural analysis is based on the discretisation method which converting model into discrete model of number of elements and included degrees of freedom (DOF) such as loading, boundary conditions and material properties. Once the problem has been discretised, the main equations for each element are calculated and assembled together to give the system equation. In the next step, general format of the equations of an element type is derived, the calculation of the equations for each occurrence of that element in the body is straightforward; it is simply the question of substituting the nodal coordinates, material properties and loading conditions of the element into the general format.

The individual element equations are assembled to obtain the system equation, which describe the behaviour of the body as a whole. These generally take the form of

$$[k]\{U\} = \{F\} \quad (2.36)$$

Where $[k]$ is a square matrix, known as the stiffness matrix; $\{U\}$ is the vector of (unknown) nodal displacements or temperatures; and $\{F\}$ is the vector of applied nodal forces.

The equation above is direct problem which is comparable to the load and displacement relationship for a simple one-dimensional spring. The F represents

force and U is deflection and k is spring of stiffness. To find the displacement by a given force, the relationship is inverted. These matrixes define inherent properties of the system being studied. Energy derivations are commonly used to form the stiffness for a variety of element types. The elements have restrictions on their behaviour; the result is always a stiffness matrix that can then be treated like any other stiffness matrix and can be rotated and transformed. Additional considerations are also generated since the shape function assumption can affect the accuracy of the results. For thin structures, the most common elements are the membrane (planar), plate, shell and solid elements. Each element has a given set of nodes and displacements associated with those nodes. There are many types of elements suitable for different materials or systems. Shell/membrane elements are most widely used to simulating thin sheet structures in engineering or biological materials ([Hutton, 2005](#); [Firat, 2007](#); [Peng X. Q. and Wang Y, 2011](#); [Lei et al, 2014](#)).

The membrane element refers to two-dimensional triangular and rectangular elements extending flat elements. The membrane element has a stiffness or rigidity without rotation perpendicular to the plane of the element. It may optionally be located in the space, but the resulting force must be located in the plane of the element. The flat plate element is similar to the two-dimensional element plate. There are two-plane rotation and normal displacement degrees of freedom. These elements could be used to model plate bending behaviour of two dimensions. The three-dimensional solid element is a variable 4- to 20- node or a 21- or 27-node isoperimetric element applicable to general 3-D analysis. Eight-node unit has some linear variation of stress throughout the element. Solid element has no rotational stiffness. The most common version is the eight-node solid elements; also called tetrahedron (tetrahedral) and hexahedral (hex) is a popular mesh generation and the use of adaptive mesh refinement. ([ABAQUS, 6.11](#))

Traditionally, FE modelling was used to predict the behaviour of materials or structures under different loading condition ([Reusch and Estrin, 1998](#); [Dini et al, 2009](#); [Podshivalov et al, 2011](#)) over a wide range of industries. Recently, many research works explored the use of FE modelling to inversely predict the material properties by coupling FE modelling with different inverse programs ([Guo et al, 2004](#); [Kajberg and Wilman, 2007](#); [Kim and Choi, 2008](#)). For example, [Louche et al,](#)

(2009) has developed an impact test model to study the thermo mechanical behaviour of an ABS polymer structural component by comparing the result of experimental data and numerical data. In another study, FE modelling was used to model a collapsible PET water fountain bottles by using Pro/Engineering software. In this study, bottle with different wall thickness were tested and simulated in order to determine the material properties (Masood et al, 2005). In another work Cao et al, (2009) developed an inverse program to predict the viscoelastic properties of materials based on indentation tests with a flat punch. The program was successfully used to characterise the compressible elastic properties of thin sheet samples. The approach has also been used in research of new materials. In the work on hydrogels by (Sasson et al (2012) as potential implant material of the Nucleus Pulposus (NP) within the intervertebral disk, a spherical tip indenter was used to test the hydrogel surfaces shown in Figure 2.10. A digital image correlation (DIC) technique was used with the indentation test in order to process the full-field surface strains where the indenter contacts the hydrogel and then compare the data with those predicted by the FE model. For the data with $D=20$, the FE model with Ogden model showed reasonable agreement with the testing data, but the comparison with a larger chamber is less good.

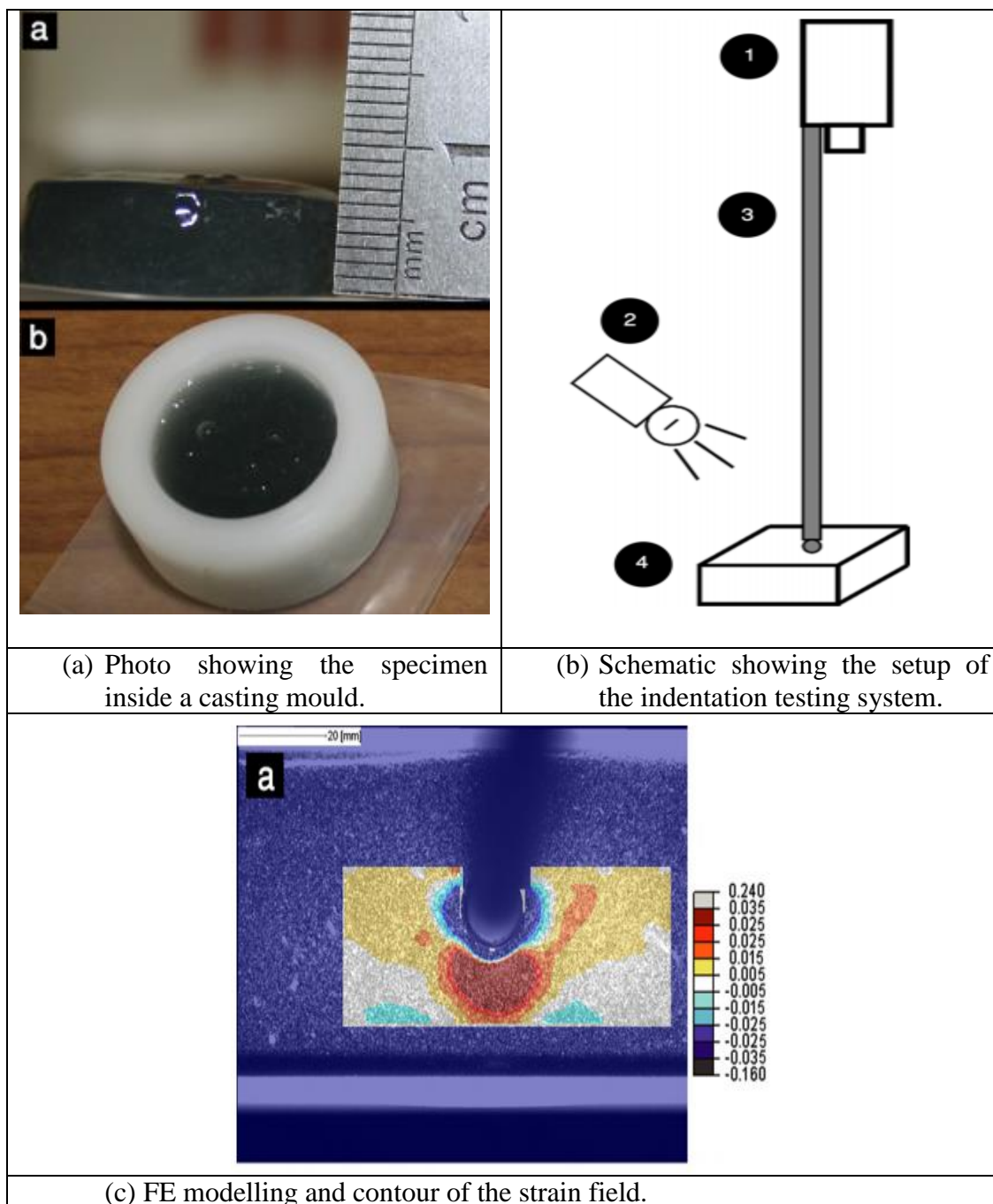


Figure 2.10 Indentation test of hydrogel with high cross-linked polymeric network. (*Sasson A. et al, 2012*).

2.9 Different inverse modelling approaches and their applications in material properties prediction

Inverse material parameter identification normally involves the use of combined experimental and numerical methods to determine the properties/variables that are not readily available from nonstandard tests. Inverse modelling has been applied to many problems in engineering fields (*Buljak V. and Maier G., 2012; Tang L. and Walters C. L., 2014; Sun G. Y. et al, 2014*). General areas in inverse problems in engineering mechanics were the subjects of mathematical and computational aspects of inverse problems, parameter or system identification, shape determination, sensitivity analysis, optimization, material property characterization, thermal inverse problems, and other engineering applications (*Tanaka and Dulikravick, 2000*). Parameter estimation can be treated as one form of inverse problem of optimisation that deals with the determination of the mechanical system with unknown material properties, geometry sources or boundary conditions, from the knowledge of response to given excitations on its boundary (*Neaupane and Sugimoto, 2003*). A successful program for predicting material parameters has to be accurate, efficient and robust. Whether or not all these can be achieved are dependent on the testing method(s) used, inverse program, optimisation method etc. There are many methods to estimate the parameter problems, typically interactive data processing method, parametric method, Kalman filter method, neural networks method etc. (*Corigliano A. and Mariani S., 2004; Saleeb A.F. et al, 2004; Tyulyukovskiy E. and Huber N., 2006; Puel G. et al, 2013; Kim T.H., Kim Y.M., 2015*). In materials testing, inverse modelling is normally combined with non-standard tests under more complex conditions to determine the material parameters. The uses of a range of tests have been explored including suction, tension, torsion, bending test or indentation (*Vannah and Childress, 1996; Vescovo et al, 2002; Mattei and Zahouani, 2004*). Each method has its advantages and disadvantages which made them only suitable for different conditions.

2.9.1 Inverse parameter identification based interactive property searching approach

In an interactive property searching approach, the properties are modified in the optimisation loop, and then new numerical data is produced and compared to the target. The input was modified again after comparison between predicted data and target until the numerical result is within a reasonable range of the target. Normally the user defines an objective function based program to measure the material parameters, an lower objective function represents a better fit between the numerical data and the experimental target. One example use a direct and inverse modelling to determine the material parameter is shown in Figure 2.11. The FE model of the indentation test is shown in Figure 2.11(a), the flow chart (Figure 2.11(b)) shows the structure of the inverse program to estimate the material parameters from the indentation curve. ([Saux et al, 2001](#)). The interactive method is easy to understand, however, it requires the model to be re-run many times, which can be time and resources consuming. Figure 2.12 shows another approach used by [Ren et al, \(2006\)](#) in determining the elastic properties from *in vivo* surface tension tests. This approach firstly determines a rough range of the data and then refines the material parameters. This method could effectively predict the material parameters with reduce the amount of computation works required. However, before using this approach, good pre-knowledge of the material required for the user.

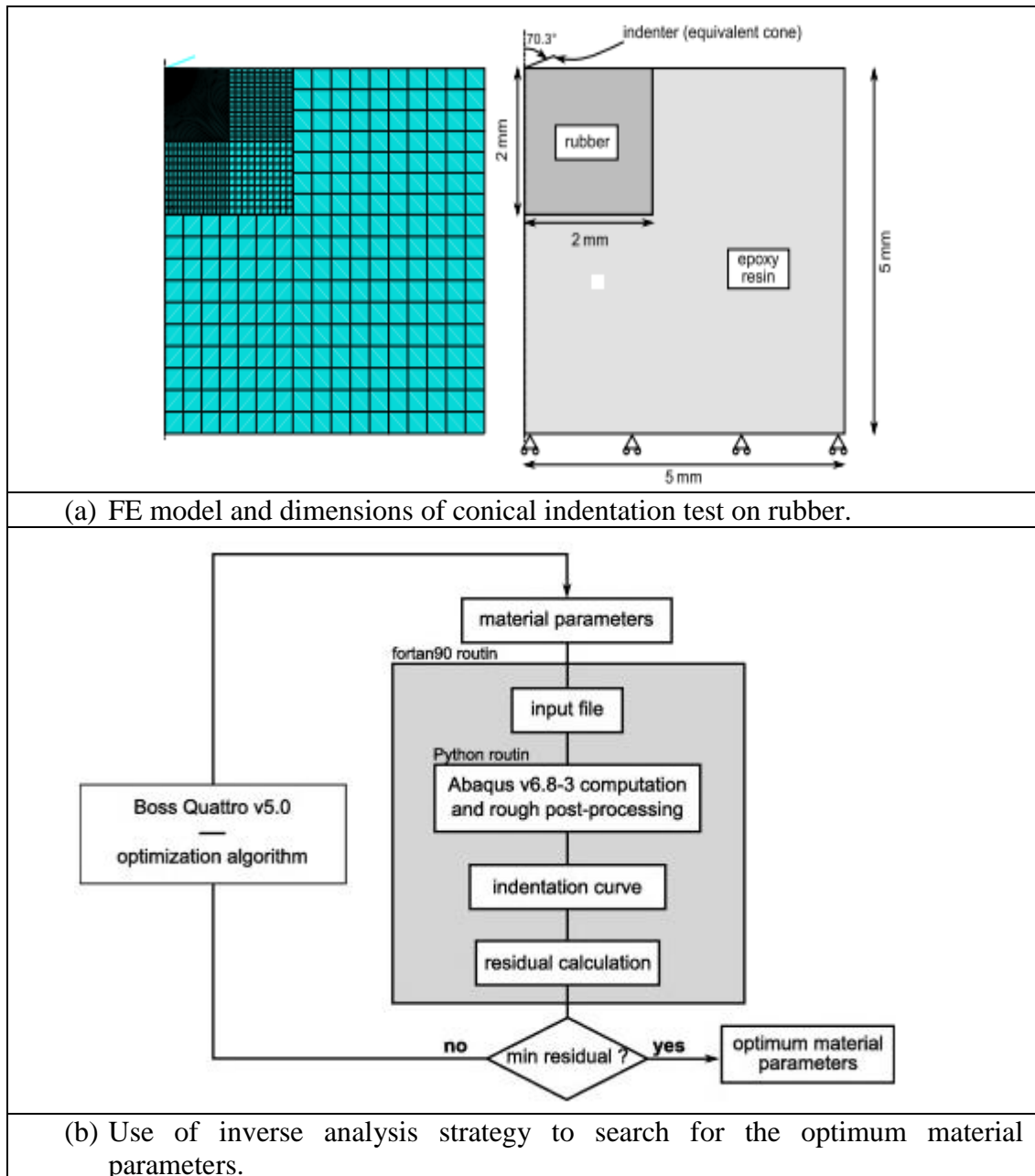


Figure 2.11 Inverse modelling approaches for characterising rubber materials based on indentation tests. (Saux et al, 2001).

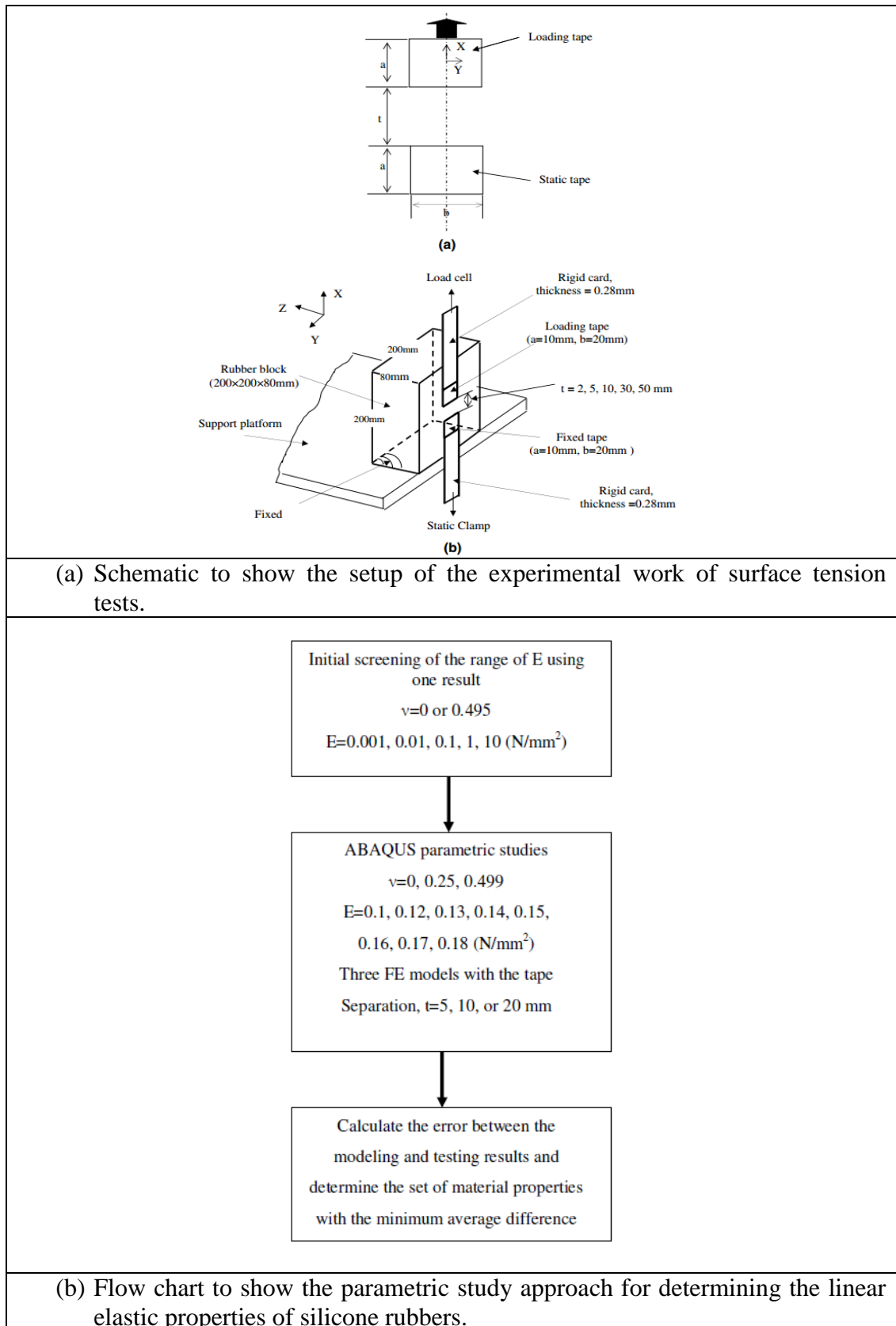


Figure 2.12 Typical parametric studies based inverse FE modelling method for inverse material properties identification of rubber block based on a surface tension test. (Ren et al, 2006).

2.9.2 Artificial Neural Network (ANN)

Recently, Artificial Neural Network (ANN) algorithms have been used to model complex non-linear relationship based on indentation test results. [Huber et al \(2001\)](#) presented artificial neural network model to determine the constitutive properties of thin films on a substrate based on the depth–load curves of spherical indentation. Their models enabled the material properties of both the thin film and the substrate to be identified from a single indentation load–displacement curve. [Tho et al, \(2004\)](#) proposed an artificial neural network model to characterise elasto-plastic material properties of metals following the power law work hardening rule. [Kapoor et al, \(2005\)](#) and [Araujo et al, \(2006\)](#) employed ANN technique to predict mechanical properties of an alloy with a laminated structure based on a two layered system. In addition, [Tyulyukovskiy and Huber \(2007\)](#) used neural networks combined with FE model and experiments to analyse bulk material and thin films for their creep behaviour. Figure 2.13 lists the key input and output of an ANN program involved in the work using ANN by [Lobato et al, \(2010\)](#).

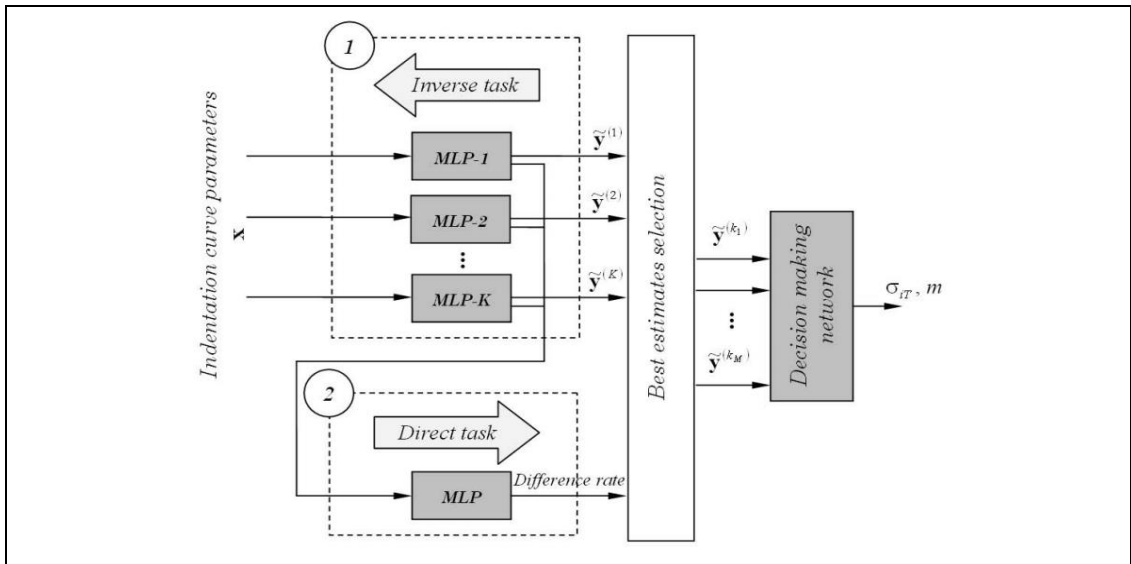


Figure 2.13 Structure of direct and inverse neural network modelling. ([Mishulina O. A. et al, 2011](#)).

[Harsono \(2009\)](#) used a single neural network approach (Figure 2.14(a)) in studying the prediction of yield stress and work hardening coefficients based on data from indenter with different angles. The input is the surface of the ratio between work

done and total energy (W_R/W_t) and the ratio of the curvature ratio of the curves of two different indenter angles (C_1/C_2) (Figure 2.14(b)). The comparison between the ANN predictions is listed in Table 2.1 in comparison with the target value.

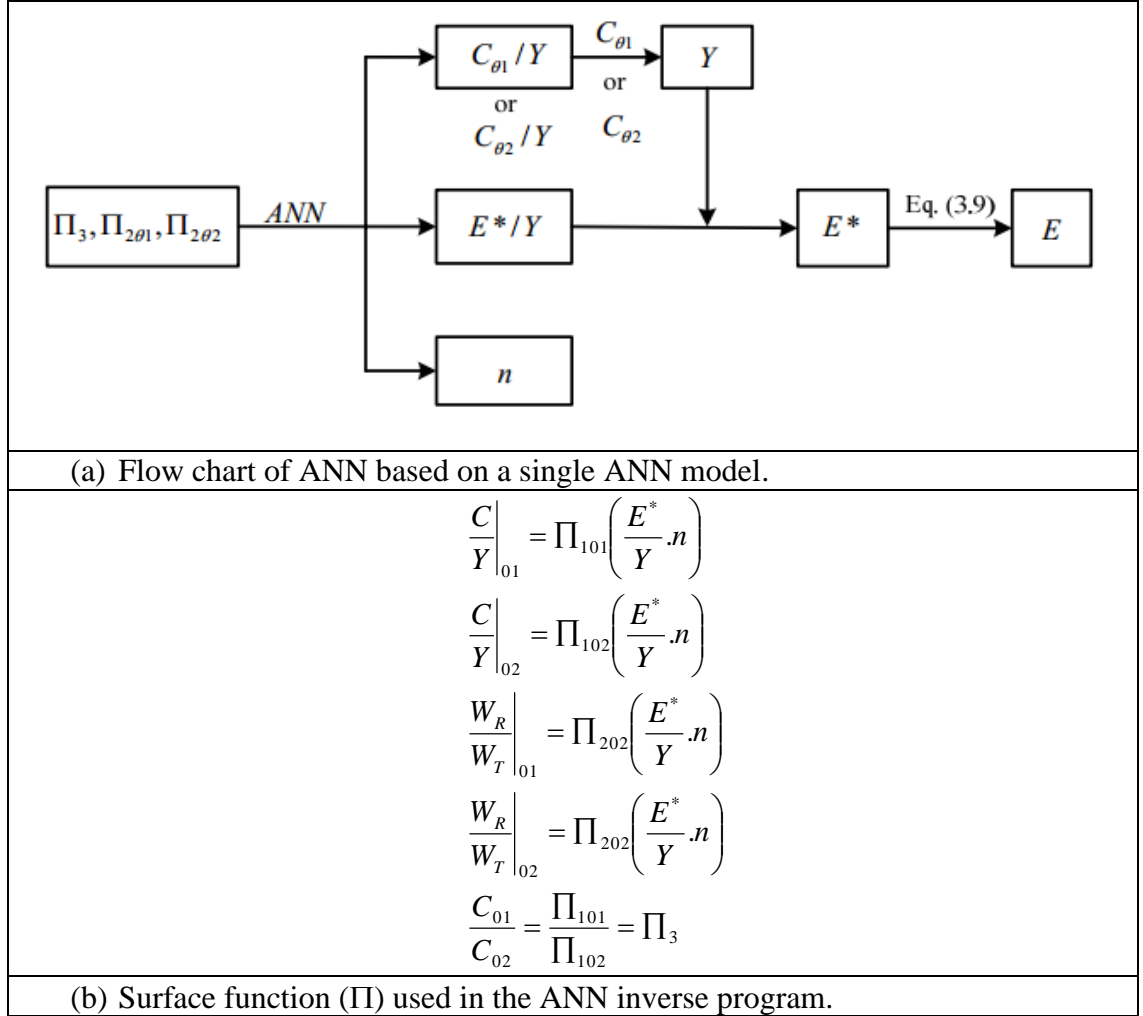


Figure 2.14 A single ANN system used in predicting plastic properties based on conical indentation (a) and the surface equations representing the relationship between the P-h curve parameters and material properties (b) (Harsono, 2009).

Table 3. Prediction from artificial neural network model.

	Al6061	Al7075	Steel	Iron
E^* (GPa)				
Actual	72.4	73.4	194.3	170.8
Predicted	72.7	73.1	195.6	170.0
Deviation (%)	0.5	0.4	0.7	0.5
E (GPa)				
Actual	69.0	70.1	210.0	180.0
Predicted	69.3	69.8	211.8	179.0
Deviation (%)	0.5	0.4	0.8	0.6
Y (MPa)				
Actual	275.0	500.0	500.0	300.0
Predicted	276.3	508.3	489.6	297.9
Deviation (%)	0.5	1.6	2.1	0.7
n				
Actual	0.050	0.122	0.100	0.250
Predicted	0.049	0.117	0.106	0.253
Deviation (%)	2.3	4.5	5.6	1.2

Table 2.1 Comparison of the predicted material properties obtained from ANNs algorithm with inputs for various combinations of three-sided pyramidal indenter tips. (*Tho et al, 2004*).

The ANN predicted yield strength shows a good agreement but the work hardening coefficients showed a relatively high deviation. This shows that ANN can be used to predict the materials properties but not necessarily will achieve high accuracy for all the material parameters. This does not imply that program is not useful but to highlight the fact that when developing ANN, the goal should be try to achieve the best possible outcome can be achieved rather than purely to produce accurate number on limited cases. In another work of using ANN program on EVA foams (*Su et al, 2010*), it was found that ANN can be used in direct P-h curve prediction, but the inverse property prediction process was not necessarily unique.

2.9.3 An optimisation method with post data processing –the Kalman filter method

Figure 2.15 is a flow chart showing the procedure for a Kalman filter method to obtain the parameter of the material properties of foams and human heel pad (*Li B.et al, 2009*). In the work, experiment and numerical data have been stored into the database and Kalman filter program was used to search for material parameters. Once the comparison between the experiment and numerical data match over several

data points, the program will stop and present the material properties as a final result. This method provides an efficient computation a framework to compare the experimental and numerical data. In this method, the unknown variable can be effectively estimated than interactive methods, but a simulation space has to be produced first.

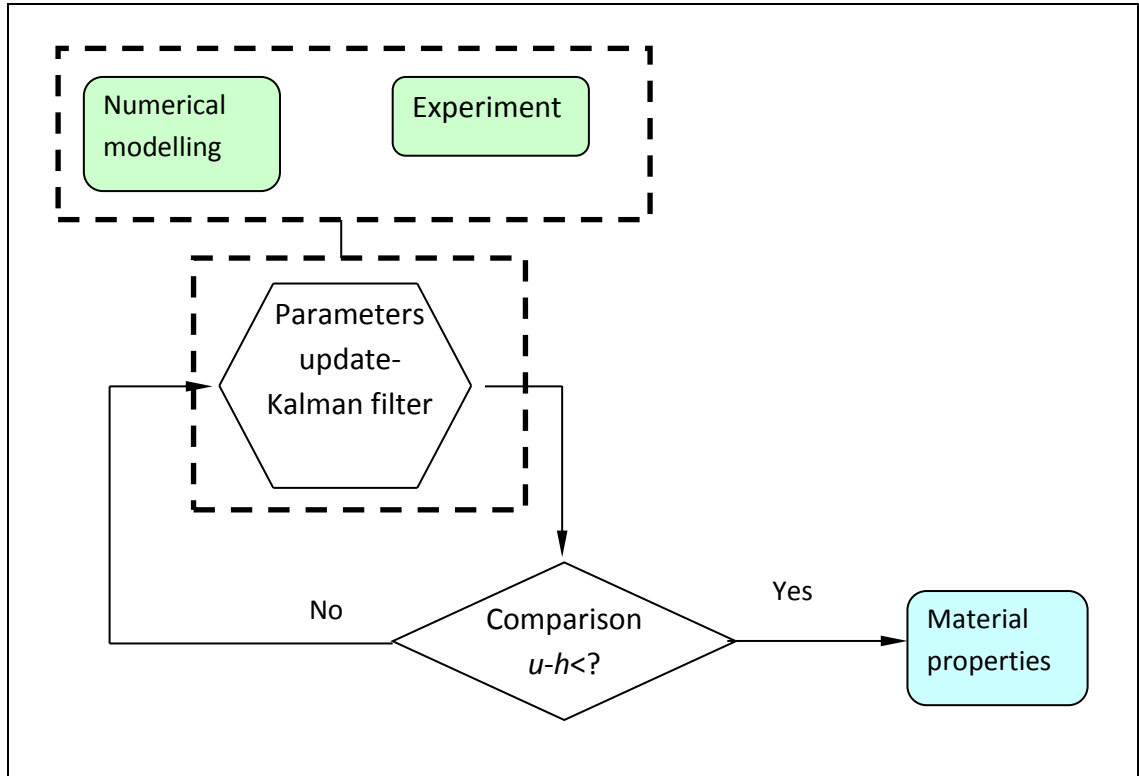


Figure 2.15 Post-modelling approach based on the Kalman Filter method.

The Kalman filter has been used in seeking unknown parameters of homogeneous material models (*Hoshiya and Saito, 1984; Aoki et al, 1997; Nakamura et al, 2000; Gu et al, 2003; Delalleau et al, 2006*). *Neaupane and Sugimoto (2003)* used an extended Kalman filter coupled with finite element method to formulate an inverse problem and estimate the thermal boundary in the form of a heat transfer coefficient (HTC). In their research a simple non-linear formulation based on steady-state heat conduction was incorporated in the Kalman filter loop. From the laboratory experiment, steady state temperatures were measured at predefined locations. The heat transfer coefficient (HTC) was estimated inversely from the measurements (*Neaupane and Sugimoto, 2003*). *Gu et al, (2003)* developed an inverse analysis

model based on the Kalman filter technique to characterise elastic-plastic properties of graded materials, in which the material properties varies across the sectional area. The results showed an excellent agreement between the indentation load-displacement curve from finite element analysis with estimated properties and that of measured record, which assures a high degree of accuracy in the current measurement procedure. Recently, [Li \(2009\)](#) has developed an inverse program based the Kalman filter approach and successfully used it to study foams and human heel pad.

2.9.4 An objective functions method for optimisation

The objective function method involves calculating the difference between two curves. The final material property sets were determined by finding the property data that give a minimum objective function value. This is a straight forward approach commonly used in comparing the similarity of two sets of data. The objective function method is normally defined by the sum of the squares of the differences between the computational and experimental data for the same time or strain level.

$$G = \sum_{i=1}^n \left(\frac{Fi,e - Fi,n}{Fi,e} \right)^2 \quad (2.37)$$

Where G is objective function value, (Fi,e) is experimental data, and (Fi,n) is computation data.

The objective function has been used to determine material constants within unified creep constitutive equations based on experimental data ([Simunek J. & De Vos J.A., 1999](#), [Li B. et al, 2002](#), [Lin J. et al, 2002](#), [Cao J. & Lin J., 2008](#)). [Lin J. et al, 2002](#) used objective function method to characterise the effect of hardening and softening state variables on superplastic flows of metal and alloys. By using the objective optimisation method, the work overcome the difficulties associated with identifying the difference between predicted and experimental data. In another study, [Harish G. et al, 2000](#) has successfully used an objective function to identify material parameters of hyperelastic foam material used to provide grasping force in artificial hands.

2.10 Main challenges testing thin membranes and properties identification.

Many efforts have been made to study thin membranes of rubber like materials using different strain energy functions in describing the material behaviour. (*Guo Z. and Sluys L. J., 2006; Selvadurai, 2006, Zhao et al, 2006*). The potential use of an inverse modelling program requires satisfactory convergence and consistency conditions. This includes an accurate FE model of the system and effective experimental setup to achieve a reasonable robustness for the inverse modelling technique (*Aernouts J. et al, 2010; Erdemir A. et al, 2006*). In addition, for hyperelastic material models, a wide range of material parameters is required to be able to access the uniqueness of program. This requires expensive modelling work to build a large simulation space and allow the program to compare with experimental result. Many inverse analyses still uses conventional methods to calculate and analyse the data. Analysis of the data and editing the material parameters manually is very time-consuming and ineffective. An effective programming technique has to be used to improve the accuracy and decrease the time of data mining. In ABAQUS, many users using linked between FORTRAN and C++ to run user-subroutine codes such as VUMAT and UMAT (*Lee W. B. and Chen Y. P., 2010; Toda N. et al, 2010; Mishnaevsky L. et al, 2014*). These developments offer an opportunity to develop a data processing program combining FE modelling, parametric studies, data process and analysis to reduce the complexity of the inverse program, this is very important for application oriented development of inverse modelling. Another potential area is to use the Python programming, which is much easy to implement and directly compatible with ABAQUS.

Indentation bending testing is an important characterisation method for thin membranes. It is important to develop an effective framework of inverse modelling based on programming base method to characterise the material parameter. However, this is a very challenging task due to the fact that the testing and predicted result can be affected by many factors including the selection of material models and strain energy functions as well as the testing conditions. The effect of the sample size (such as thickness) and the indenter size is also not well defined, this may vary with the materials and strain levels. This makes it much more difficult to define a robust inverse program and data analysis procedure. All these could be effectively established by developing a modern Python programming language as a tool to

search a wide range of material parameters set for rubber-like in smart and quicker method to characterise the material properties. Another area is the potential effects of new material behaviours. Recently many new materials are being explored such as negative Poisson's ratio or Modulus materials ([Evans K.E. and Alderson A., 2000](#); [Sanami M. et al., 2014](#); [Alderson K., et al, 2014](#); [Brighenti R., 2014](#); [Shufrin I. et al, 2015](#)). These materials hold the potential to open up new application areas. For example, material with negative Poisson's ratio has been found applications in many areas such as fabrics ([Sloan M.R. et al, 2011](#); [Subramani P. et al, 2014](#); [Ge Z. and Hu H., 2015](#)). It is important to establish the effects of these features (such as negative Poisson's ratio) on the material behaviour under indentation bending test.

CHAPTER THREE

INVERSE FINITE ELEMENT (FE) MODELLING METHOD TO DETERMINE THE HYPERELASTIC MATERIAL PARAMETERS BASED ON INDENTATION BENDING TESTS

3.1 Introduction

As shown in Figure 3.1, there are three main parts in the work: experimental tests, FE modelling and inversed program. The experiment work is carried out with latex rubber sheet of different thicknesses and diameters. Standard tests including uniaxial test and planar test are used to characterise the material and produce input material data for the FE model to assess its accuracy and evaluate the suitability of different strain energy functions. Relaxation tests based on indentation bending tests are also performed; the result is to be presented in Chapter 4. The testing data is also used the target to assess the accuracy of the inverse FE program for material parameters estimation.

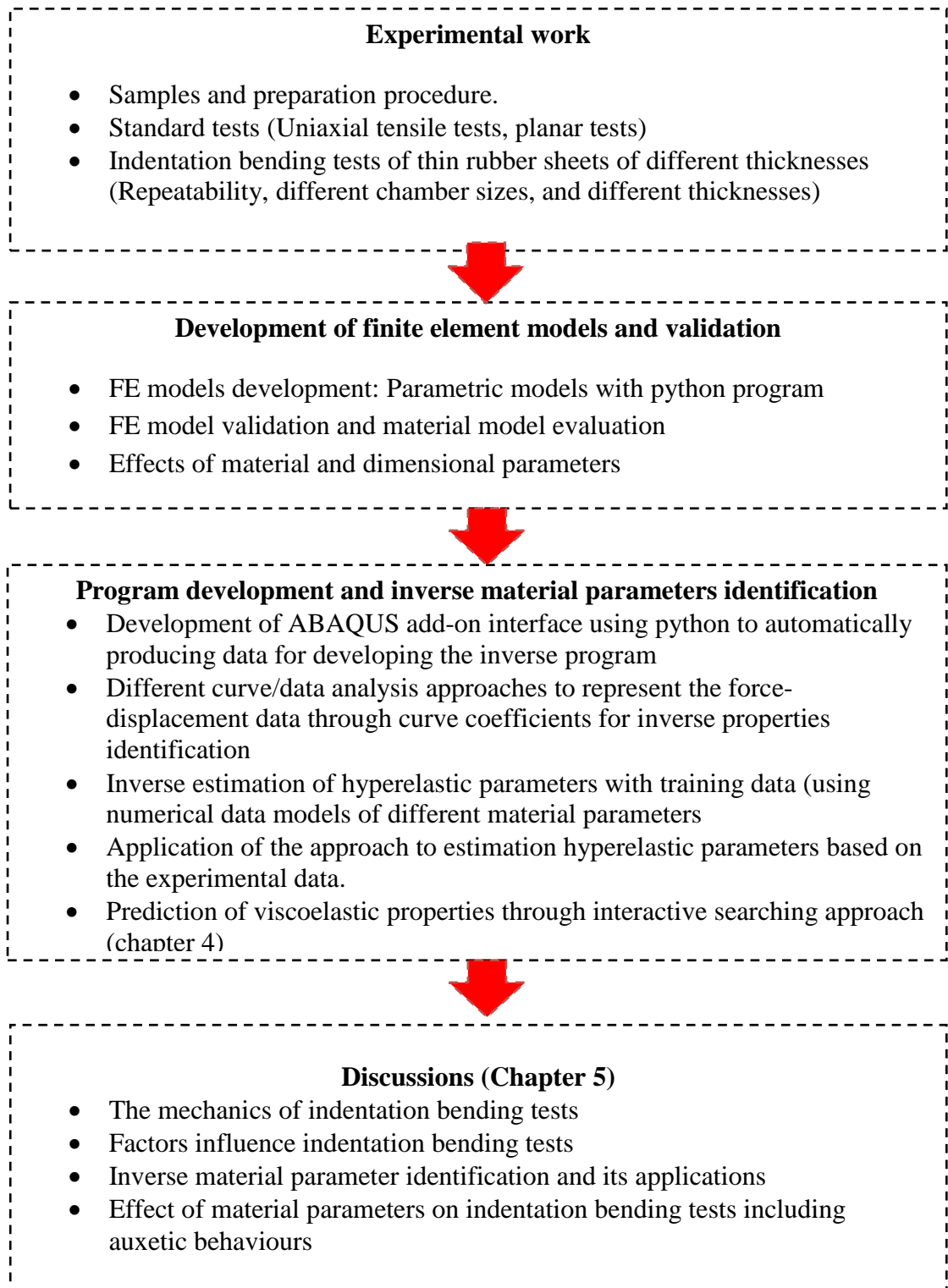


Figure 3.1 Flow chart showing the research work: The experimental tests, numerical modelling and inverse FE modelling.

Finite element (FE) models of indentation bending tests are developed using ABAQUS ([ABAQUS 6.11](#)). The effects of element size and the frictional conditions represented by different friction coefficients are investigated using parametric studies. The FE model is validated by comparing the FE result with experimental data. The FE model with linear elastic material models is validated against analytical solutions from published papers and known the analytical solution for specific conditions (e.g. point loading condition) ([Komaragiri U. et al, 2005](#)). An ABAQUS add-in parametric program has been developed using the Python code to produce systematic data over a wide range of material parameters. Three main approaches have been developed to characterise/represent the force-displacement data through different curve parameters, which are to be detailed in section 3.4. The validity and accuracy of the inverse program is systematically assessed using training data (i.e. using numerical data as the target data for the inverse program) before being used to analyse the experimental data. An inverse program is also developed for estimation of the time dependent material parameters with indentation bending tests. The key viscoelastic parameters are determined through combining experimental test data and numerical simulation results through an objective function based approach and a two stage interactive curve matching program. In the discussion (Chapter 5), several main topics are discussed in details include the mechanics of indentation bending tests, main issues/factors influencing an indentation bending test, potential applications and limitation of the inverse FE modelling approaches, and effects of material parameters including auxetic material on the material behaviour.

3.2 Experimental works and results

3.2.1 Rubber sheet sample preparation

The experimental tests were performed using liquid latex rubber as the model material. The Latex or liquid rubber is a prevulcanized emulsion which can form a highly flexible thin rubber or mould. Samples for different types of tests were moulded into different shapes, including indentation bending tests, uniaxial tensile test and planar test, as shown in Figure 3.2. All the samples were from the same batch of liquid latex under an identical processing procedure. The use of single part resins ensures that the rubber is homogeneous and the thickness is controlled by the volume of the resin. The moulding and curing process was performed at room temperature. In general liquid latex contains polymer produced by the reaction of monomers in presence of initiators or catalysts. Surfactants are used to stabilise these polymer particles in water during emulsification. After removed moisture, formation of strong bridge bonded between individual latex particles with polymers ([Steward P.A., et al, 2000](#)). To fully evaporate water within the liquid latex, sample was left in the mould for 24 hours to ensure the effect of curing process for each rubber sheet sample was comparable. The circular sample for the indentation bending tests was made using a plastic circular mould with a diameter of 40mm as shown in Figure 3.2(a). The 'dog bone' shaped sample moulded for the uniaxial tensile test is 10mm wide with a gauge length of 100mm as shown in Figure 3.2(b). The planar test sample is 120mm wide with a gauge length of 12mm as shown in Figure 3.2(c). The standard uniaxial tensile tests and planar tests are performed to characterise the material to provide data to validate the FE model and provide data to assess the accuracy of the inverse material parameters prediction.

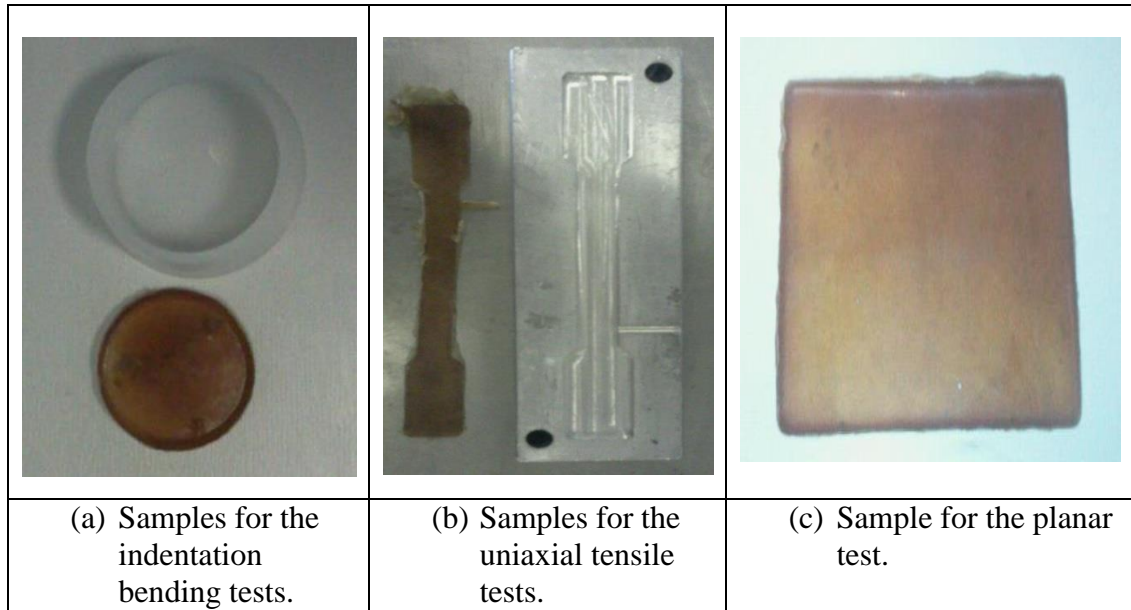


Figure 3.2 Samples of rubber sheets used in the indentation bending tests, uniaxial tensile test and planar tests.

3.2.2 Uniaxial and planar tests of the rubber material and results

The uniaxial tensile tests were performed on a standard tensile testing machine shown in Figure 3.3(a) (Model: Tinius Olsen, H50KS) equipped with 2 types of loadcells in different load ranges (10N and 500N). A 500 LC laser extensometer was used to measure the deformation of the rubber sheet by monitoring the movement of two reflective markers placed on the surface of the rubber sheet as shown in Figure 3.3(b-c). The purpose of conducting tests under different stress strain conditions was to obtain data for extracting the nonlinear material properties as there are multiple material parameters involved in the hyperelastic strain energy functions. A testing rate of 5mm/min was used in the experiments and at least three samples were tested and the average data was used. Figure 3.4 shows typical experimental data showing the force-displacement. The engineering stress over strain curve was determined and the result was plotted in Figure 3.5. These stress strain data was then used as an input into the FE model, the hyperplastic parameters could be then determined through the material evaluation function available in ABAQUS. The data could also directly be used to validate the FE model and evaluate the suitability of the linear elastic and hyperelastic models.

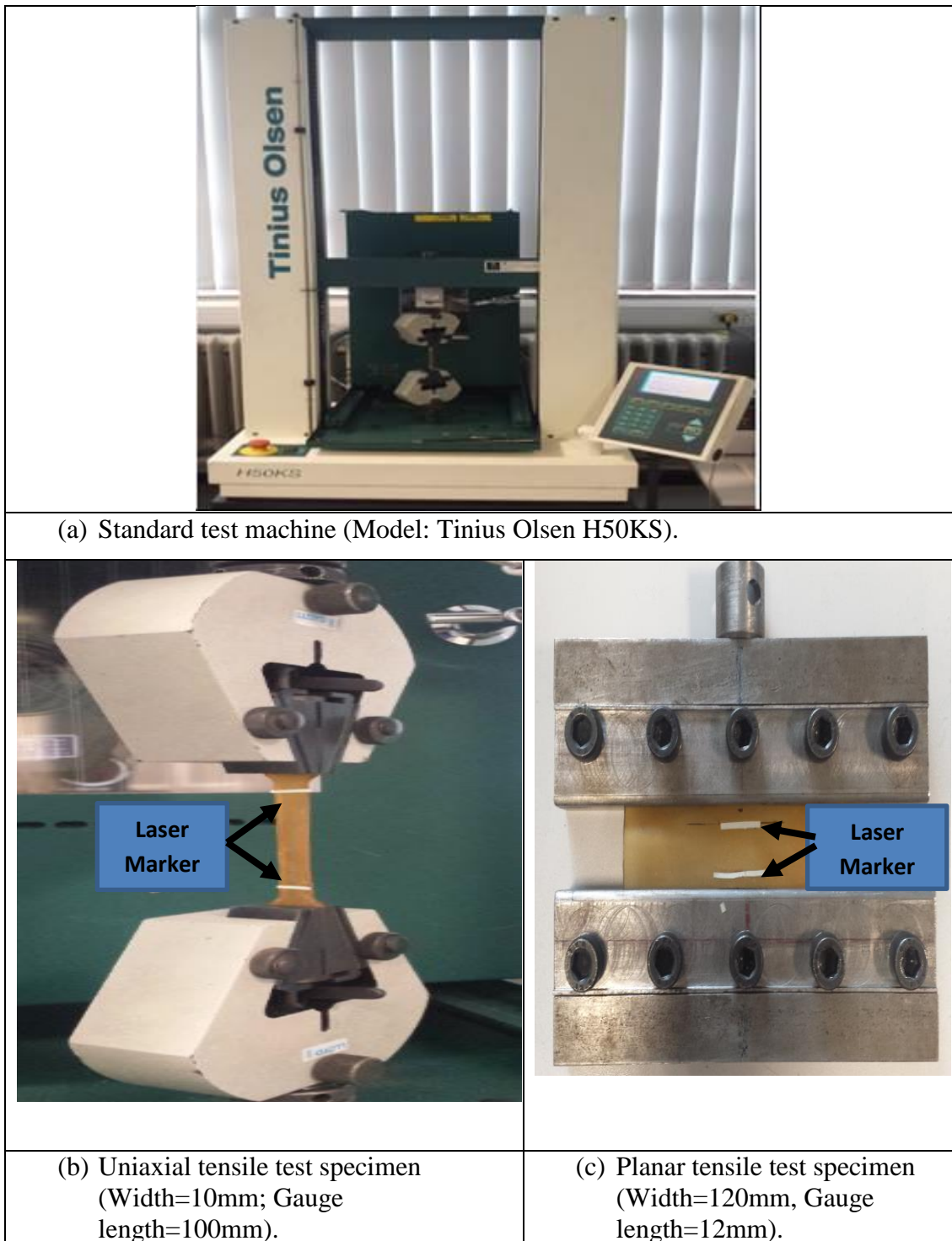


Figure 3.3 Tensile test machine (a) and the setup of the uniaxial tensile test (b) and planar tensile tests (c).

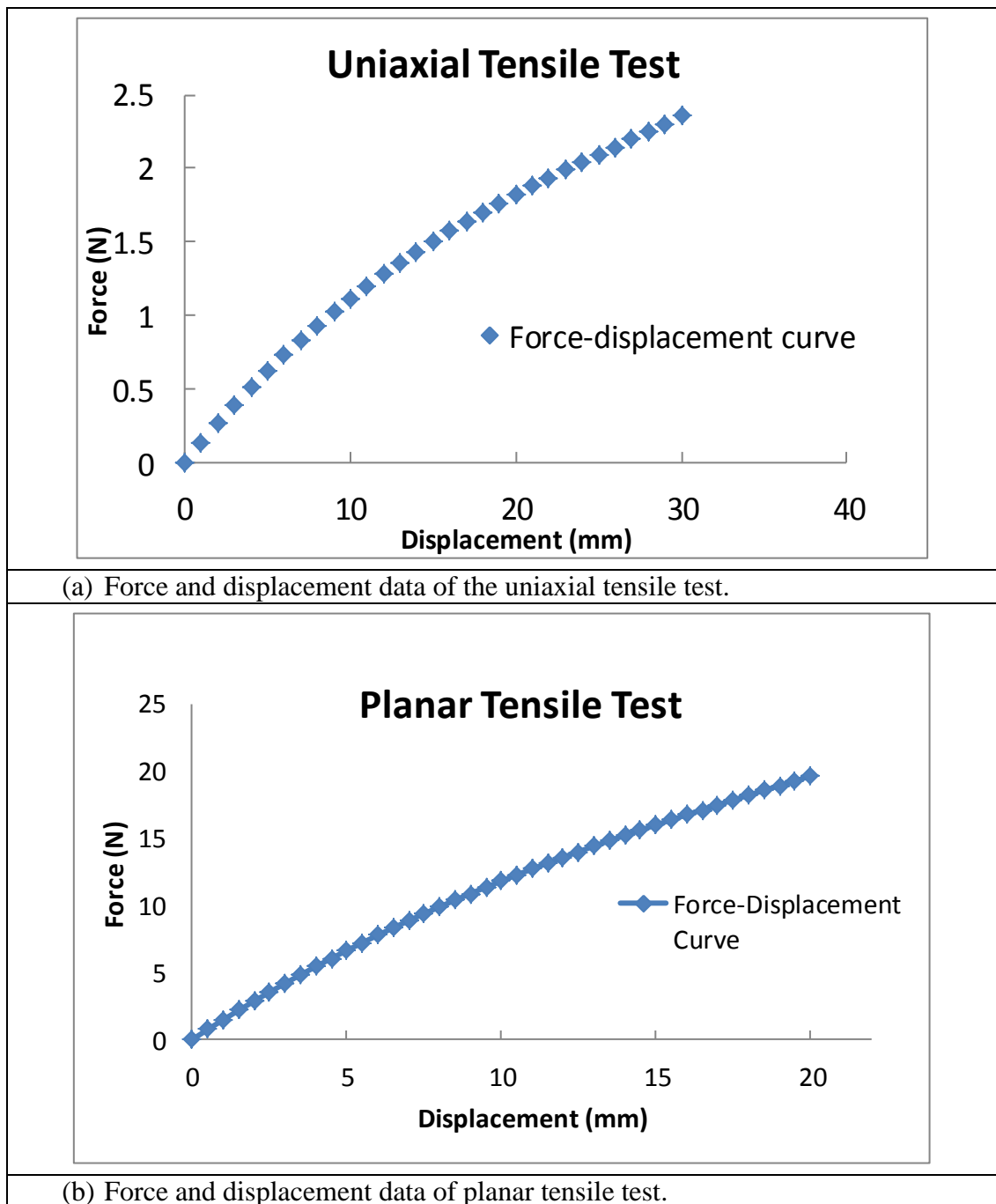


Figure 3.4 Typical force and displacement data of the uniaxial tensile test(a) and planar tensile test (b).

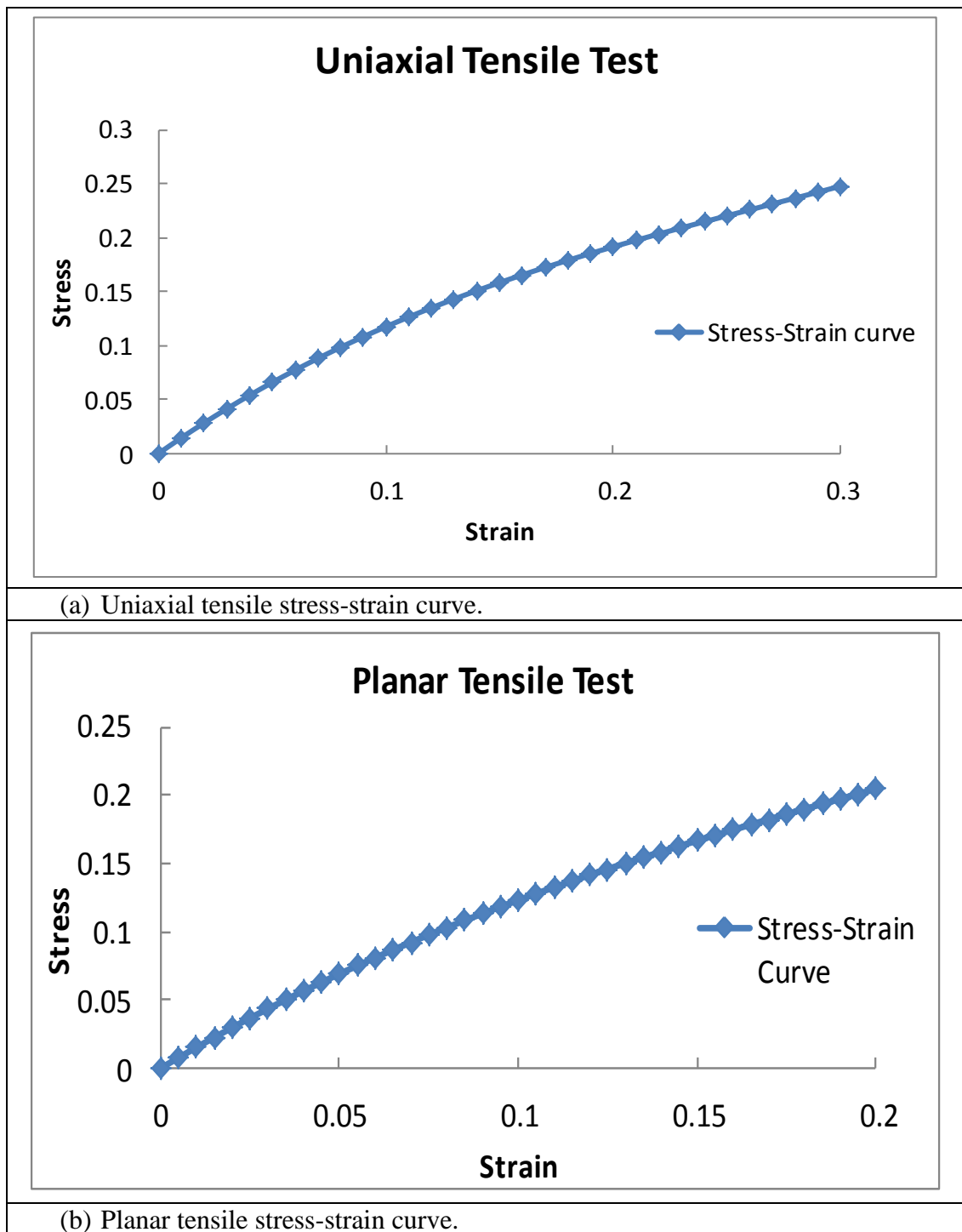


Figure 3.5 Stress-strain curves for uniaxial tensile test (a) and planar tensile test (b) of the rubber sheet.

3.2.3 Indentation bending tests and results

Figure 3.6 shows the experimental set-up of the indentation bending test system. As shown in Figure 3.6(a), the test system was setup on a standard testing machine. The indenter was connected to the cross-head of the tensile test machine with a load cell monitoring the force and the force-displacement was recorded by the computer. The accuracy of the force and displacement was calibrated by comparing from other machines. Figure 3.6(b) is a chart showing the main function of the key components and Figure 3.6(c) shows the indentation process and the sample holder. Metal cylindrical chambers of different diameters have been made which controls the dimension of the sample being tested, the two mainly sizes used in this work are 20mm and 30mm in diameter, which are designated as sample size 20 and 30 (Ch20 and Ch30). Most of the data reported in the thesis used a spherical indenter with a radius of 4mm (R4) made of stainless steel. The rubber sample was clamped onto the chamber made of brass with three evenly spaced screws (Figure 3.6(d)).

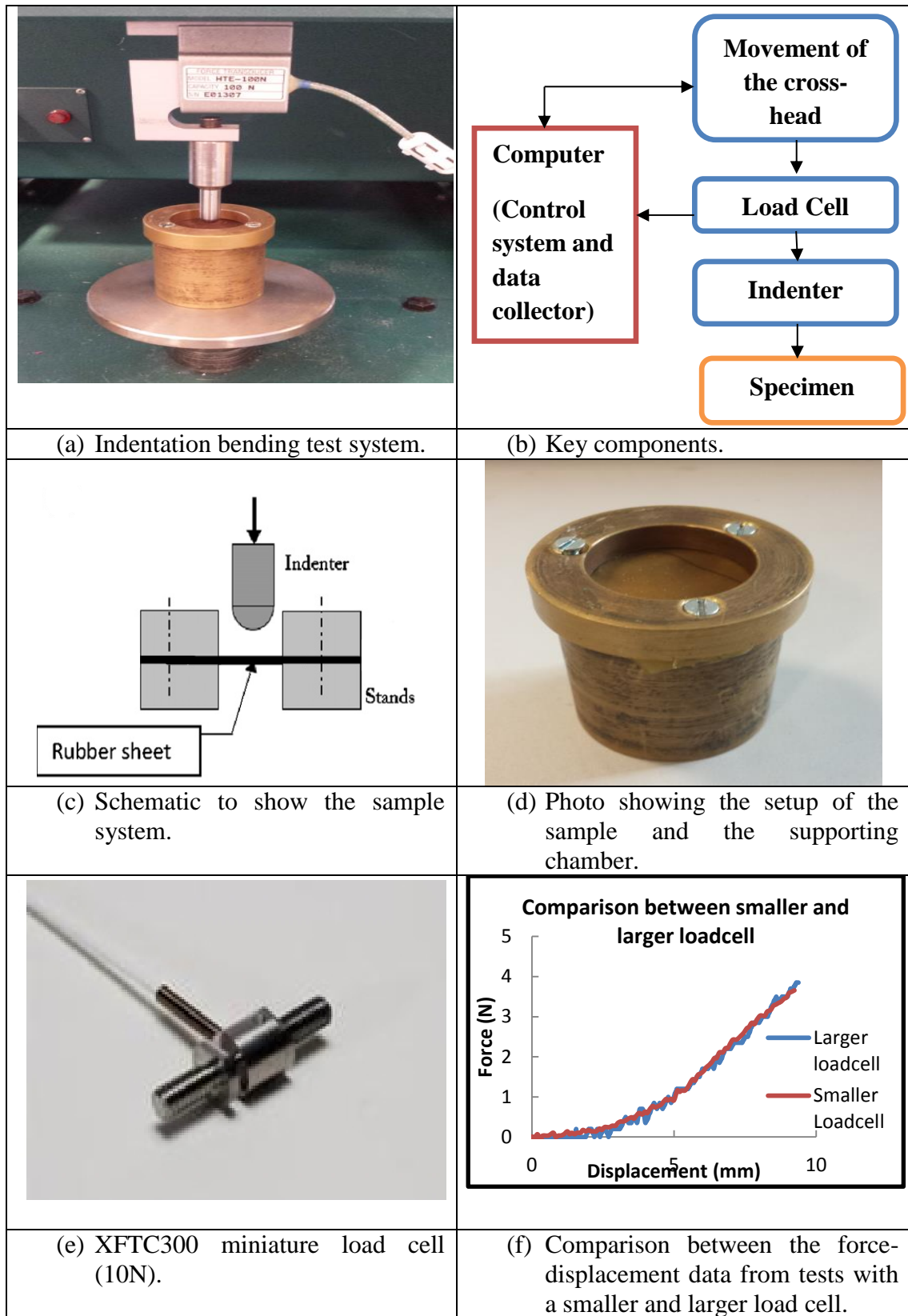


Figure 3.6 Structure and setup of the indentation bending test system (a&b), the sample holder (c&d), smaller load cell and typical force-displacement curve (e&f).

Figure 3.7 are typical experimental results showing the repeatability of the tests when using a sample size of 20 and 30mm. The initial part of the testing data is not picking up by the load due to the sensitivity of the loadcell, but it was cross compared with a smaller loadcell (10N) shown in Figure 3.6(f). The XFCT300 series of miniature load cell has a measuring range from 0-10N. With the smaller load cell, initial load of P-h curve can be determined and the curves were comparable. The limitation of the smaller load cell lies in the fact that it is unable to do large deformation especially for smaller sample size. The cross comparison between smaller and larger load cell (500N) to certain extent shows that the testing data are accurate. The average of at three testing data was used to represent the results. Figure 3.8 shows the effect of different loading rate on the force and displacement data. In the work, the tests were performed using loading (displacement) rates ranged from 1mm/min to 10 mm/min to a pre-set displacement of 10mm. The results show that there is no significant influence of the loading rate on the force-displacement data within the load range tested. A reasonable testing rate of 5mm/min was used in the experiments, which is relatively easy to control.

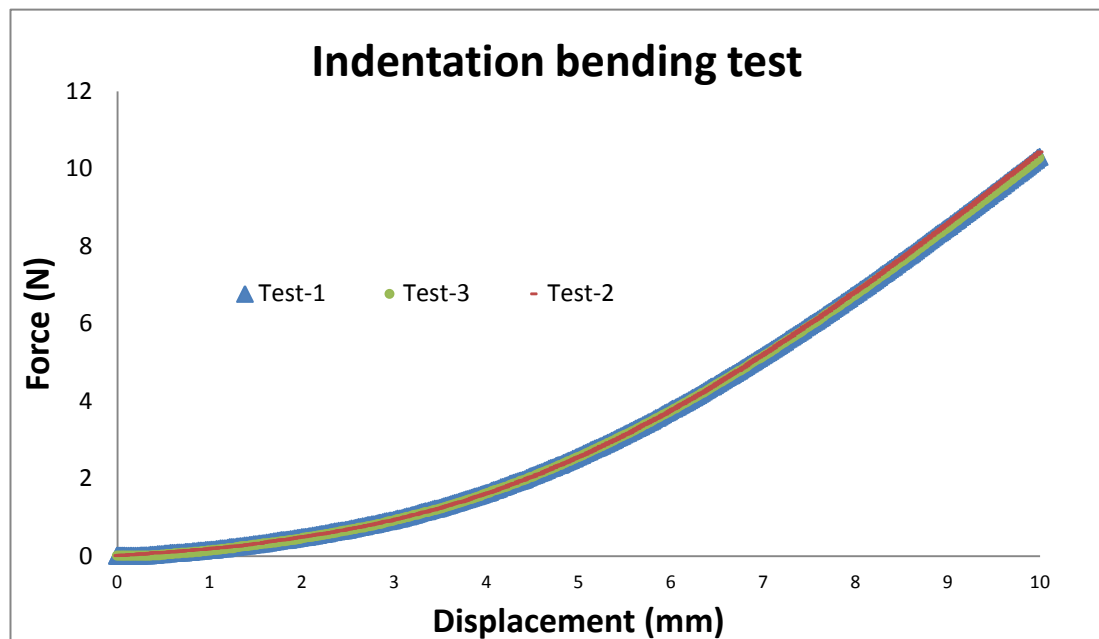


Figure 3.7 Typical experimental force-displacement data showing the repeatability of the test. (Chamber size, diameter=20mm, Sample thickness=0.8mm).

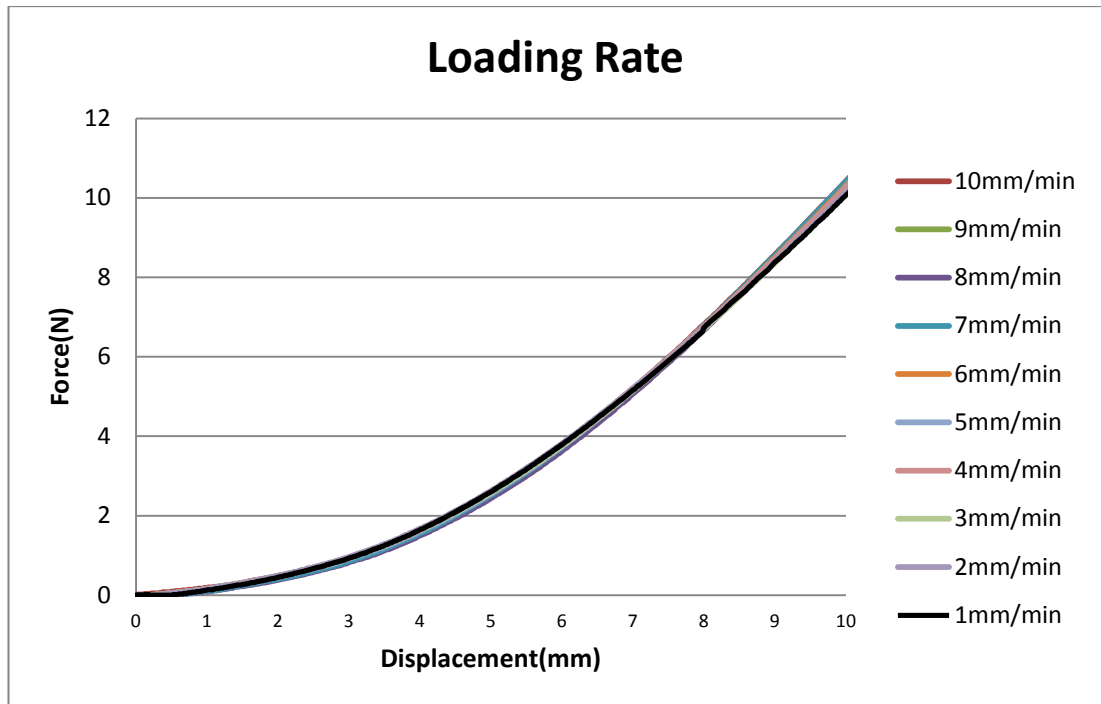
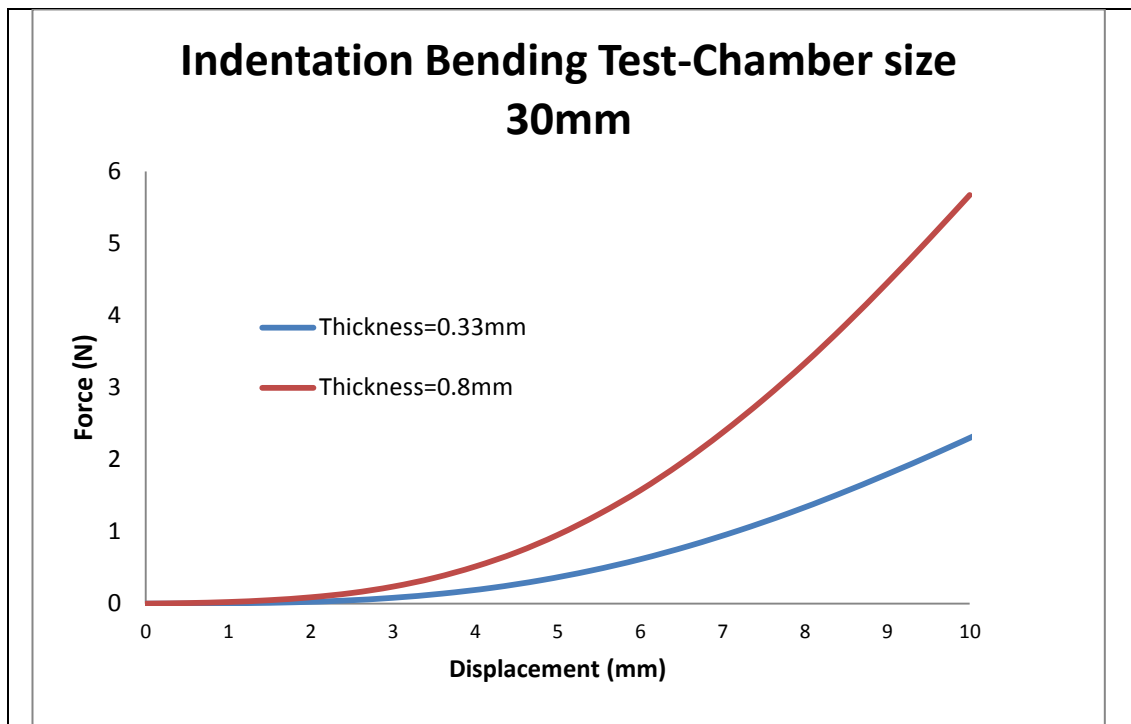
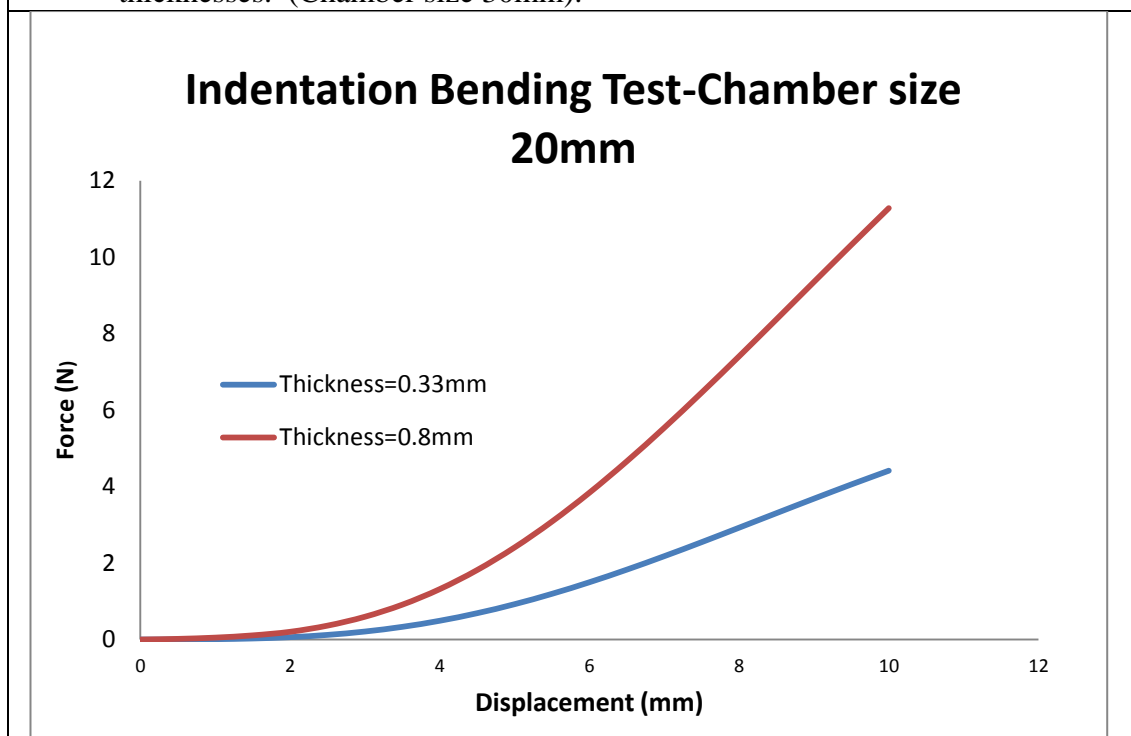


Figure 3.8 Typical testing data with different loading rates. (Sample Thickness=0.8mm; Chamber size diameter=30mm).

The effect of sample thickness on the force-displacement data was investigated by conducting tests on rubber sheets with different thicknesses made from the same batch. Figure 3.9(a&b) shows typical force and displacement data for two typical thicknesses (0.3mm and 0.8mm) with a chamber size of diameter 30mm or 20mm. In both cases, the curves have shown a similar trend but the thicker sample exhibits a higher resistant force in particular over the higher displacement range.



(a) Typical experimental force-displacement data with different sample thicknesses. (Chamber size 30mm).



(b) Typical experimental force-displacement data with different sample thicknesses. (Chamber size 20mm).

Figure 3.9 Force-displacement data of rubber sheet of different thicknesses.

3.3 FE modelling of indentation bending tests and validation.

3.3.1 Hyperelastic FE model of indentation bending test

As explained in 3.1, the FE modelling work involves initially building an FE model mimicking the indentation bending tests, then an ABAQUS add-on is developed which enables automatic generation of a large scale data over a wide range of material properties. The add-on is developed based on the .rpy file associated with ABAQUS cae file. This requires a carefully planning in building the FE model following a proper procedure (Figure 3.10), otherwise the add-on will repeat some operations unnecessarily. The procedure to build the FE model in ABAQUS is shown in Figure 3.10. The first stage of the model is to create each individual part with the same shape and dimensions to mimic the experimental work. The rubber sheet is modelled as a 3D deformable shell with S4R four-node shell element with reduced integration. This type of element has 6 degrees of freedom (3 displacement and 3 rotation components at nodes) and based on first-order-shear deformation theory in which the transverse shear strain are assumed to be constant through the thickness of the shell. The indenter is modelled as an analytically rigid part, as it is a lot stiffer ($E_{\text{steel}}=200\text{GPa}$) than the rubber sheet. Analytical rigid was used instead of discrete rigid as the shape of the indenter is smooth and is not an arbitrary shape. Analytical rigid is less expensive in terms of computational resources and time compared to that when the indenter is treated as a discrete rigid body. In the assembly section, the parts are assembled together in the correct position mimicking the experimental condition as shown in Figure 3.11(a). Two types of approaches have been used to assign the material properties. The first approach is directly inputting testing data in the form of stress-strain curves based on the standard uniaxial tensile tests and planar tests data (Figure 3.5). The second approach is using material coefficients either for linear elastic model or hyperelastic model. As shown in Figure 3.11, the clamping force on the sheet is represented by fixing the outer rim of the rubber sheet to prevent the sample from moving/sliding away. A displacement is applied to the reference point of the indenter and reaction force on the indenter is extracted to represent the resistance. Figure 3.11(c) shows the typical vertical deformation field, which illustrates that the displacement increased gradually from the central point to the edge. Figure 3.11(d) shows a typical numerical force-

displacement data extracted from the FE model. The result shows that the initial increment of the slope of curve was relatively slow and becomes much stiffer as the displacement is increased.

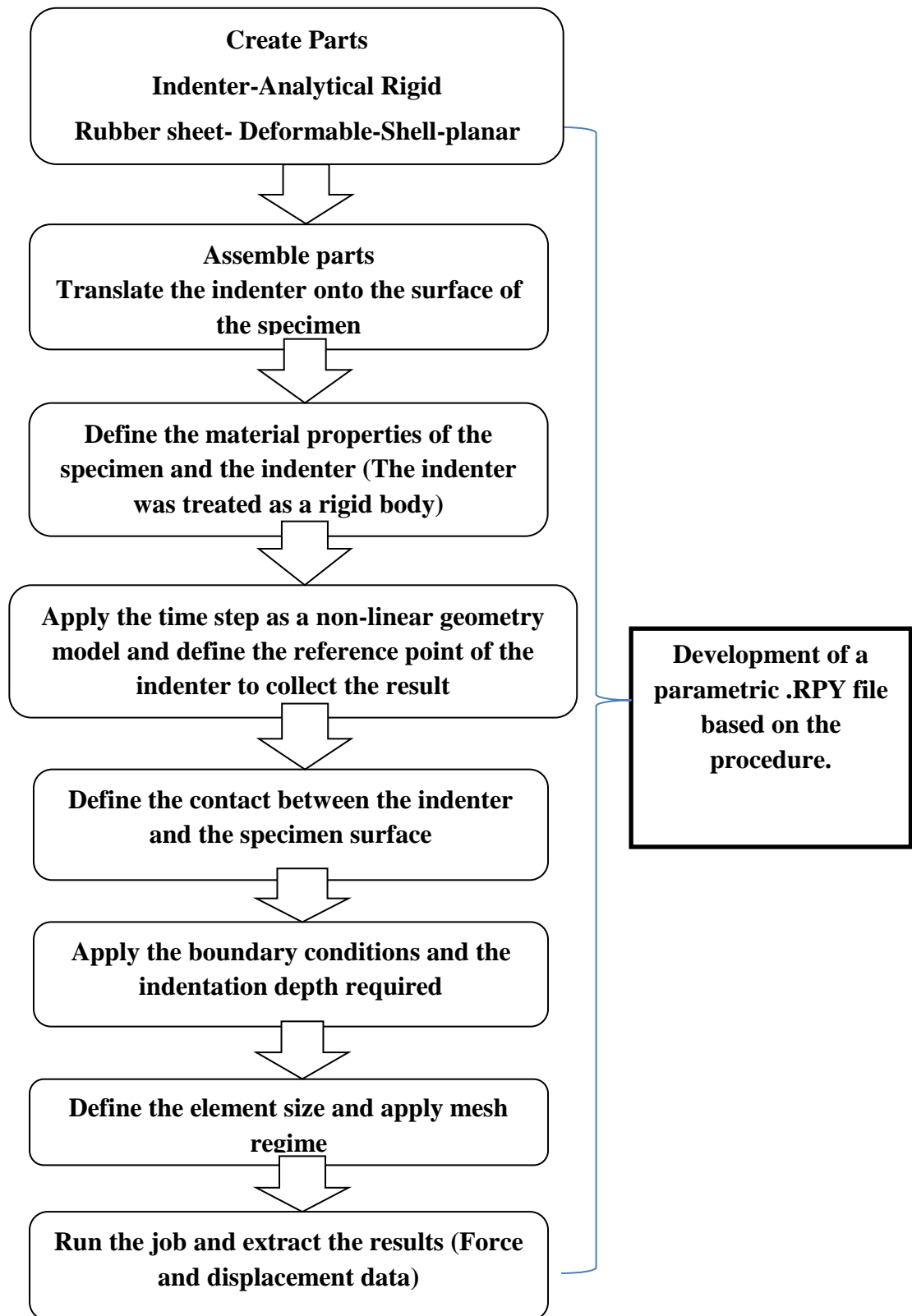


Figure 3.10 Flow chart showing the key procedure to build the ABAQUS model of the indentation bending test, which is used to produce the .RPY file.

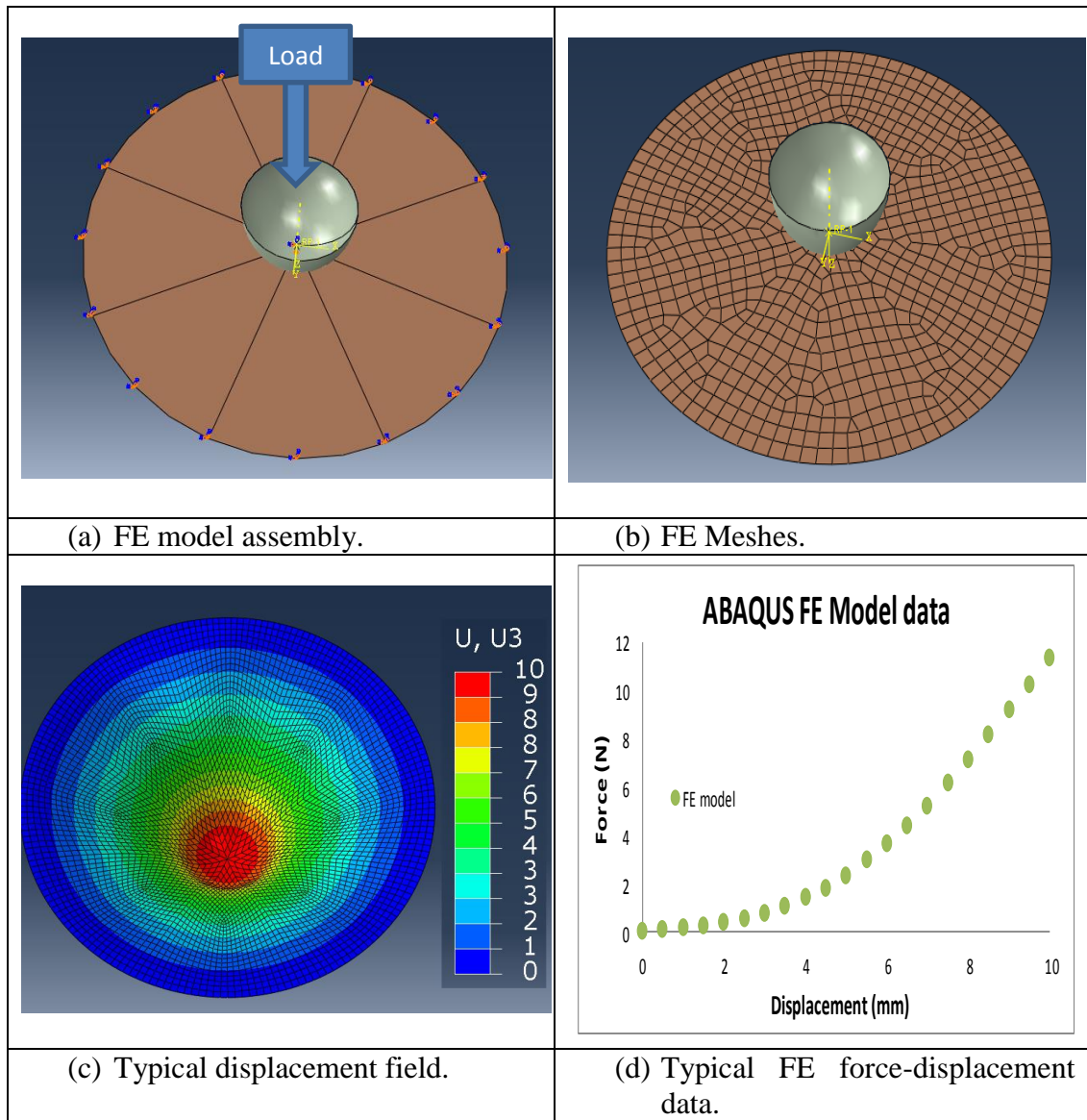


Figure 3.11 3D finite element model of the indentation bending tests (a) FE model; (b) Mesh of the model; (c) typical deformed shape (vertical displacement, U_3); (d) a typical force displacement data.

3.3.2 Mesh sensitivity tests and results

To achieve an optimum result, mesh sensitivity tests were performed in order to determine a suitable number of nodes and elements. This was done by increasing the number of elements in the model until the difference between the force-displacement data and stress-strain contour from two consecutive models became negligible. As illustrated in Figure 3.12(a-c), FE models with different mesh densities have been developed with all other parameters including material properties being kept the same. The material model used in the mesh sensitivity tests is a linear elastic model, where the properties are represented by the Young's modulus and the Poisson's ratio. The chamber size is 30mm in diameter and the sample thickness is 0.8mm. Figure 3.12(d) shows typical numerical force-displacement data extracted from FE models with different mesh sizes. It is clearly shown that, with larger elements, the curves are significantly different with much higher forces, and as the mesh size becomes smaller, the force displacement data become less sensitive to the mesh density. The FE with the finest mesh gives the highest accuracy of the numerical result, but the simulation time will increase significantly. For this model, the best choice of the mesh size is 0.1mm to achieve an optimum balance between demand on the computation resources and modelling accuracy.

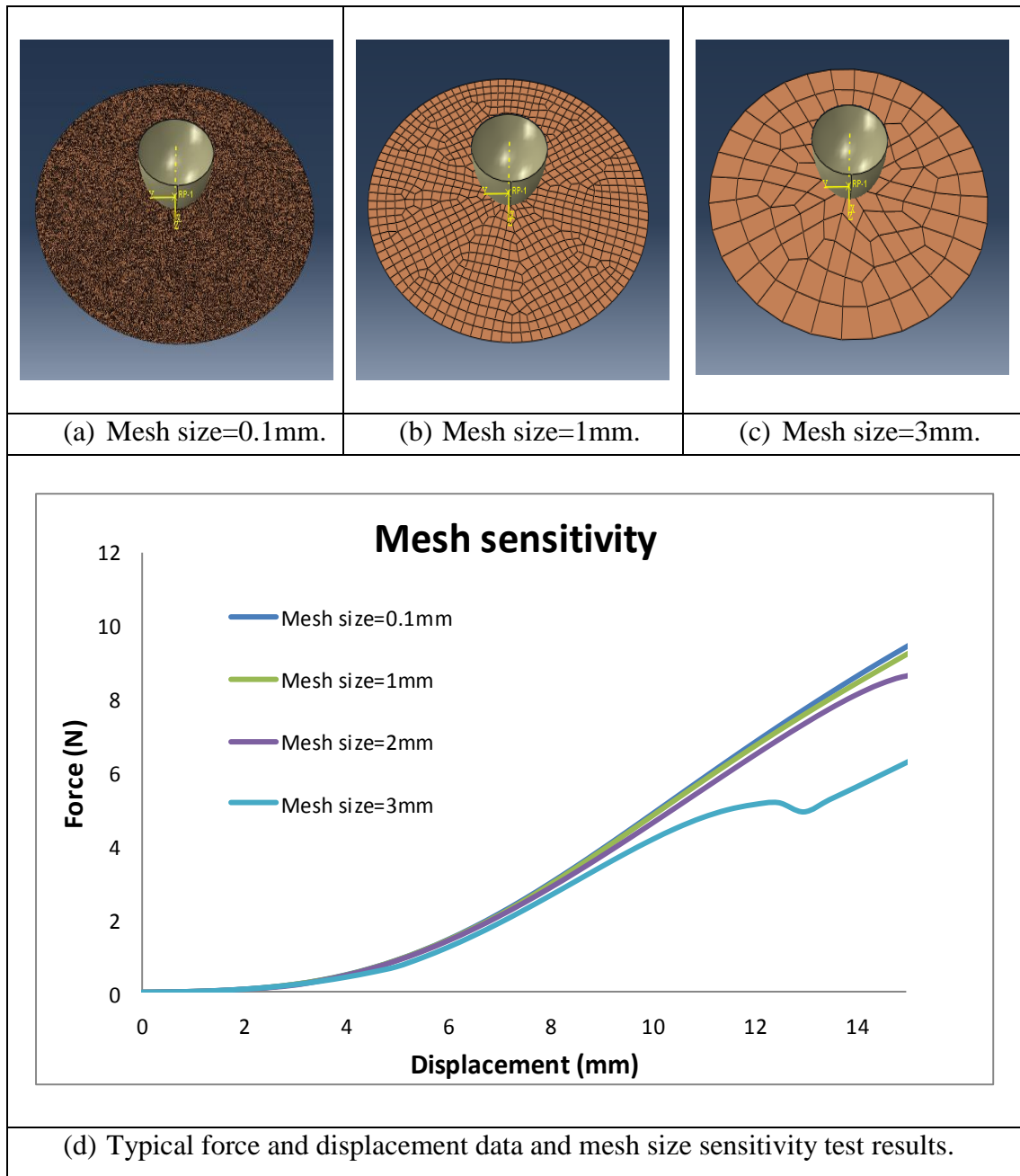


Figure 3.12 Mesh size sensitivity tests and results. (a-c): FE models with different mesh sizes for chamber diameter=30mm;(d) typical force and displacement data of FE models of different element size($E=1.25\text{Mpa}$, $\nu=0.495$).

3.3.3 Validation of the FE model with testing data and selection of suitable strain energy function for direct and inverse analysis

Different FE models with different hyperelastic models have been developed and compared to the experimental data. The most common used linear elastic model is represented by two material parameters which are Young's modulus and Poisson's ratio. The Young's modulus used $E=1.25\text{MPa}$ determined by initial part of the stress-strain curve of uniaxial tensile test data. The Poisson's ratio was set at 0.495 which is close to 0.5 as rubber is known to be an incompressible material. The suitability of several nonlinear models was assessed using the same tensile test data and planar test data as an input data but selecting different strain energy function in the FE model. Details of the strain energy functions involved are listed in Table 3.1. Figure 3.13(a&b) shows the force-displacement data when using different strain energy models together with experimental data. As shown in Figure 3.13(a), for a thicker sample, the linear elastic model match the experimental data up to a displacement of 4mm, while for a thinner sample, the force-displacement with the linear Elastic model match the experimental data up to a much higher displacement. While the numerical data with the Ogden model (1st order) is in a good agreement to the experimental data over the displacement range for all the cases. The match between experimental data and numerical data suggests that the FE model is valid and accurate. The validated FE model will be used to investigate the effect of key testing and material parameters on the testing results and to develop an inverse FE modelling approach to predict the material parameters.

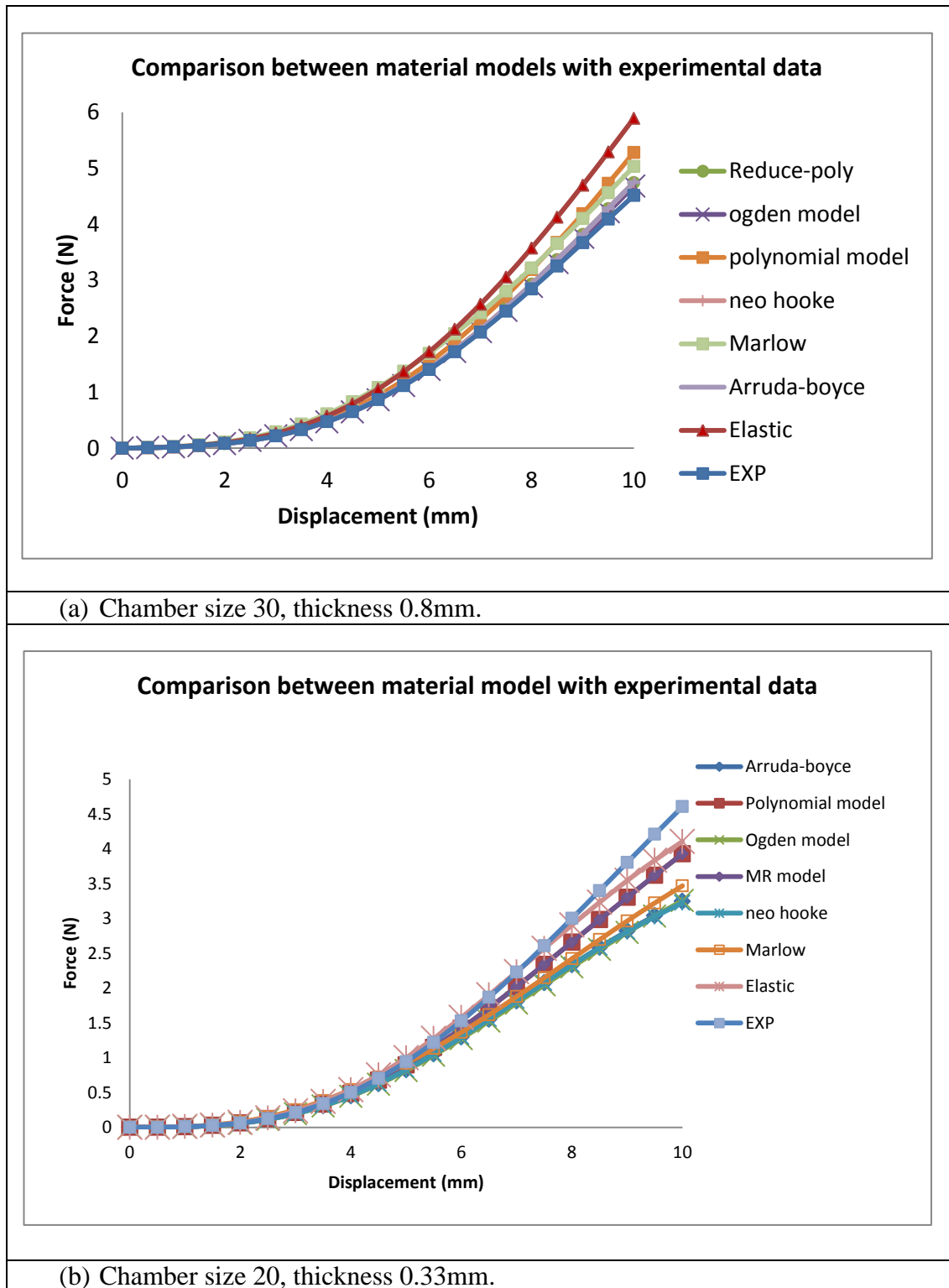


Figure 3.13 Comparison between experiment result and FE results with different material models based on the combination of tensile test and planar test data of the rubber sheet.

There are some material models, for which the FE data is also close to the experimental data including Mooney Rivlin, polynomial, Neo Hooke and Arruda-boyce. However, preliminary works reveals clear limitation of these models such as suitability of a wider range of materials or lack of uniqueness, or interlinking between the material parameters, therefore the main work will be focused on the 1st order of the Ogden model, represented by the two material parameters μ and α .

Table 3.1: List of different material models assessed in this work.

Material Models	Governing Equations	Main material parameters
Linear Elastic model	$\sigma = E\epsilon$	E, and ν
Mooney Rivlin model	$W = C_{01}(\bar{I}_2 - 3) + C_{10}(\bar{I}_1 - 3) + D_1(J - 1)^2$	C10 and C01
Ogden model	$U = \sum_{i=1}^N \frac{2\mu}{\alpha_i^2} (\bar{\lambda}_1^{\alpha_i} + \bar{\lambda}_2^{\alpha_i} + \bar{\lambda}_3^{\alpha_i} - 3) + \sum_{i=1}^N \frac{1}{D} (J^{el} - 1)^{2i}$	μ, α and Di
Neo Hookean model	$W = C_1(\bar{I}_1 - 3 - 2\ln J) + D_1(J - 1)^2$	C1 and D1
Arruda-Boyce model	$W = D_1 \left(\frac{J^2 - 1}{2} - \ln J \right) + C_1 \sum_{i=1}^5 \alpha_i \beta^{i-1} (\bar{I}_1 - 3^i)$	D1, C1 and β

3.4 Inverse FE modelling for material parameters prediction

In an inverse FE process, the materials parameters are determined by determining the material property sets which produce a numerical results best match the target experimental data. One key aspect is how to represent the curves. For indentation of elastic-plastic materials, the curve can be represented by the curvature ($C \sim P/h^2$), while for the force-displacement data of indentation bending tests of a hyperelastic material, it is not clear which is the best way. In this work, three approaches are proposed and their suitabilities to be used to extract the hyperelastic material parameters from the force-displacement data are evaluated. The main results will be focused on the Ogden model to illustrate the working structure of the program where the two main parameters are $\mu(\mu)$ and $\alpha(\alpha)$. The three approaches are briefly explained below.

Curvature (P/h^3) approach

The first approach is designated as “curvature approach”, which involves calculating the curvature value (P/h^3 , where P is force and h is the indentation depth) over the small displacement section of the force displacement curve.

$$P = Ch^3 \quad (3.1)$$

This idea is based on the Schwerin equation for a point loading condition. ([Komaragiri et al, 2005](#)). The analytical solution (equation 3.2) is based on a modified Schwerin point loading condition with consideration of the influence of the Poisson's ratio.

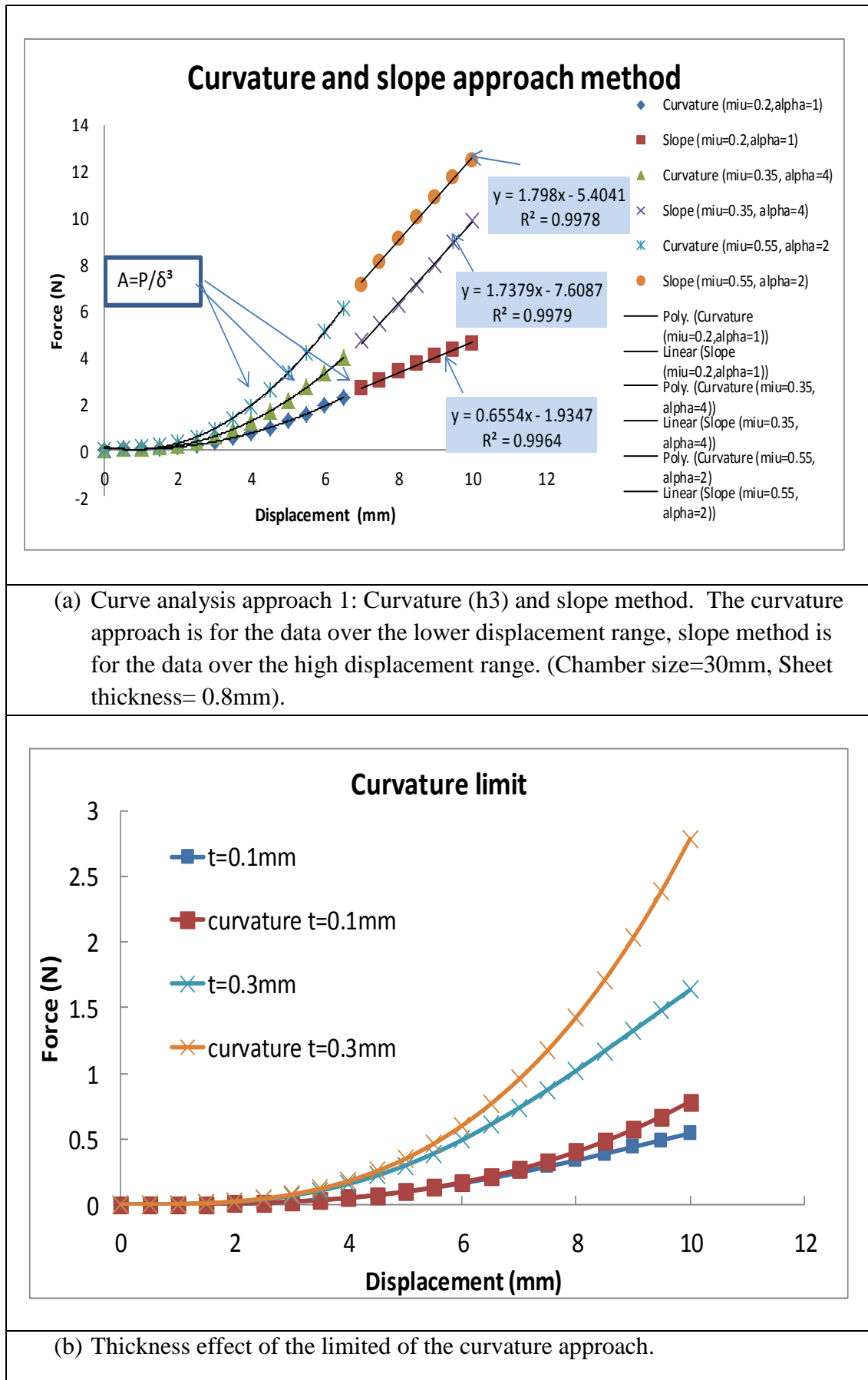
$$h = f(\nu)a \left(\frac{P}{Eat} \right)^{\frac{1}{3}} \quad (3.2)$$

In the equation, ‘ a ’ is the diameter of the chamber; ‘ h ’ is the indentation depth/deflection; ‘ P ’ is the force (N) and ‘ t ’ is the thickness. $f(\nu)$ is a material constant if the Poisson's ratio is known. As shown in Figure 3.14 (a), preliminary analysis shows that the initial part of the data follows this relationship. So, for a situation where the chamber diameter ‘ a ’, and sample thickness is fixed, potentially these relationship of the P/h^3 may still be valid and can be used to approximately

represent the material resistance. Details are presented in section 5.1 on the mechanics of indentation bending tests. If we designated C as $C(h^3)$ to distinguish it from the C for indentation test on elastic-plastic materials ([Li J. et al, 2012](#); [Marteau J. et al, 2012](#)), then $C(h^3)$, the curvature value, is the function of $\mu(\mu)$ and $\text{Alpha}(\alpha)$ with different material parameters but same chamber size and thickness.

$$C(h^3)=f(\mu, \alpha) \quad (3.3)$$

This curvature could potentially provide a mechanism of representing the curve through a single curvature value, which will make the inverse FE modelling process mathematically viable and much easier to program by establishing the relationship between the curvature and the material parameters. Similar approach has been used in dealing with elastic-plastic materials for indentation tests, where $P=Ch^2$ ([Gouldstone A. et al, 2007](#); [Zeng K. and Chiu C. H., 2001](#); [Giannakopoulos A. E., 2006](#); [Zisis Th., 2011](#)). Table 3.2 below shows the correlation coefficient when using the curvature to fit the P-H data for different sample thicknesses. In this process, the curvature value of each p-h curve with different thicknesses was calculated and then this C value is used to recalculate the force (P) of each curve by equation 3.1. As shown in Table 3.2 the correlation coefficient, the approach for the thinner sample is better than thicker samples, this approach is not applicable for some thicker samples. As shown in Figure 3.14 (b), comparison between two curves, one from experiment data and the other from $C(h^3)$ calculation. For the case with a thickness of 0.1mm, the result is close to the numerical data. However, for thickness 0.3mm the curve calculate by $C(h^3)$ becomes different from the original data. The curve starting to split after 6.5mm indentation depth. This is used as the limit for the force-displacement data for the curvature based approach.



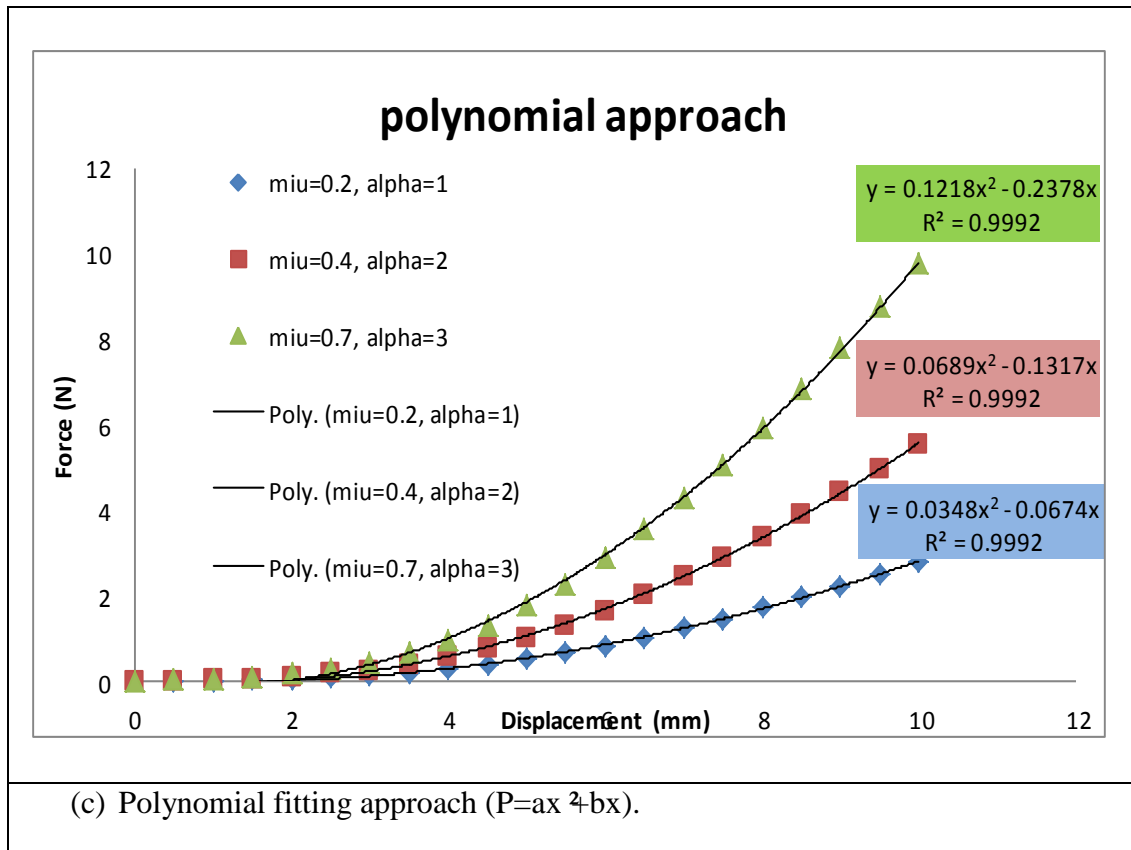


Figure 3.14 Typical feature of the P-h curve that provides coefficients representing the force displacement data to be used in the inverse FE modelling program.

Table 3.2: Correlation coefficient of curve fitting using $C(h^3)$ with different sample thicknesses. (Indentation depth 6.5mm)

Sample thickness	Correlation coefficient of two curve
0.1	0.999521
0.2	0.999467
0.3	0.999394
0.4	0.999307
0.5	0.999202
0.6	0.999076
0.7	0.998926
0.8	0.998748
0.9	0.998539
1.0	0.998295
1.5	0.996455
2.0	0.993462

Slope approach

The second method is designated as “slope approach”, which involves using the linear part of the curve at relatively large displacement. Analysis/observation of the data over a wide range of material properties revealed that the force-displacement data roughly follow a linear relationship at larger displacement. This part of the curve could be represented by the slope and intercept value. As illustrated, the coefficient of correlation is good enough to represent the data through this approach. If we treat the data as a linear line, then there are two parameters, one is the slope, and the other one is the intersection point with the horizontal axis. Both could be a function of the material parameters. These data are likely to provide another potential approach to inversely predict the material parameters by establishing the relationship between their relations with the material parameters. This approach might be more stable as it is using a trend and intercepting point.

Polynomial coefficients approach

The third method is designated as “polynomial approach”, which involves fitting the force displacement curve using second order polynomial equation as illustrated in Figure 3.14(b). Second order polynomial equation $P=ax^2+bx$ and the interception was set as ‘0’, as based on the physics, when the displacement is zero, then the force should be zero. In this approach, each of the curves could be represented by a combination of ‘a’ and ‘b’ values, both are function of the material properties, which potentially can be used in an inverse FE program for identifying the material parameters from an indentation bending test.

Further details of each of these three approaches and typical inverse modelling results are to be presented in the following sections. In each case, the use of single chamber size data and dual chamber (chambers of different sizes) is comparatively studied. The main purpose is to assess the accuracy, robustness and uniqueness of the inverse results, which are important for practical application of inverse FE modelling programs for material property identification. Once the force displacement data is characterised through curve parameters, then it is relatively easy to mathematically work out the relation between the material parameter and the curvature parameter (e.g. the curvature, slope etc.). Then the material parameters can be predicted. This requires generating data over a wide range of material properties and a proper approach to establish the mathematic link.

3.5 Structure of the data analysis and inverse material parameters identification program

Figure 3.15 shows the process to produce and analyse the data. In the first part of the work, an ABAQUS add-on python program is developed to generate a series of models within a potential range of material properties to form a simulation space as shown in Figure 3.16. The Pseudo code illustrating the main steps and functions structure of the program are listed in Table 3.3. The range and the density of data in the simulation space can be properly controlled using the ABAQUS add-on. The ABAQUS add-on program allow the user to generate, execute and gather the results from multiple analyses with different input parameters such as dimensional parameters or material parameters. In the next step, several python programs are developed to be able to automatically determine all the curve parameters including the curvature, slope, intercept, and 1st and 2nd order of polynomial trendline coefficients. A program is then developed in MatLab to produce three dimensional surface plot representing the mathematic relationship between the curve parameter (curvature, slope, intercept, or 2nd order of polynomial coefficient) and the material parameters (μ and α). The suitability of several different surface equations are to be coded and assessed as listed Table 3.4. A different program is developed for each equation in MatLab, which is then used to determine the surface plot coefficient (e.g. a, b, c, d, e or f) and evaluate their suitability in describing the relationship between the curve coefficients of the force displacement data and the material properties. The best one which is generally applicable to a range of data is the 3D parabolic equation. A MatLab program is used to solve this equation format to directly form a function between a material parameter and the curve parameters with 3 dimensional least-square polynomial methods. This provide a mathematical mean to estimate the material parameters either based on different parameters of the same curve or by combination of two different approaches with two chamber sizes. Some key code, procedure and results are to be presented in the following sections.

Table 3.3: Pseudo code to show main steps and functions of the program.

<p><i>Algorithm 1: paramatricStudy</i></p>
<p><i>Input: inputRequest, nodeSet, dataFromInputFile</i> <i>Output: tempFile, resultODB, resultReport, failedJobList</i></p> <ol style="list-style-type: none"> 1. inputRequest, request data from user(Dimension of the model, Material parameters and range, interaction properties, mesh type and mesh size) 2. tempFile, store variables from user inputRequest 3. materialParameterRange, define the range of material parameters 4. nodeSet, define a nodeSet for the reference point of the indenter 5. dataFromInputFile, create parametric rpy file 6. Update dataFromInputFile with inputRequest 7. $i=1$ 8. Create a Simulation Job-[i]with dataFromInputFile 9. While $i \leq \text{materialParameterRange}$: <ol style="list-style-type: none"> 10. Submit the Job-[i] in ABAQUS 11. OpenjobMessage from ODB[i] to read the job status 12. If jobMessage is Job-completed: <ol style="list-style-type: none"> 13. Open ODB[i] 14. NodeSet, obtain nodal force and displacement of the indenter 15. resultsReport, write results (force-displacement data) as a report (.rpt) 16. resultsODB[i], convert .rpt files of force and displacement into a plain text file following a structured framework for later access 17. $i+=1$ 18. Else: <ol style="list-style-type: none"> 19. Return the job[i] which has been failed to user, failedJobList 20. $I+=1$(continue while loop without break) 21. Return resultODB 22. Goto slopeFunction
<p>Where:</p> <p>inputRequest is a user interface to allow user input and asking questions.</p> <p>tempFile is a temporary file to store all the user input variables and range of material parameters</p> <p>materialParameterRange is a number of different material parameter sets for the numerical model need to be run</p> <p>nodeSet is a node set to record the reaction force and displacement from the history output</p> <p>dataFromInputFile is a rpy file which can be edited such as dimensions of the model, hyperelastic model material parameter, friction coefficient, mesh type, mesh size and job name.</p> <p>resultODB is a text file to store the force-displacement results corresponding to each material parameter sets ('α' and 'μ' for the Ogden model).</p> <p>failedJobList is a text file to store the job names of failed models</p>

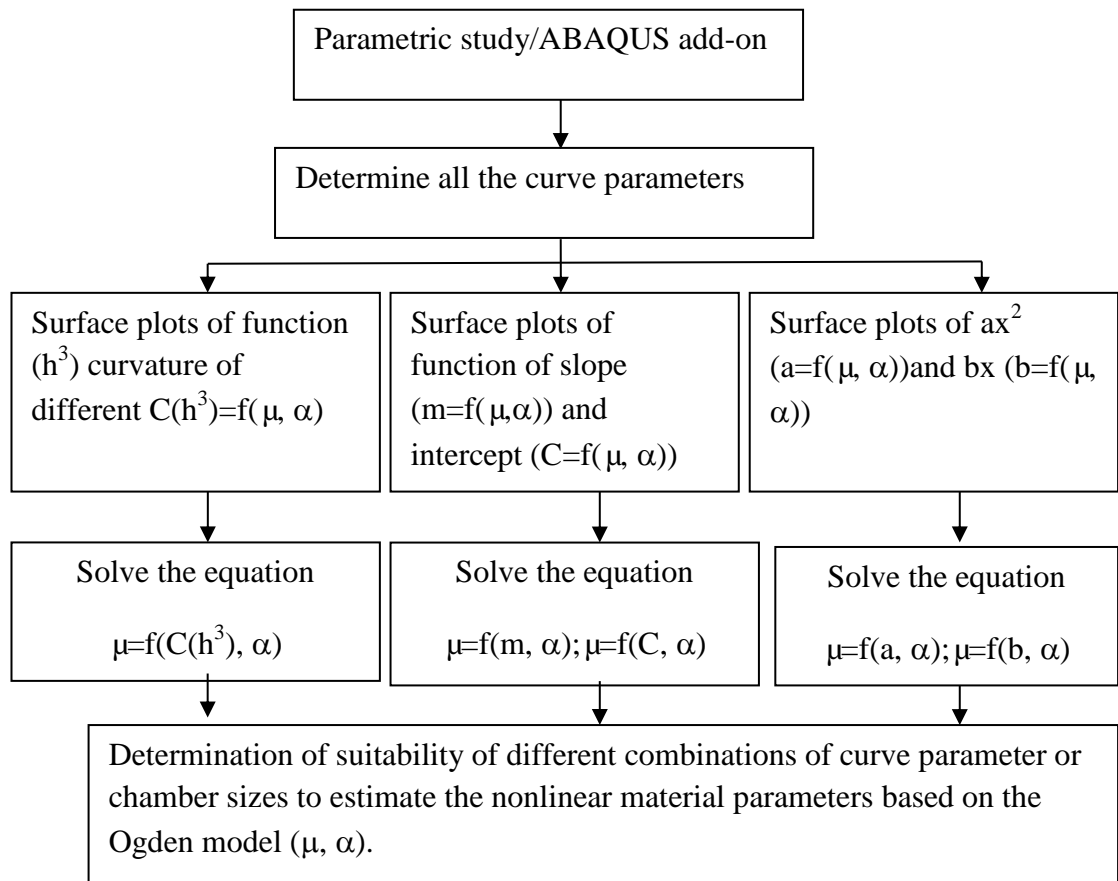


Figure 3.15 Structure of the program to estimate the material parameters.

```

C:\rpy-new>python option.py
Would you like to run single job or multiple jobs?
-----
Please select <1>.Single or <2>.Multiple jobs.2
Thank you.....
Indentation and Indentation bending module
-----
Please select <1>.Indentation module or <2>.Indentation Bending module.2
Thank you.....
Indentation bending model-Elastic or visco-Elastic material model
-----
Please select <1>.Elastic and Hyperelastic or <2>.Visco-elastic:1
Thank you.....
You had selected multiple jobs of Indentation bending module
-----
Please select material model.
Please select <1>.Elastic, <2>.Mooney Rivlin, <3>.Ogden, or <4>.Arruda_Boyce:3
Thank you...
Please wait...
You have selected Multiple jobs of Indentation bending module_Ogden material mod
el.
What is the the Radius of the sample <mm>?15
What is the Radius of indenter<mm>?4
What is the Thickness of the sample <mm>?0.8
What is the friction coefficient between indenter and plate?0.01
What is the indentation depth?10
What is the Mesh size of the plate?0.1
Please wait...
Abaqus License Manager checked out the following license(s):
"cae" release 6.11 from Jensen-TOSH
<1023 out of 1024 licenses remain available>.
Enter the first miu number start with:0.2
Enter the first alpha number start with:0.5
How many number of miu iteration?5
How many number of alpha iteration?5
What is the number of increment for miu?0.05
What is the number of increment for alpha?0.5_
  
```

Figure 3.16(a) Screen print of the add-on program.

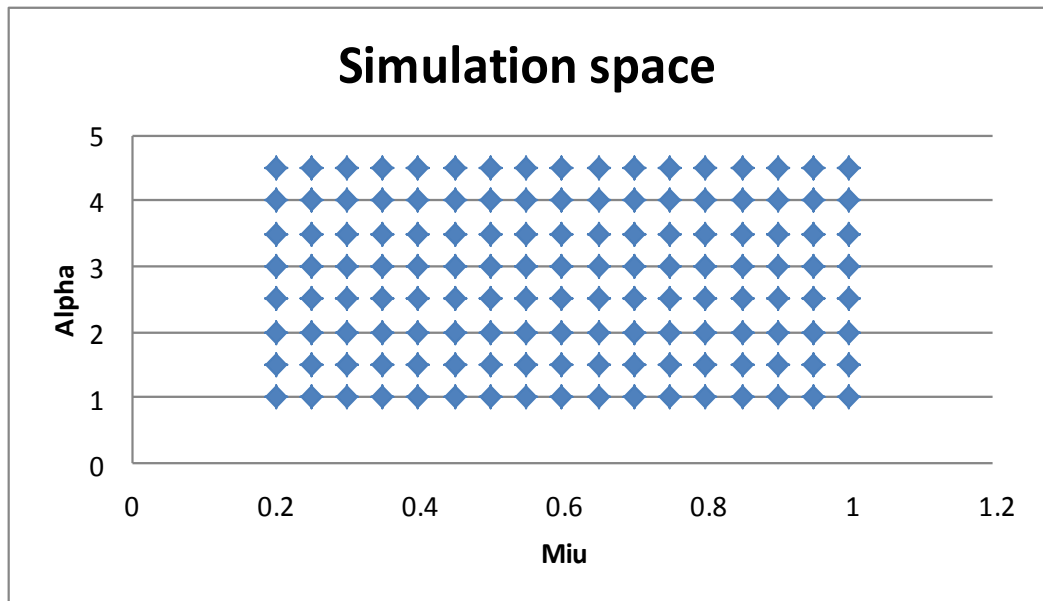


Figure 3.16(b) Large range of material parameters (μ :0.2-1, α :1-4.5)

Table 3.4: Different 3D surface equations evaluated.

Function	Equation
Plane	$z = z_0 + ax + by$
3D least squares polynomial(3 terms)	$z = ax^3 + bxy^2 + c$
3D least squares polynomial(6 terms)	$z = a + bx + cx^2 + dxy + ey + fy^2$

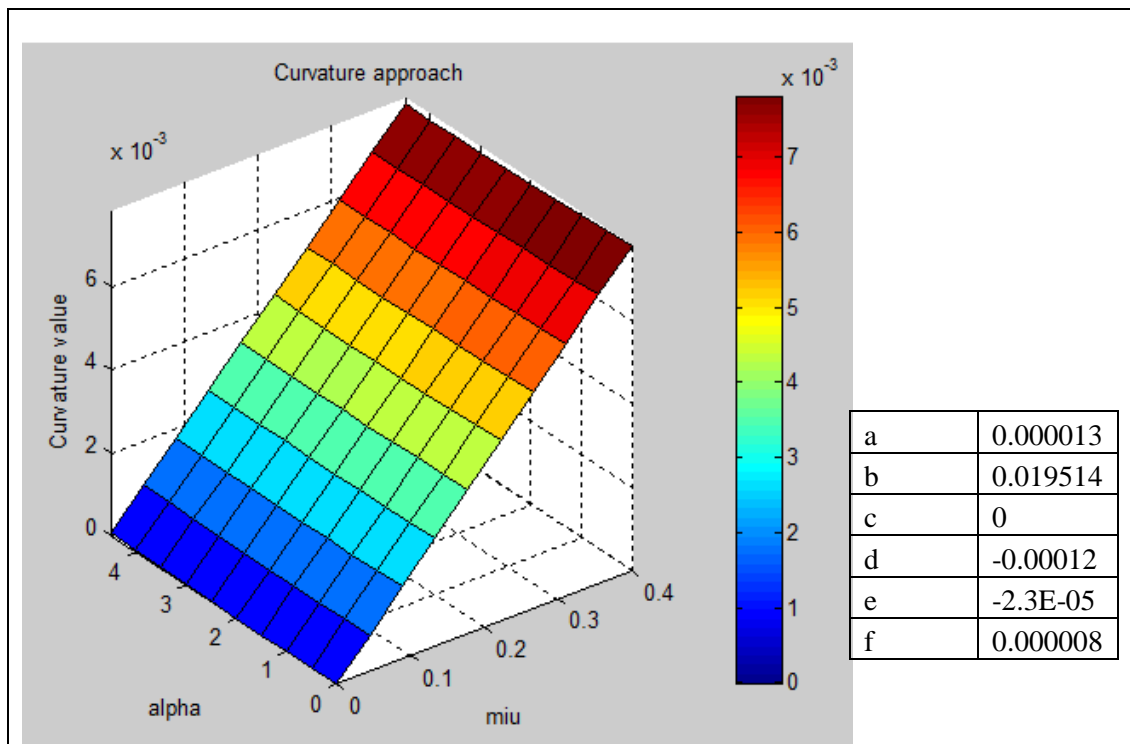
3.6 P/h³ Curvature approach and results

As outline in the last section, in the curvature approach, the initial part of the curve is fitted using $P=Ch^3$. A program in python is developed to automatically calculate the C value from the force-displacement data for each set of material parameters. In most of the case, the coefficient of fitting is over 99%. This was done initially in excel to evaluate the ideas, and then a MatLab based program was developed to automatically calculate the curvature values. The coding program involves discreting the data into different depth points, and then the curvature can be calculated following equation:

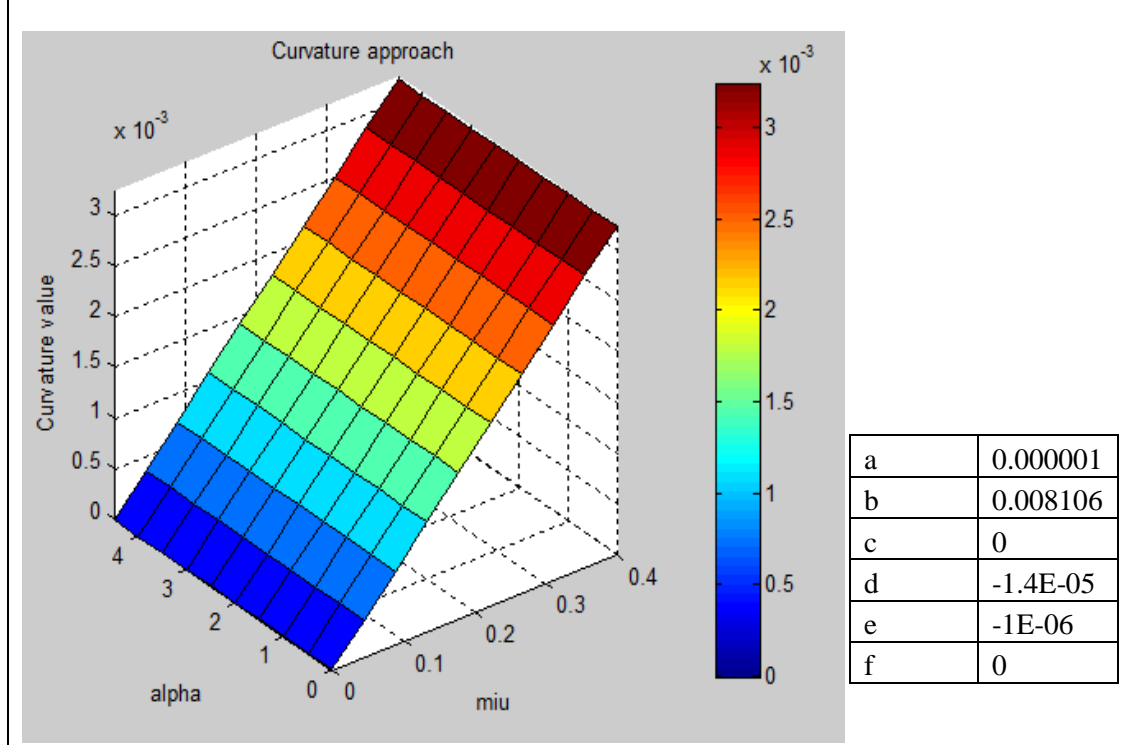
$$C(h^3) = \left[\frac{P_i}{h_i^3} \right]_{i=0}^N \quad (3.4)$$

This program can also calculate the coefficients of fitting.

Once the curvature values corresponding to the material properties over the whole domain of data (Figure 3.16 (b)) are determined, the 3D surface is determined using a code written in MatLab. Figure 3.17 shows the surface plot of full parabolic equation $z=a+bx+cx^2+dxy+ey+fy^2$ and the key parameters with different chamber diameters. For both chamber size of 20mm and 30mm, the coefficient of 3D surface fitting is over 99 and 98% respectively. This equation would provide a means to mathematically predict all the potential sets of material parameters when the force displacement data is known.



(a) Curvature approach with 3D paraboloid equation for Chamber size 20mm.



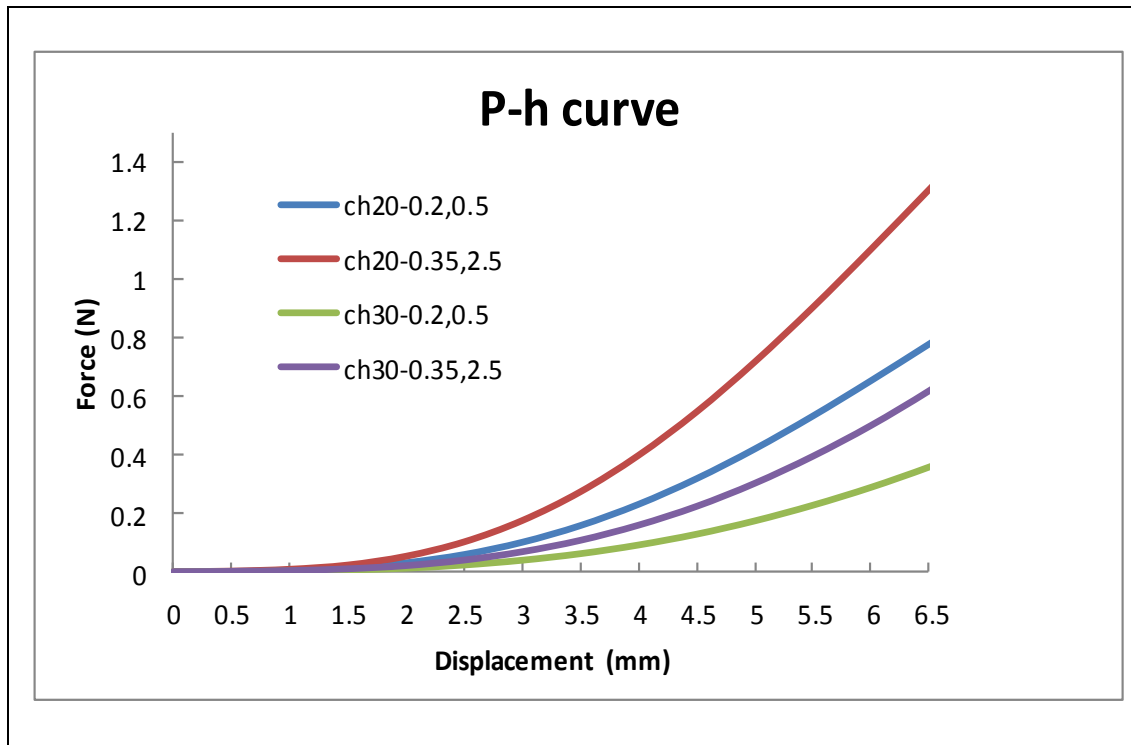
(b) Curvature approach with 3D paraboloid equation for Chamber size 30mm.

Figure 3.17 Surface plot for Curvature vs. (μ , α) (Sheet thickness=0.3mm).

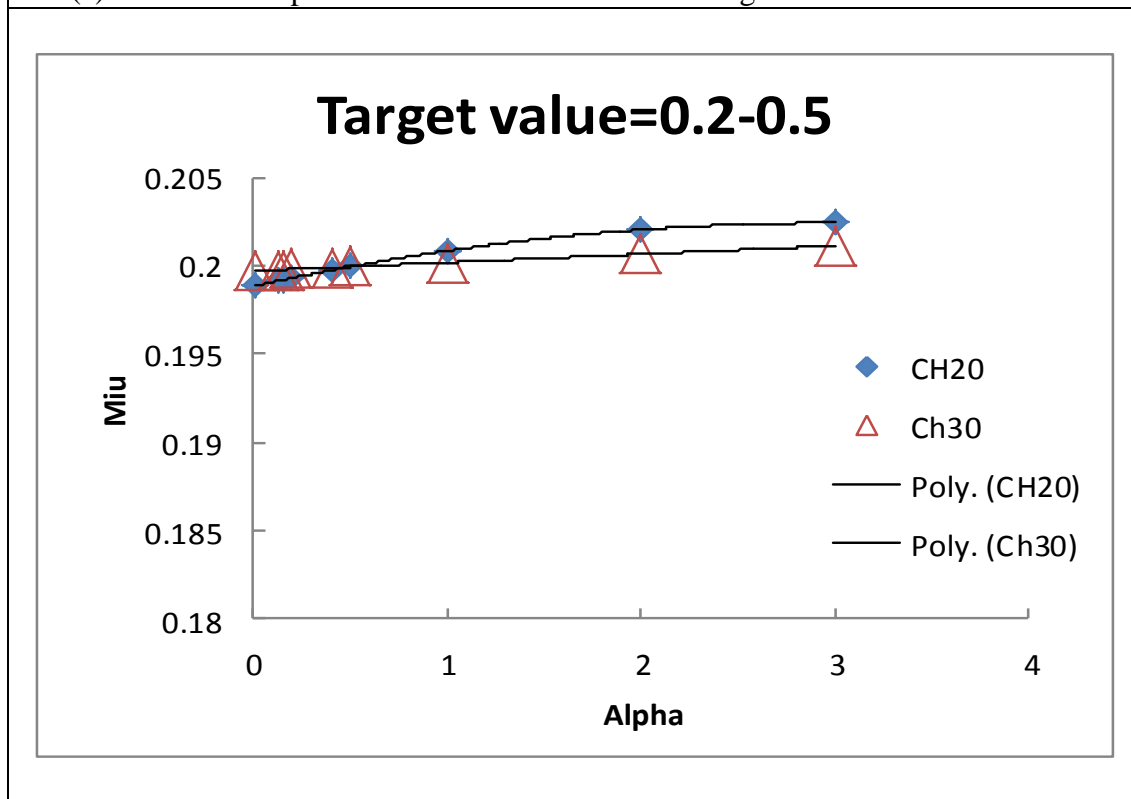
The results have been assessed using training data, i.e. using FE data with known material properties. This could simplify the process as for training data, the material properties are known as the target. Created a smaller range of simulation space with 25 potential material properties and used one of the material property as a target to assess the accuracy of the program. Two typical examples are shown in Figure 3.18(a) with the P-h curves of the two material property sets (i.e. a pair of μ and α) with two different chamber sizes. For each set of material properties, there is a curvature value. Then based on the equation, we can work out all the potential material properties which could produce the target curvature value. Given the format of the equation, there are many sets of material properties. As shown in Figure 3.18(b & c), for both chamber size 20mm and 30mm, for a known curvature value (based on the target material property set), the surface equation could identify a range of material property sets which fits the equation (data on the line). Mathematically, curvature values of the force-displacement data corresponding to the material data set on the line will all close to the target value. The data symbols plotted are just a few representative points, the line is a polynomial trendline. This suggests that based on a single chamber data, the inversely determined material properties are not unique. This is a common problem in inverse modelling, the surface function developed provided a quick way to identify all the material property sets. This is important as it provides an effective way to identify this material property sets which have identical force-displacement data. Then new approach can be developed to improve the uniqueness of the inverse modelling program.

One common practical approach in inverse modelling is to combine potential material properties for different dimension/stress strain conditions to improve the non-uniqueness. This has been shown to be effective in some tests and inverse modelling. For example, dual indenter methods ([Swaddiwudhipong S. et al, 2005](#); [Le M. Q., 2009](#)), for which data associated with different shaped indenters are jointly used in the inverse Fe modelling approach to be able to extract more than one material parameters from indentation tests. As shown in Figure 3.18 (b&c), we tried combine the data for different chambers size. As shown in the Figure 3.18 (b), there is a cross point between the curve for Chamber size 20 and 30, so this suggests mathematically, this could produce an better result by using the data with different chamber sizes. However, in this case, all the data of the potential properties for

chamber size 20 and 30 are still very close, so in a practical application, it will be difficult to use this method, i.e. based on the curvature method, to produce a unique result even though data from different chambers sizes are used. However, the results clearly shows that surface function approach is an effective way to identify all the potential material set with confidence which will provide important info for inverse material identification with other physical curve parameters which are to be presented in the following sections.



(a) Force and displacement curve used in the training data.



(b) Predicted material property sets which has a curvature value close to the target value. Target ($\mu=0.2$, $\alpha=0.5$).

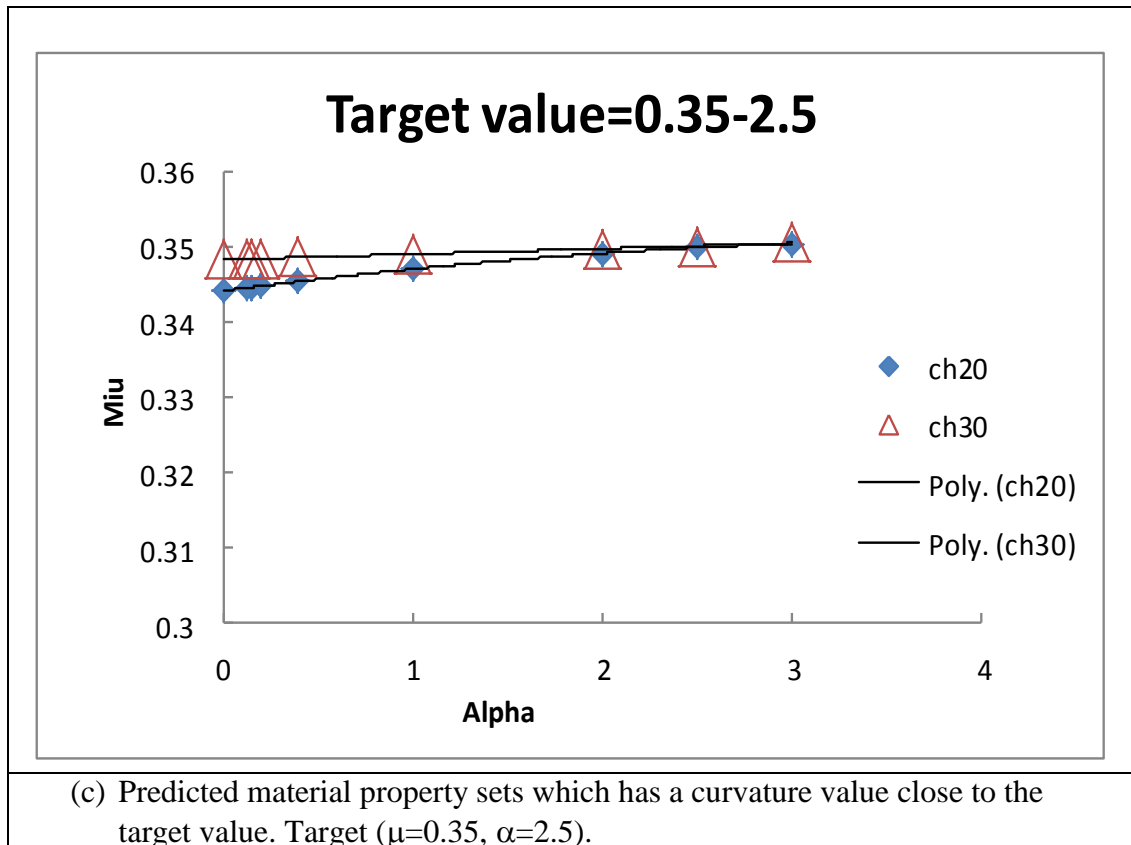


Figure 3.18 The $p-h$ curves used in the training data as the target; (b & c) predicted material parameters with two different chamber size based on the curvature approach. (Sheet thickness=0.3mm).

3.7 Slope method and results

In the slope method, the key curve parameter is the slope of the data at higher indentation depth. For this approach, the depth needs to be determined at which the method (which is applicable to most of the data) can be used to represent the data. A program needs to be developed to calculate the slope and interception for a range of data. This involves discreting the data into different depth points, and then the slope value can be calculated following:

$$m = \frac{\sum (x - \bar{x})(y - \bar{y})}{\sum (x - \bar{x})^2} \quad (3.5)$$

Where \bar{x} and \bar{y} are the mean of the known x's and known y's. In this case, y is the force, x is the displacement. Typical example of the pseudo code is shown in Table 3.5.

Table 3.5: Pseudo code shows the algorithm of the program to obtain slope value.

<p><i>Algorithm 2: slopeFunction</i></p>
<p><i>Input: tempFile, resultsODB,</i> <i>Output: overAllNumericalSlope, overAllNumericalIntercept</i></p> <ol style="list-style-type: none"> 1. tempFile, obtain the material parameters (μ and α) from user input 2. resultsODB, obtain all the ODB results from database 3. materialParameterRange, obtain the range of material parameters from tempFile 4. readCurve, read data from the resultODB column by column 5. x, define displacement column of readCurve as x 6. y, define force column of readCurve as y 7. countNumberI, compute number of row in x and y (to determine the number of data point for each force-displacement curve)) 8. $i=1$, starting with the first number of resultsODB[i], then updated in each calculation loop. 9. while $i < \text{materialParameterRange}$: 10. $j=1$ 11. For $j < \text{countNumberI}$: 12. Calculate SumX=Sum(x_j) & SumY=Sum(y_j) 13. $j+=1$ 14. Calculate meanX and meanY by divide SumX and SumY with countNumberI 15. For $i < \text{countNumberI}$: 16. $j=1$, starting with first data of x[j] and y[j] 17. Calculate slope value of the linear section of the force-displacement curve with the regression equation $\text{Where } \text{numericalSlope}[j] = \frac{\sum (x_j - \bar{x})(y_j - \bar{y})}{\sum (x_j - \bar{x})^2}, \bar{x} \text{ is MeanX and } \bar{y} \text{ is MeanY}$ <ol style="list-style-type: none"> 18. $j+=1$ 19. Save numericalSlope[j] into a text file, overAllNumericalSlope 20. For $j < \text{countNumberI}$: 21. $j=1$, starting with first data of x[j] and y[j] 22. Calculate slope value of the linear section of the force-displacement curve with the regression equation 23. Where numericalIntercept= Average($y_j - \text{numericalSlope}[j] * x_j$) 24. $j+=1$ 25. Save numericalIntercept into a text file, overAllNumericalIntercept 26. $i+=1$ 27. Return overAllNumericalSlope and overAllNumericalIntercept 27. Goto 3DSurcfaceEquationFunction

Where:

readCurve is a function to read the data from text file

x is a column to store a displacement data from the **readCurve**

y is a column to store a force data from the **readCurve**

countNumerI is a integer variable to store number of rows for each column of **x** and **y**

SumX is a summation of $x(i=1,2,3,...)$

SumY is a summation of $y(i=1,2,3,...)$

numericalSlope[j] is a slope value for each force-displacement curve ($j=1,2,3,...$)

numericalIntercept[j] is a intercept value for force-displacement curve ($j=1,2,3,...$)

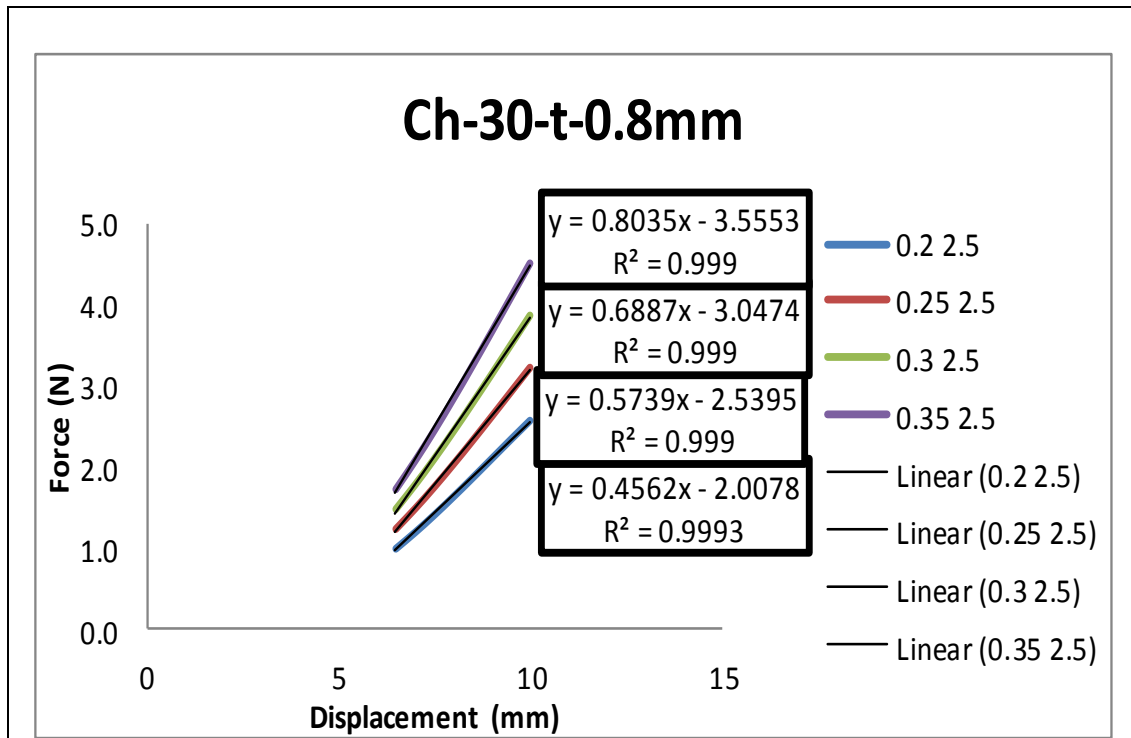
MeanX is the average of $x(i=1,2,3,...)$

MeanY is the average of $y(i=1,2,3,...)$

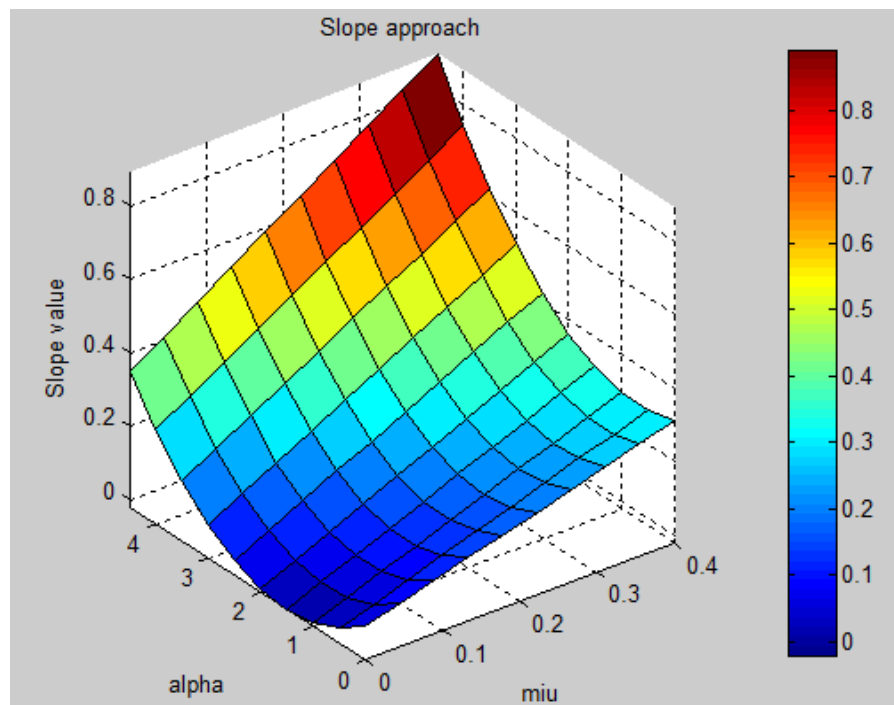
overAllNumericalSlope is a text file to store the slope value for all the numerical curve

overAllNumericalIntercept is a text file to store the intercept value for all the numerical curve

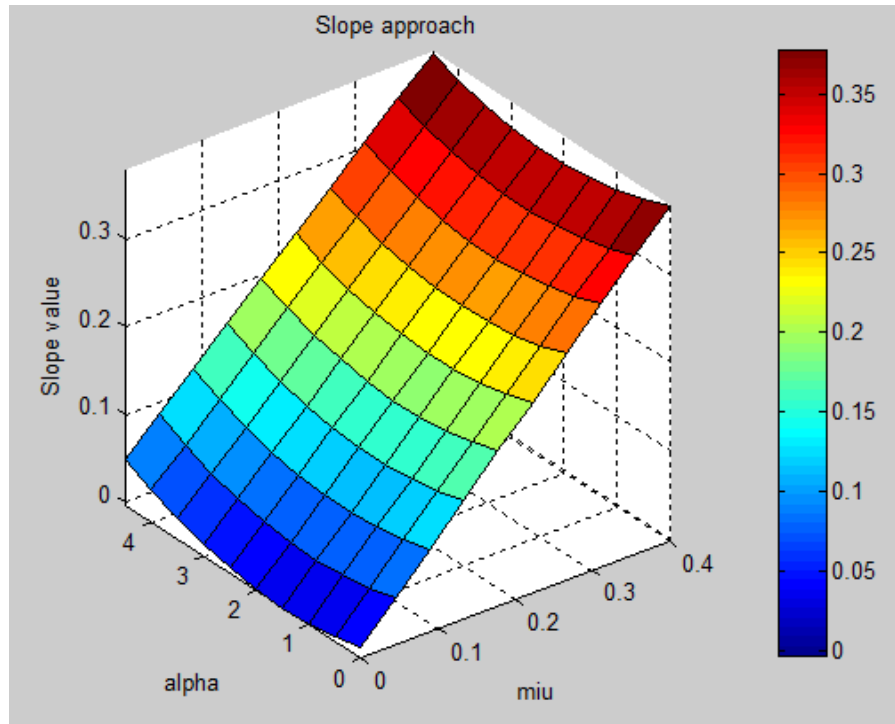
Figure 3.19(a&b) shows the 3D surface plot of slope as a function of the material parameters for chamber size 20mm and chamber size 30mm, respectively. It clearly shows that the equation and the surface plot for the two chamber size are different. The surface plot for chamber size 30mm is significant flatter than that for chamber size 20mm. Based on the surface equation, potential material properties for a target slope data could be mathematically determined by solving the equation in MatLab. Figure 3.20 (a&b) shows two cases in training data. These data shows that for both chamber size 20 and 30, there are several material properties combination could match the slope value, however the data for chamber size 30 shows much less change with the value/magnitude in the parameter ' μ ' than that for chambers 20. More importantly, there is a clear cross point, which represent this property point can match the slope value for both chamber size 30 and chamber size 20. The point is very close to the target property value.



(a) Illustration of the slope method to extract the slope value from the force-displacement data.



(b) 3D paraboloid equation for Chamber size 20mm.



(c) 3D paraboloid equation for Chamber size 30mm.

Figure 3.19 Surface plot for slope vs. (μ , α) ($t=0.3\text{mm}$). (a) Chamber size =20, and
(b) Chamber size =30mm.

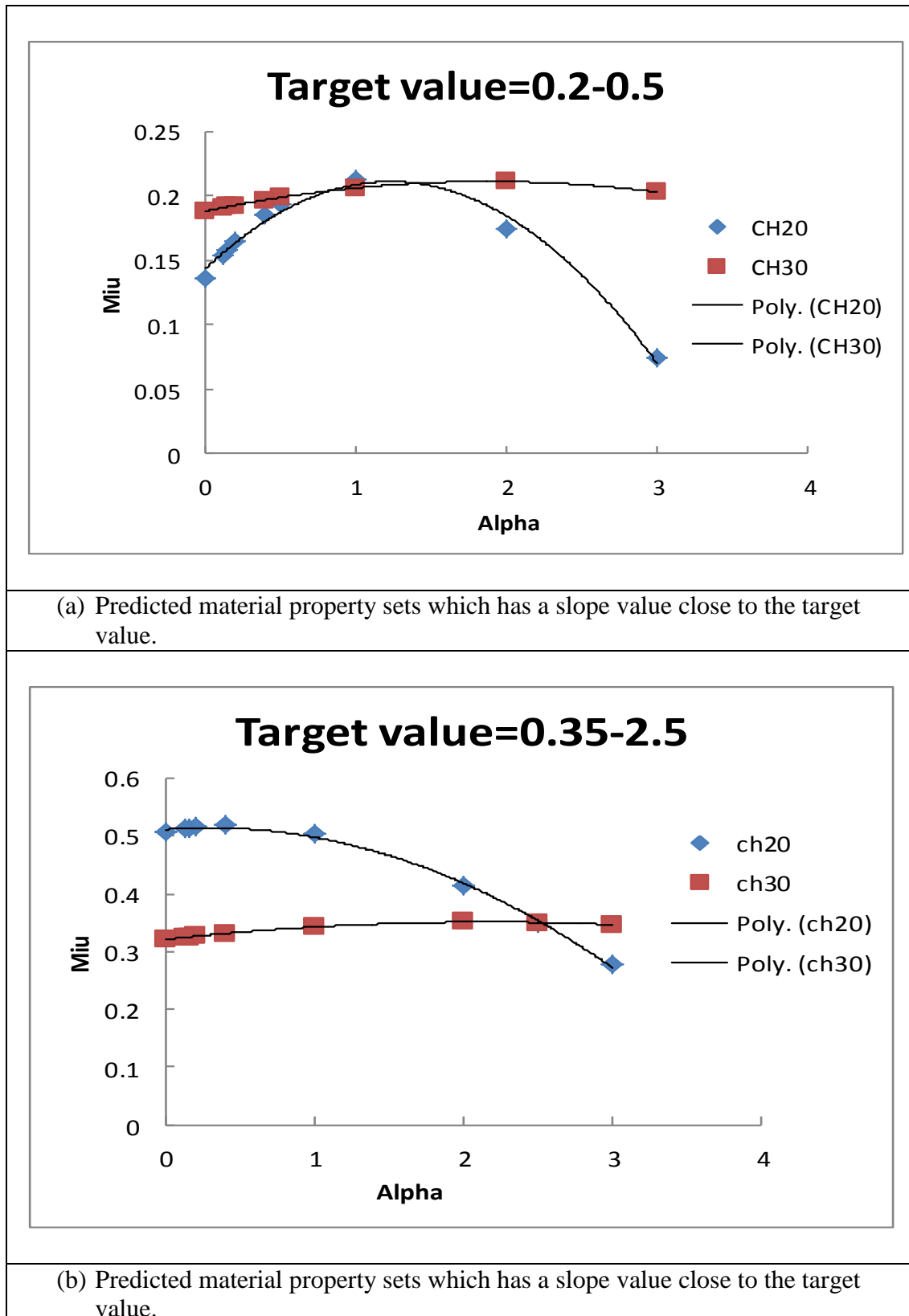


Figure 3.20 Typical materials sets predicted based on the surface plot equations of the slope and the use of data from two chamber sizes to predict the material parameters (Sheet thickness=0.3mm).

FE model has been performed based on the properties of these cross point, the result confirmed that both cross point can produce identical/comparable force displacement curves, this suggest that the result is still not unique but the program is able to narrow the potential material properties to a manageable number of properties. In this case, there are only two points, which will give a clear focus point for the property searching process. Similar analysis has been conducted on several target material properties and the results are listed in Table 3.6 and 3.7. In all the cases, the prediction accuracy is within 3% for μ .

Table 3.6: Typical data in training data to predict the material parameters with two chamber size using slope approach. (Sample thickness=0.8mm).

Target Value		Prediction Result		Percentage error %	
μ	α	μ	α	μ	α
0.2	0.5	0.206	1	3	100
0.2	2.5	0.198	2.5	1	0
0.3	1	0.3	1	0	0
0.3	1.5	0.299	1.5	0.3	0
0.3	2.5	0.3	2.5	0	0
0.35	1	0.345	0.7	1.43	30
0.35	2	0.349	2	0.28	0
0.35	2.5	0.3508	2.5	2.5	0
0.4	0.5	0.41	1	2.5	100
0.4	2.5	0.401	2.5	0.25	0

Table 3.7: Typical data in training data to predict the material parameters with two chamber size using slope approach. (Sample thickness=0.3mm).

Target Value		Prediction Result		Percentage error %	
μ	α	μ	α	μ	α
0.2	0.5	0.205	0.9	2.5	80
0.2	2.5	0.2	2.5	0	0
0.3	1	0.3	1	0	0
0.3	1.5	0.3	1.5	0	0
0.3	2.5	0.3	2.5	0	0
0.35	1	0.34	0.8	2.9	20
0.35	2	0.35	2.1	0	5
0.4	0.5	0.41	1	2.5	100
0.4	2.5	0.401	2.5	0.25	0
0.35	2.5	0.35079	2.5	0.2257	0

3.8 Polynomial curve fitting approach and results

As shown in Figure 3.14, the force-displacement curves could be fitted by 2nd order polynomial trendline equation. The first order coefficients and the second order coefficients potentially is the function of ‘μ’ and ‘α’. Typical 2nd order of polynomial correlation coefficient of different FE data have been plotted into bar chart as shown in Figure 3.21. The range of the correlation coefficients is within 0.974- 0.998. For each force displacement data, there are two parameters. A program has been developed to fit/determine these two parameters for a wide range of material data. The main least square fitting 2nd order of polynomial equation is as following:

$$\begin{aligned}
 a_0 n + a_1 \sum_{i=1}^n x_i + \dots + a_k \sum_{i=1}^n x_i^k &= \sum_{i=1}^n y_i \\
 a_0 \sum_{i=1}^n x_i + a_1 \sum_{i=1}^n x_i^2 + \dots + a_k \sum_{i=1}^n x_i^{k+1} &= \sum_{i=1}^n x_i y_i \\
 a_0 \sum_{i=1}^n x_i^k + a_1 \sum_{i=1}^n x_i^{k+1} + \dots + a_k \sum_{i=1}^n x_i^{2k} &= \sum_{i=1}^n x_i^k y_i
 \end{aligned}$$

Or, in matrix form

$$\begin{bmatrix}
 n & \sum_{i=1}^n x_i & \dots & \sum_{i=1}^n x_i^k \\
 \sum_{i=1}^n x_i & \sum_{i=1}^n x_i^2 & \dots & \sum_{i=1}^n x_i^{k+1} \\
 \vdots & \vdots & \ddots & \vdots \\
 \sum_{i=1}^n x_i^k & \sum_{i=1}^n x_i^{k+1} & \dots & \sum_{i=1}^n x_i^{2k}
 \end{bmatrix}
 \begin{bmatrix}
 a_0 \\
 a_1 \\
 \vdots \\
 a_k
 \end{bmatrix}
 =
 \begin{bmatrix}
 \sum_{i=1}^n y_i \\
 \sum_{i=1}^n x_i y_i \\
 \vdots \\
 \sum_{i=1}^n x_i^k y_i
 \end{bmatrix}$$

We can obtain the matrix for a least squares fit by writing

$$\begin{bmatrix}
 1 & x_1 & \dots & x_1^k \\
 1 & x_2 & \dots & x_2^k \\
 \vdots & \vdots & \ddots & \vdots \\
 1 & x_n & \dots & x_n^k
 \end{bmatrix}
 \begin{bmatrix}
 a_0 \\
 a_1 \\
 \vdots \\
 a_k
 \end{bmatrix}
 =
 \begin{bmatrix}
 y_1 \\
 y_2 \\
 \vdots \\
 y_n
 \end{bmatrix}$$

By multiplying the sides with transpose of the first matrix then gives

$$\begin{bmatrix} 1 & 1 & \cdots & 1 \\ x_1 & x_2 & \cdots & x_n \\ \vdots & \vdots & \ddots & \vdots \\ x_1^k & x_2^k & \cdots & x_n^k \end{bmatrix} \begin{bmatrix} 1 & x_1 & \cdots & x_1^k \\ 1 & x_2 & \cdots & x_2^k \\ \vdots & \vdots & \ddots & \vdots \\ 1 & x_n & \cdots & x_n^k \end{bmatrix} \begin{bmatrix} a_0 \\ a_2 \\ \vdots \\ a_n \end{bmatrix} = \begin{bmatrix} 1 & 1 & \cdots & 1 \\ x_1 & x_2 & \cdots & x_n \\ \vdots & \vdots & \ddots & \vdots \\ x_1^k & x_2^k & \cdots & x_n^k \end{bmatrix} \begin{bmatrix} y_1 \\ y_2 \\ \vdots \\ y_n \end{bmatrix}$$

So

$$\begin{bmatrix} y_1 \\ y_2 \\ \vdots \\ y_n \end{bmatrix} = \begin{bmatrix} 1 & x_1 & x_1^2 & \cdots & x_1^k \\ 1 & x_2 & x_2^2 & \cdots & x_2^k \\ \vdots & \vdots & \vdots & \ddots & \vdots \\ 1 & x_n & x_n^2 & \cdots & x_n^k \end{bmatrix} \begin{bmatrix} a_1 \\ a_2 \\ \vdots \\ a_k \end{bmatrix} \quad (3.6)$$

In matrix notation, the equation for a polynomial fit is given by

$$y = Xa.$$

This can be solved by premultiplying by the transpose X^T ,

$$X^T y = X^T X a.$$

This matrix equation can be solved numerically where

$$a = (X^T X)^{-1} X^T y.$$

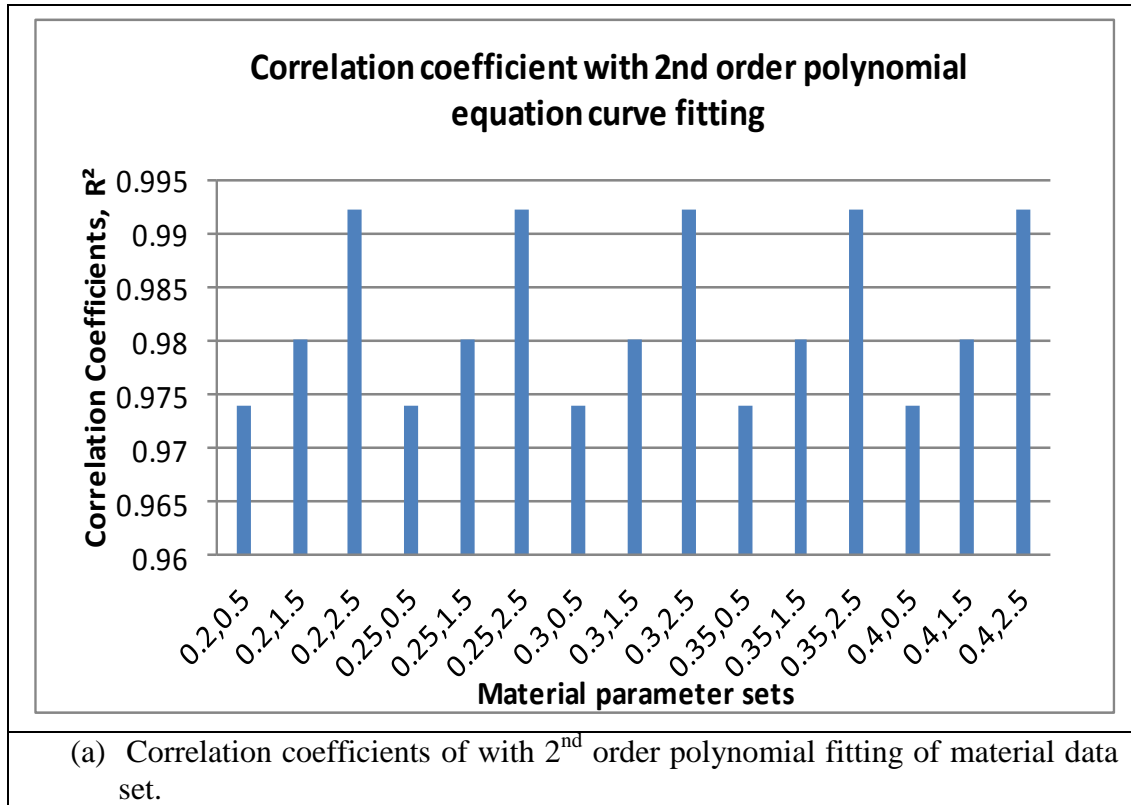
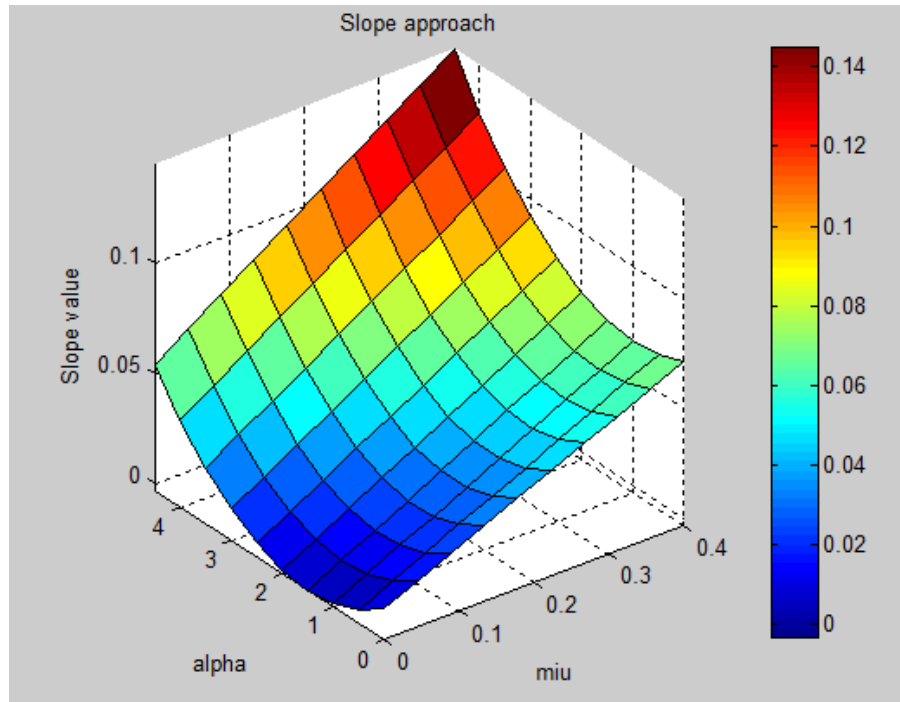


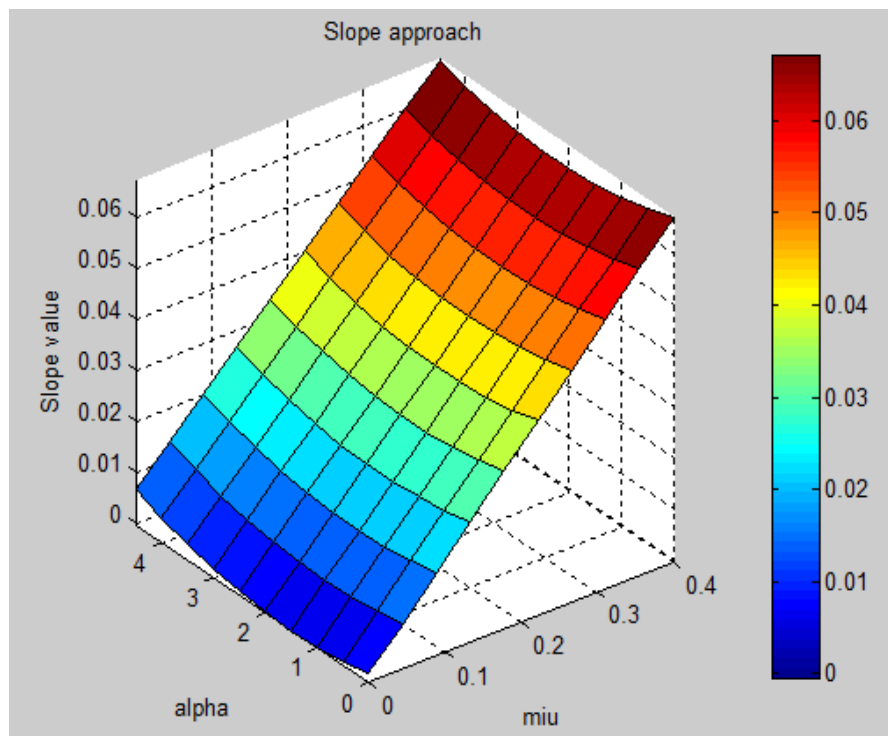
Figure 3.21 Typical correlation coefficients when fitting the force-displacement data with 2nd order polynomial trendlines.

Based on these equations, the two polynomial coefficients ('a' and 'b') could be evaluated for every different set of material properties over a wide range of simulation space. Typical 3D surface plot of parameter 'a' is plotted in Figure 3.22, Figure 3.22(a) is for chamber size 20mm and Figure 3.22(b) is for chamber size 30mm. In both cases, the coefficient 'a' increase with the ' μ ' and ' α '. To check the accuracy and consistency of the ax^2 approach in predicting material properties for a given target value, training data has been performed with two chamber size and different thicknesses. As shown in Figure 3.23(a), there are several material sets for both chamber size 20 and 30. The data for chamber size 20 exhibits a curved shape, while the data for chamber size 30 is close to a linear line. There are two cross point, one of them is very close to the target data ($\mu=0.2$ $\alpha=0.5$). Similar trend can be observed in another set of data when the target is $\mu=0.202$, $\alpha=1.8$. The material property sets for chamber size 30 follows a linear trend, while the material property sets follows a curved distribution for chamber 20. One of the cross point is in agreement with the target material property. These data shows that there will be multiple materials property sets having similar 2nd order polynomial coefficient from

one chamber size test. One potential approach is to use two chambers with different sizes, which will narrow the material property down to only two points. Similar approach has been evaluated when using the first order polynomial coefficient 'b', some typical data are shown in Figure 3.24. The overall trend is similar to the predicted data based on the 2nd order polynomial coefficient. But the quality of some data is less smooth as the data shown in Figure 3.23. The 2nd order coefficient 'a' and first order coefficient 'b' has been evaluated with thicker samples. Typical results for the case of a sample 0.8mm thick are shown in Figure 3.25. The data clearly shows that the approach is capable of predicting the target material properties. Similarly when using a sample with thickness of 0.8mm, the data based on the surface function for the first order coefficient 'b' shows a similar trend (Figure 3.26), but the quality of the data is less good than the data for 'a' as shown in Tables 3.8 and 3.9.



(a) 3D parabolic surface for Second order Polynomial coefficient 'a'(chamber size 20mm).



(b) 3D parabolic surface for Second order Polynomial coefficient 'a' (chamber size 30mm).

Figure 3.22 Surface plot for second order coefficient a vs. (μ, α) ($t=0.8\text{mm}$, chamber size =20 (a) and 30mm (b)).

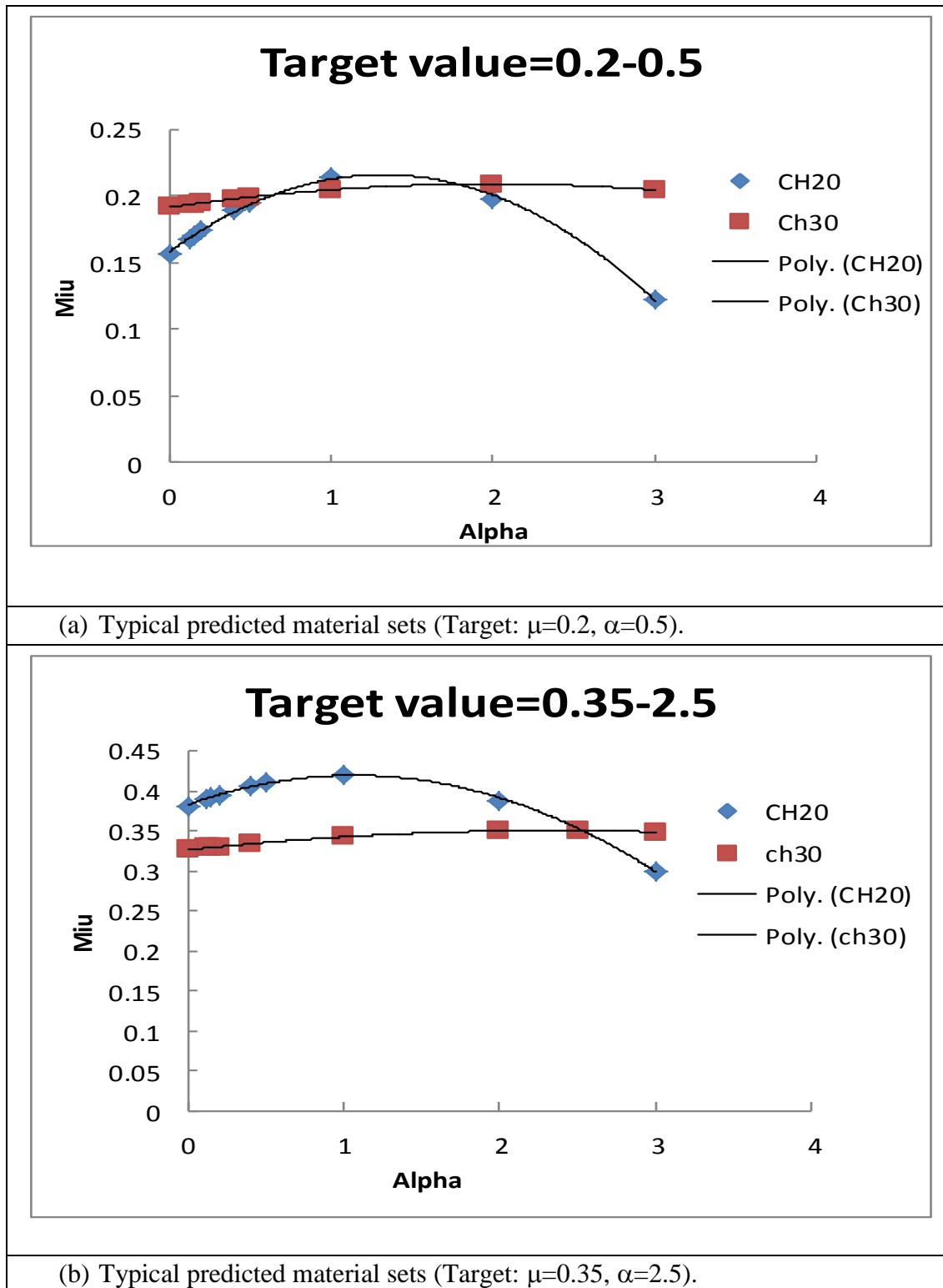
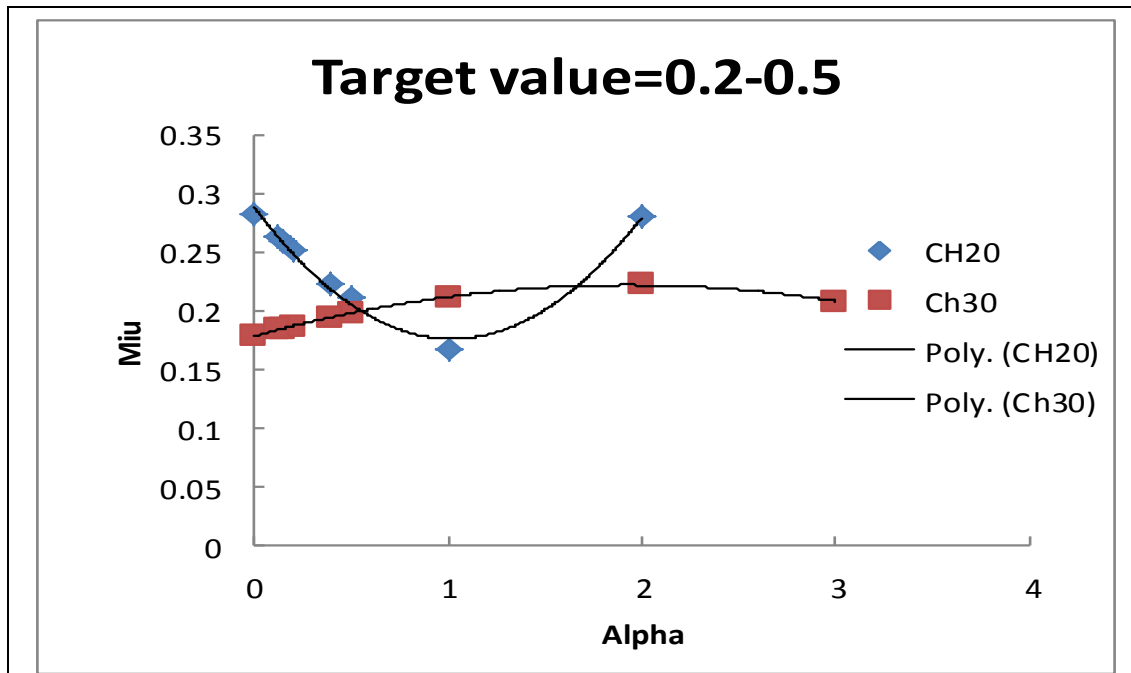
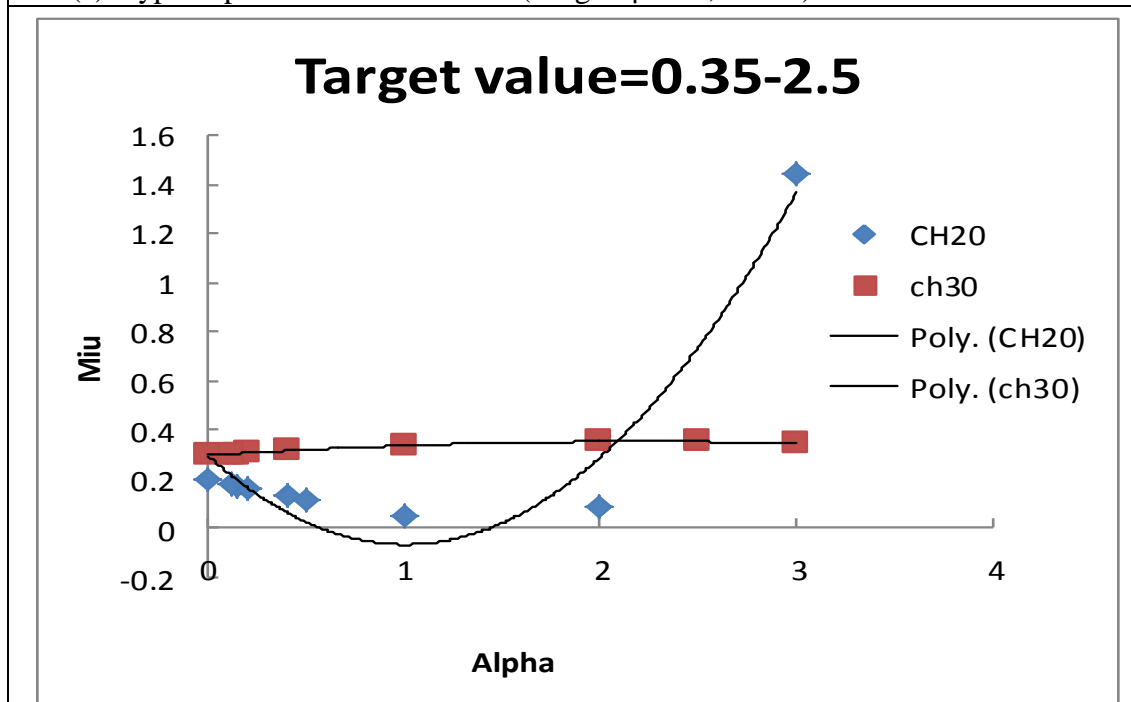


Figure 3.23 Typical material sets predicted based on the surface plot equations of the second order polynomial coefficient 'a' and the use of data from two chamber sizes to predict the material parameters (Sheet thickness=0.3mm).

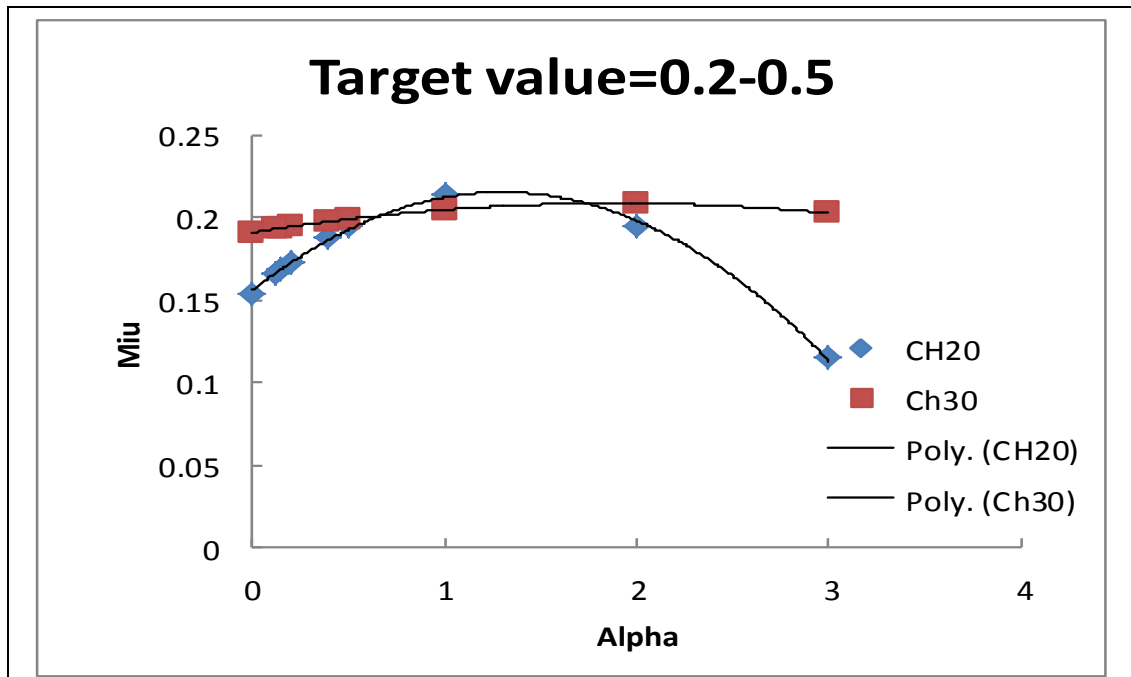


(a) Typical predicted material sets (Target: $\mu=0.2$, $\alpha=0.5$).

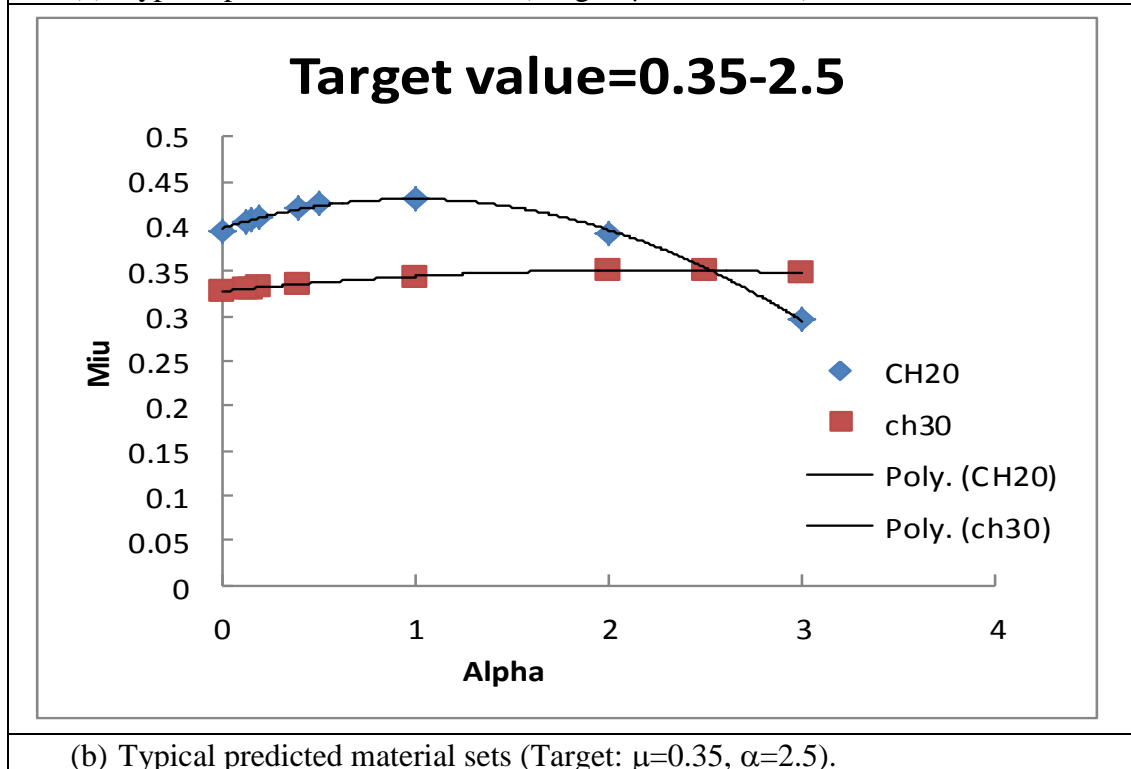


(b) Typical predicted material sets (Target: $\mu=0.35$, $\alpha=2.5$).

Figure 3.24 Typical materials sets predicted based on the surface plot equations of the first order polynomial coefficient 'b' and the use of data from two chamber sizes to predict the material parameters (Sheet thickness=0.3mm).



(a) Typical predicted material sets (Target: $\mu=0.2$, $\alpha=0.5$).



(b) Typical predicted material sets (Target: $\mu=0.35$, $\alpha=2.5$).

Figure 3.25 Typical materials sets predicted based on the surface plot equations of the second order polynomial coefficient 'a' and the use of data from two chamber sizes to predict the material parameters (Sheet thickness=0.8mm).

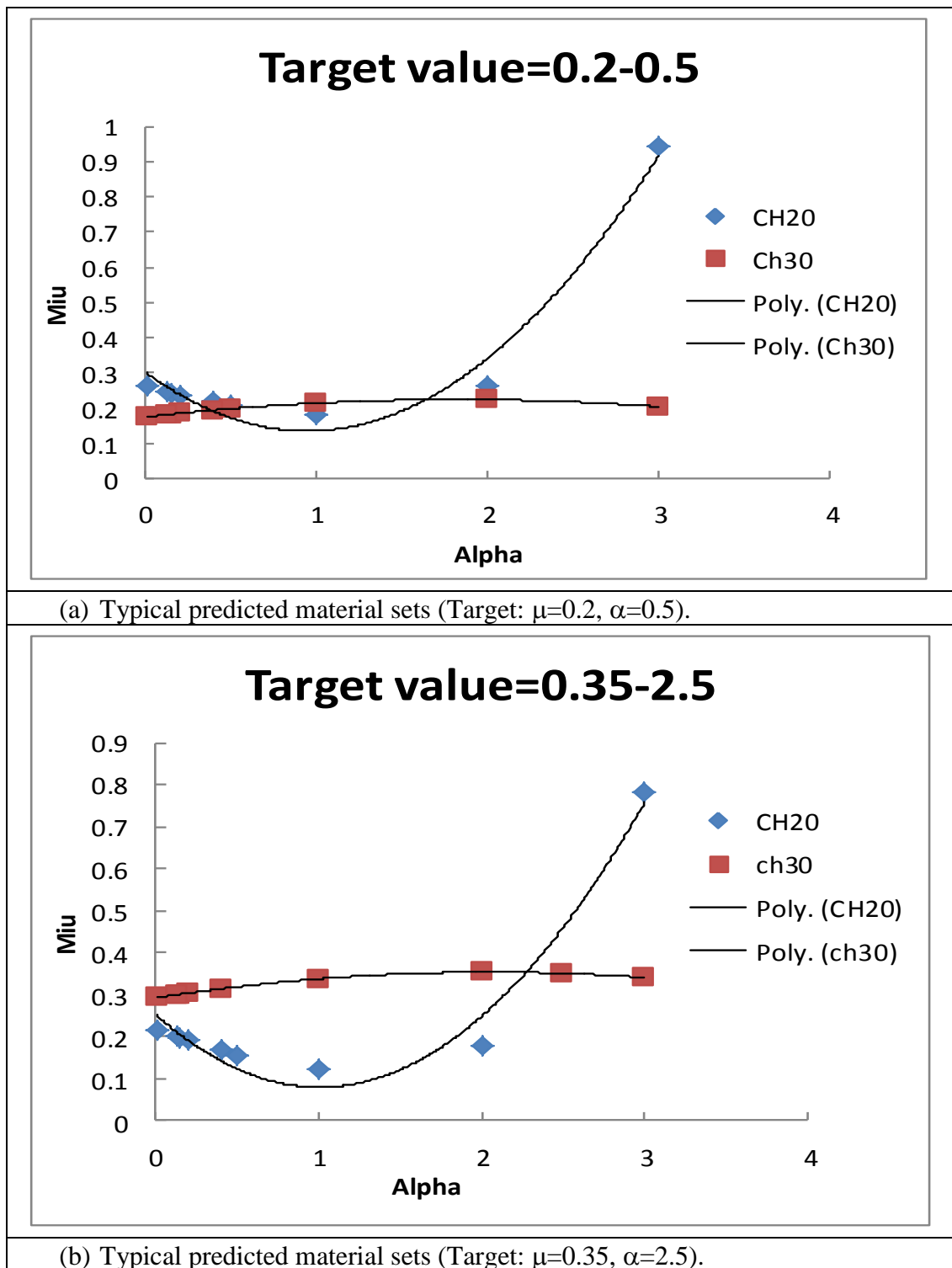


Figure 3.26 Typical materials sets predicted based on the surface plot equations of the first order polynomial coefficient ‘b’ and the use of data from two chamber sizes to predict the material parameters. (Sheet thickness=0.8mm).

Table 3.8: Typical results of training data to predict the material parameters with two chamber size using coefficient ‘a’ approach. (Sample thickness=0.8mm).

Target Value		Prediction Result		Percentage error %	
μ	α	μ	α	μ	α
0.2	0.5	0.206	0.6	3	20
0.2	2.5	0.199	2.5	0.5	0
0.3	1	0.3	1	0	0
0.3	1.5	0.3	1.6	0	6.7
0.3	2.5	0.3	2.5	0	0
0.35	1	0.35	1	0	0
0.35	2	0.35	2	0	0
0.4	0.5	0.41	1	2.5	100
0.4	2.5	0.4	2.5	0	0
0.35	2.5	0.3505	2.5	0.1429	0

Table 3.9: Typical results of training data to predict the material parameters with two chamber size using coefficient ‘b’ approach. (Sample thickness=0.8mm).

Target Value		Prediction Result		Percentage error %	
μ	α	μ	α	μ	α
0.2	0.5	0.2	0.5	0	0
0.2	2.5	0.2	2.3	0	8
0.3	1	0.3	1.4	0	40
0.3	1.5	0.3	1.5	0	0
0.3	2.5	0.3	2.3	0	8
0.35	1	0.37	1.3	5.7143	30
0.35	2	0.35	1.8	0	10
0.4	0.5	0.41	0.3	2.5	40
0.4	2.5	0.401	2.3	0.25	8
0.35	2.5	0.35	2.3	0	8

3.9 Inverse materials properties identification based on combination of different curve parameters

Another approach evaluated in this work is to use the combination of different curve parameters from the same force displacement curve. The combination of two approaches in one chamber size is potentially more effective way to predict the material than using the data from two chamber sizes, because one testing data is only needed instead of two. This is a more straight forward method to extract the material properties from a wide range of material parameters set. Main approaches tested included (i) combination of curvature and slope, (ii) slope and interception, (iii) combination of second order and first order polynomial coefficients etc. Table 3.10 shows a typical example of pseudo code to show how the slope and intercept program can be used to predict the material parameters. In the first part, an experimental is input to the program, then the curvature value and the slope is calculated using the program. The value is then feed into the surface equation between the curvature-and parameter (μ and α) and the surface equation between the slope and the parameter (μ and α). The equation is solved and the set of material parameters is determined. In the next stage, the material parameter (μ and α) fits both the curvature and slope surface equations was identified as the target material parameter.

Algorithm 4: MaterialParameterPredictionFunction

Input: expCurve, coefficientSlope, coefficientIntercept

Output: resultMaterialParameter

1. **expCurve**, obtain experimental curve from user
2. **coefficientslope**, read the 3D surface coefficient of slope function (Algorithm 3)
3. **coefficientIntercept**, read 3D surface coefficient of intercept function (Algorithm 3)
4. **readCurve**, read data from the **expCurve**
5. **x**, define displacement column of **readcurve** as x
6. **y**, define force column of **readCurve** as y
7. **countNumberI**, compute number of row in **x** and **y** (to get the number/length of numerical data)
8. $i=1$, starting with number of **x[i]** and **y[i]**
9. For $i < \text{countNumberI}$:
10. Calculate **SumX**=Sum(**x_i**) & **SumY**=Sum(**y_i**)
11. $i+=1$
12. Return **SumX** and **SumY**
13. Calculate **meanX** and **meanY** by divide **SumX** and **SumY** with **countNumberI**
14. For $i < \text{countNumberI}$:
15. $i=1$, starting with number of **x[i]** and **y[i]**
16. Calculate slope value of the final linear curve with the equation of the regression line

$$\text{Where } \text{expSlope} = \frac{\sum (x_i - \bar{x})(y_i - \bar{y})}{\sum (x_i - \bar{x})^2}, \bar{x} \text{ is MeanX and } \bar{y} \text{ is MeanY}$$

17. $i+=1$
18. Return **expSlope**
19. For $i < \text{countNumberI}$:
20. $i=1$, starting with first data of **expCurve**
21. Calculate intercept value of the linear curve with the equation of the regression
Where **expIntercept** += Average(**y_i**-**expSlope*****x_i**)
22. $i+=1$
23. Return **expIntercept**
24. Save the data for **expSlope** and **expIntercept** individually into text file
25. Solve **3DequationSlope** with 3dimensional least-square polynomial method $a+bx+cx^2+dxy+ey+fy^2-z=0$, where **z** is **expslope**, a, b, c, d, e and f is from **coefficientSlope**.
26. Solve **3DequationIntercept** with 3dimensional least-square polynomial method $a+bx+cx^2+dxy+ey+fy^2-z=0$, where **z** is **expIntercept**, a, b, c, d, e and f is from **coefficientIntercept**.
27. Obtain **resultMaterialParameter** by combining **3DequationSlope** and **3DequationIntercept** to get the point representing material property sets matching the surface equations for both the slope and intercept surface equation.

28. Save resultMaterialParameter into text file 29. Return resultMaterialParameter
Where: expCurve is an experimental data input by user readCurve is a function to read the data from text file x is a column to store a displacement data from the readCurve y is a column to store a force data from the readCurve countNumerI is an integer variable to store number of row for each column of x and y SumX is the summation of $x(i=1,2,3,...)$ SumY is the summation of $y(i=1,2,3,...)$ MeanX is the average of $x(i=1,2,3,...)$ MeanY is the average of $y(i=1,2,3,...)$ expSlope is the slope value for experimental curve expIntercept is the intercept value for experimental curve 3DequationSlope is the 3D surface equation for slope function 3DequationIntercept is the 3D surface equation for intercept function resultMaterialParameter is a text file for material parameter set (μ and α) predicted by combining two equations (3DequationSlope and 3DequationIntercept)

Table 3.10: Typical example of pseudo code for slope and intercept approach.

Some typical results are briefly shown from Figure 3.27 to Figure 3.28. Figure 3.27(a) shows the data from the slope and intercept method with a chamber size of 20mm and sample thickness of 0.8mm. As shown in Figure 3.27(a), the data for the slope and intercept approach are plotted together and it clearly shows that the material parameters corresponding to one of the cross point is in a good agreement with the target values. Figure 3.27(b) shows the results when combining inversely predicted data from the second order and first order polynomial curve coefficients. The results reveal a clear point which is close to the target material parameter values.

Figure 3.27(c&d) show the results for chamber size 30mm. As shown in Figure 3.27(c), there are two crossing points, one of which is close to the target value. But, in general, the data from the slope and intercept point are very close, this suggest that it is not suitable to predict the material properties for chamber size 30mm. Figure 3.27(d) shows the data for the combining inversely predicted data from the second order and first order polynomial curve coefficients. One of the crossing point matches the target value, but the difference between the two sets of data are not as clear as the data for chamber size 20mm. In general, the data from the slope and

intercept point are very close, this suggest that it is not suitable to predict the material properties for chamber size 30mm.

Similar analyses have been applied to thinner samples. Typical results are shown in Figure 3.28(a-d). As shown in Figure 3.28(a), the prediction based on the combination of slope and intercept method doesn't fully match the target value different from the case of thicker sample (as shown in Figure 3.27). In the case of prediction based on the combination the second order and first order polynomial curve coefficients, one of the crossing points matches the target very well. As shown Figure 3.28(c&d), when the chamber size is 30mm, it is difficult to identify a clear crossing point. The work shows that the program developed is able to automatically determine all potential data, this is important for determine the feasibility of different approaches in identifying the materials parameter when combining different experimental set up. The situation for smaller chamber size and thicker sample (e.g. 20mm, sample thickness=0.8mm), the situation is much clearer. In both cases for combined Slope-Intercept method (Figure 3.27(a)) and the combined polynomial parameters approach (Figure 3.27(b)), there is a clear cross point that match the target values, this suggest that it is a better approach for practical application.

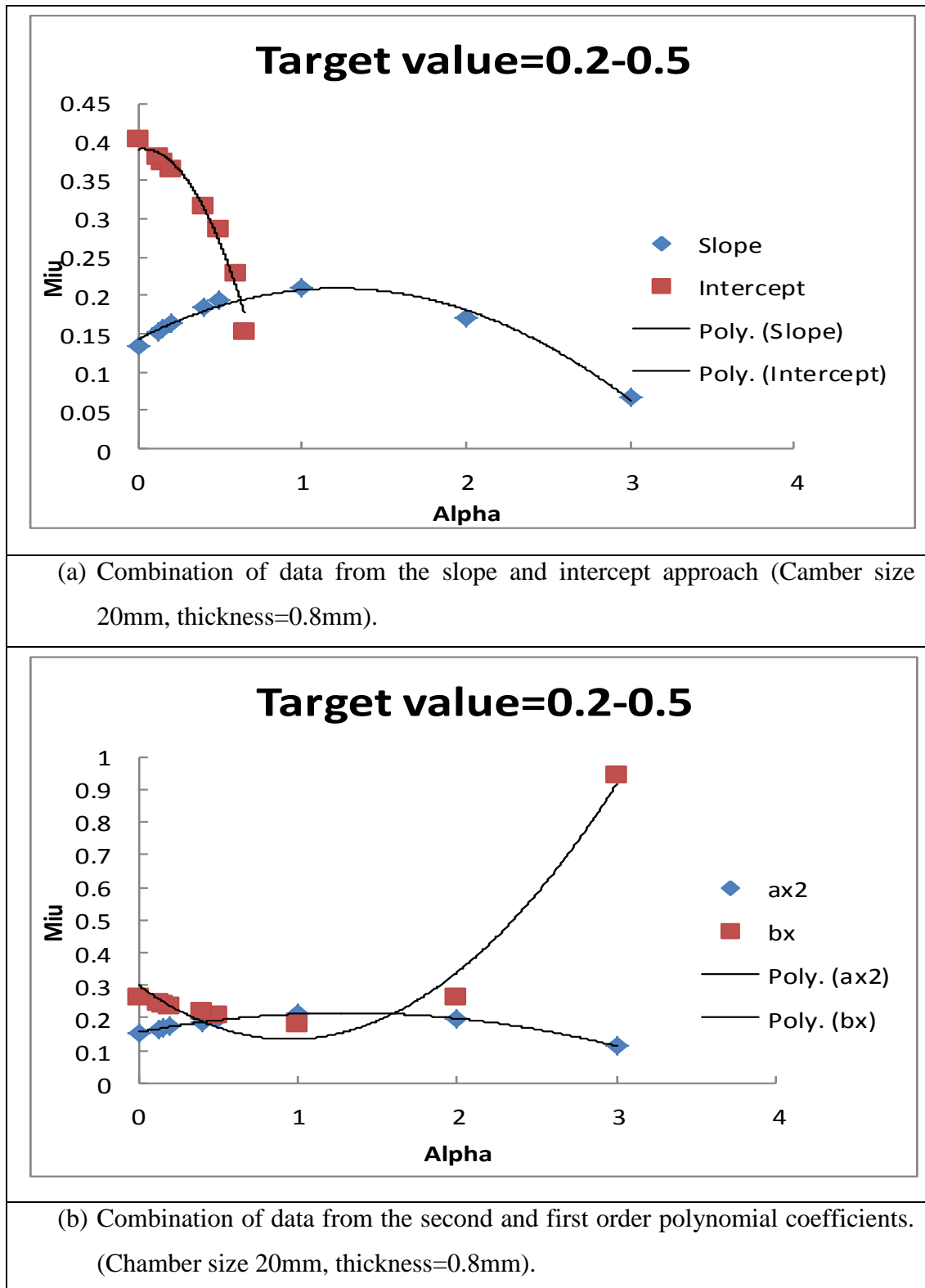
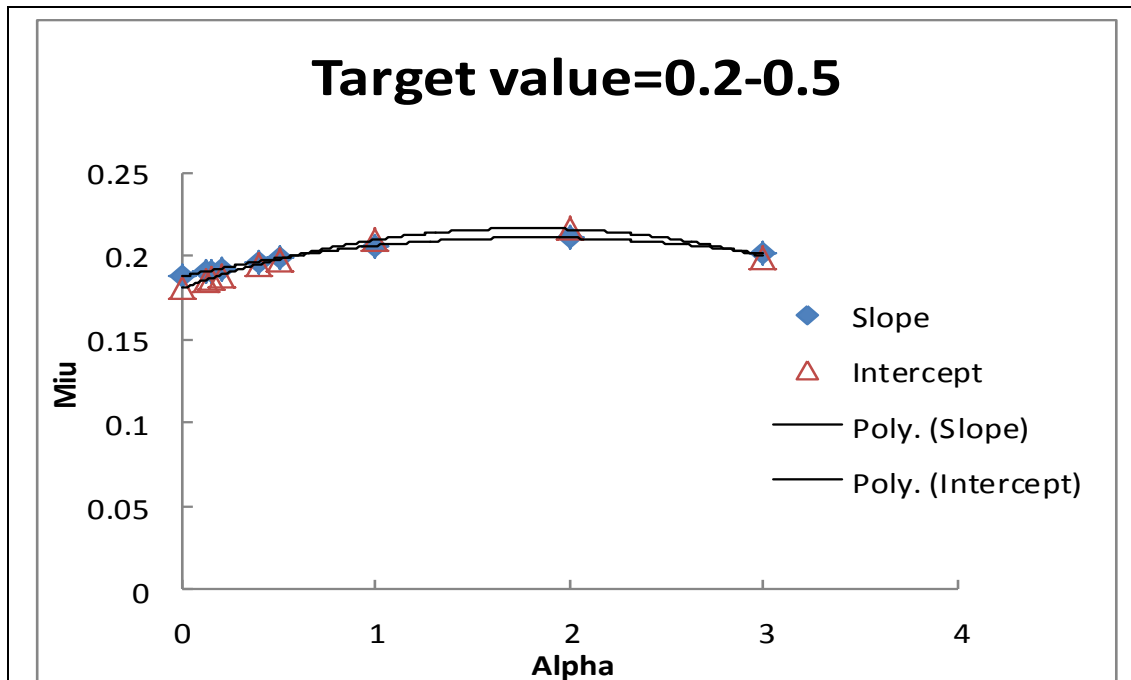
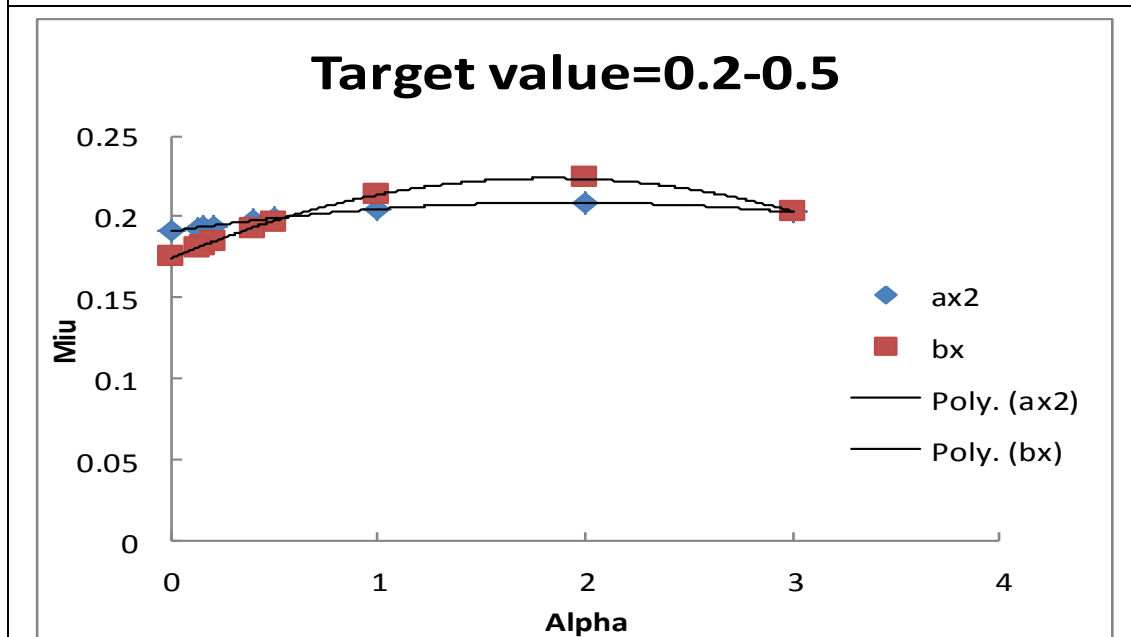


Figure 3.27 (a&b) Data to show the concept of combining the material sets based surface equation for the slope and interception method (a) and the material sets based surface equation for the second order and first order polynomial coefficients. (Chamber size=20mm, Sheet thickness=0.8mm).

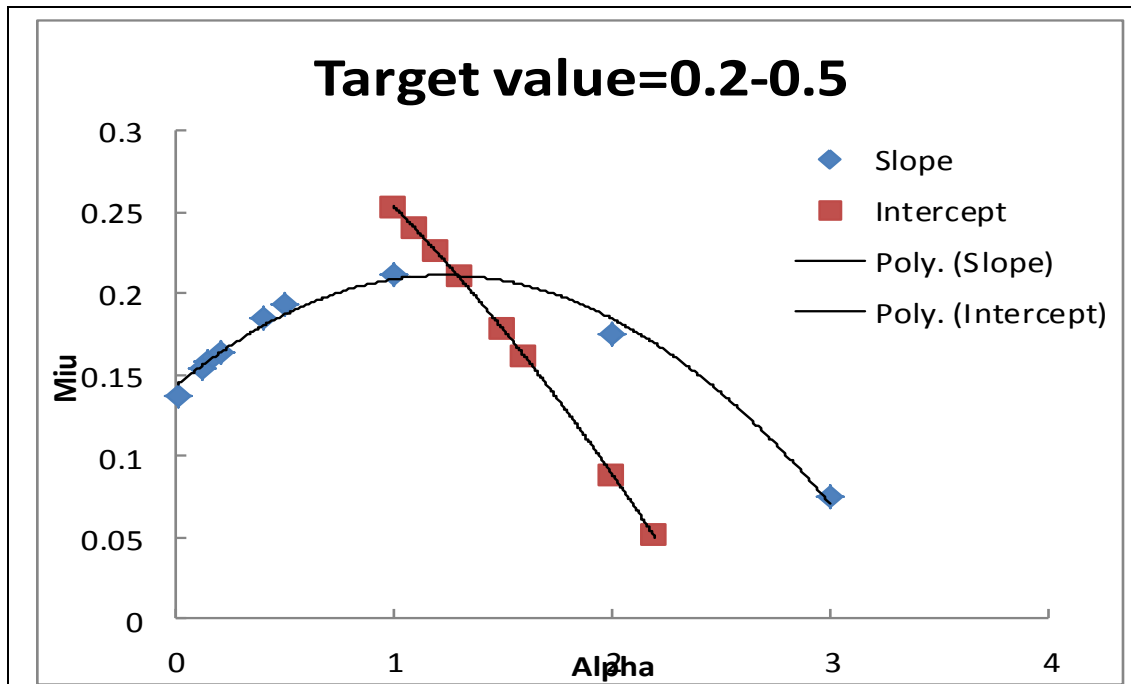


(c) Combination of data from the slope and intercept approach (Chamber size 30mm, thickness=0.8mm).

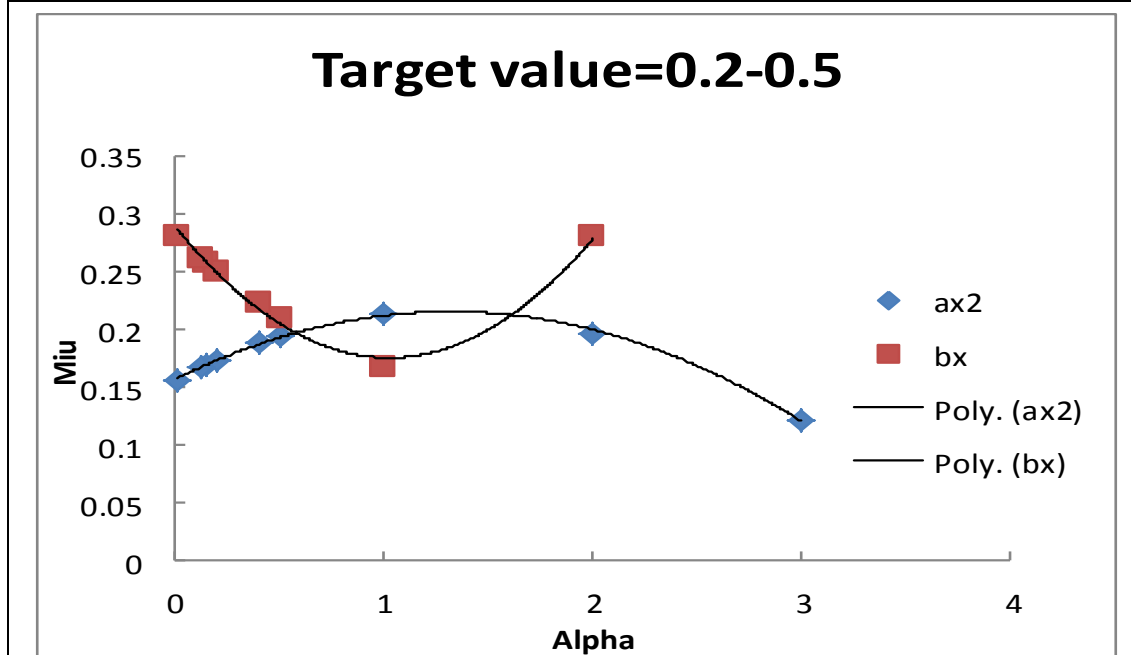


(d) Combination of data from the second and first order polynomial coefficients. (Chamber size 30mm, thickness=0.8mm).

Figure 3.27 (c&d) Data to show the concept of combining the material sets based surface equation for the slope and interception method (a) and the material sets based surface equation for the second order and first order polynomial coefficients. (Chamber size=30mm, Sheet thickness=0.8mm).

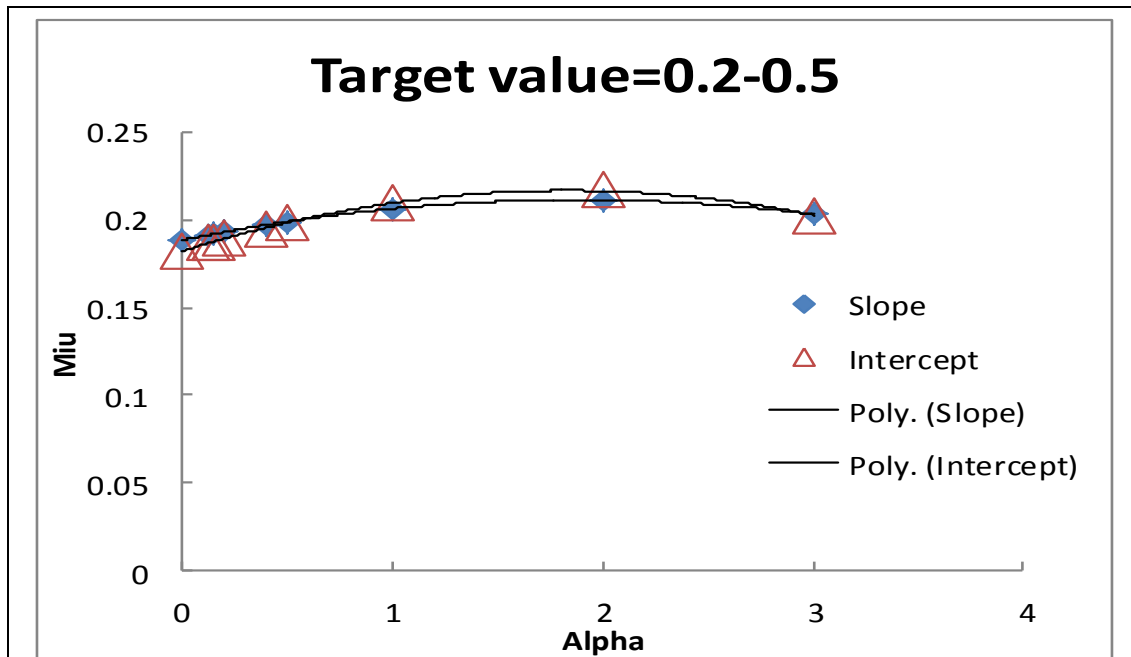


(a) Combination of data from the slope and intercept approach.

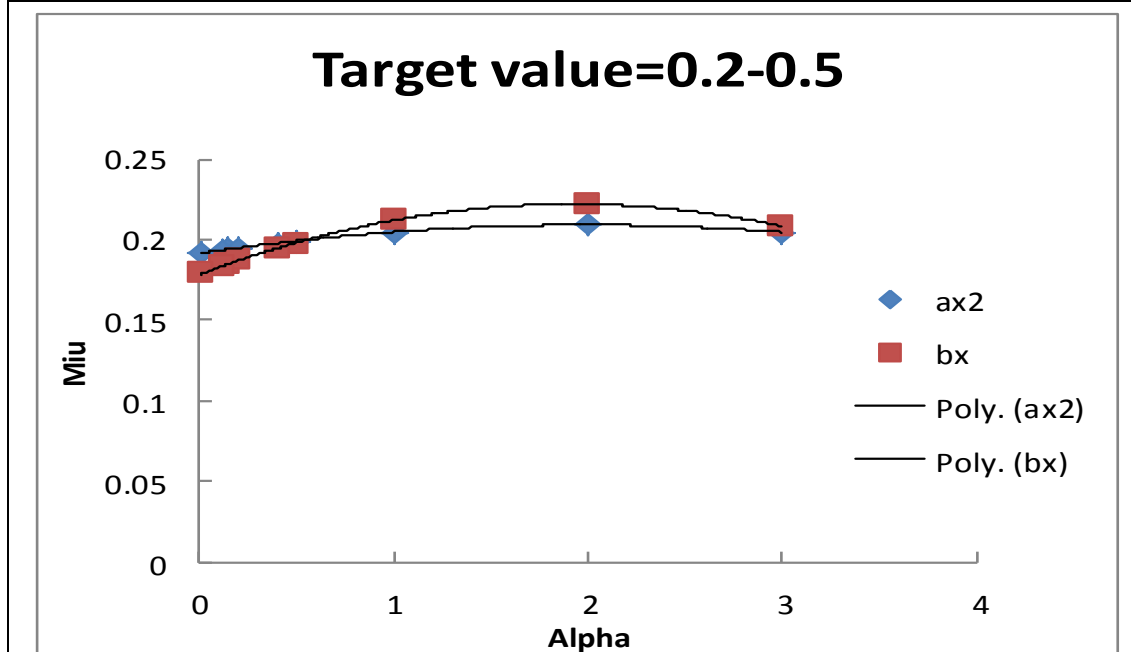


(b) Combination of data from the second and first order polynomial coefficients.

Figure 3.28 (a&b) Data to show the concept of combining the material sets based surface equation for the slope and interception method (a) and the material sets based surface equation for the second order and first order polynomial coefficients. (Sample diameter=20mm, Sheet thickness=0.3mm)



(c) Typical predicted material sets (Target: $\mu=0.2$, $\alpha=0.5$) with a combined slope and intercept approach.



(d) Typical predicted material sets (Target: $\mu=0.2$, $\alpha=0.5$) with a combined ax^2 and bx approach.

Figure 3.28 (c&d) Data to show the concept of combining the material sets based surface equation for the slope and interception method (a) and the material sets based surface equation for the second order and first order polynomial coefficients. (Sample diameter=30mm)

3.10 Use of the inverse approach in analysing experimental data and comparison with the full curve objective function approach

The analysis developed using training data with selected numerical data as the target shows that by using two curve parameters from the same curve, the material parameters could be predicted using the crossing point between the data from different approaches. These approaches have been used to analyse the experimental data of samples of different thicknesses including the curvature and slope, slope and intercept, polynomial parameters 'ax²' and 'bx' approaches. The procedure is similar to that used in the training data, in which the curve parameters were determined first then the potential material parameters are determined by using the surface functions. The procedural details are not repeated to preserved clarity. Some key results are illustrated in Figure 3.29.

As shown in Figure 3.29(a), two different approaches (curvature and slope) have been performed with chamber size 20mm and plotted together to identify the material parameters. The experimental data fitted in ABAQUS from the standard tensile tests data is ($\mu=0.35$, $\alpha=2.4$). As shown in the figure, the material property at the cross point is ($\mu=0.34$, $\alpha=2.5$), which is close to the target value. As shown in Figure 3.29(b), for chamber size 30mm, the prediction material parameter sets is within in a reasonable range of the target, but there are many other data close to each other on the lines. Figure 3.29(c & d) shows the results for the data based on combination of slope and intercept point method. As shown in Figure 3.29(c), there is a clear cross points when the chamber size is 20, which is close to the target value. But for chamber size 30mm, as shown in Figure 3.29(b), there is no clear cross point.

Figure 3.29(e&f) shows the data when combining the second order and first order polynomial curve coefficients. As shown in Figure 3.29(e) for chamber size 20mm, there is a clear cross points between data from the surface equations, the material properties correspond to the cross point is within a close range of the target data. For chamber size 30mm, as shown in Figure 3.29(f), there is cross point which is in a reasonable range of the target data, However, the data line of 2nd order coefficient 'a' and data line for the first order coefficient 'b' is very close, which made it difficult to be conclusive with a clear prediction. This suggests that this ax² and bx approach is a

more robust approach than the other approach in particular with a smaller chamber size.

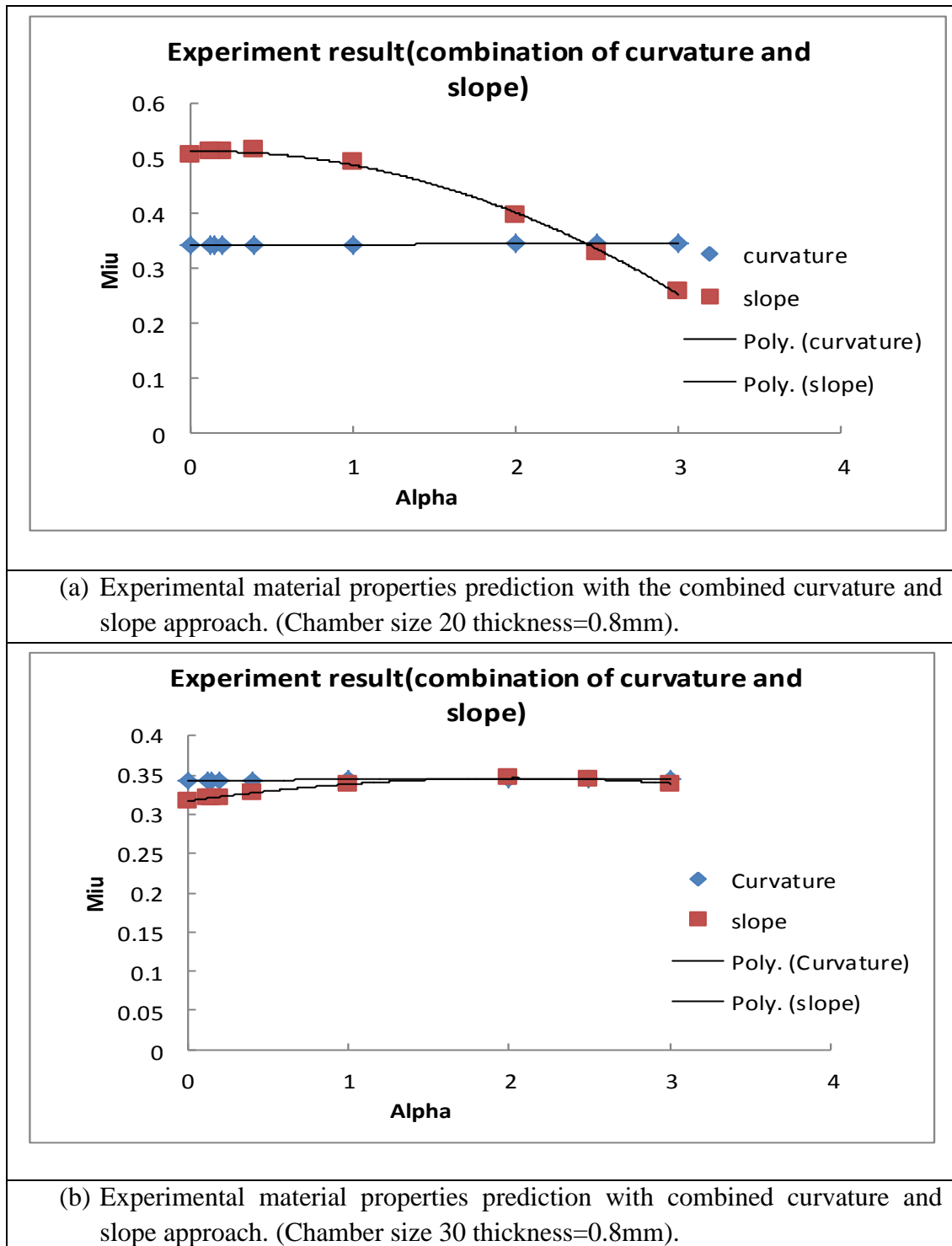
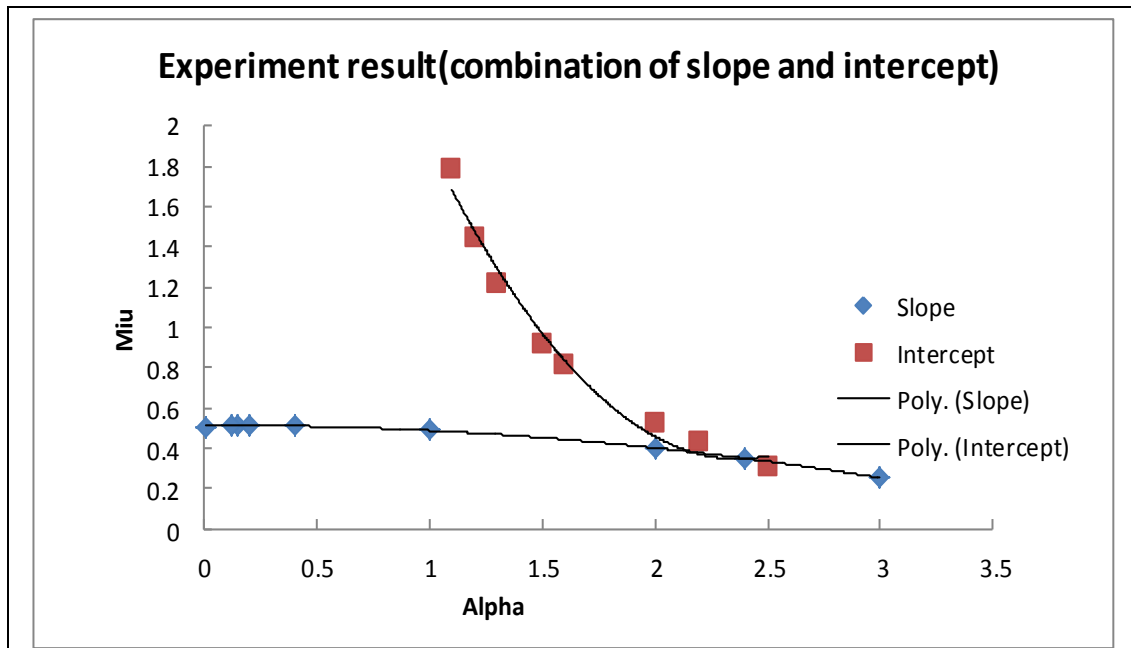
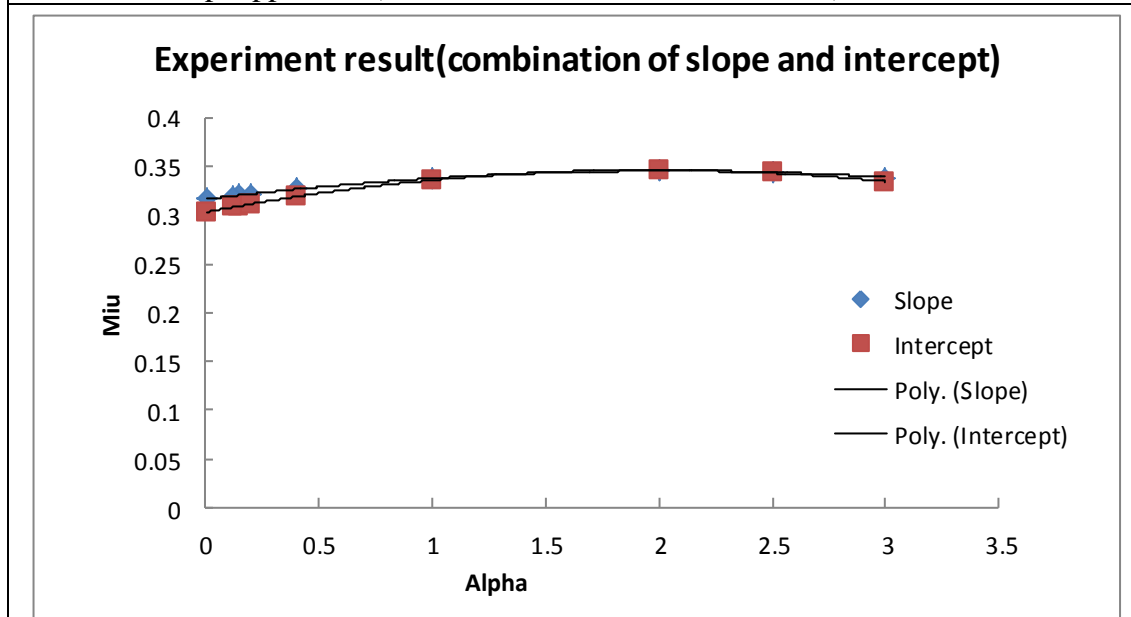


Figure 3.29 (a-b) Materials parameters prediction based on the experimental data with the combined curvature and slope approach for chamber size 20 (a) and chamber size 30 (b). (Sheet thickness=0.8mm, Target value: $\mu=0.35$, $\alpha=2.4$)

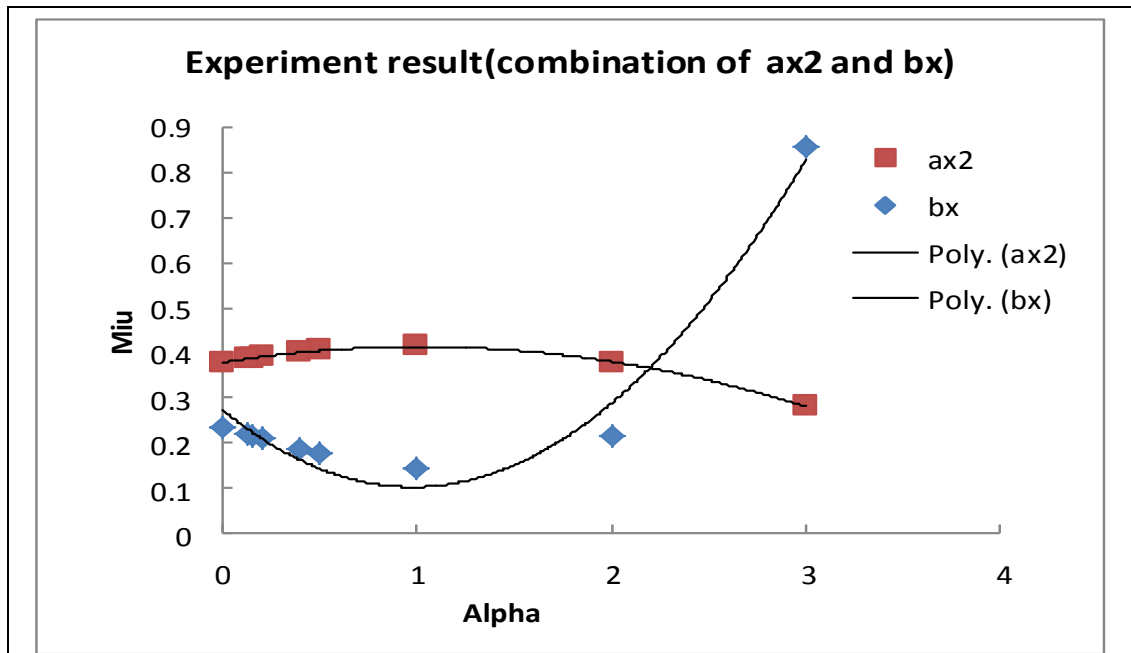


(c) Experimental material properties prediction with combined slope and intercept approach. (Chamber size 20 thickness=0.8mm).

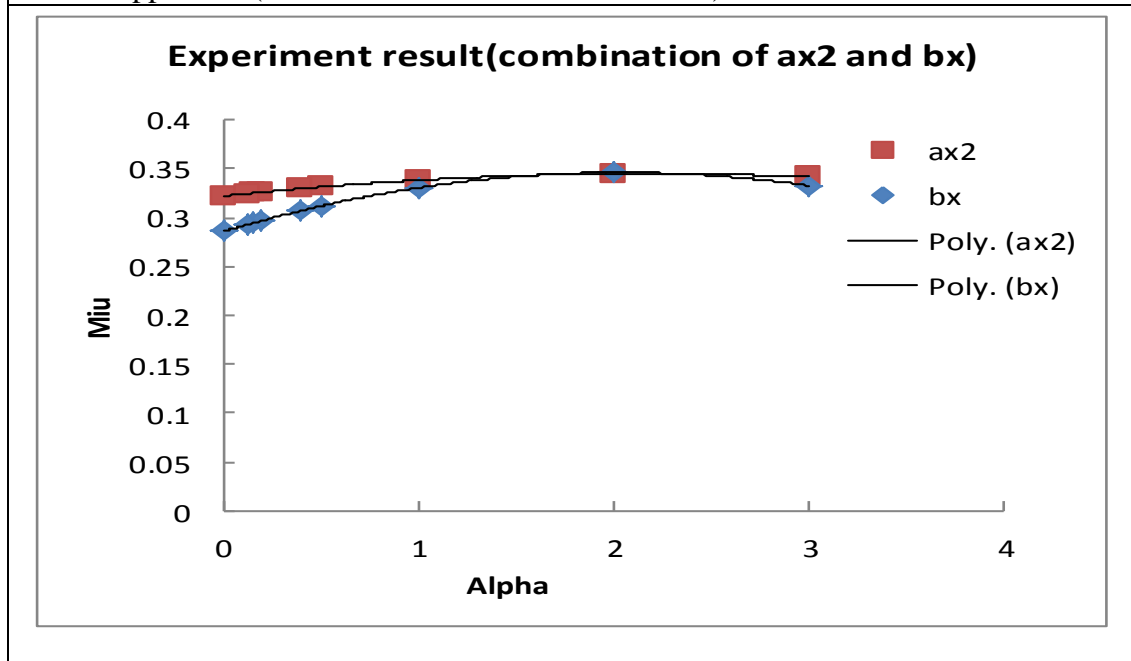


(d) Experimental material properties prediction with combined slope and intercept approach. (Chamber size 30 thickness=0.8mm).

Figure 3.29 (c-d) Materials parameters prediction based on the experimental data with the combined slope and intercepts approach for chamber size 20 (a) and chamber size 30(b). (Sheet thickness=0.8mm, Target value: $\mu=0.35$, $\alpha=2.4$).



(e) Experimental material properties prediction with combined ax^2 and bx approach. (Chamber size 20 thickness=0.8mm).



(f) Experimental material properties prediction with ax^2 and bx approach. (Chamber size 30 thickness=0.8mm).

Figure 3.29 (e-f) Materials parameters prediction based on the experimental data with the combined 2nd and 1st polynomial equation coefficients approach for chamber size 20 (a) and chamber size 30(b). (Sheet thickness=0.8mm, Target value: $\mu=0.35$, $\alpha=2.4$).

Figure 3.30 is a bar chart showing the comparison between inversely predicted properties from the experimental data with three different approaches. For chamber size 20, most of the prediction in a good agreement with the target values. For chamber size 30, the values are within a reasonable range. The predicted $\mu(\mu)$ value is very close to the target value but the values for Alpha(α) are slightly out of range.

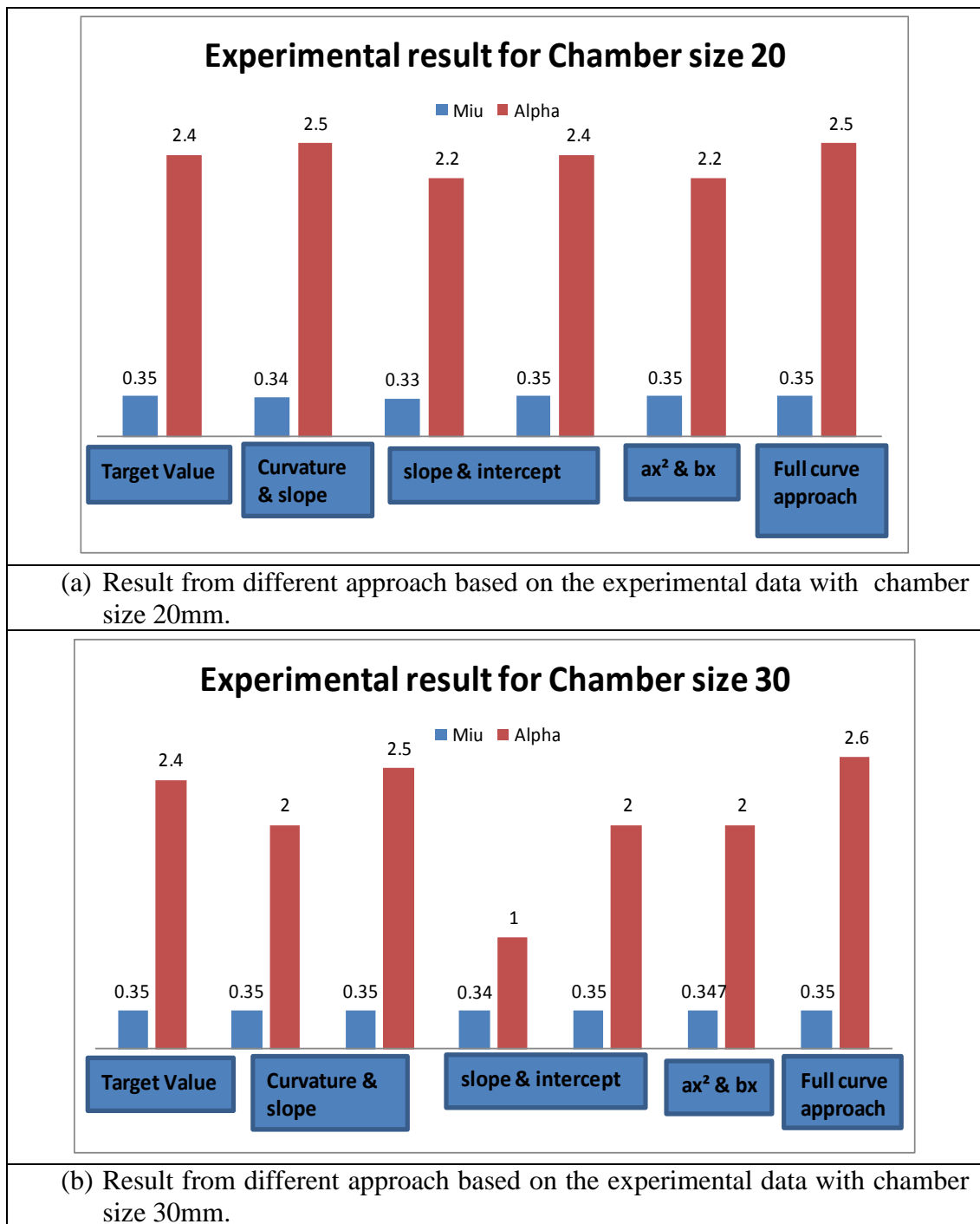


Figure 3.30 A Bar chart comparing the predicted data from different approaches.

3.11 Discussion

Application and mechanics of indentation bending tests.

Indentation bending test is a convenient testing method to characterise the material properties in the form of thin soft samples. The material covered is relevant to many industrial sectors such as biomechanics and material engineering. The advantages of the indentation bending test is that it only requires small amounts of material sample. Many efforts have been made to analytically represent the force displacement data (*Begley M. R. et al, 2004; Scott O.N. et al, 2004; Ju B. F. et al, 2005; Ahearne M. et al, 2009*) but most of these analytical approaches are only applicable to limited conditions. In addition, most of the analytical solution is only based on the Young's modulus. The use of an inverse FE modelling allows a much more flexible approach without the requirement of strict conditions, but requires large data asset and processing. As illustrated in this work, this can be addressed using a computer program to automatically generate and process data. The main focus of the project is in developing a practical program to identify all the potential materials parameters, the data would then be used to establish optimum condition for materials parameter identification by combining different test dimensions and the data.

As presented in sections 3.1-3.10, this work has developed some key computer programs which are important to make the inverse property identification process. The first program is the ABAQUS add-on which allows the user to generate the FE data over a wide range of material properties, once the original FE model is validated. This involves allowing the user to control both the range and the data density. This can be easier to use in other situations. Secondly, the program has been developed to allow the calculation of the key curve parameters. This made it much easier and quicker. Most importantly it allows the processing to follow the same format. All the data can be processed in exactly the same way. The program developed determines the 3D surface plot is one of the important programs. In preliminary work, many different equations have been tried but the results shows that it could not accurately represent the data. The 3D surface plot clearly demonstrates the relationship between key curve parameters and the nonlinear material parameters. This program has allowed us to processing multiple curve parameters format, force-displacement curves and conveniently compare/assess the uniqueness and accuracy

of the inverse material parameter identification process. It also made the evaluation of different approaches in combining different tests much easier. One major problem for inverse FE based material parameter identification may suffers from non-uniqueness, this has been reported in many other form of testing in tension, compression or indentation, in particular when using hyperelastic strain energy functions (*Sasson A. et al, 2012; Erdemir A. et al, 2006; Moerman K.M. et al, 2009; Gras L. L. et al, 2012; Chang C.T. et al, 2015*). The approach in using the surface plot equation could make the processing in using data from different experimental set (such as dual indenter method) and in this work dual chamber method much easier. This allows the feasibility of different approaches to be more efficiently evaluated.

With the help of the programs developed, this work has assessed many different combinations including jointly using the data from different chambers (sample sizes) and the combination of different curve parameters. The dual chamber size method showed some improvement in terms of the robustness of the predicted results but with the depth of this work, this is still difficult to predict nonlinear parameters. The option of combining the curve parameters could gave a new direction. Most of the combination of curve parameters (Figure 3.18(b&c)) mathematically showed a clear cross point, which suggests that the method is theoretically feasible. But there are a few situations where the data from different curve parameters are still very close, so practically it will not be possible to distinguish the material parameter accurately and robustness. The best result is shown with chamber 20 and thicker sample. This suggests that using a relatively smaller chamber or sample size will be a better option. As shown in the work in the training data (using numerical data) and analysing the experiment data, these approaches could produce predicted data close to the target data.

Factors affect the indentation bending test and FE modelling process

The indentation bending test usually represented by force and displacement ($p-h$) curve, where force (p) is the resistance of the material and depth (h) of the indenter. There are many factors which might affect the $p-h$ curve such as indenter shape and size, chamber size, and experimental conditions, etc. These factors have to be carefully considered when using the indentation bending test and FE modelling process. For each of the material models studied, the effect of mesh size has been

assessed by different meshing scheme to ensure the model is accurate and valid. Different strain energy function and linear elastic models were compared to testing data to further validate the FE model. Loading rate is another important factor has to be studied and has been assessed in the early stage of the work by comparing the p - h curve with different loading rate range from 1-10mm/min. The results showed no significant difference for all the loading rates studied. This could eliminate one of the factors for FE modelling as it could reduce the uncertainty of the results due to rate dependent material model. Another important factor which might affect the p - h curve is friction coefficient. This has been assessed in the earlier stage of the work by comparing the p - h curve with different coefficients and showed testing data is less than 0.1 friction coefficient. This could assumed that frictionless between two surfaces and provide a significant advantage for inverse FE modelling. Different from other small sample tests such as indentation tests, indentation bending tests is sensitive to the size of the chamber. When a smaller chamber is used, for the same displacement the strain level is higher. This actually has generated a situation when the dual chamber size approach can be used. In addition, for hyperelastic properties, a smaller sample size is more sensitive.

Sensitivity of the predicted material properties due to variations of the input data is essentially an intrinsic characteristic of inverse processes. In this work, the input data were taken from a numerical model, but, in a real testing situation, there can be potentially both system and random errors. Factor such as indenter diameter, roundness of the indenter tips, accuracy of the recorded indentation force or depth and chamber position which may influence the measurement results (Dao et al., 2001). One of the major issues may affect the prediction work is misalignment of the experiment setup such as indenter and chamber holder. All these needs to be carefully controlled to avoid error in the inverse FE modelling process.

3.12 Conclusion

In this work, the use of inverse FE modelling and indentation bending test for material properties (hyperelastic Ogden model) identification has been systematically studied. A parametric FE model has been developed and validated simulating the indentation tests of thin latex rubber samples made in the laboratory. An ABAQUS add-on program has been developed to automatically update the material parameters and extract the force-displacement data. Different curve analysis approaches in representing the force-displacement curve have been proposed including: (1) using ratio of P/h^3 for the low load region, (2) using the effective slope at higher load and (3) using the second order polynomial curve fitting parameters. The effectiveness of these three approaches in providing data to inverse material parameters identification is evaluated supported by several programs. The result shows that use of these curve fitting parameters could effectively simplify the inverse FE modelling process and allow the use of surface plot equations to establish a mathematical relationship between curve coefficients and material parameters. These relationships could effectively open up the possibility in improving the uniqueness of inversely predicted material property sets by combining either data from different testing conditions or different curve data from the same test.

A MatLab program has been developed to determine the surface equation between the key curve coefficients and the material parameters based on FE data with an Ogden model. Work based on the data from a single indenter tests shows that there are multiple material property sets that could produce identical force-displacement data. This confirms that the results are not unique. A program has been developed which allows systematic studies with different approaches including dual chamber size and combining two curve parameters approach. Several approaches have been evaluated by combining the surface equation for different curve parameters or testing conditions (i.e. sample sizes), including (1) combination of curvature and slope; (2) combination of slope and intercept, (3) combination of 2nd and 1st polynomial equation coefficients approach. The program is evaluated using numerical training data and experimental data. The results show that combining different curve fitting approaches method with a smaller chamber size is more effective than using the dual

chamber size approach. The combination of 2nd and 1st polynomial equation coefficients approach offers the optimum accuracy and flexibility.

CHAPTER FOUR

CHARACTERISATION OF THE VISCOELASTIC MATERIAL PARAMETERS OF MATERIALS FROM INDENTATION BENDING TESTS.

4.1 Introduction

In this chapter, an inverse FE program is developed to characterise the viscoelastic material parameters of thin sheet samples based on indentation bending tests. As shown in Figure 4.1, in the first part, a set of relaxation tests based on the indentation bending system was conducted. Latex rubber with different thicknesses were produced and tested. The creep properties of the latex rubber are inversely estimated by combined experimental data and FE modelling program. The repeatability and effect of experimental condition on relaxation testing are established. The accuracy of the predicted viscoelastic parameters is assessed by comparing the testing results with standard tensile relaxation test. The factors affect the viscoelastic tests and the inverse parameter identification process is discussed. Two inverse modeling approach have been developed, one is based on an objective function searching approach, the other one is based a staged interactive approach. The accuracy of these two approaches are comparatively studied through both training dataand against experimental data.

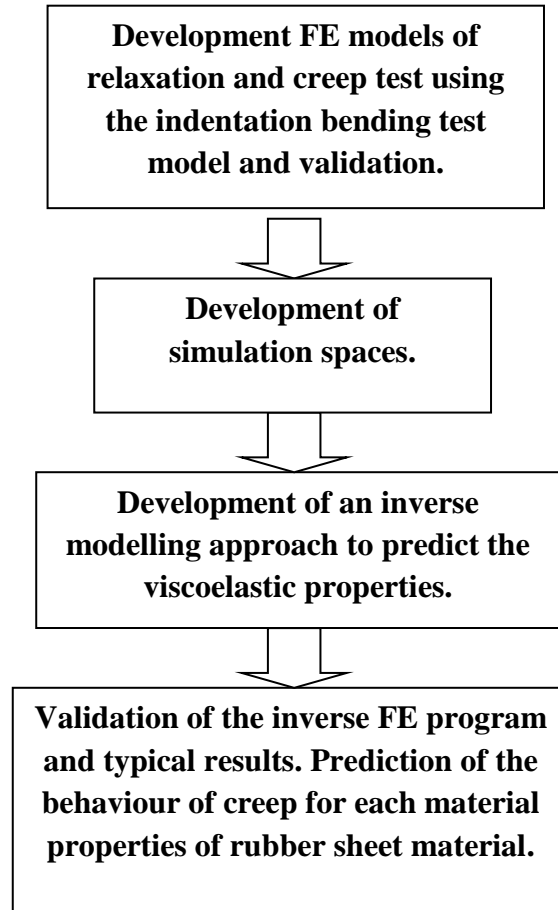


Figure 4.1 Flow chart showing the main work in developing an inverse modelling procedure to extract the relaxation coefficients from indentation bending tests.

4.2 Experimental work and results

4.2.1 Materials

Specimens for standard tensile stress relaxation tests and indentation bending relaxation test were produced by latex liquid emulsion as shown in Figure 4.2(a) and (b). Large rubber sheet were cut in round shape for indentation bending relaxation tests and dog-bone shaped standard tensile test specimen is used for tensile stress relaxation tests.

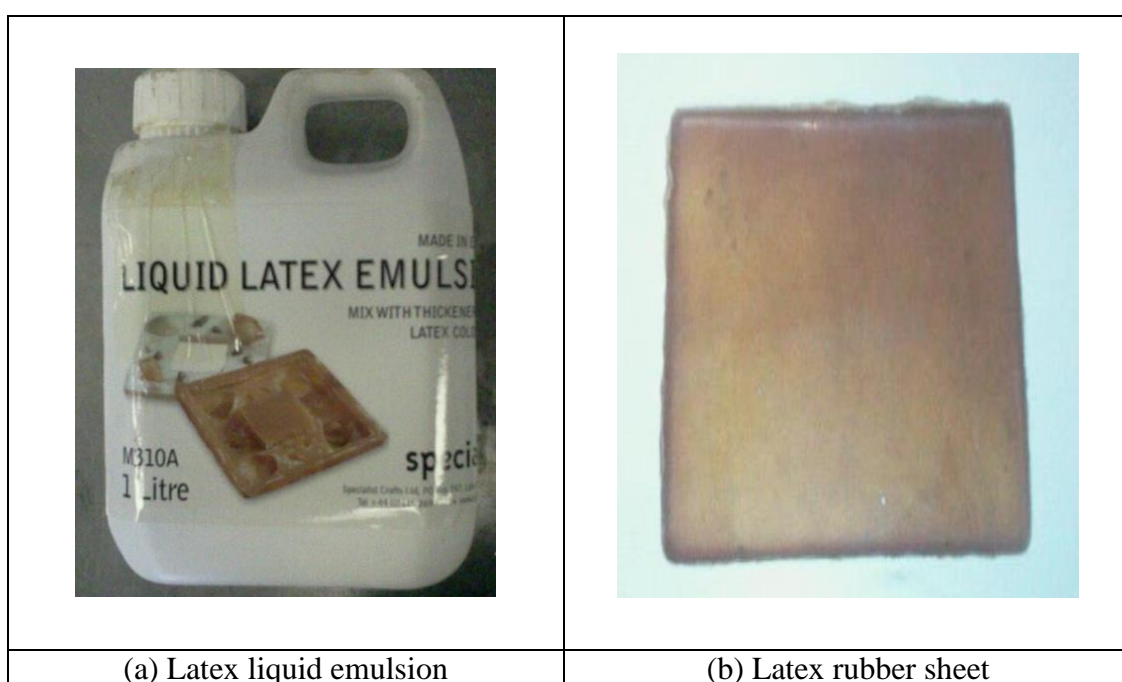


Figure 4.2 Latex liquid emulsion and specimen material.

4.2.2 Relaxation tensile test

The tensile stress relaxation tests were performed on a standard tensile testing machine (model: Tinius Olsen, H50KS) as shown in chapter 3 (Figure 3.3(a)) with a 10N load cell. In the test, a dog bone shaped specimen is pulled to a predefined displacement with a constant strain rate. The movement of the cross head is stopped when the required displacement is reached and the sample is held at that position. The load, which decreases with time is monitored from the load cell. Figure 4.2(c) shows a typical force-time data of relaxation tensile test. Different loading rate were

performed to check the sensitivity of force-time data on the strain rate. In these cases the relaxation tensile test was not significantly affected by the strain rate as shown in Figure 4.3.

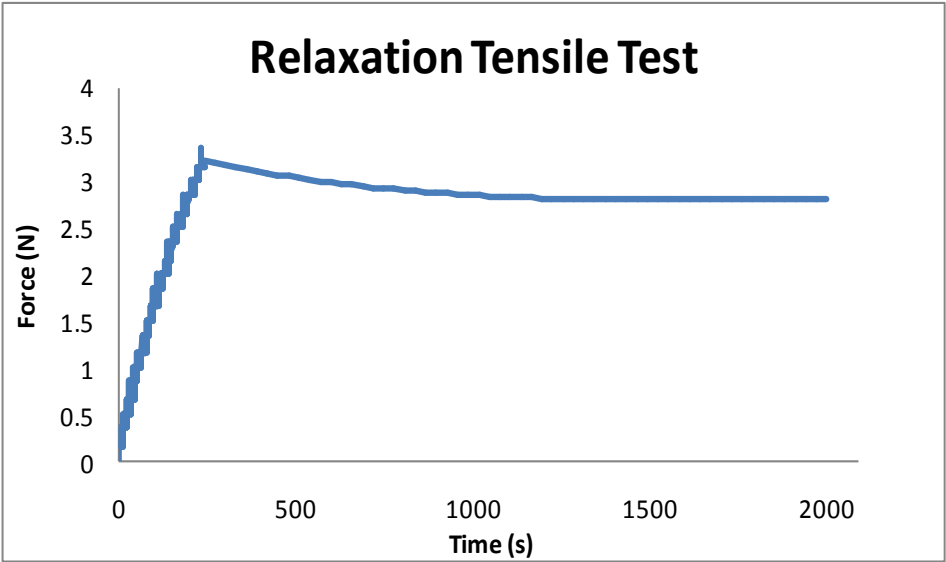


Figure 4.2 (c) Typical force-time data for relaxation tensile test of the latex rubber material.

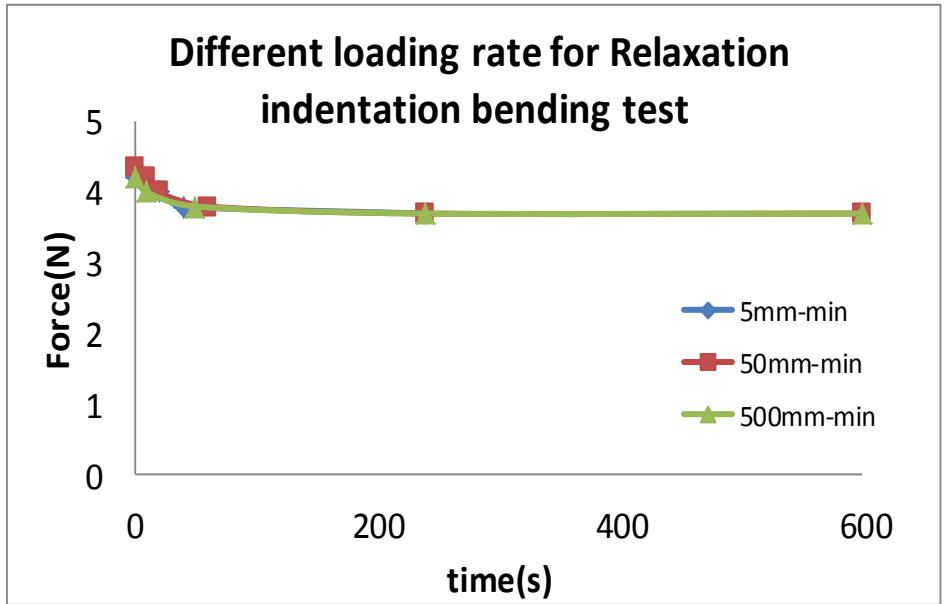


Figure 4.3 Force-time data with different loading rate.

4.2.3 Indentation bending test and relaxation tests

For the indentation bending relaxation test, round latex rubber sample is clamped tightly on a cylindrical frame with 3 evenly spaced screws to ensure no slipping occurs during the test. A stainless indenter 4mm in radius is used. The indenter was stopped at a specific depth and hold at that position with the time and force being recorded. These data would provide data as the input to the FE inverse modelling program to determine the viscoelastic parameters. Samples of different thicknesses were produced to check the thickness effect on the force displacement and the relaxation process. Figure 4.4 shows the force and time data for the indentation bending relaxation test for different thickness (1.9mm, 0.34mm and 0.24mm).

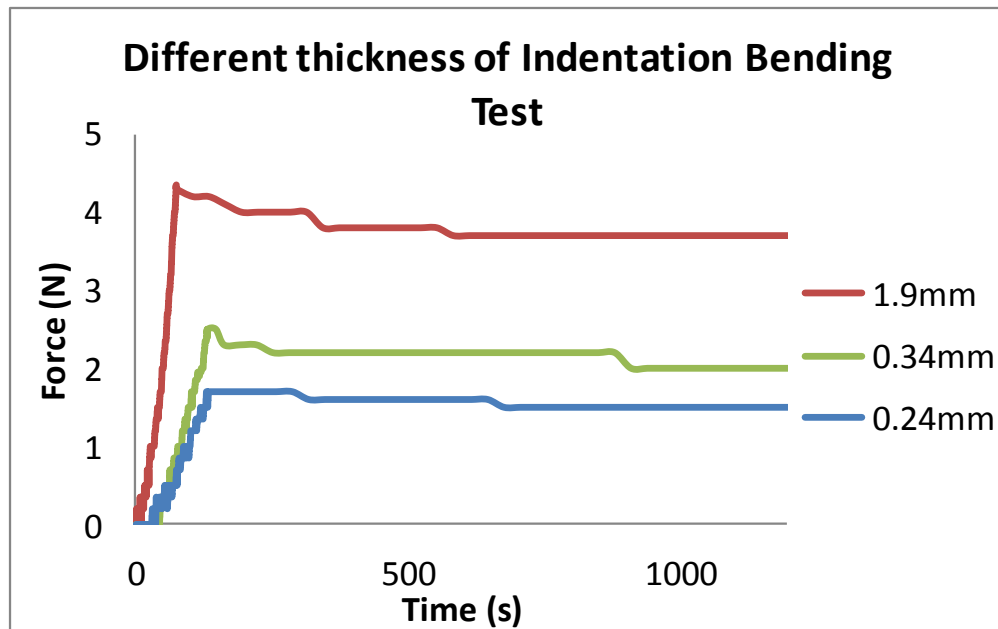


Figure 4.4 Typical force-time data of relaxation indentation bending test on samples of different thicknesses (R=4mm, Chamber size=30mm, and thickness=0.24, 0.34, 1.9mm).

4.3 FE model and inverse identification of creep parameters

The setup of FE model for simulating the relaxation test is the same as the one to simulate an indentation bending test but two steps are applied in the analysis. Step 1 is to move the indenter to a predefined depth; step 2 is to hold the indenter at the depth over a period of time. Relaxation tensile test has been conducted and converted into normalised shear modulus over time as shown in Figure 4.5. The relaxation shear test data in term of stress against time is used as an input test data into ABAQUS. First of all, the shear stress is normalised by the initial stress ([Hibbit, Karlson and Sorensen Inc., 2002](#)).

$$G_R(t) = \frac{E(t)}{2(1+\nu)} \quad (4.1)$$

Where G_R and $E(t)$ are shear and Young modulus as a function of time and ν is the Poisson's ratio.

The shear relaxation modulus can be written in a dimensionless form

$$g_R(t) = \frac{G_R(t)}{G_R(0)} \text{ or } g_R(t) = \frac{G_R(t)}{G_0} \quad (4.2)$$

Where $G_0 = G_R(0)$ is the instantaneous shear modulus.

From the formula above, the shear relaxation modulus $g_R(t)$ could be obtained which is required by the ABAQUS software together with time(s) as the input

The long term normalised shear compliance or modulus is calculated based on the formula below:

$$g_{\text{inf}} = \frac{G_{\text{inf}}}{G_0} \quad (4.3)$$

Where g_{inf} is long term normalised shear modulus,

$$G_{\text{inf}} = \frac{E_{\text{inf}}}{2(1+\nu)} = \frac{E(t)}{2(1+\nu)}$$

$E(t)$ is the Young modulus for maximum shear stress,

$$G(0) = \frac{E(0)}{2(1 + \nu)} \quad (4.4)$$

Where $E(0)$ = Young's modulus of the material. (*Canovic S. and Concalves, 2005*). Table 4.1 listed the key time point and data to obtain normalised shear stress from the tensile stress relaxation tests.

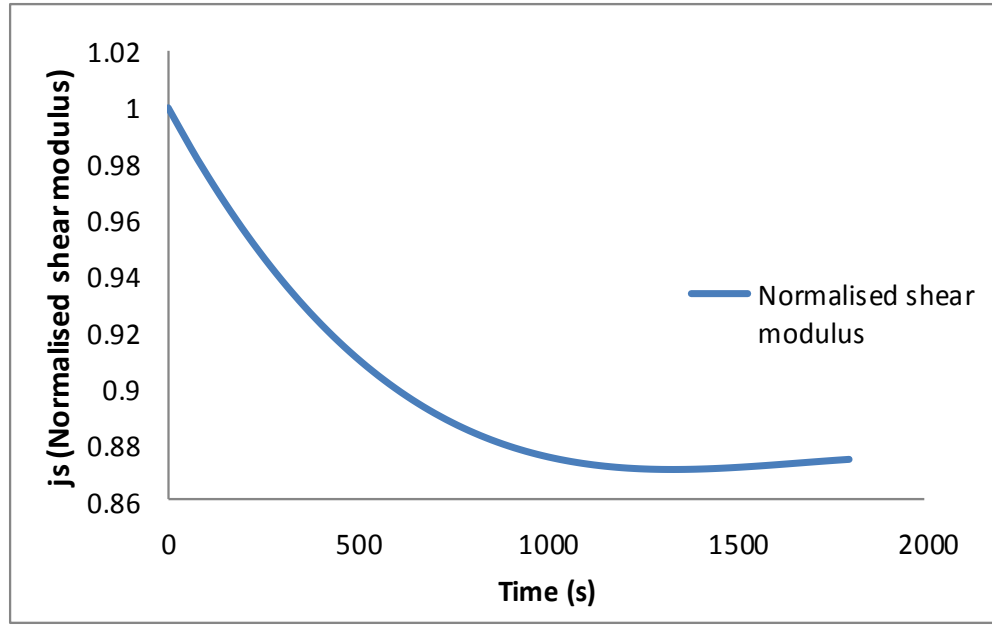


Figure 4.5 Typical normalised shear modulus-time for ABAQUS input parameters to fit the Prony series coefficients.

Table 4.1: The key time point and data to obtain normalised shear stress.

Tensile stress	Time(s)	E(t)	G(t)	G(t)(E max)	$gR = G(t)/G(t)M_{ax}$
21.75815	200	5439.538	1970.847	1970.847016	1
20.77145	400	5192.862	1881.472	1970.847016	0.954651
20.14917	600	5037.293	1825.106	1970.847016	0.926052

The FE model used is shown in Figure 4.6(a) and validated by the testing data, as detailed in Chapter 3. The numerical data is shown in Figure 4.6(b), the loading curve is simulated with hyperelastic parameters (Ogden model) and force relaxation part is modelled based on creep material parameters from the tensile stress testing data. Several visco-hyperealstic models have been developed and the force-time data

is plotted in Figure 4.7. The result shows that the Ogden hyperelastic model is suitable for modelling both the loading and relaxation process. Figure 4.8 shows the accuracy of Ogden model to describe the non-linear stress-strain behaviour.

For the viscoelastic model, ABAQUS only allow to use Prony series (Eq. 4.1), which is normally used to describe the viscoelasticity of materials ([Chen T.K., 2000](#); [Mills N.J., 2006](#)).

$$G(t) = G^\infty + \sum_{i=1}^N G_i \exp(-t / \tau_i) \quad (4.5)$$

Where,

- $G(t)$ is Shear modulus of time dependent
- G^∞ is long term shear modulus
- G_i is Shear modulus at the observation i
- t is the time in second
- and τ_i is material constant.

The material constant for the Prony series are G modulus and $\text{Tau}(\tau_i)$, which needs to be inversely predicted with indentation bending relaxation tests.

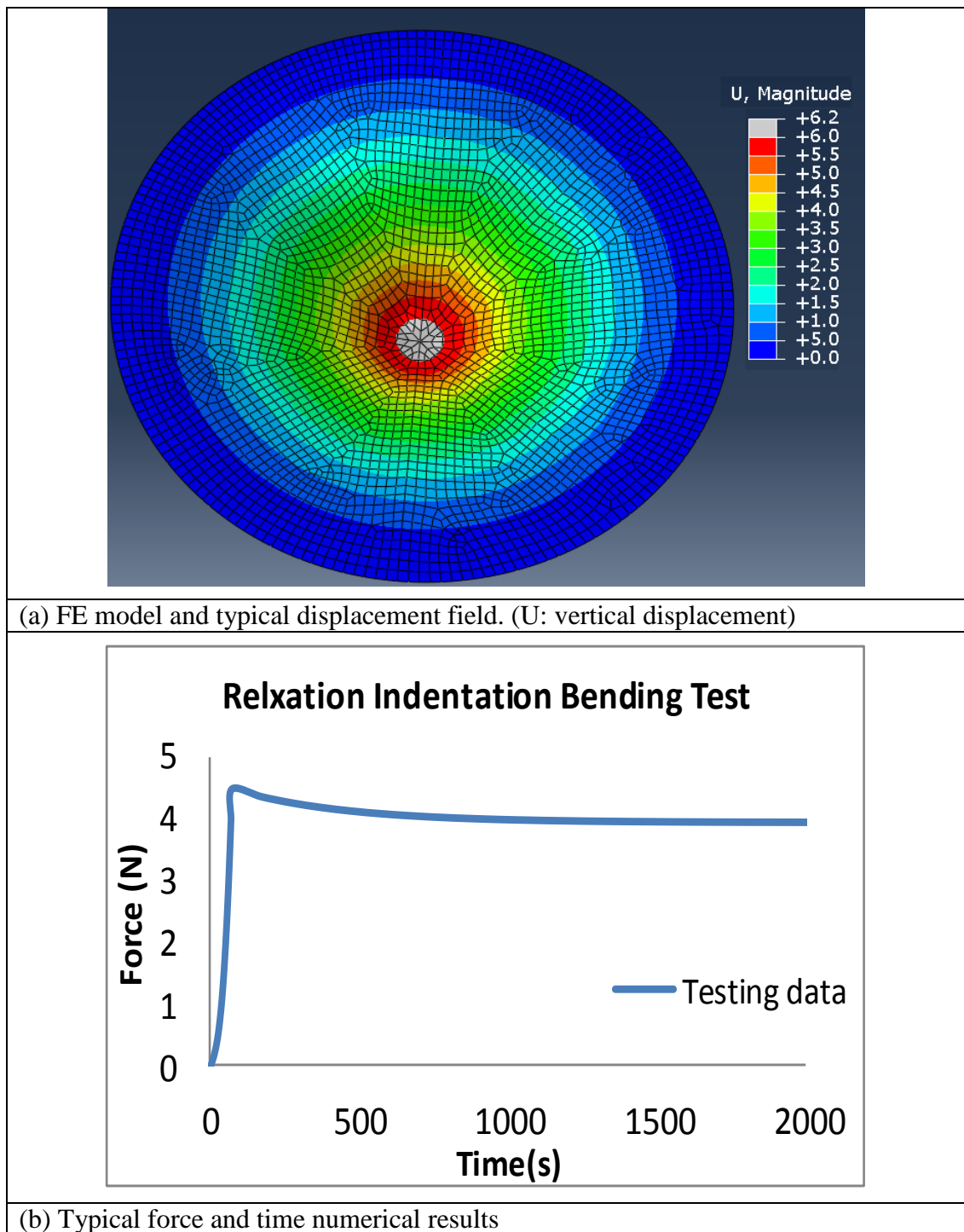


Figure 4.6 Typical FE modelling result using the tensile relaxation as direct input to the FE model.

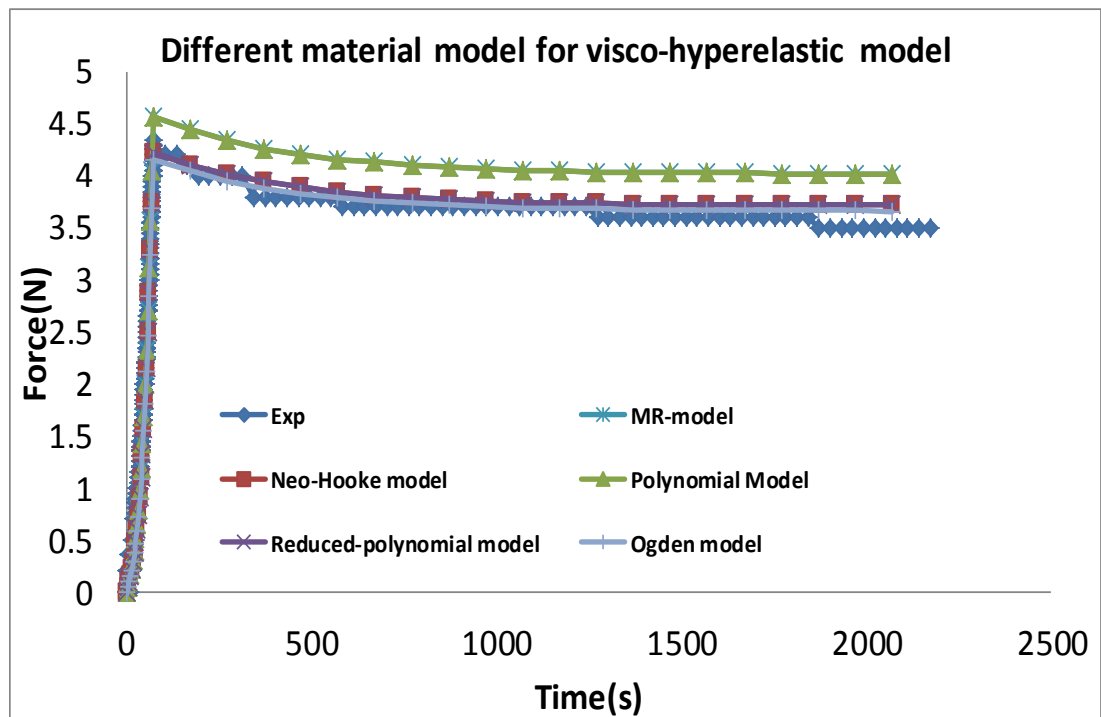


Figure 4.7 Comparison between experiment result and FE results with different material model.

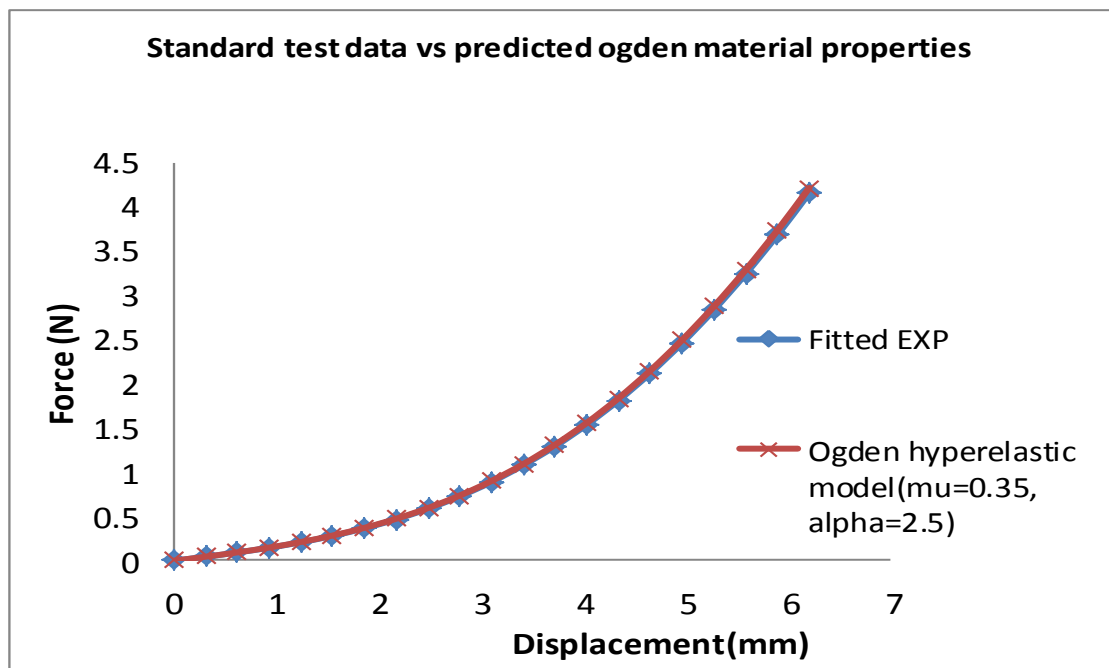


Figure 4.8 Comparison between fitted standard test data versus the data based on predicted material parameters.

4.4 Inverse program and results

Figure 4.9 shows the procedure of an objective function based inverse modelling approach which consist of three parts: experiment works, FE modelling and the inverse program. The input to the program (e.g. experimental results) is in the form of force-time data. Then FE parametric studies were used to generate relaxation test data over a potential range of material properties. The numerical data were then processed to form simulation surfaces. The inverse program will explore the simulation spaces to search for the material parameter which gives a force-time response matching the experimental data represented by an objective function.

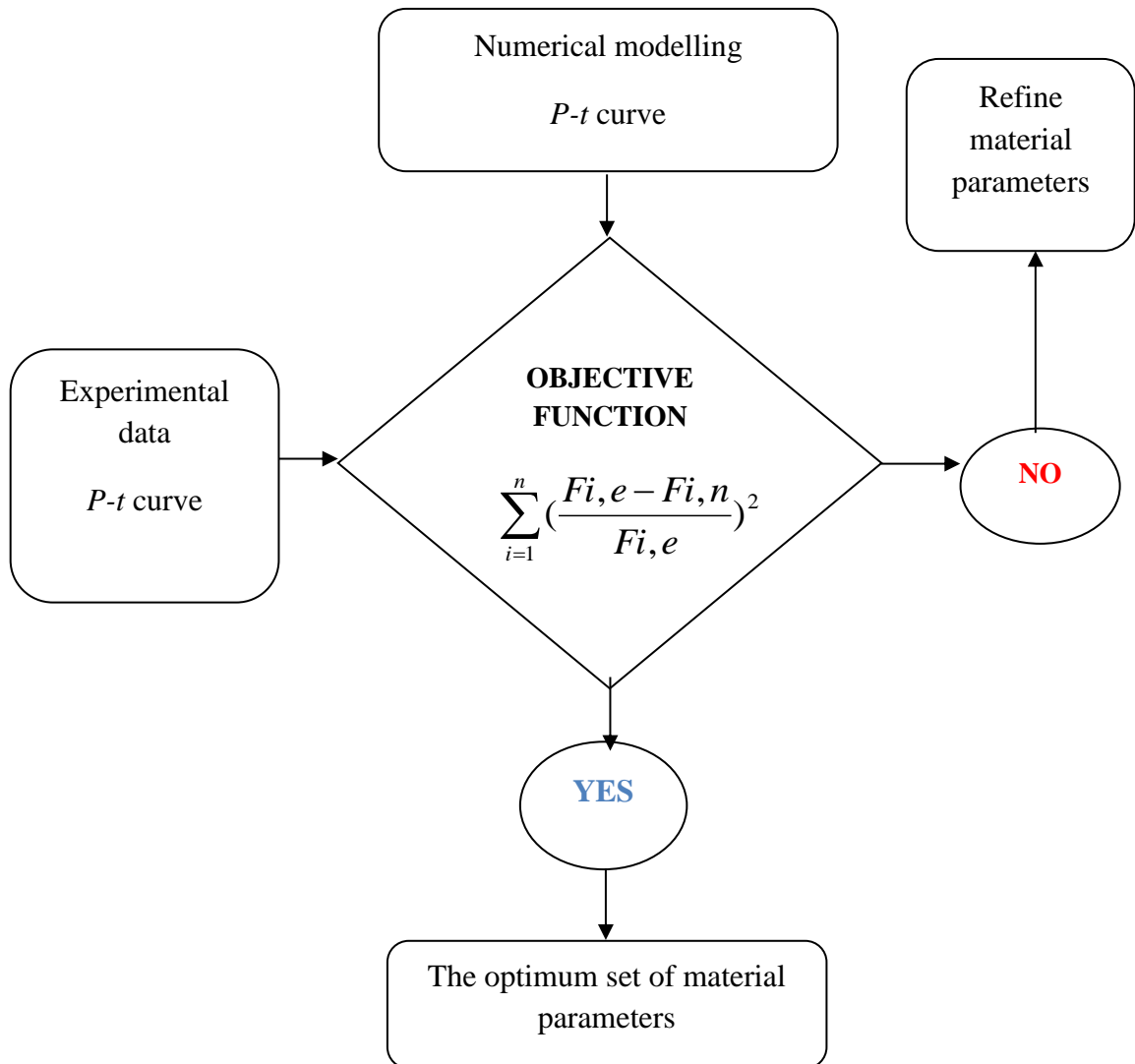


Figure 4.9 Flow chart to show the inverse modelling approach to predict the visco-hyperelastic properties.

To assess the accuracy of the program, training data were conducted by using data with known material parameters as shown in Figure 4.11. The difference between the relaxation curves for each set of material properties and the target was calculated using objective functions of the force at different time points. Figure 4.12 plots the surface of the objective function value over the property domains against the material parameters (G and τ_i). The 3D surface plot represents the objective function value, x and y-axis is the material parameters (G and τ_i). The minimum value point could be determined as $G=0.2$ and $\tau_i=250$. As shown in Figure 4.13 where the objective function value gets lower when the material parameters move closer to the target value. Similar accuracy has been observed with other target data in the training data. These suggest that the objective function approach is an effective method in estimating the creep parameters.

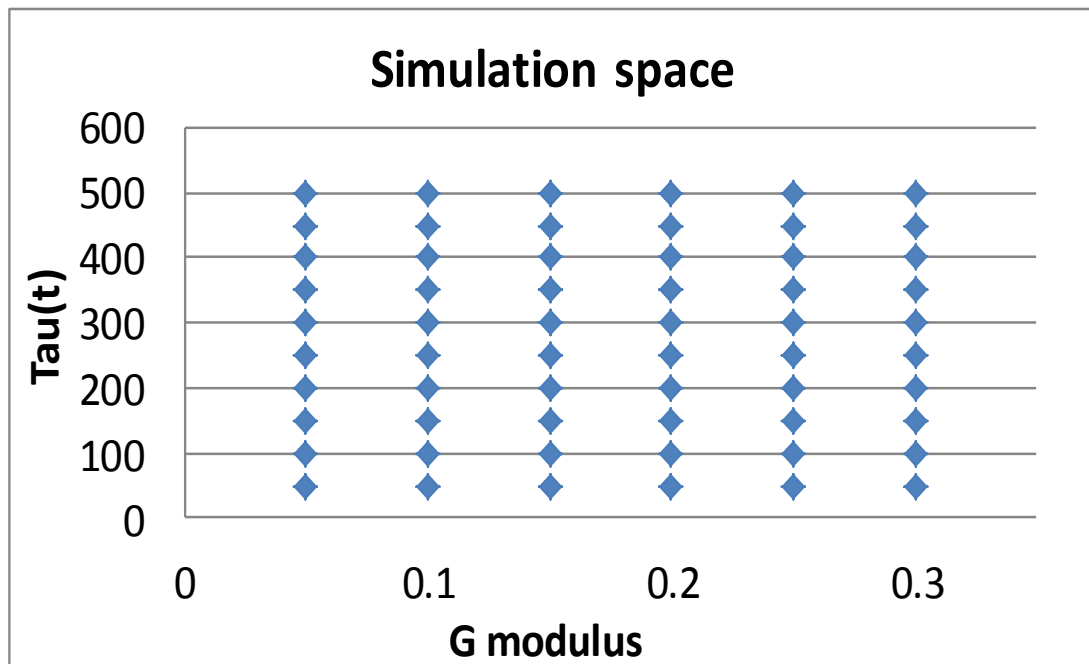


Figure 4.10 Simulation space for Prony series properties.

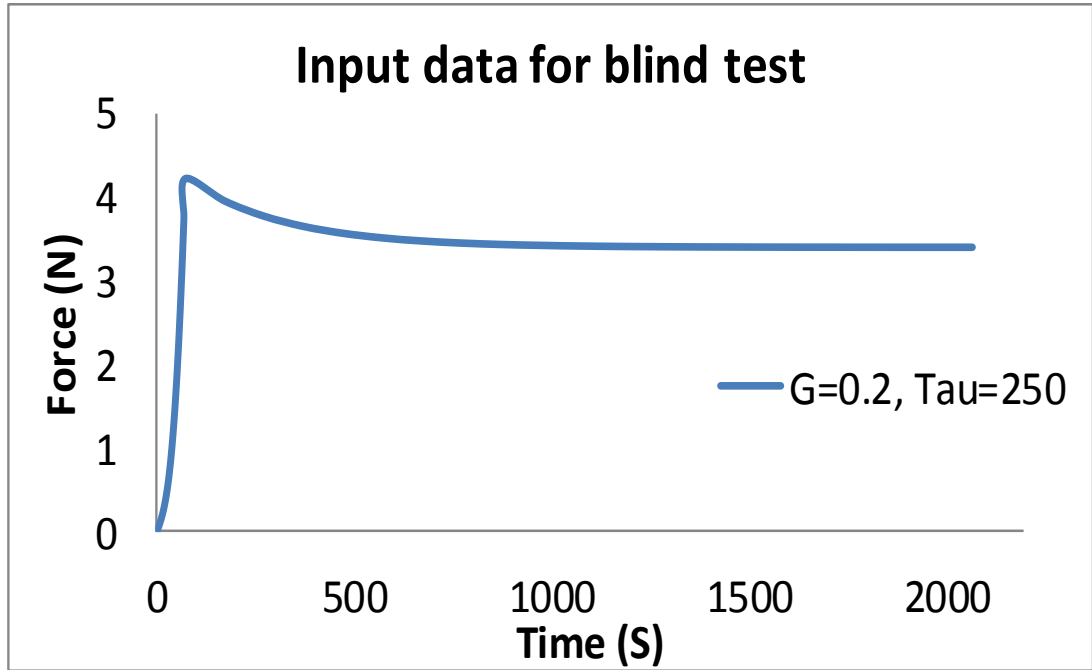
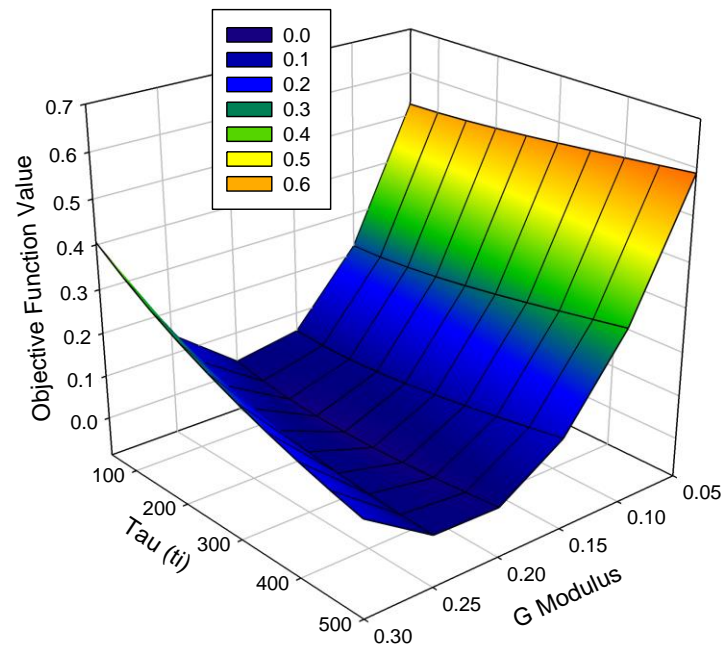


Figure 4.11 Numerical data used as a target in the training data to predict the visco-hyperelastic parameters.



$$f=1.0138-9.5588*x-0.0003*y+23.7808*x^2+4.45E7*y^2$$

Figure 4.12 Surface plots of the Objective Functions for training data with known material properties.

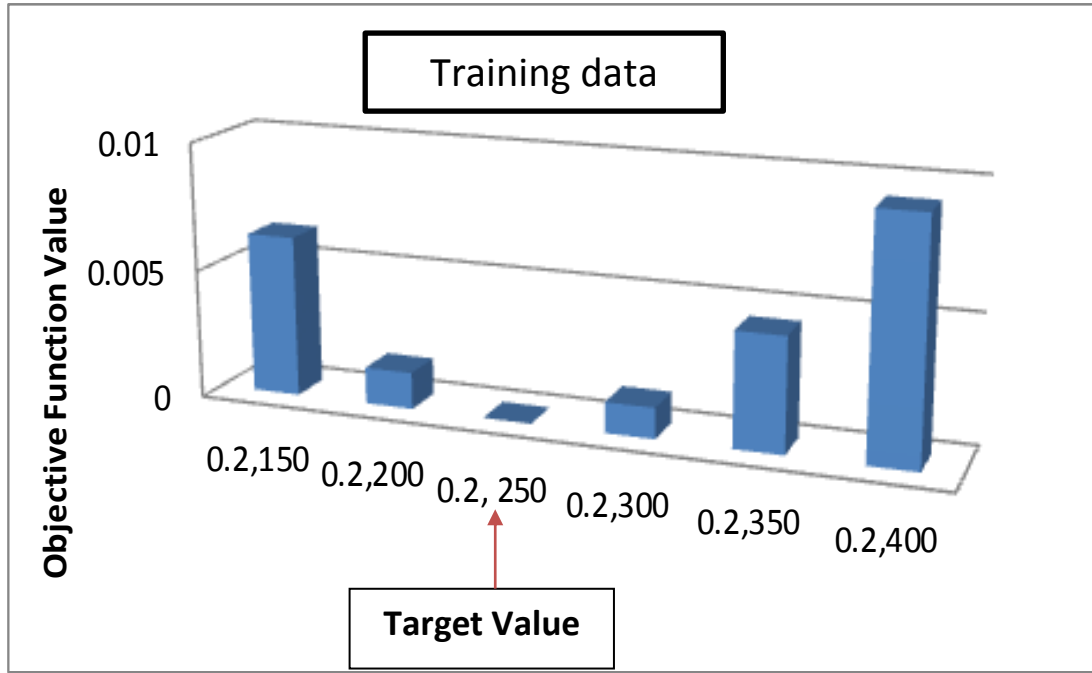
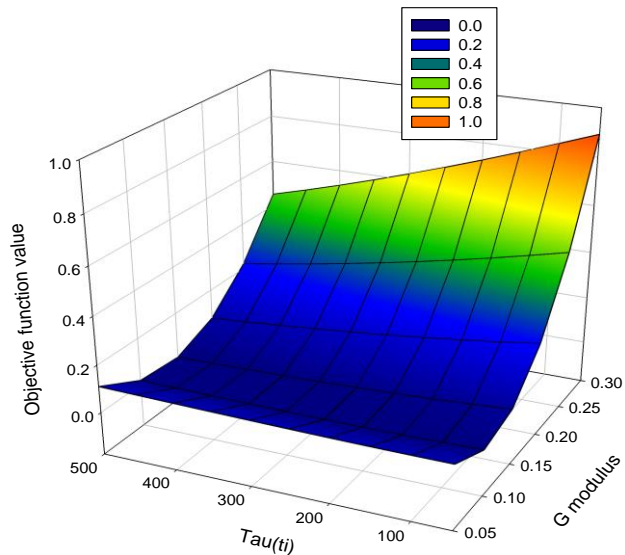


Figure 4.13 Typical objective function values for some property sets against target ($G=0.2$ and $\tau=250$).

Figure 4.14 shows the surface plot of the objective functions using the experiment test data as input. Due to the limited property range of the simulation space, the prediction of the material properties is not in a perfect match to the data estimated from the tensile relaxation tests.



$$f=0.3889-4.7470*x-0.0005*y+19.9816*x^2+2.5E-7*y^2$$

Figure 4.14 Surface plot of objective function against the experimental data.

Figure 4.15 shows the lowest objective function is (G modulus=0.15 and τ_i =500) where the fitted standard test data is (G modulus=0.125 and τ_i =370). This suggests that the variation of the simulation space need to be refined. The accuracy of the inversely predicted material parameters is tested by comparing the numerical data and the target as shown in Figure 4.16. The red coloured cross line is numerical result fitted by tensile testing data, the blue dot line is experimental result and green colour triangle is numerical force-time data based the material property sets with the lowest objective function value. The curve clearly shows that these three are in a reasonable agreement. But there are still some differences between the curves. The results highlighted a disadvantage of the objective function based approach, as it requires the simulation need to be positioned within a reasonable range, which might be difficult in a real situation. To improve this situation, python programming was used as an interactive searching tool which has the flexibility on the property range. Details of the program and typical results are to be presented in the next section.

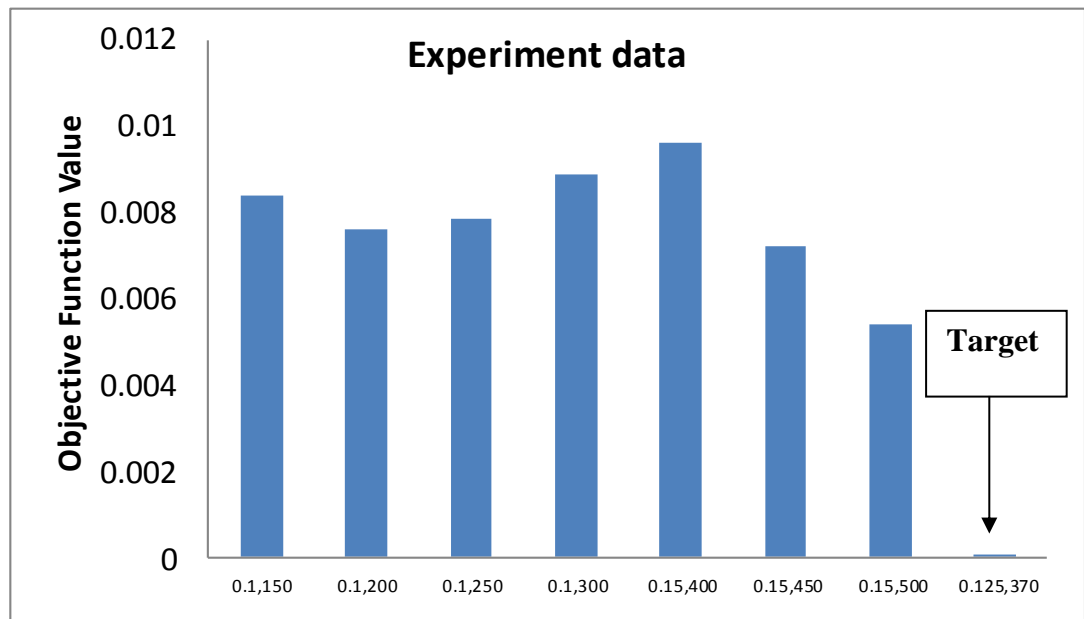


Figure 4.15 Typical objective function values of some material property sets against the experimental data. The results show that the inverse program method has produced a result close to the true material properties extracted from the standard tensile relaxation tests.

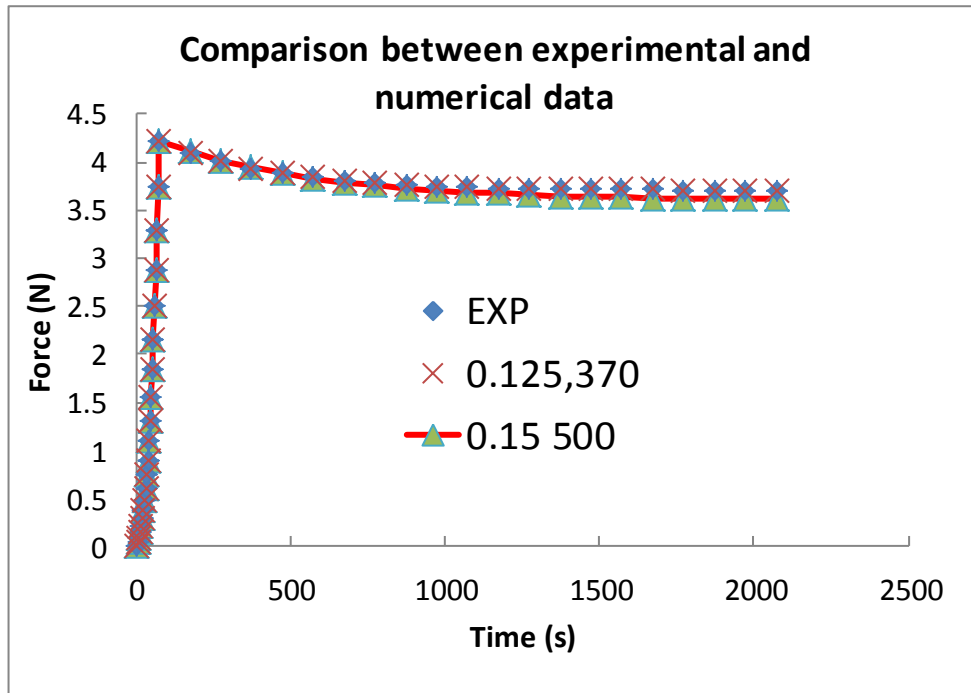


Figure 4.16 Typical force-time curve based on predicted material parameters with low objective function values together with experimental curve.

4.5 Development of a staged interactive searching program in Python and results

To overcome the problem with objective function based inverse modelling, a new interactive searching program is developed in python. A new staged based approach is implemented, i.e. searching for the G modulus first, then searching for the parameter τ_i . This will effectively reduce the time to total searching time. This concept is based on the trend shown in Figure 4.14. As shown in the surface plot, the change of the objective function is much more sensitive to G modulus than the parameter τ_i . As shown in Figure 4.17, the program consists of three main parts. The programs allow the user to input the dimensions of the indenter, chamber size, thickness and experimental data of the rubber. In the second part, the ABAQUS INP file will be updated and submit for calculation. The program will automatically extract the data from the ABAQUS ODB file and compare the results with the experiment data. Several loops will be performed until the numerical data is in a close agreement with the experimental data. Once the G value has been estimated, the program will go into the second stage searching for the parameter τ_i . The sensitivity of Prony series has been tested to check the different influence of the increment of G and τ_i on the relaxation curve. Figure 4.18(a) shows that the G value mainly affects the initial relaxation stage, while the parameter τ_i has a stronger influence on the curve over a longer time. The accuracy of the program depends on the increment of the material parameters, where if the increment is high the accuracy will decrease *vice versa* lower the increment of the material parameters will increase the accuracy of the program. In this case, every increment of the G parameters is 0.05 and for parameter τ_i is 1. The searching time is also important for this case to avoid wait for longer time to complete each search. Material parameters refinement has been create where the program consist of variation of the parameters increments shows in table 1. The aim of using different parameters increment is to speed up the search when the target is still far away from the input.

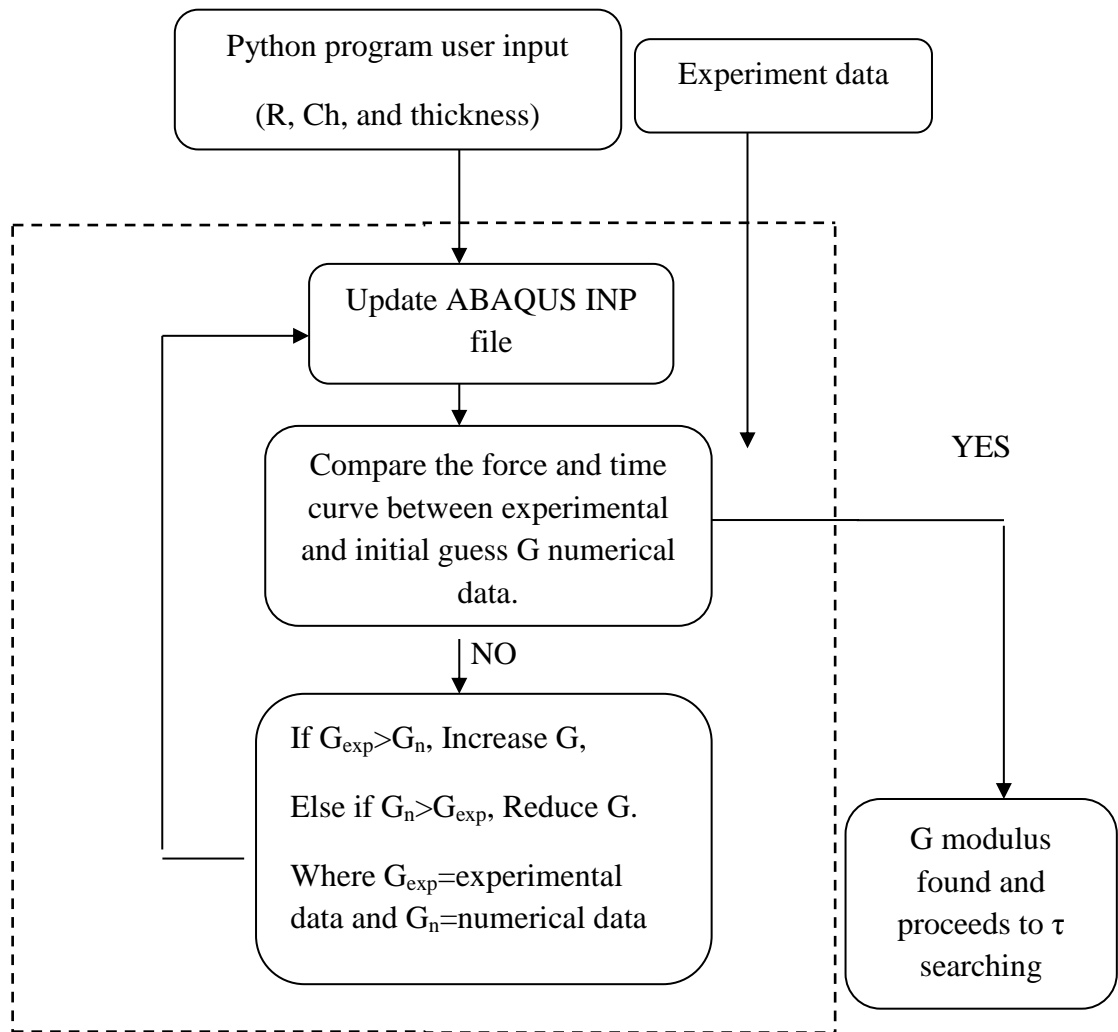


Figure 4.17 Flow chart to show the procedure of the python program to search for G and τ of the Prony series parameter.

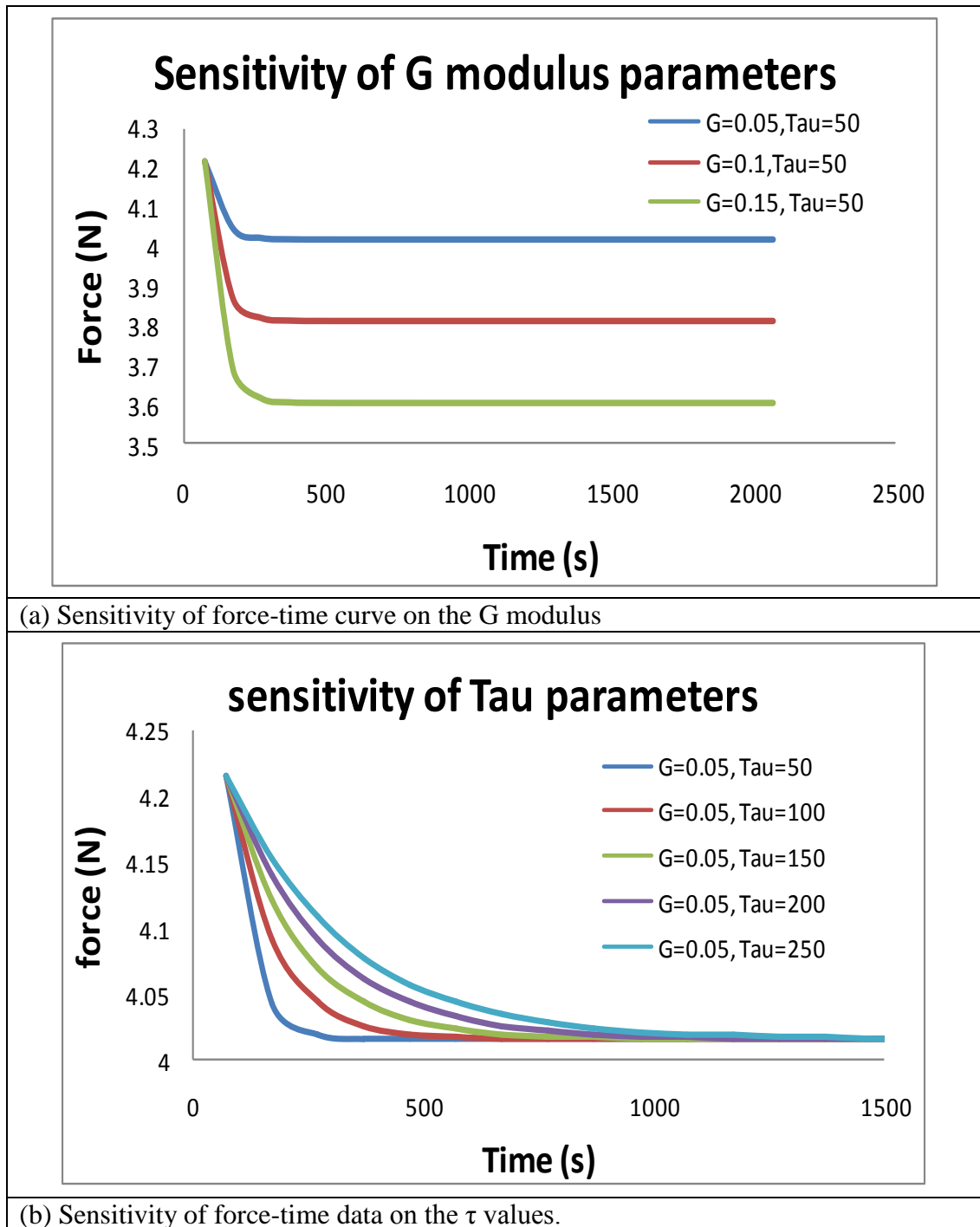


Figure 4.18 Sensitivity test of Prony series parameters.

Table 4.2: Variation of parameters increment.

Variation of parameter increment		
Objective function value	Parameter increment (G Modulus)	Parameter increment τ_i
>0.05	0.5	50
>0.02	0.4	40
>0.01	0.3	30
>0.005	0.2	20
>0.001	0.1	10
>0.000001	0.05	1

Table 4.3: Training data for python searching program.

Input		Target		%error	
G	τ_i	G	τ_i	G	τ_i
0.3	100	0.3	100	0	0
0.25	400	0.25	401	0	-0.25
0.1	250	0.1	248	0	0.8

The following Table 4.3 are the training data used to assess the python searching program accuracy. Three known material parameters have been used as an input into the program, and the returned results from the program are very accurate as shown in Table 4.4. The accuracy achieved is better than the prediction based on the objective function approach. In addition, it can be applied to samples of different thickness flexibly. Figure 4.19 compared the predicted G shear modulus and the parameter τ_i from the experimental data with different sample thicknesses. It is clearly shown that the parameters predicted between samples of different thickness are comparable, and in all the case, close to the target value predicted from standard tensile stress relaxation tests. These values are used in the FE model to predict the force-time data, the result is shown in Figure 4.20. In all the three cases, the numerical data showed a

good agreement with the original raw test data of different sample thicknesses. This suggests that the two stage interactive searching approach is an effective way of estimating the relaxation parameters from indentation bending tests.

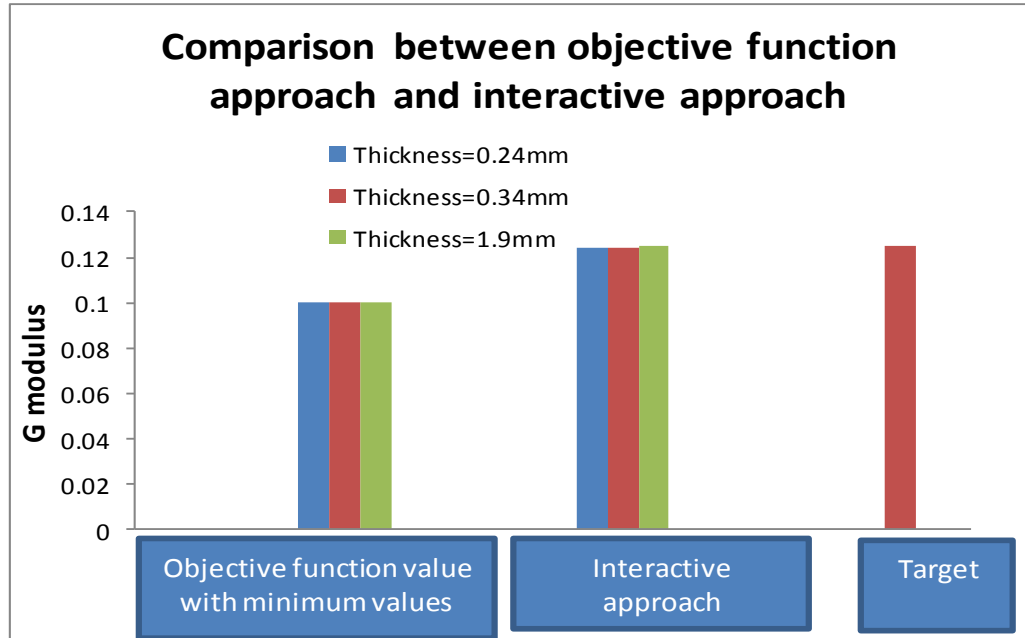


Figure 4.19 (a) Comparison between the predicted G modulus based on the Objective function approach and the interactive searching approach and the target value (based on the standard tensile stress relaxation test).

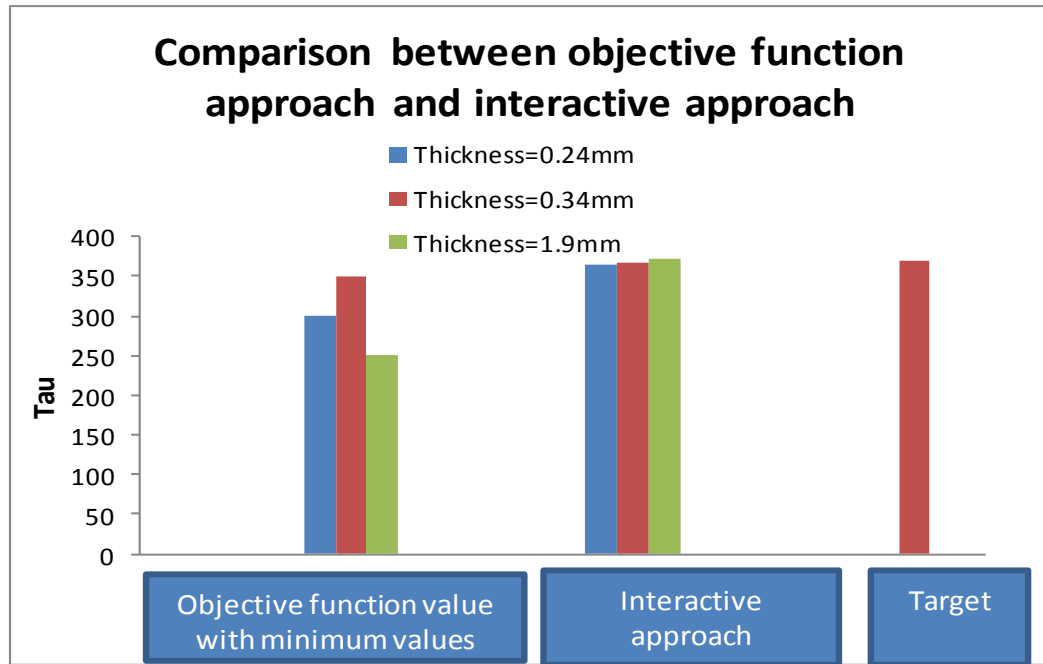


Figure 4.19 (b) Comparison between the predicted τ based on the Objective function approach and the interactive searching approach and the target value (based on the standard tensile stress relaxation test).

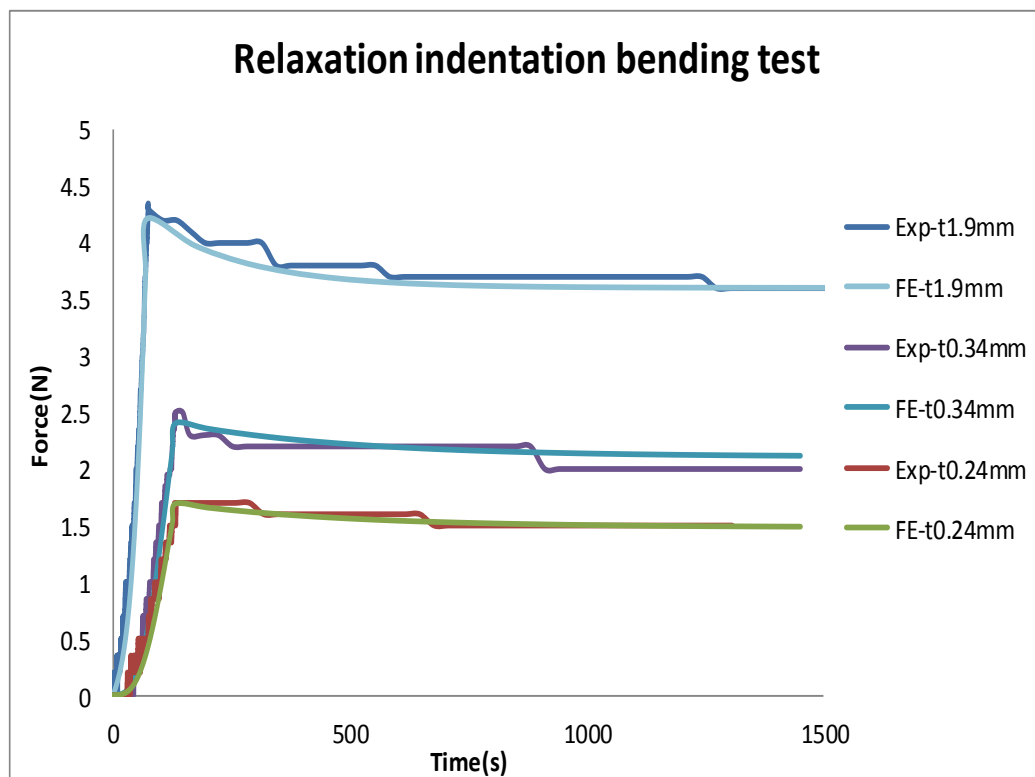


Figure 4.20 Comparison between experimental relaxation data and numerical force-time data using the predicted relaxation parameters in an indentation bending tests.

4.6 Summary

In this chapter, Relaxation indentation bending test has been performed and different inverse FE programs have been comparatively applied to estimate the viscoelastic parameters from the test data. Relaxation indentation bending test of different thickness latex rubber samples have been tested. FE models simulating the relaxation indentation bending of viscoelastic material behaviour have been developed and factors such as mesh sensitivity, hyperelastic material model were systematically studied. Relaxation tensile test and relaxation shear test also directly be used to validate the FE model and evaluate the suitability of the hyperelastic and viscoelastic model. Simulation spaces over a wide range of material parameters have been developed for thickness samples, which successfully provided the data for the material parameters prediction. Two inverse parameter identification programs have been developed. One program is based on full objective function approach; the other is a two staged interactive searching approach. These programs were evaluated in both training data using numerical data as the target and relaxation test data of the natural latex rubber sample. The work shows that the viscoelastic parameter could be determined through an inverse program, but the two stages based interactive searching program developed is more effective and flexible in running larger property domains.

CHAPTER FIVE

EFFECTS OF POISSON'S RATIO ON THE DEFORMATION OF THIN MEMBRANE STRUCTURES UNDER INDENTATION

5.1 Introduction

As detailed in Chapter 2, many engineering and medical conditions involve deformation/deflection of thin shells/membranes with a clamped boundary, such as pressure sensors, valves and actuators as well as biological tissues (*Scott O. N. et al, 2004, Ju B. F. et al, 2005, Selvadurai A. P. S., 2006, Egan P. et al, 2007, Aheame M. et al, 2010*). The material deformation in these cases covers a wide spectrum of strain levels from small deformation to large displacement with samples of different thicknesses. The resulting force displacement curve (P-h curves) in an indentation bending test is dependent on the properties of the material, the structure and dimensions of the sample. Many studies have been conducted into the mechanics of membranes under localised load with different loading or boundary conditions (*Perlrine R. et al, 2000, Haughton D. M., 2001, Liu K. K. & Ju B. B., 2001, Oyen M. L. et al, 2004, Scott O. N. et al, 2004, Ju B. F. et al, 2005, Selvadurai A. P. S., 2006, Egan P. et al, 2007*). Most of these works have been focused on material with a positive Poisson's ratio. It is important to expand the study to some new materials groups under indentation bending, in particular Negative Poisson's ratio materials. These types of materials get fatter when they are stretched, or become smaller when compressed, in contrast to conventional materials (like rubber, glass, metals, etc.) (*Evans K. E. & Alderson A., 2000, Alderson K. et al, 2014*). Many advances have been made recently to produce material with negative Poisson's ratios at different length scales (*Pozniak A. A. & Wojciechowski K. W., 2014, Sanami M. et al, 2014, Sun J. et al, 2014, Ge Z. & Hu H., 2015, Lim T. C., 2015, Shufrin I. et al, 2015*). A detailed investigation on the potential effects of Poisson's ratio and auxeticity on the force-displacement data, the material deformation and its interaction with the indenter during indentation tests is important to explore the use of auxetic materials in different applications.

Due to the nature of loading and sample configuration, the effect of Poisson's ratio for sample with clamped edge conditions is complicated being affected by material properties as well as the experimental conditions (such as sample thickness and indenter size, etc.). Within the loading domain, the deformation mode may change with depth. In the bending/plate domain, the load is known to be not affected by the auxeticity of the materials (*Timoshenko S. & Woinowski-Krieger S., 1987*). But in the

membrane or transition between plate and membrane behaviour, positive or negative Poisson's ratio theoretically would potentially have different effects under localised loading conditions (*Timoshenko S. & Woinowski-Krieger S., 1987, Komaragiri U. et al., 2005*). It is essential to study the effect of Poisson's ratio on the material behaviour in both point loading and finite contact conditions (such in the case of a spherical indenter). In these conditions which are different from the loading conditions of standard tests, the effect of material properties on the material behaviour is directly influence by the dimensions of the experimental samples as well as the loading conditions. A detailed understanding of these factors will help to establish the effects of the Poisson's ratio with a focus on the influence of auxeticity, which will help to further develop material testing methods and extend the use of auxetic materials in many relevant industrial fields.

In this chapter, numerical models of a thin membrane under point loading and finite contact conditions with a spherical indenter have been developed. The FE model for the spherical indentation model is fully validated against experiment data of latex rubber samples (as a model material) of different thicknesses and sizes. The FE model simulating point loading of thin membranes is compared to analytical solutions for materials of different thicknesses and effects of the Poisson's ratio with different sample thickness and deflection depth is analysed. FE models with finite contact are developed to simulate thin membranes incorporating auxetic behaviour and their deformation mechanisms under an indentation bending test is studied. The effect of auxeticity on the P-h curves, deformation profile and contact is presented and discussed with reference to deformation mechanisms and potential use of auxeticity.

5.2 Experimental and FE models

Figure 5.1(a) shows schematically the setup of the indentation bending test. In the test, a spherical indenter is pressed onto a thin membrane supported by a circular frame which provides a fixed boundary condition. The diameter (designated as chamber size) and height of the supporting chamber) is 30mm and 50mm, respectively. The radius of the indenter is 4mm. A rubber sheet with a thickness of 0.8 mm was made out of a latex resin by casting. The Young's modulus of the rubber sheet is 1.25MPa. The sample was made by mixing the latex coagulant and emulsion (ABL Resin & Glass, UK) at room temperature followed by degassing in a vacuum casting machine to remove entrained air, then pouring into an aluminum mold and cured at room temperature to avoid any residual pre-strain. The samples were characterised in uniaxial tensile tests and planar tests on a tensile test machine (Tinius Olsen Ltd (H50KS)), the data was used to validate the FE modeling results from the indentation bending tests. The indenter used is made of a stainless steel ball with a highly polished surface. The indentation system was mounted on a rigid supporting frame. The loading rate used in the test is 0.5mm/sec. A sensitive load cell (model: LCMS-D12TC-5N) was attached to the moving head of the actuator to monitor the force during the test. The displacement of the indenter is monitored by a linear variable displacement transducer (LVDT) and controlled by a computer.

The FE of the test is developed using the finite element code ABAQUS 6.11. Figure 5.1 (b&c) shows the FE models developed to study the deformation of membranes under finite contact condition (b) and under point loading condition (c). The membrane was modelled with shell elements (type S3 and S4R). There are total ~15000 elements in the model with finer meshes over the region under the indenter in order to establish the contact area. Both element types are general purpose conventional stress displacement shells with 3 or 4 nodes. These elements allow transverse shear deformation. They use thick shell theory as the shell thickness increases and become discrete Kirchhoff thin shell elements as the thickness decreases. The use of mixed types of elements effectively improved the efficiency of the FE model. The rim of the rubber sheet was fully fixed to represent the effect of the clamping rig. Preliminary work showed that the numerical results from this simplified (but more efficient) boundary condition were comparable to a solid model

with full boundary conditions. A full 3D model also allows the evaluation of potential effects of misalignment etc. The main work reported in this paper is based on a linear elastic law in which the properties were represented by Young's modulus (E) and the Poisson's ratio (ν). Linear elastic models have been used previously to describe rubber like membranes at relatively lower strain levels (*Ju B. F. et al, 2005, Scoot O. N. et al, 2004*). In this work, the suitability of elastic modelling is also compared to several hyperelastic models to further validate the FE model and establish a displacement range, within which the Elastic mode is fully valid. The use of linear elastic modelling allows effective evaluation of the effect of Poisson's ratio and auxeticity on the material behaviour in terms of force displacement data and deformation behaviour.

As shown in Figure 5.1 (b&c), two loading conditions have been investigated. One (Figure 5.1(b)) is to apply a point load at the centre of the circular membrane; this is designed to compare the FE modelling results with analytical solutions. The other one (Figure 5.1(c)) is a finite contact situation in which indenters of different sizes are simulated. In this case, contact has been defined between the indenter and specimen. Sensitivity tests have been performed to assess the influence of mesh size, boundary conditions, and frictional condition in order to ensure the FE model is accurate with an optimum requirement with regard to computational resources. A python program has been developed in which the material properties and sample thickness can be changed systematically.

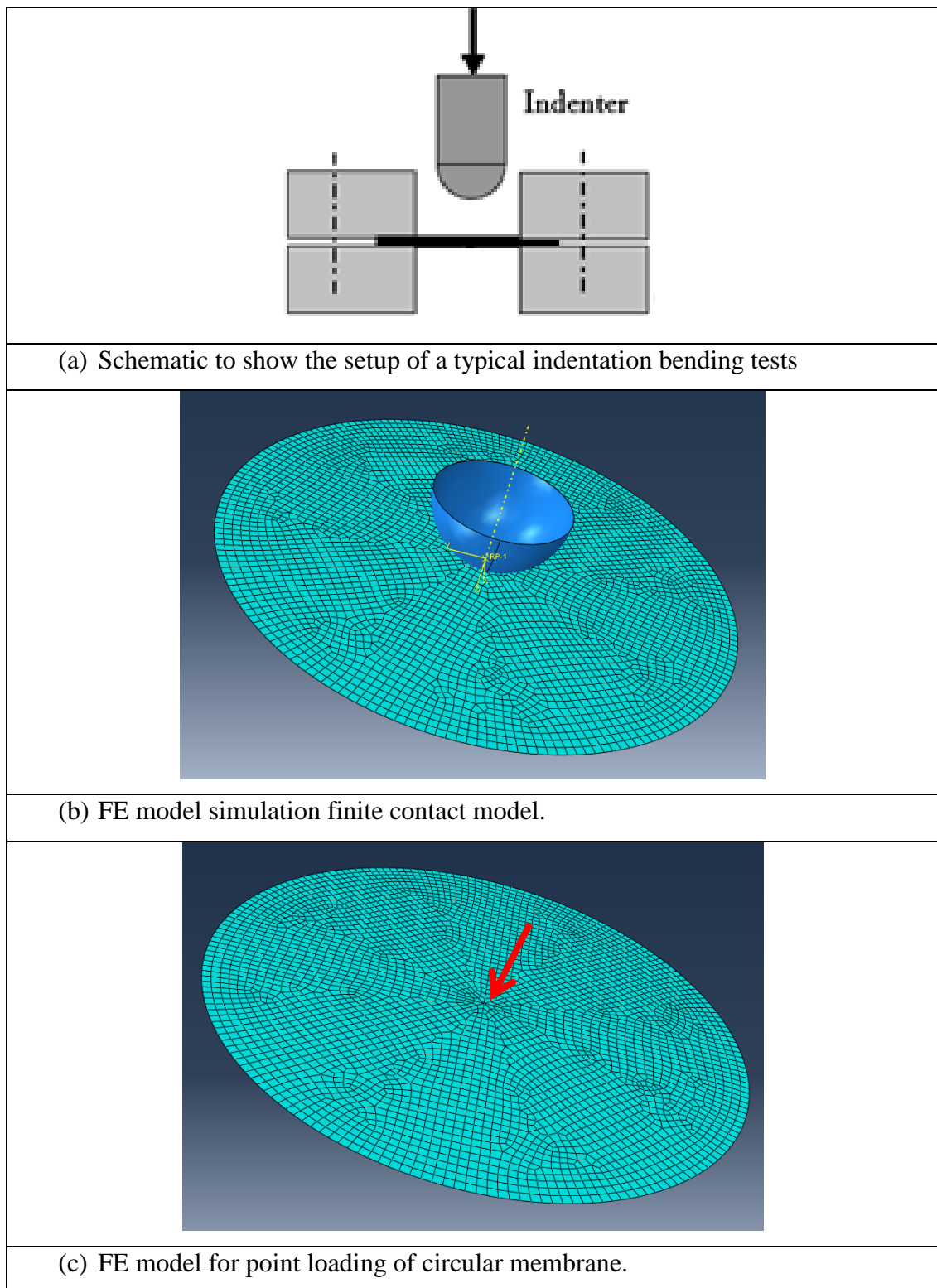
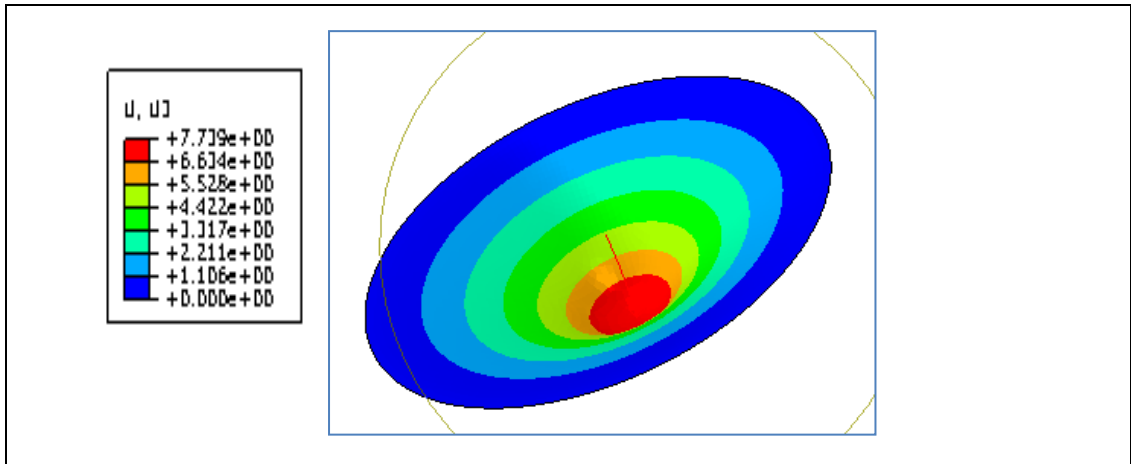


Figure 5.1 Setup of a typical indentation bending tests (a) and FE model for finite contact (b) and point loading (c) of thin membranes. The rim of the circular membrane is fixed at all degree of freedom.

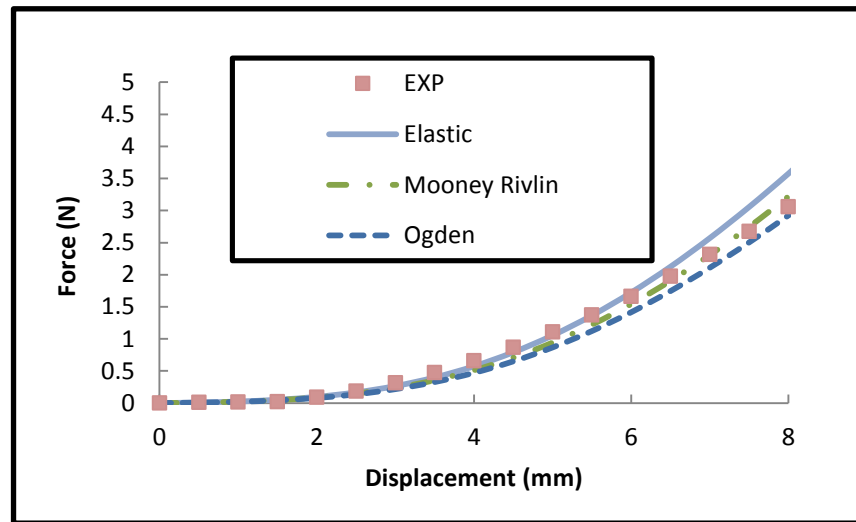
5.3 Results and discussion

5.3.1 Comparison between experimental data and FE modelling

Figure 5.2(a) shows the displacement fields and comparison between test data of the latex rubber sample and FE modelling with elastic properties (solid line) and hyperelastic properties (dashed line). Details of the Ogden and Mooney Rivlin strain energy function could be found in [the ABAQUS 6.11 Theory Manual](#). The elastic property is based on tensile tests and hyperelastic property was based on the combination of tensile and planar tests. The material test data is not shown to preserve clarity. The data in Figure 5.2 clearly shows that the FE data with elastic properties is in a good agreement with the testing data up to a displacement of 5mm. While the hyperelastic models can produce data up to much larger displacement. Given the current work is focused on investigating the effects of Poisson's ratio, the modelling is limited to the strain range where the elastic model is valid. Similar agreements could be found between FE and experimental data over a wide range of sample thickness and indenter sizes which confirms that the FE model is valid and accurate. This is essential to be able to predict the effect of Poisson's ratio and auxeticity.



(a) Typical deflection fields of membrane under indentation.



(a) Experimental force deflection data and FE results with elastic and hyperelastic material law. ($E=1.25\text{MPa}$).

Figure 5.2 Comparison of experimental and numerical data with Elastic and hyperelastic model to validate the FE model.

5.3.2 Deformation of a thin membrane under point loading conditions.

Figure 5.3 compares the FE modelling results and analytical solution. The analytical solution (equation 1) is based on a modified Schwerin point loading condition with consideration of the influence of the Poisson's ratio (*Komaragiri U. et al, 2005*).

$$\delta = f(\nu)a \left(\frac{P}{Ea} \right)^{\frac{1}{3}} \quad (5.1)$$

Where:

$$f(\nu) \approx 1.049 - 0.146\nu - 0.158\nu^2 \quad (5.2)$$

In equation (1), 'a' is the diameter of the chamber; 'δ' is the indentation depth/deflection; 'P' is the force (N) and 't' is the thickness. The data presented in Figure 5.3 are for membrane thickness of 0.1mm, E=1.25MPa and Poisson's ratio of 0.495 and -0.495 (these value are used rather than 0.5 to improve the modelling efficiency). In both cases, the FE data and the analytical data show a good agreement.

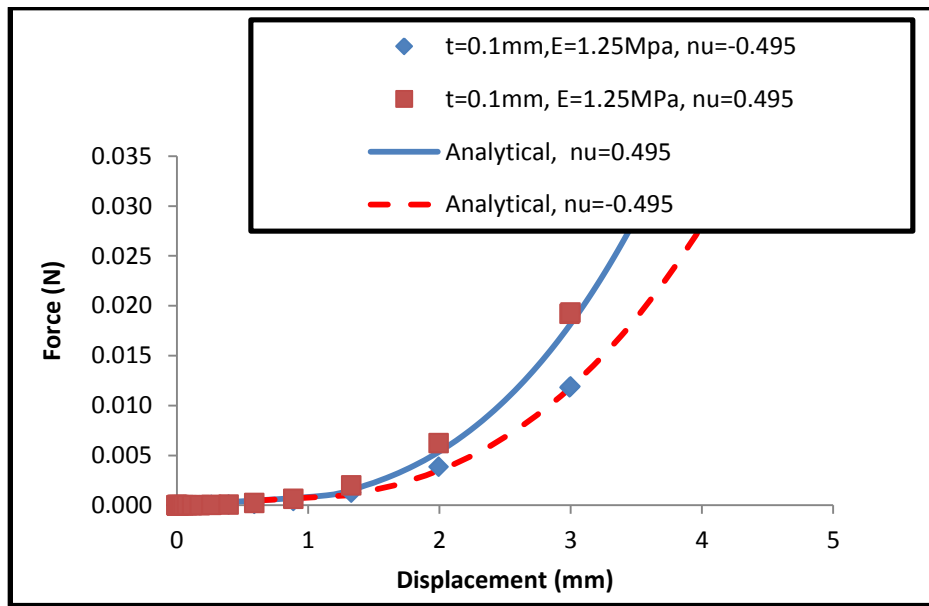


Figure 5.3 Comparison between FE and analytical solution for point Loading Condition of circular membrane with negative and positive poisson's ratio.

According to the analytical solution, P is related to δ^3 . Figure 5.4 plots (P/δ^3) vs. displacement. At lower displacement, P/δ^3 decreases with displacement following a similar trend between negative and positive Poisson's ratio, and then eventually reach to a stable value. With thin samples Figure 5.4(a), there is a clear effect of auxeticity, (P/δ^3) is much lower with negative Poisson's ratio. As the thickness of the sample increase, the effect of negative Poisson's ratio become less significant, as shown in Figure 5.4(b&c). In the case where thickness is 1mm, the difference between positive and negative Poisson's ratio is much less significant.

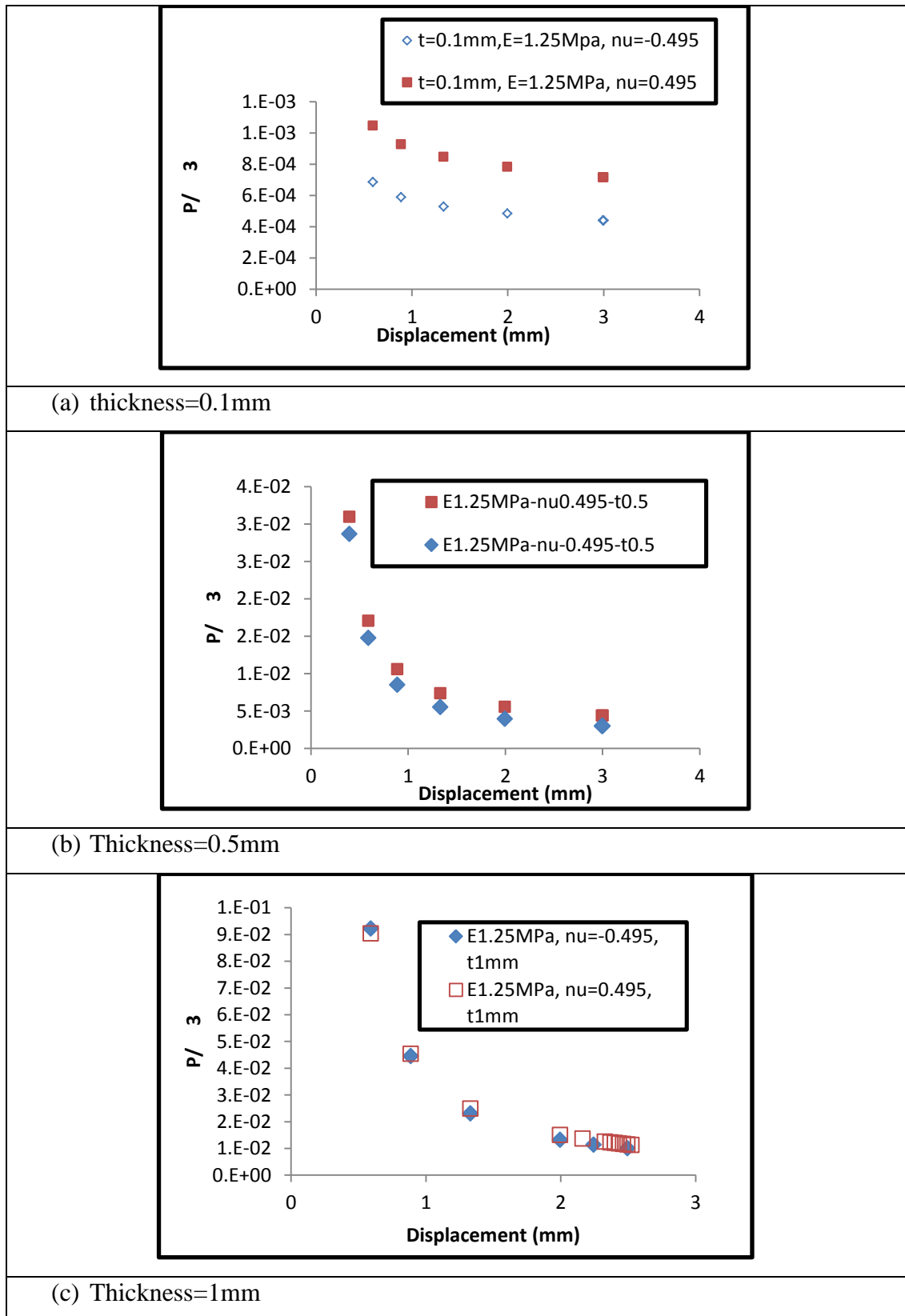


Figure 5.4 Variation of curvature parameter (P/δ^3) with positive and negative Poisson's ratio for samples of different thicknesses under point loading.

5.3.3 Effect of Poisson's ratio on the deformation of membranes under finite contact conditions.

In the finite contact case, an indenter is pressed onto the surface. Figure 5.5 shows typical force displacement data with an indenter size of R4mm. The data shows that the force displacement of a finite contact conditions is different from the analytical solution derived for point loading in particular at high indentation depths. Preliminary work also showed that only when the indenter size is smaller than 0.5mm, the result can be approximated by the analytical solution (result not shown). As shown in the data, the membrane with negative Poisson's ratio is weaker than the corresponding one with a positive Poisson's ratio. This is also observed for other E values. In other words, a material with a negative Poisson's ratio has better sensitivity to the load change. This could be a beneficial factor in situation such as sensors or some biological tissue such as bladder tissues. Figure 5.6 plots P/δ^3 data for different indenter sizes. Results show that, in all cases, the membrane deformation zone can be effectively represented/approximated by a cubic relationship, i.e. P/δ^3 , which could provide an effective way in material data comparisons. Comparing to the data metric for point loading conditions (Figure 5.4), the P/δ^3 reached a stable constant zone at certain displacement ranges (in this case, after 1mm depth). This is probably due to the interaction between the membrane and the indenter. This could be a very useful feature in representing the force displacement data. In the data for each indenter size, the P/δ^3 is lower for the membrane with negative Poisson's ratio. Figure 5.7 shows the P/δ^3 for samples of different thickness. It clearly shows that samples with different thickness show a different trend in reaching a full membrane domain and the effect of auxeticity becomes more significant with increasing depth for thicker samples.

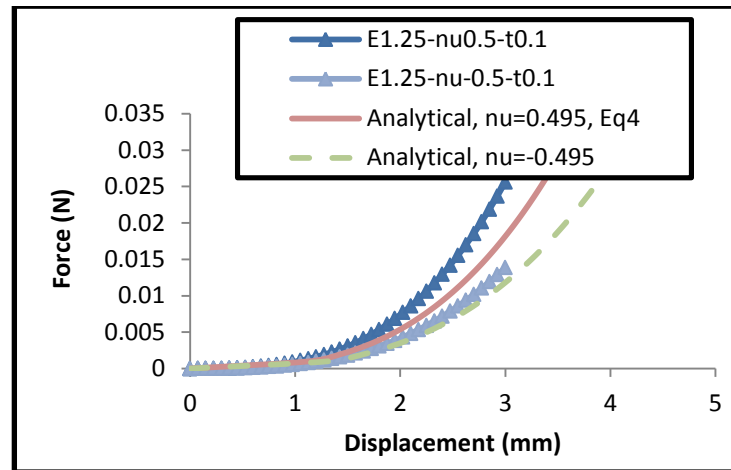


Figure 5.5 Force displacement curves for Limit Contact Model. The solid and dash lines are data based on analytical solution for point loading (Eq. 5.1).

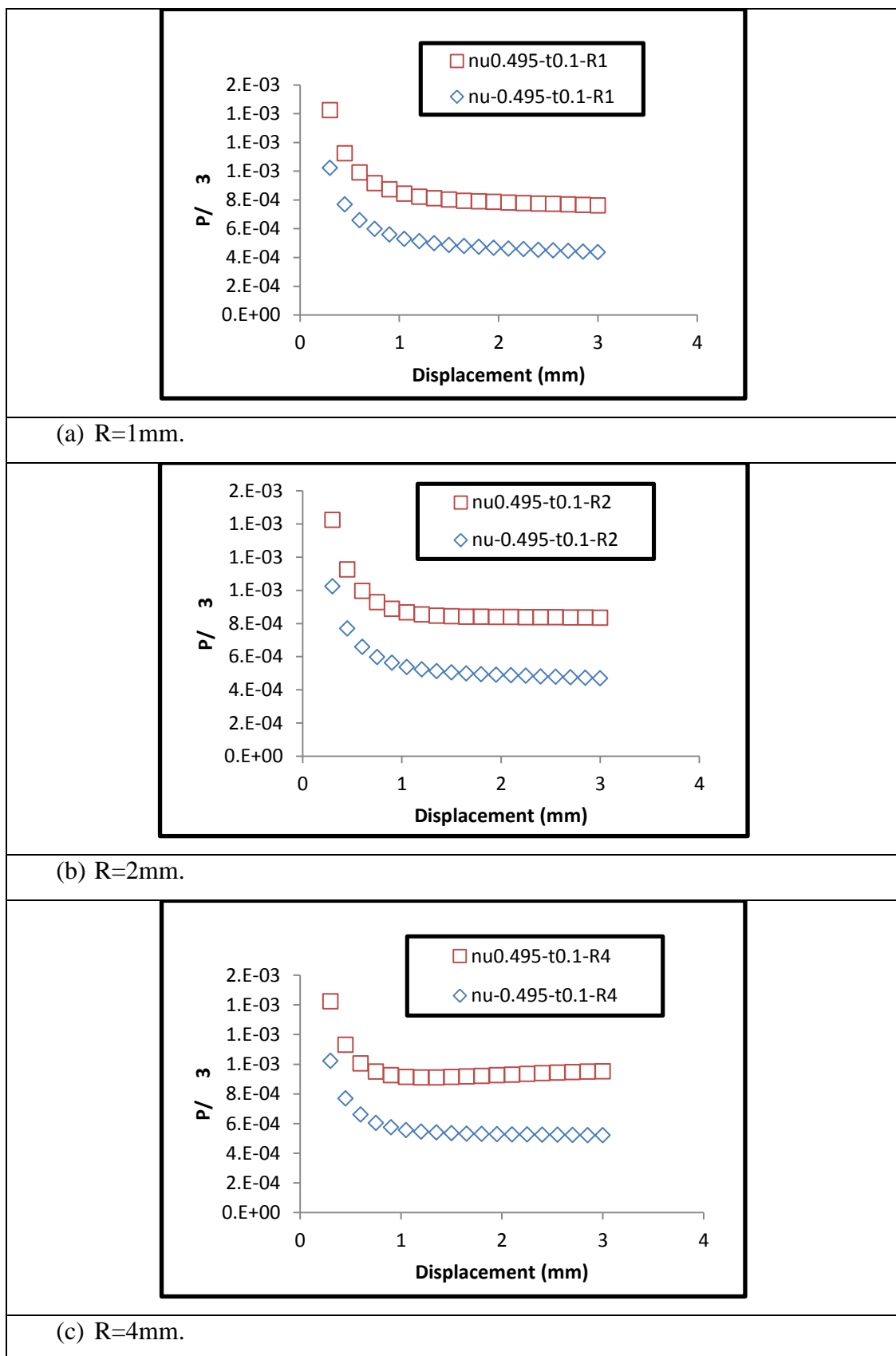


Figure 5.6 Curvature Parameter (P/δ^3) vs. depth for different indenter sizes (R1, 2, and 4mm, sample thickness=0.1mm).

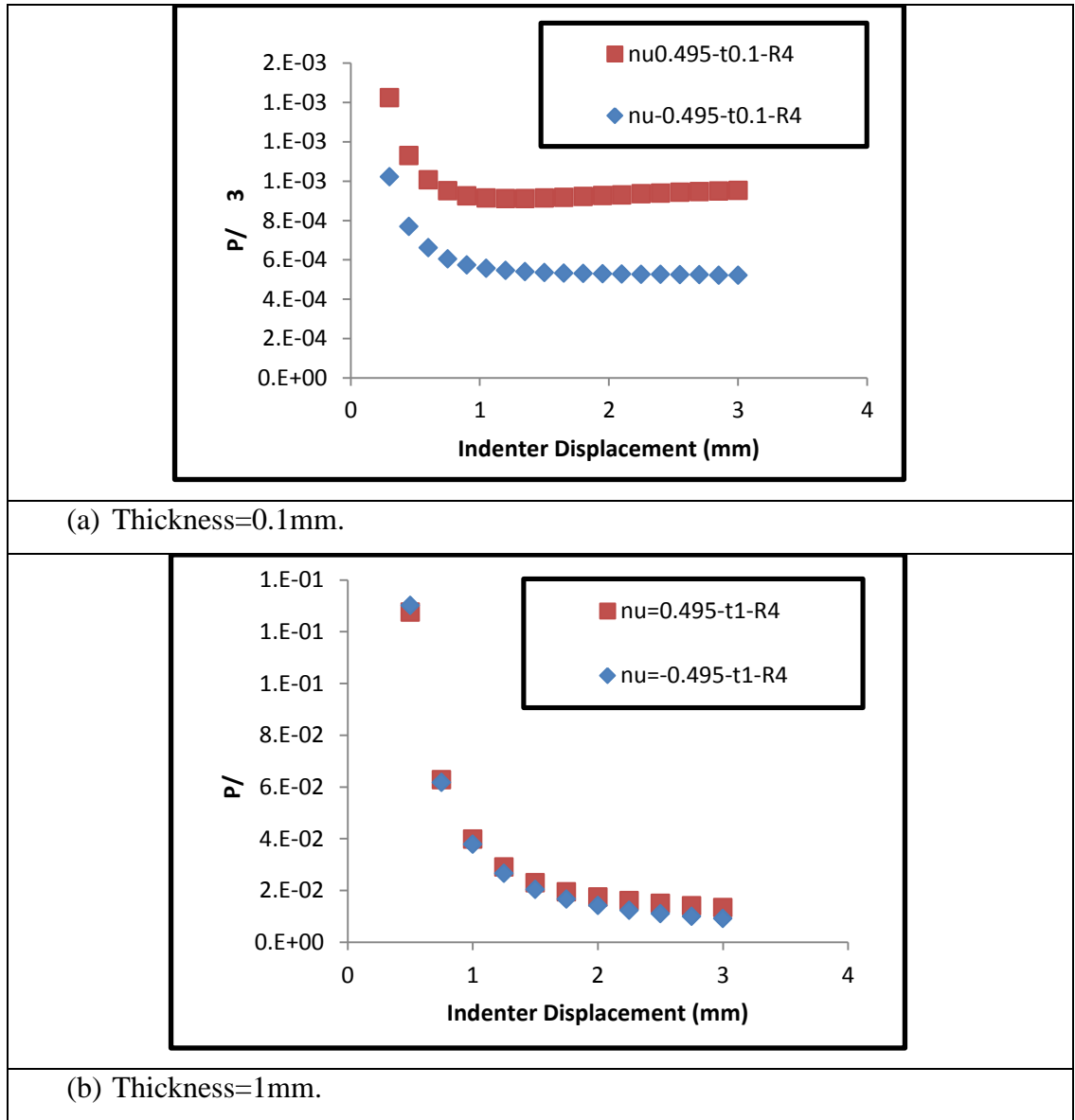


Figure 5.7 Effect of auxeticity on the P/δ^3 for samples of different thickness.

The results clearly show that auxeticity has direct influence on the force displacement relationship. The detailed deformation is analysed to establish the effect of auxeticity on the displacement profile for both the vertical and lateral direction. Different from standard material tests, the displacement profile is an important feature for thin membrane tests. The profile may provide means to represent the deformation of the materials, which has been explored by several researchers ([Ju B. F. et al, 2005](#), [Selvadurai A. P. S., 2006](#)). It is important to analyse the potential effects of auxeticity on the displacement profile and contact conditions. Figure 5.8 plots a typical profile of vertical deflection (U_2) with positive and negative Poisson's ratio. In the figure, the x-axis used is the distance from the centre

point normalised by the radius of the chamber (15mm). (0 represents the central point, 1 represents the position of the edge). For thin samples, the displacement profile between the positive and negative Poisson's ratio is slightly different (Figure 5.8(a)). But in the central part and near the clamp edge, the displacement profile is comparable. This is probably due to restraint from the indenter and the edge effects. But with thicker specimen, there is no difference in the displacement profile between positive and negative Poisson's ratio. This is probably due to the transition to the plate deformation domain.

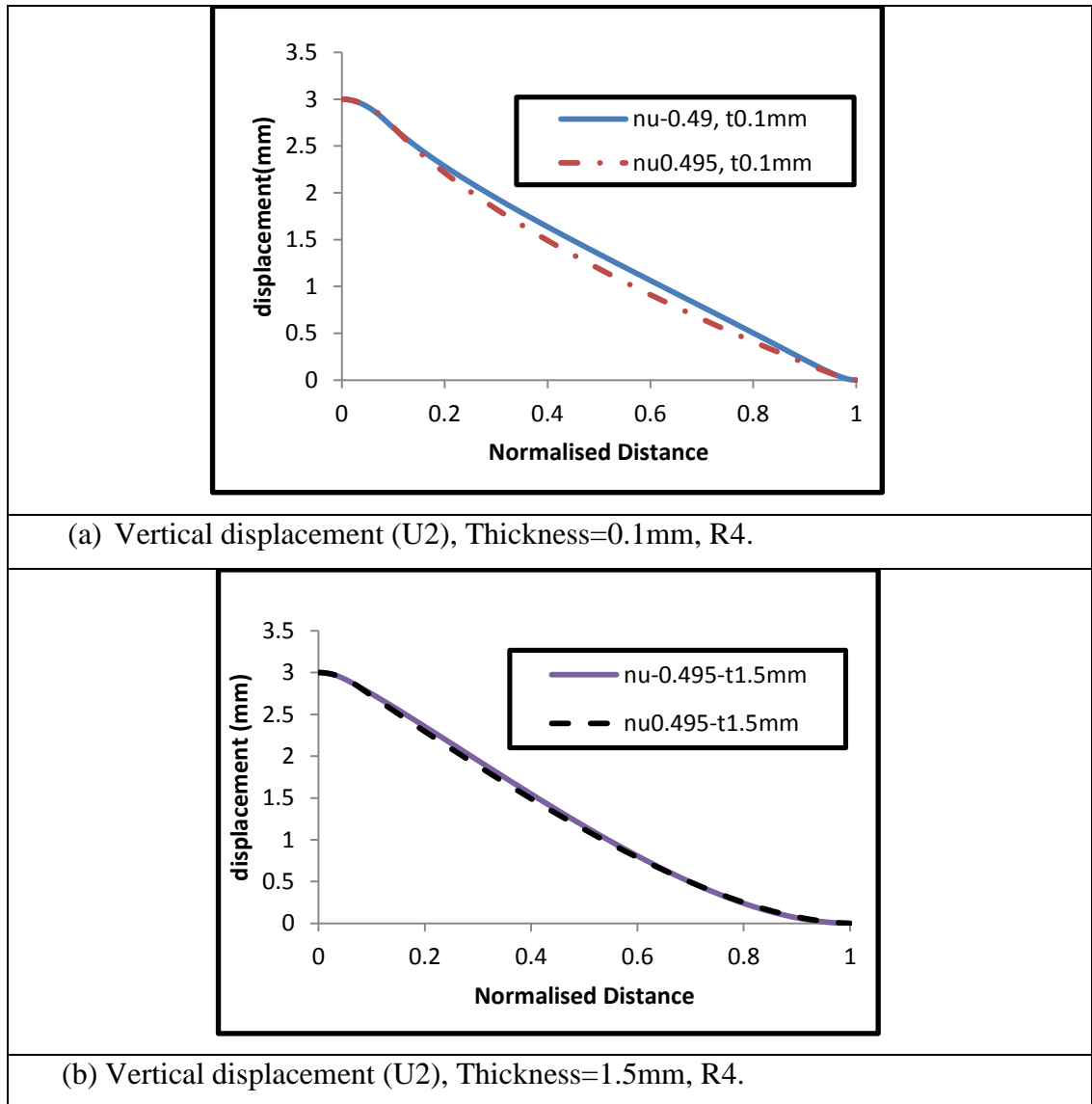


Figure 5.8 Effect of auxeticity on the displacement (Vertical displacement, U2) profile with different sample thickness.

Figure 5.9(a) compares the distribution of lateral displacement between positive and negative Poisson's ratio. In general, the values are very low, but there is a clear difference between these two sets of data. The data suggests that a negative Poisson ratio results in a positive circumferential strain as compared to a predominantly negative circumferential strain in the case of a positive Poisson's ratio. Figure 5.9 (a&b) compares the profile of lateral displacement of samples with different thickness at an indentation depth of 3mm, in all cases, the auxeticity showed a clear influence on the profile. With finite contact problems, the contact area is another important character. This is studied by plotting the contact stress. Figure 5.10 shows the contact pressure for samples of different thicknesses. In both cases, the contact area for the negative Poisson's ratio one is smaller than the one with positive Poisson's ratio. This is in reasonable agreement with the data on the deformation profiles and force displacement data.

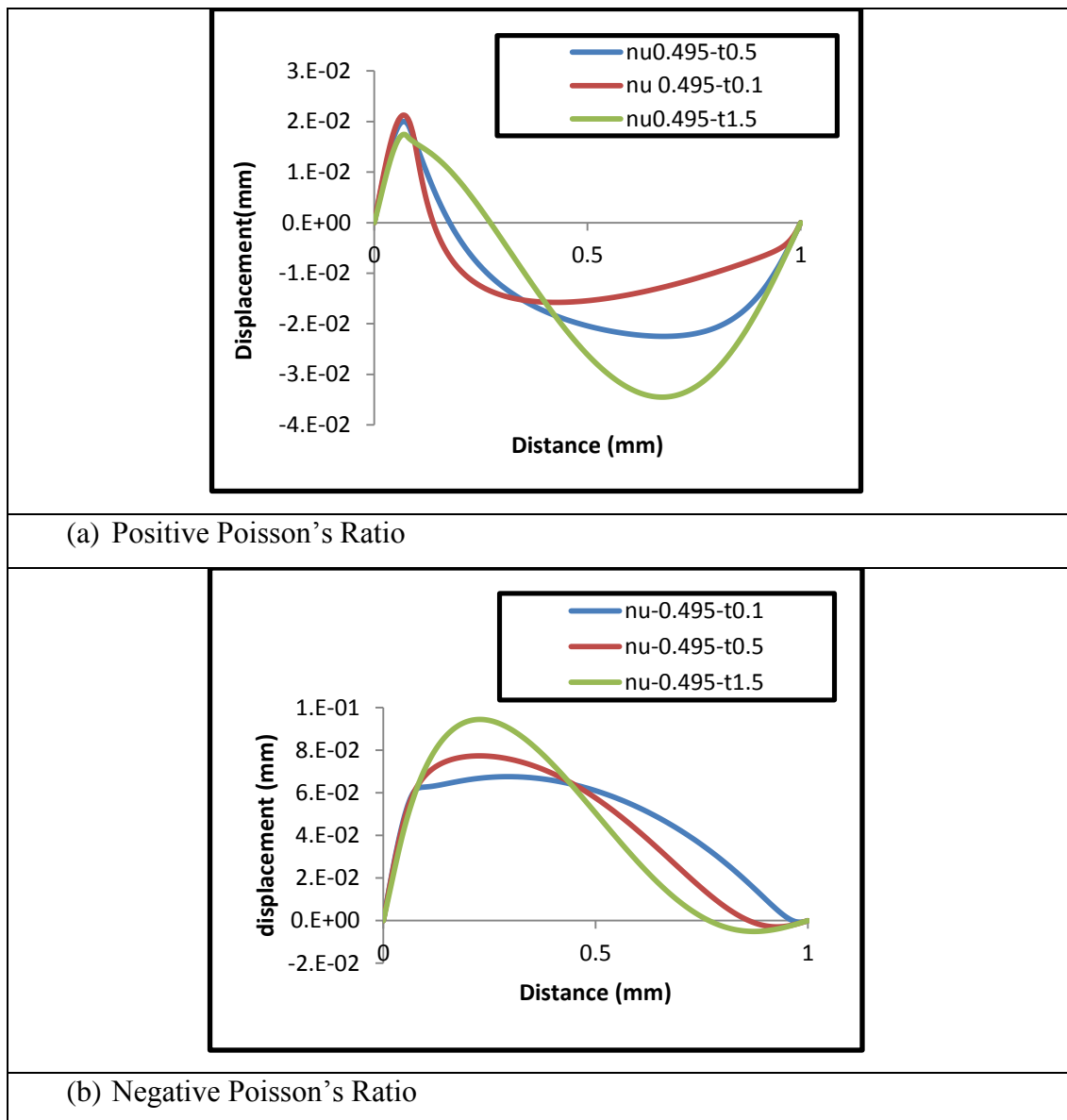


Figure 5.9: Axial displacement (U1) Profile with different sample thicknesses.

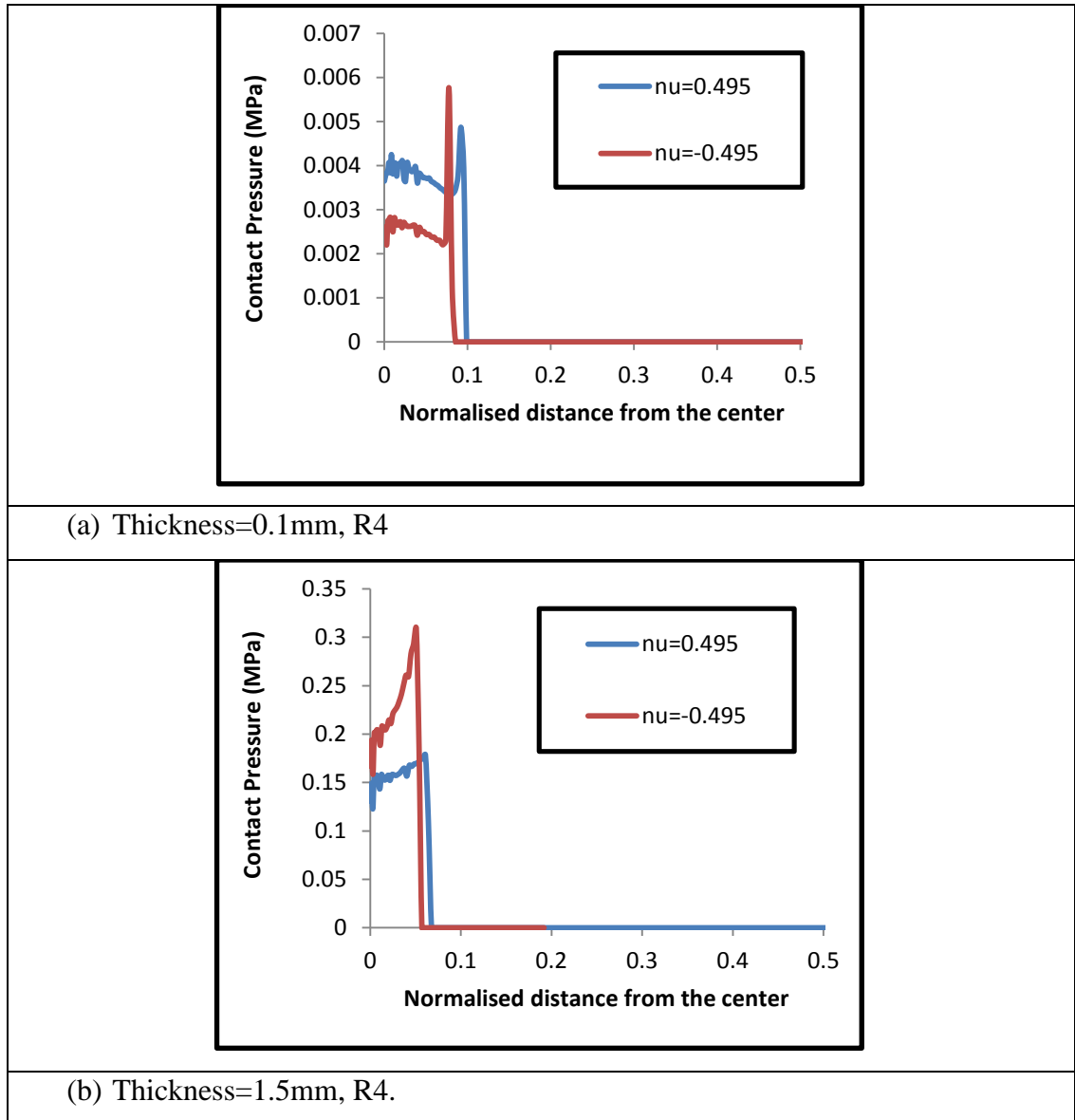


Figure 5.10 Effect of Poisson's Ratio on the contact stress showing the effect of auxeticity on the contact area.

The effect of the auxeticity on the contact and the deformation of thin plate is a complex process, as the deformation of the region in contact with the indenter and the remaining region of the membrane could be through different deformation regimes (*Komaragiri U. et al, 2005*). The contact pressure is affected by many factors such as the friction, thinning of the samples and chamber size, which require a systematic further investigation. The change of the contact area observed is in reasonable agreement with the effects of negative Poisson's ratios. In general, for an auxetic membrane, there is a tendency for lateral strain ' ϵ_θ ' to be positive causing expanded radius. An expanded radius, in the case of finite contact, would naturally

give a decreased contact area. This in turn may affect the overall indentation resistance. Further work is required to investigate if these changes of the contact area have partially contributed to the relative lower force for materials with a negative Poisson's ratio.

5.4 Summary

In this chapter, the deformation of circular elastic membranes with a clamped edge under point loading and finite contact conditions is systematically studied incorporating auxeticity behaviour. The effect of Poisson's ratio on the deformation of the material is established. The feasibility and limitation of an analytical solution is assessed. The work shows that the P/δ^3 relationship is applicable to describe the force displacement data over the membrane domain for both point loading and finite contact conditions. It is shown that negative Poisson's ratio has direct influence on the membrane deformation domain; the force is relatively lower, which could be beneficial as the material will be more sensitive to load change. The deflection profile is slightly different between positive and negative Poisson's ratio, while the contact area for negative Poisson's ratio is relative smaller. This work has highlighted some important characteristics of membranes with negative Poisson's ratio, further work is required to quantify these effects with consideration of relative dimensions between sample thickness and chamber size.

CHAPTER SIX

CONCLUSIONS AND FUTURE WORKS

6.1 Summary and conclusion

In this work, the use of inverse FE modelling and indentation bending test for material properties identification has been systematically studied. A parametric FE model has been developed and validated simulating the indentation tests of thin latex rubber samples made in the laboratory. Rubber samples were tested in standard uniaxial tensile, planar tests, the hyperelastic material parameters are determined and used as the target for the inverse material parameter identification program. The influence of factors such as mesh size sensitivity and choice of material model on the modelling results was systematically studied. An ABAQUS add-on program has been developed to automatically update the material parameters and extract the force-displacement data. Simulation spaces over a wide range of material parameters have been developed, which successfully provided the numerical data for the inverse approach for material properties prediction. Different curve analysis approaches in representing the force-displacement curve have been proposed including: (1) using ratio of P/h^3 for the low load region, (2) using the effective slope at higher load and (3) using the second order polynomial curve fitting parameters. The effectiveness of these three approaches in providing data to inverse material parameters identification is evaluated supported by several programs. The result shows that use of these curve fitting parameters could effectively simplify the inverse FE modelling process and allow the use of surface plot equations to establish a mathematical relationship between curve coefficients and material parameters. These relationships could effectively open up the possibility in improving the uniqueness of inversely predicted material property sets by combining either data from different testing conditions or different curve data from the same test.

The work has been supported by several new programs to process and analysis the data. A MatLab program has been developed to determine the surface equation between the key curve coefficients and the material parameters based on FE data with an Ogden model. Work based on the data from a single indenter tests shows that there are multiple material property sets that could produce identical force-displacement data. This confirms that the results are not unique. Several approaches have been evaluated by combining the surface equation for different curve parameters or testing conditions (i.e. sample sizes). A program has been developed

and implemented in the inverse FE modelling which allows systematic studies with different approaches including dual chamber size, thickness or combining two curve parameters approach. The program is evaluated using training data with numerical and experimental data. The results demonstrate combining different curve fitting approaches method with a smaller chamber size is more effective than using the dual chamber size approach.

Relaxation indentation bending test has been performed and different inverse FE programs have been comparatively applied to estimate the viscoelastic parameters from the test data. One program is based on full objective function approach; the other is a two staged interactive searching approach. These programs have been evaluated in both training data using numerical data as the target and relaxation test data of the natural latex rubber sample. The work shows that the viscoelastic parameter could be determined through an inverse program, but the two staged based interactive searching program developed is more effective and flexible in running larger property domains.

The deformation of circular elastic membranes with a clamped edge under point loading or finite contact conditions is systematically studied incorporating auxeticity behaviours (Negative Poisson's ratio). The effect of Poisson's ratio on the deformation of the material is established. The feasibility and limitation of an analytical solution is assessed. The work shows that the P/h^3 relationship is applicable to describe the force displacement data over the membrane domain for both point loading and finite contact conditions. It is shown that negative Poisson's ratio has direct influence on the membrane deformation domain; the resistance force of a membrane with a negative Poisson's ratio is relatively lower, which could be beneficial for application such as sensors, as the material will be more sensitive to load change. The deflection profile is slightly different between positive and negative Poisson's ratio, while the contact area for negative Poisson's ratio is relative smaller. This work has highlighted some important characteristics of membranes with negative Poisson's ratio, further work is required to quantify these effects with consideration of relative dimensions between sample thickness and chamber size.

6.2 Recommendations for future works

This work has established a series of programs and framework for developing FE models of indentation bending tests and inverse materials parameters identification.

The work can be extended into the following areas:

1. Use of the method in investigating temperature effects on materials. Rubber materials could be used in different temperatures, which directly influence the load bearing capacity and creep behaviour. The indentation bending tests could potentially be a convenient way to establish the material behaviour at different temperatures.
2. Use of the method to study the effect of composition or curing time on the properties of rubber or gels. A special shaped mould could be made, which allows the making of very thin rubber samples. Some thin silicone rubber could be made by simply spin the rubber in a container, and then the thin sheet can be tested.
3. Further develop the program into a web based tool in running ABAQUS model and analysing data.

References

- ABAQUS**, User's Manual, version 6.11, Hibbitt, Karlsson & Sorensen. Inc.
- Aernouts J., Couckuyt I., Crombecq K., Dirckx J.J.J.**, 2010, "Elastic characterization of membranes with a complex shape using point indentation measurements and inverse modelling". *International journal of Engineering science*. Vol. 28, pp.599-611.
- Aernouts J., Aerts J.R.M., Dirckx J.J.J.**, 2012, "Mechanical properties of human tympanic membrane in the quasi-static regime from in situ point indentation measurements". *Hearing Research*. Vol.290, pp.45-54.
- Afshar R., Berto F.**, 2011, "Stress concentration factors of periodic notches determined from the strain energy density". *Theoretical and Applied Fracture Mechanics*. Vol.56, pp.127-139.
- Ahearne M., Liu K. K., El Haj A. J., Then K. Y., Rauz S., Yang Y.**, 2010, "Online monitoring of the mechanical behavior of collagen hydrogels: Influence of corneal fibroblasts on elastic modulus". *Tissue Engineering. Part C*. Vol.15, pp.1-11.
- Alderson K.L., Pickles A.P., Neale P.J., Evans K.E.**, 1994, "Auxetic polyethylene: The effect of a negative poisson's ratio on hardness". *Acta Metallurgica et Materialia*. Vol.42, pp.2261-2266.
- Alderson K., Alderson A., Grima J.N., Wojciechowski K.W.**, 2014, "Auxetic Material and Related systems". *Physica status solidi (b)*. Vol.251, No.2, pp.263-266.
- Ali A., Hosseini M., Sahari B.B.**, 2010, "A Review of Constitutive Models for Rubber-Like Materials". *American J. of Engineering and Applied Sciences*. Vol.3, No.1, pp.232-239.
- Ali M.N., Rehman I.U.**, 2015, "Auxetic polyurethane stents and stent-grafts for the palliative treatment of squamous cell carcinomas of the proximal and mid oesophagus: A novel fabrication route". *Journal of Manufacturing System*. Vol.37, pp.375-395.
- Almagableh A., Mantena P.R., Al-Ostaz A.**, 2009, "Creep and Stress Relaxation Modeling of Nanoclay and Graphite Platelet Reinforced Vinyl ester Nanocomposites". *Composite Structures and Nano-Engineering Research*. The University of Mississippi, University, MS 38677.

- Aoki S., Amaya K., Sahashi M., Nakamura T.,** 1997, “Identification of Gurson's Material Constants by Using Kalman Filter”. *Computational Mechanics*. Vol.19, No.6, pp.501-506.
- Arciniega R.A., Reddy J.N.,** 2007, “Tensor-based finite element formulation for geometrically nonlinear analysis of shell structures”. *Comput. Method Appl. Mech. Engrg.* Vol.196, pp.1048-1073.
- Argatov I.I.,** 2012, “Mathematical modeling of linear viscoelastic impact: Application to drop impact testing of articular cartilage”. *Institute of Mathematics and Physics, Aberystwyth University, Ceredigion, Wales, UK.*
- Araujo A.L., Lopes H.M.R., Vaz M.A.P., MotaSoares C.M., Herskovits J., Pedersen P.,** 2006, “Parameter estimation in active plate structures”. *Computers and Structures*. Vol.84, pp.1471-1479.
- Avellanads M., Swart P. J.,** 1998, “Calculating the performance of 1-3 piezo composites for hydrophone applications: An effective medium approach”. *Journal of the Acoustical Society of America*. Vol.3, pp.1449-1467.
- Bader D.L., Knight M.M.,** 2008, “Biomechanical analysis of structural deformation in living cells”. *Med. Biol. Eng. Comput.* Vol.46, pp.951-963.
- Bechir H., Chevalier L., Idjeri M.,** 2010, “A three-dimensional network model for rubber elasticity: The effect of local entanglements constraints”. *International Journal of Engineering Science*. Vol.48, pp.265-274.
- Begleya M. R., Mackin T. J.,** 2004, “Spherical indentation of freestanding circular thin films in the membrane regime”. *Journal of the Mechanics and Physics of Solids*. Vol.52, pp.2005-2023.
- Boulénouar A., Benseddiq N., Mazari M.,** 2013, “Strain energy density prediction of crack propagation for linear elastic materials”. *Theoretical and Applied Fracture Mechanics*. Vol.67-68, pp.29-37.
- Boubaker M.B., Corre B.L., Meshaka Y., Jeandel G.,** 2014, “Finite element simulation of the slumping process of a glass plate using 3D generalized viscoelastic Maxwell model”. *Journal of Non-Crystalline Solids*. Vol.405, pp.45-54.
- Breslavsky I.D., Amabili M., Legrand M.,** 2014, “Nonlinear vibrations of thin hyperelastic plates”. *Journal of Sound and Vibration*. Vol.333, pp.4668-4681.
- Brighenti R.,** 2014, “Smart behaviour of layered plates through the use of auxetic materials”. *Thin-Walled Structures*. Vol.84, pp.432-442.

- Brown R.P., Bennett, F.N.B.**, 1981, "Compression stress relaxation Polymer Testing". Elsevier Ltd. Vol.2, pp.125-133.
- Brunig M.**, 1998, "Nonlinear Finite element analysis based on a large strain deformation theory of plasticity". Computers and Structural. Vol.69, pp.117-128.
- Budday S., Nay R., De Rooij R., Steinmann P., Wyrobek T., Ovaert T.C., Kuhl E.**, 2015, "Mechanical properties of gray and white matter brain tissue by indentation". Journal of the Mechanical Behavior of Biomedical Materials. Vol.46, pp.318-330.
- Buljak V., Maier G.**, 2012, "Identification of residual stresses by instrumented elliptical indentation and inverse analysis". Mechanics Research Communication. Vol.41, pp.21-29.
- Burke M.**, 1997, "A stretch of the imagination". New Scientist. Vol.154, pp.36-39.
- Cameron A.R., Frith J.E., Gomez G.A., Yap A.S.**, 2014, "The effect of time-dependent deformation of viscoelastic hydrogels on myogenic induction and Rac1 activity in mesenchymal stem cells", Biomaterials. Vol.35, pp.1857-1868.
- Canovic S. & Goncalves J.**, 2005, "Modelling of the response of the New Svinesund Bridge". Concrete Structures. Master's Thesis. Chalmers University of Technology
- Cao J., Lin J.**, 2008, "A study on formulation of objective functions for determining material models". International Journal of Mechanical Sciences. Vol.50, pp.193-204.
- Cao Y. P., Ma D. C., Raabe D.**, 2008. "The use of flat indentation to determine the viscoelastic properties in the time and frequency domains of a soft layer to a rigid substrate". Acta Biomaterialia. Vol.5, pp.240-248.
- Cao Y. P., Ma D. C., Raabe D.**, 2009, "The use of flat punch indentation to determine the viscoelastic properties in the time and frequency domains of a soft layer bonded to a rigid substrate". Acta Biomaterialia. Vol.5, pp.240-248.
- Carter F.J., Frank T.G., Davies P.J., Mclean D., Cuschieri A.**, 2001, "Measurements and modelling of the compliance of human and porcine organs". Medical Image Analysis. Vol.5, pp.231-236.
- Carson W.S., Gerling G.J., Krupski T.L., Kowalik C.G., Harper J.C., Moskaluk C.A.**, 2011, "Material characterization of ex vivo prostate tissue via spherical indentation in the clinic". Medical Engineering & Physics. Vol.33, pp.302-309.
- Chan E.P., Crosby A.J.**, 2006, "Fabricating microlens arrays by surface wrinkling". Advanced Material. Vol.18, pp.3228-3242.

- Chan N., Evans K.E.**, 1997, "Microscopic examination of the microstructure and deformation of conventional and auxetic foams". *Journal of Materials Science*. Vol.32, pp.5725-5736.
- Chandrasekaran C.**, 2010, "Rubber Seals for Fluid and Hydraulic Systems". A volume in Plastic Design Library. pp.71-78.
- Chandra P.K., Sobral P.J.do. A.**, 2000, "Calculation of viscoelastic properties of edible films: Application of three models". *Cienc. Tecnol. Aliment.* Vol.20, no.2, pp.250-256.
- Chang C.T., Chen Y.H., Lin C.C.K., Ju M.S.**, 2015, "Finite element modelling of hyper-viscoelasticity of peripheral nerve ultrastructures". *Journal of Biomechanics*. Vol.48, pp.1982-1987.
- Charles J., Gunasekaran S.**, 2015, "Experimental and theoretical investigations of natural rubber (cis-1,4-polyisoprene) using coloumb attenuating and Hartree-Fock theoretical methods". *Optik*. Vol.127, pp.279-287.
- Chaudhari C.V., Bhardwaj Y.K., Patil N.D., Dubey K.A., Kumar V., Sabharwal S.**, 2005, "Padiation-induced vulcanisation of natural rubber latex in presence of styrene-butadiene rubber latex". *Radiation Physics and Chemistry*. Vol.72, pp.613-618.
- Chen S.H., Soh A.K.**, 2008, "The capillary force in micro- and nano-indentation with different indenter shapes". *International Journal of Solids and Structures*. Vol.45, pp.3122-3137.
- Chen T.K.**, 2000, "Determining a Prony Series for a Viscoelastic Material From Time Varying Strain Data". National Aeronautics and Space Administration, Langley Research Center, Hampton, Virginia.
- Chicot D., De Baets P., Staia M.H., Puchi-Cabrera E.S., Louis G., Delgado Y.P., Vleugels J.**, 2013, "Influence of tip defect and indenter shape on the mechanical properties determination by indentation of a TiB_2 -60% B_4C ceramic composite". *International Journal of Refractory Metals and Hard Materials*. Vol.38, pp.102-110.
- Choi J.B., & Lakes R.S.**, 1994, "Analysis of elastic modulus of conventional foams and of re-entrant foam materials with a negative Poisson's ratio". *International Journal of Mechanical Sciences*. Vol.37, pp.51-59.
- Corigliano A. & Mariani S.**, 2004, "Parameter identification in explicit structural dynamics: performance of the extended Kalman filter". *Comput. Meth. Appl. Mech. Engrg.* Vol.193, pp.3807-3835.

- Coombs D.J., Laz P.J., Rao M., Smith S.D., Bushelow M., Rullkoetter P.J.,** 2012, “Stepwise Validated Finite Element model of the Human Lumbar Spine”. SIMULIA Customer Conference, University of Denver, Denver, CO.
- Crocker L.E., Duncan B.C., Urquhart J.M., Hughes R.G., Olusanya A.,** 2011, “The application of rubber material models to analyse flexible adhesive joints”. National Physical Laboratory, Teddington, UK.
- Cui T., Chao Y.J., Van Zee J.W.,** 2013, “Thermal stress development of liquid silicone rubber seal under temperature cycling”. *Polymer Testing*. Vol.32, pp.1202-1208.
- Dai X.H., Wang Y.C., Bailey C.G.,** 2010, “Numerical modelling of structural fire behaviour of restrained steel beam-column assemblies using typical joint types”. *Engineering Structures*. Vol.32, pp.2337-2351.
- Daisley G.R., Dastgir M.G., Ferreira F.C., Peeva L.G., Livingston A.G.,** 2006, “Application of thin film composite membranes to the membrane aromatic recovery system”. *Journal of Membrane Science*. Vol.286, pp.20-36.
- Darja R., Tatjana R., Alenka P.C.,** 2013, “Auxetic Textiles”. *Acta Chim. Sloc.* Vol.60, pp.715-723.
- De Haan Y.M., Sluimer G.M.,** 2001, “Standard linear solid model for dynamic and time dependent behaviour of building materials”. Faculty of Civil Engineering and Geosciences, Delft University of Technology.
- Delalleau A., Josse G., Lagarde J.M., Zahouani H., Bergheau J.M.,** 2006, “Characterization of the mechanical properties of skin by inverse analysis combined with the indentation test”. *Journal of Biomechanics*. Vol.39, pp.1603-1610.
- Dias V., Odenbreit C., Hechler O., Scholzen F., Zineb T.B.,** 2014, “Development of a constitutive hyperelastic material law for numerical simulations of adhesive steel-glass connections using structural silicone”. *International journal of adhesion & Adhesive*. Vol.48, pp.194-209.
- Diridollou S., Berson M., Vabre V., Black D., Karlsson B., Auriol F., Gregoire J.M., Yvon C., Vaillant L., Gall Y., Patat F.,** 1997, “An in vivo method for measuring the mechanical properties of the skin using ultrasound”. *Ultrasound in Med. & Biol.* Vol. 24, pp.215-224.
- Drozdov A.D.,** 1999, “A model for the non-linear viscoelastic response and physical aging in glassy polymers”. *Compt. Theor, Polym. Sci.* Vol.9, pp.73-87.

- Egan P., Whelan M.P., Lakestani F., Connelly M.J.,** 2007, “Small punch test: An approach to solve the inverse problem by deformation shape and finite element optimization”. Computational Materials Science. Vol.40, pp.33-39.
- Erdemir A., Viveiros M.L., Ulbrecht J.S., Cavanagh P.R.,** 2006, “An inverse finite-element model of heel-pad indentation”. Journal of Biomechanics. Vol.39, pp.1279-1286.
- Erisken C., Kalyon D.M., Zhou J., Kim S.G., Mao J.J.,** 2015 “Viscoelastic properties of dental pulp tissue and ramifications on biomaterial development for pulp regeneration”. JOE. Vol.41, pp.1711-1717.
- Ericksen J.L., & Rivlin R.S.,** 1948, “Large Elastic Deformations of Homogeneous Anisotropic Materials”. Journal of Rational Mechanics and Analysis. Vol.3, No.3.
- Evans K.E. & Alderson A.,** 2000, “Auxetic Material: Functional Materials and Structures from Lateral Thinking!”. Advanced Materials. Vol.19, No.9, pp.617-628.
- Fagan M.J.,** 1992, “Finite element analysis”. Theory and practice. Essex: Longman.
- Firat M.,** 2007, “Computer aided analysis and design of sheet metal forming processes: Part I – The finite element modelling concepts”. Material and Design. Vol.28, pp.1298-1303.
- Fontanella C.G., Forestiero A., Carniel E.L., Natali A.N.,** 2013, “Analysis of heel pad tissues mechanics at the heel strike in bare and shod conditions”. Medical Engineering & Physics. Vol.35, pp.441-447.
- Fredrik N., Maria N.,** 2006, “FE-Modelling of PC/ABS-Experimental Tests and Simulations”. Division of Solid Mechanics. pp.1-83.
- Friis S., McLaughlin J.K., Mellekjaer L., Kjoller K.H., Blot W.J., Boice J.D., Fraumeni J.F. Olsen J.H.,** 1997b, “Breast implants and cancer risk in Denmark”. International Journal of Cancer. Vol. 71, pp.956-958.
- Gac P.Y.L., Roux G., Verdu J., Davies P., Fayolle B.,** 2014, “Oxidation of vulcanized polychloroprene: A kinetic study”. Polymer Degradation and Stability. Vol.109, pp.175-183.
- Galantai A.,** 2000, “The theory of Newton’s method”. Journal of Computation and Applied Mathematics. Vol.124, pp.25-44.
- Ge Z. & Hu H.,** 2015, “Deformation behaviors of three-dimensional auxetic spacer fabrics”. Journal of the Textile Institute. Vol.106, pp.101-109.

- Giannakopoulos A.E.**, 2006, “Elastic and viscoelastic indentation of flat surfaces by pyramid indentors”. *Journal of the Mechanics and Physics of Solids*. Vol.54, pp. 1305-1332.
- Giannakopoulos A.E., Triantafyllou A.**, 2007, “Spherical indentation of incompressible rubber-like materials”. *Journal of the Mechanics and Physics of Solids*. Vol.55, pp.1196-1211.
- Gouldstone A., Chollacoop N., Dao M., Li J., Minor A.M., Shen Y.-L.**, 2007, “Indentation across size scales and disciplines: Recent developments in experimentation and modelling”. *ActaMaterialia*. Vol.55, pp.4015-4039.
- Gras L.L., Mitton D., Viot P., Laporte S.**, 2012, “Hyper-elastic properties of the human sternocleido mastoideus muscle in tension”. *Journal of the Mechanical Behaviour of Biomedical Materials*. Vol.15, pp.131-140.
- Gu Y., Nakamura T., Prchlik L., Sampath S., Wallace J.**, 2003, “Micro-indentation and inverse analysis to characterize elastic-plastic graded materials”. *Materials science and Engineering*. Vol.A345, pp.223-233.
- Guo Z., Sluys L.J.**, 2006, “Computational modelling of the stress-softening phenomenon of rubber-like materials under cyclic loading”. *European Journal of Mechanics and Solids*. Vol.25, pp.877-896.
- Guo Y.Q., Li Y.M., Bogard F., Debray K.**, 2004, “An efficient pseudo-inverse approach for damage modeling in the sheet forming process”. *Journal of Material Processing Technology*. Vol.151, pp.88-97.
- Ha-Anh T., Vu-Khanh T.**, 2005, “Prediction of mechanical properties of polychloroprene during thermos-oxidative aging”. *Polymer Testing*. Vol.24, pp.775-780.
- Hibbit, Karlson and Sorensen Inc.**, 2002, *Abaqus/standard version 6.3, User's Manual, Theory Manual and Keywords Manual*, Hibbit, Karlson, and Soresen Inc., U.S.A.
- Hamaguchi H., Samejima Y., Kani N.**, 2009, “A Study of Aging Effect on Rubber Bearings After About Twenty Years in Use”. 11th World Conference on Seismic Isolation, Energy Dissipation and Active Vibration Control of Structures, GuangZhou, China.
- Han L.H., Noble A., Burcher M.**, 2002, “A Novel Ultrasound Indentation System for Measuring Biomechanical Properties of In Vivo Soft Tissue”. *Ultrasound in Med. & Biol.* Vol.29, No.6, pp.813-823.

Harsono E., Swaddiwudhipong S., Liu Z.S., 2009, “Material characterization based on simulated spherical-Berkovich indentation tests”. *Scriptamaterialia*. Vol.60, pp.972-975.

Haslach H.W., Humphrey J.D., 2004, “Dynamics of biological soft tissue and rubber: internally pressurized spherical membranes surrounded by a fluid”. *International Journal of Non-Linear mechanics*. Vol.39, pp.399-420.

Hassan M.A., Abouel-Kasem A., Mahmoud A., El-Sharied, Yusof F., 2012, “Evaluation of the material constants of nitrile butadiene rubbers (NBRs) with different carbon black loading (CB): FE-simulation and experimental”. *Polymer*. Vol. 53, pp. 3807-3814

Hassan M.A., Kasem A.A., El-Sharied M.A., Yusof F., 2012, “Evaluation of the material constants of nitrile butadiene rubbers (NBRs) with different carbon black loading (CB): FE-simulation and experimental”. *Polymer*. Vol.53, pp.3807-3814.

Haughton D.M., 2001, “Nonlinear Elasticity: Theory and Applications”. (Fum Y.B., Ogden, R.W. (Eds), Cambridge University Press). Vol.283, pp.233-267.

Hayes W.C., Bodine A.J., 1978, “Flow-independent viscoelastic properties of articular cartilage matrix”. *Journal of Biomechanics*. Vol.11, pp.407-419.

Heinrich C., Waas A.M., Wineman A.S., 2009, “Determination of material properties using nanoindentation and multiple indenter tips”. *International Journal of Solids and Structures*. Vol.46, pp.364-376.

Henni A.H., Schmitt C., Tremblay M.E., Hamdine M., Heuzey M.C., Carreau P., Cloutier G., 2011, “Hyper-frequency viscoelastic spectroscopy of biomaterials”. *Journal of the Mechanical Behaviour of Biomedical Materials*. Vol.4, pp.1115-1122.

Hoshiya M., Saito E., 1984, “Nonlinear structural identification using extendedKalman filter”. *Computers and Structures*. Vol.52, No.4, pp.1757-1770.

Hosseini M., Shalili S.M.R., Fard K.M., 2013, “An indentation law for doubly curved composite sandwich panels with rigid-plastic core subjected to flat-ended cylindrical indenters”. *Composites Structures*. Vol.105, pp.82-89.

Huang H., Agafonov V., Yu H., 2013, “Molecular electrical transducers as motion sensors: A review”. *Sensor*. Vol.13, pp.4581-4597.

Huber N., Tsakmakis Ch., 1999. “Determination of constitutive properties from spherical indentation data using neural networks. Part I: the case of pure kinematic hardening in plasticity laws”. *Journal of the Mechanics and Physics of solids*. Vol.47, pp.1569-1588.

- Huber N., Tsakmakis Ch.**, 2001, “A neural network tool for identifying the material parameters of a finite deformation viscoplasticity model with static recovery”. *Computer Methods in Applied Mechanics and Engineering*. Vol.191, pp.353-384.
- Humphrey J.D.**, 2002, “Cardiovascular solid mechanics: cell, tissues, and organs”. New York: Springer.
- Hutton D.V.**, 2004, “Fundamentals of Finite Element Analysis”. The McGraw-Hill Companies.
- Ismail H., Leong H.C.**, 2001, “Curing characteristics and mechanical properties of natural rubber/chloroprene rubber and epoxidized natural rubber/chloroprene rubber blends”. *Polymer Testing*. Vol.20, pp.509-516.
- Israel A. B.**, 1966, “A Newton-Raphson method for the solution of systems of equations”. *Journal of Mathematical Analysis and Applications*. Vol.15, pp.243-252.
- Jaunich M., Stark W.**, 2009, “Monitoring the vulcanization of rubber with ultrasound: Influence of material thickness and temperature”. *Polymer Testing*. Vol.28, pp.901-906.
- Jiang T.Z., Xue P., Butt H.S.U.**, 2014, “Plate Shaper Design for Dynamic Testing of Viscoelastic Materials Using Polymeric SHPB”. *International Journal of Impact Engineering*. Ph.D. Thesis.
- Johannknecht R., Jerrams S.J.**, 1999, “The need for equi-biaxial testing to determine elastomeric material properties”. *Constitutive Models for Rubber*. pp73-75.
- Ju B. F., Ju Y., Saka M., Liu K. K., Wan K. T.**, 2005. “A systematic method for characterizing the elastic properties and adhesion of a thin polymer membrane”. *International Journal of Mechanical sciences*. Vol.47, pp.319-332.
- Kabwe A.M., Fester V.G., Slatter P.T.**, 2010, “Prediction of non-Newtonian head losses through diaphragm valves at different opening positions”. *Chemical Engineering Research and Design*. Vol.88, pp.959-970.
- Kraaij G., Zadpoor A. A., Tuijthof G.J.M., Dankelman J., Nelissen R.G.H.H., Valstar E. R.**, 2014, “Mechanical properties of human bone-implant interface tissue in aseptically loose hip implants”. *Journal of the Mechanical Behaviour of Biomedical Materials*. Vol.38, pp.59-68.
- Kim B.K., Lee S.B., Lee J., Cho S.Y., Park H.M., Yeom S.H., Park S.H.**, 2012, “A Comparison Among Neo-Hookean Model, Mooney-Rivlin Model, and Ogden

Model for chloroprene Rubber”. International Journal of Precision Engineering and Manufacturing. Vol.13, No.5, pp.759-764.

Koumi K.E., Nelias D., Chaise T., Duval A., 2014, “Modeling of the contact between a rigid indenter and a heterogeneous viscoelastic material”. Mechanics of Materials. Vol.77, pp.28-42.

Khor C.Y., Abdullah M.Z., Ani F.C., 2011, “Study on the fluid/structure interaction at different inlet pressures in molded packaging”. Microelectronic Engineering. Vol.88, pp.3182-3194.

Kajberg J., Wikman B., 2007, “Viscoplastic parameter estimation by high strain-rate experiments and inverse modelling-Speckle measurements and high-speed photography”. International Journal of Solids and Structures. Vol.44, pp.145-164.

Kapoor R., Pal D., Chakravartty J.K., 2005, “Use of artificial neural networks to predict the deformation behavior of Zr–2.5Nb–0.5Cu”. Journal of Materials Processing Technology. Vol.169, pp.199–205.

Ke Y.C., Yao X.F., Yang H., Liu X.Y., 2014, “Kinetic friction characterizations of the tubular rubber seals”. Tribology International. Vol.72, pp.35-41.

Kim N.S., Choi H.S., 2008, “The prediction of deformation behavior and interfacial friction under hot working conditions using inverse analysis”. Journal of Material Processing Technology. Vol.208, pp.211-221.

Kim T.H. & Kim Y.M., 2015, “Interactive transient flamelet modelling for soot formation and oxidation processes in laminar non-premixed jet flames”. Combustion and Flame. Vol.162, No.5 pp.1660-1678.

Komaragiri U., Begley M.R., Simmonds J.G., 2005, “The Mechanical Response of Freestanding Circular Elastic Films Under Point and Pressure Loads”. Journal of Apply Mechanic. Vol. 17, No.2, pp.203-212.

Kwag G.H., Kim P.S., Han S., Choi H.K., 2005, “Ultra high cis polybutadiene by monomeric neodymium catalyst and its tensile and dynamic properties”. Polymer. Vol.46, pp.3782-3788.

Lakes R., Thelen D., Decker C., 2009, “Material properties of tendon: Introduction”. University of Wisconsin.

Lee A.Y., Mahler N., Best C., Lee Y.-U., Breuer C.K., 2014, “Regenerative implants for cardiovascular tissue engineering”. Tissue Engineering Program and Surgical Research.

- Le Gac P.Y., Arhant M., Davies P., Muhr A.,** 2015, "Fatigue behavior of natural rubber in marine environment: Comparison between air and sea water". *Materials and Design*. Vol.65, pp.462-467.
- Le M. Q.,** 2009, "Material characterization by dual sharp indenters". *International Journal of Solids and Structures*. Vol.46, pp.2988-2998.
- Lee W.B., Chen Y.P.,** 2010, "Simulation of micro-indentation hardness of FCC single crystals by mechanism-based strain gradient crystal plasticity". *International Journal of Plasticity*. Vol.26, pp.1527-1540.
- Lei G.H., Sun H.S., Ng C.W.W.,** 2014, "An approximate analytical solution for calculating ground surface settlements due to diaphragm walling". *Computers and Geotechnics*. Vol.61, pp.108-115.
- Li B., Gu Y.D., English R., Rothwell G., Ren X.J.,** 2009, "Characterisation of nonlinear material parameters of foam based on indentation tests". *Materials & Design*. Vol.30, No.7, pp.2708-2714.
- Li B., Lin J., Yao X.,** 2002, "A novel evolutionary algorithm for determining unified creep damage constitutive equations". *International Journal of Mechanical Sciences*. Vol.44, pp.987-1002.
- Li H., Tung K.K., Paul D.R., Freeman B.D.,** 2011, "Effect of film thickness on auto-oxidation in cobalt-catalyzed films". *Polymer*. Vol.52, pp.2772-2783.
- Li J., Li F.G., He M., Xue F.M., Zhang M.J., Wang C.P.,** 2012, "Indentation technique for estimating the fracture toughness of 7050 aluminium alloy with the Berkovich indenter". *Materials and Design*. Vol.40, pp.176-184.
- Licht C.,** 2013, "Thin linearly viscoelastic Kelvin-Voigt plates". *C. R. Mecanique*. Vol.341, pp.697-700.
- Lim T.C.,** 2015, "Auxetic Materials and Structures". Springer, Singapore.
- Lim Y.Y., Chaudhri M.M.,** 2006, "Indentation of elastic solids with a rigid Vickers pyramidal indenter". *Mechanics of Materials*. Vol.38, pp.1213-1228.
- Lin J., Cheong B.H., Yao X.,** 2002, "Universal multi-objective function for optimising superplastic-damage constitutive equations". *Journal of Materials Processing Technology*. Vol. 125-126. pp.199-295.
- Liu K.K., Ju B.B.,** 2001, "A novel technique for mechanical characterization of thin elastomeric membrane". *J Phys D: Appl Phys*. Vol.24, pp.91-94.

Liu Q., 2006, "Literature Review: Materials with Negative Poisson's Ratios and Potential Applications to Aerospace and Defence". Australia: Defence Science and Technology Organisation.

Lobato J., Canizares P., Rodrigo M.A., Piuleac C.G., Curteanu S., Linares J.J., 2010, "Direct and inverse neural networks modelling applied to study the influence of the gas diffusion layer properties on PBI-based PEM fuel cells". International Journal of Hydrogen Energy. Vol.35, pp.7889-7897.

Louche H., Coudol F.P., Arrieux R., Issartel J., 2009, "An experimental and modeling study of the thermomechanical behavior of an ABS polymer structural component during an impact test". International Journal of Impact Engineering. Vol.36, pp.847-861.

Love A.E.H., 1944, "Mathematical theory of elasticity". 4th edition, New York: Dover Publication, Inc.

Lu L.Y., Lin G.L., Shih M.H., 2012, "An experimental study on a generalized Maxwell model for nonlinear viscoelastic dampers used in seismic isolation". Engineering Structure. Vol.34, pp.111-123.

Malvern L.E., 1969, "Introduction to the mechanics of a continuous medium". New Jersey: Prentice-Hall, Inc.

Marteau J., Mazeran P.E., Bouvier S., Bigerelle M., 2012, "Zero-Point Correction Method for Nanoindentation Tests to Accurately Quantify Hardness and Indentation Size Effect". Strain. Vol.48, pp.491-497.

Martins P.A.L.S., Natal Jorge R.M., Ferreira A.J.M., 2007, "A Comparative Study of Several Material Model for Prediction of Hyperelastic Properties: Application to Silicone-Rubber and Soft Tissues". Strain. Vol.42, pp.135-147.

Masood, S.H., KeshavaMurthy V., 2005, "Development of collapsible PET water fountain bottle". Journal of Materials Processing Tech. Vol.162-163, pp.83-89.

Mattei C.P., Zahouani H., 2004, "Study of adhesion forces and mechanical properties of human skin in vivo". Journal of Adhesion Science and Technology. Vol.18, No.15-16, pp.1739-1758.

Mazurkiewicz D., 2009, "Problems of numerical simulation of stress and strain in the area of the adhesive-bonded joint of a conveyor belt". Achieves of Civil and Mechanical Engineering. Vol.4, pp.2-91.

Mills N.J., 2006, "Finite Element Models for the viscoelasticity of open-cell polyurethane foam". Cellular Polymers. Vol.25, No.5.

- Mills N., Zhu H.**, 1999, "The high strain compression of closed cell polymer foam". *Journal of the Mechanics and Physics of Solids*. Vol.47, pp. 669-695.
- Mills N.J., Fitzgerald C., Gilchrist A., Verdejo R.**, 2003, "Polymer foams for personal protection: cushions, shoes and helmets". *Composites Science and Technology*. Vol.63, pp.2389–2400.
- Mishnaevsky L., Levashov E., Valiev R.Z., Segurado J., Sabirov I., Enikeev N., Prokoshkin S., Solov'yov A.V., Korotitskiy A., Gutmanas E., Gotman I., Rabkin E., Psakh'e S., Dluhos L., Seefeldt M., Smolin A.**, 2014, "Nanostructured titanium-based materials for medical implants: Modeling and development". *Materials Science and Engineering R*. Vol.81, pp.1-19.
- Mishulina O.A., Kruglov L.A., Bakirov M.B.**, 2011, "Neural networks committee decision making for estimation of metal's hardness properties from indentation data". *Optical Memory and Neural Networks*. Vol.20, No.2, pp.132-138.
- Moerman K.M., Holt C. A., Evans S.L., Simms C.K.**, 2009, "Digital image correlation and finite element modelling as a method to determine mechanical properties of human soft tissue *in vivo*". *Journal of Biomechanics*. Vol.42, pp.1150-1153.
- Monteiro E., He Q.-C., Yvonnet J.**, 2011, "Hyperelastic large deformations of two-phase composites with membrane-type interface". *International Journal of Engineering Science*. Vol.49, pp.985-1000.
- Mooney M.**, 1940, "A theory of large elastic deformation". *J. Appl. Phys.* Vol.11, pp.582-592. (in *Atkin and Fox*, 1980)
- Moreu Y. M., Mills N.J.**, 2004, "Test Method-Rapid hydrostatic compression of low density polymeric foams". *Polymer Testing*. Vol.23, pp.313-322.
- Mottahedi M., Dadalau A., Hafla A., Verl A.**, 2010, "Numerical analysis of relaxation test based on Pronyseris material model". *University of Stuttgart*.
- Nakamura T., Wang T., Sampath S.**, 2000, "Determination of properties of graded materials by inverse analysis and instrumented indentation". *Actamaterialia*. Vol.48, No.17, pp.4293-4306.
- Neaupane K.M., Sugimoto M.**, 2003, "An inverse boundary value problem using the Extended Kalman filter". *Science Asia*. Vol.29, pp.121-126.
- Nguyen C.T., Vu-Khanh T., Lara J.**, 2004, "Puncture characterization of rubber membranes". *Theoretical and Applied Fracture Mechanics*. Vol.42, pp.25-33.

- Nordgren F., Nyquist M.**, 2006, "FE-Modelling of PC/ABS-Experimental tests and simulations". Division of Solid Mechanics, Sony Ericsson.
- Oehme A., Gebauer U., Gehrke K.**, 1993, "Homopolymerization and copolymerization of butadiene with a neodymium catalyst". *Journal of Molecular Catalysis*. Vol.82, pp.83-91.
- Ogden, R.W.**, 1972a, "Large deformation isotropic elasticity-on the correlation of theory and experiment for incompressible rubber like solids". *Proceedings of the Royal Society Lond.* Vol.A326, pp.565-84.
- Ogden R.W.**, 1972b, "Large deformation isotropic elasticity-on the correlation of theory and experiment for compressible rubberlike solids". *Proceedings of the Royal Society Lond.* Vol.A328, pp.567-83.
- Ogden R.W., Saccomandi G., Sgura I.**, 2004, "Fitting hyperelastic models to experimental data". *Computational Mechanical*. Springer-Verlag.
- Oyen M.L., Cook R.E., Calvin S.E.**, 2004, "Failure of Human Fetal Membrane Tissues". *J Mater Sci: Mater Med*. Vol.15, pp.651-658.
- Pamplona D.C., Weber H.I., Sampaio G. R.**, 2014, "Analytical, numerical and experimental analysis of continuous indentation of a flat hyperelastic circular membrane by a rigid cylindrical indenter". *International Journal of Mechanical Sciences*. Vol.87, pp.18-25.
- Park S.W., Schapery R.A.**, 1999, "Methods of interconversion between linear viscoelastic material functions. Part I-a numerical method based on Prony series". *International Journal of Solids and Structures*. Vol.36, pp.1653-1675.
- Peng X.Q., Wang Y.**, 2011, "Numerical Validation of a Fiber-Reinforced Hyperelastic Constitutive Model for Human Intervertebral Disc Annulus Fibrosus". *Journal of Mechanics in Medicine and Biology*. Vol.11, No.1, pp.163-176.
- Perlrine R., Kombluh R., Joseph J., Heydt R., Pei Q., Chiba S.**, 2000, "High-field deformation of elastomer dielectrics for actuators". *Mater Sci Eng C*. Vol.11, pp.89-100.
- Petre M.T., Erdemir A., Cavanagh P.R.**, 2007, "Determination of elastomeric foam parameters for simulations of complex loading". *Computer Methods in Biomechanics and Biomedical Engineering*. Vol.9, No.4, pp.231-242.
- Peyraut F., Feng Z.-Q., He Q.-C., Labed N.**, 2009, "Robust numerical analysis of homogeneous and non-homogeneous deformation". *Applied Numerical Mathematics*. Vol.59, pp.1499-1514.

- Pinchuk L., Wilson G.J., Barry J.J., Schoephoerster R.T., Parel J.M., Kennedy J.P.,** 2008, "Medical applications of poly(styrene-block-isobutylene-block-styrene)("SIBS"). *Biomaterials*. Vol.29, pp.448-460.
- Podshivalov L., Fischer A., Yoseph P.Z.B.,** 2011, "3D hierarchical geometric modeling and multiscale FE analysis as a base for individualized medical diagnosis of bone structure". *Bone*. Vol.48, pp.693-703.
- Pozniak A.A., Wojciechowski K.W.,** 2014, "Poisson's ratio of rectangular anti-chiral structures with size dispersion of circular nodes". *Physica Status Solidi B*. Vol.251, pp.367-374.
- Presti D.L.,** 2013, "Recycled tyre rubber modified bitumens for road asphalt mixtures: A literature review". *Construction and Building Materials*. Vol.49, pp.863-881.
- Puel G., Bourgeteau B., Aubry D.,** 2013, "Parameter identification of nonlinear time-dependent rubber bushing models towards their integration in multibody simulations of a vehicle chassis". *Mechanical Systems and Signal Processing*. Vol.36, No.2, pp.354-369.
- Puskas J.E., Fray M.E., Tomkins M., Santos L.M.D., Fischer F., Alstadt V.,** 2009, "Dynamic stress relaxation of thermoplastic elastomeric biomaterials". *Polymer*. Vol.50, pp.245-249.
- Rajagopal K.R.,** 2009, "A note on a reappraisal and generazation of the Kelvin-Voigt model". *Mechanics Research Communication*. Vol.36, pp.232-235.
- Ridha H., Thurner P.J.,** 2013, "Finite element prediction with experimental validation of damage distribution in single trabeculae during three-point bending tests". *Journal of the Mechanical Behavior of Biomedical Materials*. Vol.27, pp.94-106.
- Ren X.J., Smith C.W., Evans K.E., Dooling P., Burgess A., Wiechers J., ZahlanN.,** 2006, "Experimental and numerical investigations of the deformation of soft materials under tangential loading". *International Journal of Solids and Structure*. Vol.43, pp.2364-2377.
- Renaud C., Cros J.-M., Feng Z.-Q., Yang B.T.,** 2009, "The Yeoh model applied on the modelling of large deformation contact/impact problems". *International Journal of Impact Engineering*. Vol.36, pp.659-666.

- Renaud F., Dion J.L., Chevallier G., Tawfiq I., Lemaire R.,** 2011, “A new identification method of viscoelastic behavior: Application to the generalized Maxwell model”. *Mechanical Systems and Signal Processing*. Vol.25, pp.991-1010.
- Reusch F., Estrin Y.,** 1998, “FE-analysis of mechanical response of simple structures with random non-uniformity of material properties”. *Computational Materials Science*. Vol.11, pp.294-308.
- Roh J.H., Roy D., Lee W.K., Gergely A.I., Puskas J.E., Roland C.M.,** 2015, “Thermoplastic elastomers of alloocimene and isobutylene triblock copolymers”. *Polymer*. Vol.56, pp.280-283.
- Roylance D.,** 2001, “Engineering Viscoelasticity”. Department of Materials Science and Engineering Massachusetts Institute of Technology Cambridge.
- Saiful Islam A.B.M., Hussain R.R., Jumaat M.Z., Rahman M.A.,** 2013, “Nonlinear dynamically automated excursions for rubber-steel bearing isolation in multi-storey construction”. *Automation in Construction*. Vol.30, pp.265-275.
- Saleeb A.F., Marks J.R., Wilt T.E., Arnold S.M.,** 2004, “Interactive software for material parameter characterization of advanced engineering constitutive models”. *Advances in Engineering Software*. Vol.35, No.6, pp.383-398.
- Samad M.S.A., Ali A., Sidhu R.S.,** 2011, “Durability of automotive jounce bumper”. *Material and Design*. Vol.32, pp.1001-1005.
- Sanami M., Ravirala N., Alderson K., Alderson A.,** 2014, “Auxetic Materials for Sport Applications”. *Procedia Engineering*. Vol.72, pp.453-458.
- Sasson A., Patchornik S., Eliasy R., Robinson D., Haj-Ali R.,** 2012, “Hyperelastic mechanical behaviour of chitosan hydrogels for nucleus pulposus replacement- Experimental testing and constitutive modelling”. *Journal of the mechanical behaviour of biomaterials*. Vol.8, pp.143-153.
- Sasso M., Palmieri G., Chiappini G., Amodio D.,** 2008, “Characterization of hyperelastic rubber-like material by biaxial and uniaxial stretching tests based on optical methods”. *Polymer Testing*. Vol.27, pp.995-1004.
- Sato K., Toda A.,** 2004, “Modeling of the Peeling Process of Pressure-sensitive Adhesive Tapes with the Combination of Maxwell Elements”. *Journal of the Physical Society of Japan*. Vol.73, No.8, pp.2135-2141.
- Saux V.L., Marco Y., Bles G., Calloch G., Moyne S., Plessis S., Charrier P.,** 2011, “Identification of constitutive model for rubber elasticity from micro-

indentation tests on natural rubber and validation by macroscopic tests”. *Mechanics of Materials*. Vol.43, pp.775-786.

Scott O.N., Begley M.R., Komaragiri U., Mackin T.J., 2004. “Indentation of freestanding circular elastomer films using spherical indenters”. *ActaMaterialis*. Vol.52, pp.4877-4885.

Selvadurai A.P.S., 2006, “Deflection of a rubber membrane”. *Journal of the Mechanics and Physics of Solids*. Vol. 54, pp. 1093-1119.

Shabana A.A., 2012, “Computational Continuum Mechanics”, 2nd edition, New York: Cambridge University Press.

Shufrin I., Pasternak E., Dyskin A.V., 2015, “Hybrid materials with negative Poisson’s ratio inclusions”. *Int. J. Eng. Sci.* Vol.89, pp.100-120.

Simunek J., Vos J.A. de., 1999, “Inverse Optimization, calibration and Validation of Simulation Models at the Field Scale”. Wageningen Pers, Wageningen, The Netherlands, pp.431-445.

Slaughter W.S., 2002, “The liberalized theory of elasticity”. Birkhauser.

Sloan M.R., Wright J.R., Evans K.E., 2011, “The helical auxetic yarn – A novel structure for composites and textiles; geometry, manufacture and mechanical properties”. *Mechanics of Materials*. Vol.42, No.9, pp.476-486.

South J.T., 2001, “Mechanical Properties and Durability of Natural Rubber Compounds and Composites”. Virginia Polytechnic Institute and State University.

Srivastava V.K., Maiti M., Jasra R.V., 2011, “Synthesis and utilization of alternative chain transfer agent in cobalt catalysed 1,3-butadiene polymerization reaction to produce cis-polybutadiene rubber”, *European Polymer Journal*. Vol.47, pp.2342-2350.

Steigmann D.J., 2005, “Puncturing a thin elastic sheet”. *Int. J. Non-Linear Mech.* Vol.40, pp.255-270.

Steward P.A., Hearn J., Wilkinson M.C., 2000, “An overview of polymer latex film formation and properties”. *Advance in Colloid and Interface Science*. Vol.86, pp.195-267.

Su X.X., Gu Y.D., Finlay J.P., Jenkinson I.D., Ren X.J., 2010, “Rapid Identification of Nonlinear Material Parameters of Foams Based on Neural Network”. *Singapore IFMBE Proceedings*. Vol.31, pp.243-246.

- Subramani P., Rana S., Oliveira D., Fangueiro R., Xavier J.,** 2014, “Development of novel auxetic structures based on braided composites”. *Materials & Design*. Vol.61, pp.286-295.
- Sun G.Y., Xu F.X., Li G.Y., Huang X.D., Li Q.,** 2014, “Determination of mechanical properties of the weld line by combining micro-indentation with inverse modelling”. *Computational Material Science*. Vol.85, pp.347-362.
- Sun J. Gao H., Scarpa F., Lira C., Liu Y., Leng J.,** 2014, “Active inflatable auxetic honeycomb structural concept for morphing wingtips”. *Smart Materials and Structure*. Vol.23, pp.125023.
- Swaddiwudhipong S., Tho K.K., Liu Z.S., Zeng K.,** 2005, “Material Characterization based on dual indenters”. *International Journal of Solids and Structures*. Vol.42, pp.69-83.
- Swain M.V.,** 1998, “Mechanical property characterisation of small volumes of brittle materials with spherical tipped indenters”. *Materials Science and Engineering*. Vol.A253, pp.160-166.
- Tanaka M., Dulikravick G.S.,** 2000, “Inverse problems in engineering mechanics” II. ISBN: 10-0080436935. Elsevier Science.
- Tang L., Walters C.L.,** 2014, “Estimation of single-grain properties of steel through inverse-engineering of microindentation experiments: Uniqueness of the solution”. *Procedia Materials Science*. Vol.3, pp.215-220.
- Taniguchi H.,** 2013, “Flexible artificial muscle actuator using coiled shape memory alloy wires”. *APCBEE Procedia*. Vol.7, pp.54-59.
- Taylor L.S., Lerner A.L., Rubens D.J., Parker K.J.,** 2002, “A kelvin-voight fractional derivative model for viscoelastic characterisation of liver tissue”. *ASME International Mechanical Engineering Congress & Exposition*. IMECE2002-32605.
- Thein-Han W.W., Shah J., Misra R.D.K.,** 2009, “Superior in vitro biological response and mechanical properties of an implantable nanostructured biomaterial: Nanohydroxyapatite-silicone rubber composite”. *ActaBiometerial*. Vol.5, pp2668-2679.
- Tho K.K., Swaddiwudhipong S., Liu Z.S., HuaJ.,** 2004, “Artificial neural network model for material characterization by indentation”. *Modelling and Simulation in Materials Science and Engineering*. Vol.12, pp.1055–1062.
- Timoshenko S., Goodier J.N.,** 1951, “Theory of elasticity”. 2nd edition, New York: McGraw-Hill Book Company.

Timoshenko S. and Woinowski-Krieger S., 1987, “In theory of plates and shells”. New York: McGraw-Hill.

Tobolsky A.V., Andrew R.D., 1945, “System manifesting superposed Elastic and Viscous Behaviour”. The Journal of Chemical Physics. Vol.13, No.1

Toda N., Kimizuka H., Ogata S., 2010, “DFT-based FEM analysis of nonlinear effects on indentation process in diamond crystal”. International Journal of Mechanical Sciences. Vol.52, pp.303-308.

Trant J.F., Sran I., Bruyn J.R., Ingratta M., Borecki A., Gillies E.R., 2015, “Synthesis and properties of arborescent polyisobutylene derivatives and a paclitaxel conjugate: Towards stent coatings with prolonged drug release”. Europe Polymer Journal. Vol.72, pp.148-162.

Traub J.F., Wozniakowski H., 1979, “Convergence and complexity of interpolatory-Newton iteration in a banach space”. Comp. & Maths with Appls. Vol.6, 00.385-400.

Tyulyukovskiy E., Huber N., 2007, “Neural networks for tip correction of spherical indentation curves from bulk metals and thin metal films”. Journal of the Mechanics and Physics of Solids. Vol.55, pp.391–418.

Vannah W.M., Childress D.S., 1996, “Indenter tests and finite element modelling of bulk muscular tissue in vivo”. Journal of Rehabilitation Research and Development. Vol.33, No. 3, pp.239-252.

Verdejo R., Mills N.J., 2004, “Hell-shoe interactions and the durability of EVA foam running-shoe midsoles”. Journal of Biomechanics. Vol.37, pp.1379-1386.

Vescovo P., Varchon D., Humbert P., 2002, “In vivo tensile tests on human skin: the Extensometers”. in Bioengineering of the Skin: Skin Biomechanic. CRC Press, USA, New York, 77-90.

Wang X., Schoen J.A., Rentschler M.E., 2013, “A quantitative comparison of soft tissue compressive viscoelastic model accuracy”. Journal of The Mechanical Behavior of Biomedical Materials. Vol.20, pp.126-136.

Weiss J.A., Gardiner J.C., 2001, “Computational Modeling of Ligament Mechanics”. Critical Reviews in Biomedical Engineering. Vol.29, No. 4, pp.1-70.

Woo C.S., Park H.S., 2011, “Useful lifetime prediction of rubber component”. Engineering Failure Analysis. Vol.18, pp.1645-1651.

- Yang L.M., Shim V.P.W., Lim C.T.**, 2000, "A visco-hyperelastic approach to modelling the constitutive behaviour of rubber". *International Journal of Impact Engineering*. Vol.24, pp.545-560.
- Yang W., Li Z.M., Shi W., Xie B.H., Yang M.B.**, 2004, "On auxetic materials". *Journal of Materials Science*. Vol.39, pp.3269-3279.
- Yeoh O.H.**, 1993, "Some forms of strain energy function for rubber". *Rubber Chemistry and Technology*. Vol.66, pp.754-771.
- Zanchet A., Carli L.N., Giovanela M., Brandalise R.N., Crespo J.S.**, 2012, "Use of styrene butadiene rubber industrial waste devulcanised by microwave in rubber composites for automotive application". *Material and Design*. Vol.39, pp.437-443.
- Zeng K., Chiu C.-h.**, 2001, "An analysis of load-penetration curves from instrumented indentation". *Acta mater*. Vol.49, pp.3539-3551.
- Zhang H.H. Li L.X.**, 2009, "Modeling inclusion problems in viscoelastic materials with the extended finite element method". *Finite Element in Analysis and Design*. Vol.45, pp.721-729.
- Zhang M.G., Cao Y.P., Li G.Y., Feng X.Q.**, 2014, "Pipette aspiration of hyperelastic compliant materials: Theoretical analysis, simulation and experiments". *Journal of the Mechanics and Physics of Solids*. Vol.68, pp.179-196.
- Zhao R., Antaki J.F., Naik T., Bachman T.N., Kameneva M.V., Wu Z.J.**, 2006, "Microscopic investigation of erythrocyte deformation dynamics". *Bio rheology*. Vol.43, pp.747-765.
- Zhu Y.F.**, 2009, "Nonlinear deformations of a thick-walled hyperelastic tube under external pressure". University of Glasgow, PhD thesis.
- Zisis Th., Fleck N.A.**, 2010, "The elastic-plastic indentation response of a columnar thermal barrier coating". *Wear*. Vol.268, pp.443-454.

Publication List

Aw C.J., Zhao H., Norbury A., Li L., Rothwell G. and Ren X.J., 2015, "Effects of Poisson's ratio on the deformation of thin membrane structures under indentation". *Phys. Status Solidi B*.pp.1–8 (2015) / DOI 10.1002/pssb.201451658 (In press).

Claiden P., Knowles G., Liu F., Wei Q., Li X., Aw C.J., Ren X.J., 2014, "Modelling of nano-filler reinforcement, filler strength and experimental results of nanosilica composites made by a precipitation method". *Computational Materials Science*. Vol. 94, pp.27-34.

Aw C.J., Ren X.J., 2015, "Faculty of Environments and Technology Research Week". (Poster Presentation).

Aw C.J., Su X. and Ren X.J., 2014, "Numerical Study of Nonlinear Material Parameters on Indentation and Indentation Bending Tests". LJMU General Research Institute Conference (1st Paper Award).

Li S., Aw C.J., Ren X.J., "Use of indentation bending tests in monitoring the curing process of silicone rubber thin film". (in preparation).

Aw C.J., Ren X.J. et al, "Characterisation of force-displacement curves and their influence on inverse material properties identification". (in preparation)

Aw C.J., Zhao H., Norbury A., Li L., Rothwell G. and Ren X.J., 2014, "Numerical Investigation of the Deformation of Thin Shell/Membrane Structures Under Indentation Bending Tests". *Auxetics and Other Materials and Models with "Negative" Characteristics (AUXETICS'14)*, Poznan (Poland) 15-19 September 2014 (Invited Talk).